INVESTIGATING THE NEXUS BETWEEN INFLAMMATION AND FERTILITY IN CATTLE

By

ZACHARY KENT SEEKFORD

A DISSERTATION PRESENTED TO THE GRADUATE SCHOOL
OF THE UNIVERSITY OF FLORIDA IN PARTIAL FULFILLMENT
OF THE REQUIREMENTS FOR THE DEGREE OF
DOCTOR OF PHILOSOPHY

UNIVERSITY OF FLORIDA

2024

To those who have been told they cannot accomplish something; let nothing hold you back, let nothing hold you down.

ACKNOWLEDGMENTS

While the original proverb states that, “it takes a village to raise a child,” I would argue that it equally “takes a village to finish a PhD.” As such, I would like to acknowledge the people who have made this dissertation come to life. First and foremost, I would like to thank my advisor, Dr. John Bromfield. When I started my PhD, I was solely a “cow-guy,” and as a student in his laboratory, I have gained an expansive breadth of skills that will serve me well in future endeavors. I am incredibly grateful for his tremendous mentorship and his ability to encourage me to rationalize hypotheses, data, and life situations at a deeper level, which has ultimately pushed me to view the world through a different lens. I would also like to thank my committee members, Dr. Pete Hansen, Dr. José Santos, Dr. Klibs Galvão, and Dr. Ricardo Chebel, for their willingness to share their advice and expertise about experiments, analyses, or life. I would also like to extend my deep appreciation for my collaborators, Dr. Jermey Block, Dr. Rafael Bisinotto, Dr. Stephanie Wohlgemuth, and Dr. Pedro Fontes, for their assistance with experiments. Furthermore, I would like to thank my master’s advisors, Dr. Alan Ealy and Dr. Vitor Mercadante, for encouraging me to pursue a PhD and attend the University of Florida. I am also deeply appreciative for the Department of Animal Sciences faculty and staff for creating such a fantastic environment to complete a degree and for the financial support.

During my PhD, I have crossed paths with numerous people who have shaped my life and my research. I would like to extend many thanks to my lab mates, both past and present; in particular, Dr. Mackenzie Dickson, Dr. Paula Molinari, Arslan Tariq, Gaby Macay, Rosabel Ramirez-Hernandez, and Rachel White for their support in research endeavors and making the lab environment fun. I would also like to thank

several fellow graduate students, specifically, Lané Haimon, Quinn Hoorn, Maura McGraw, Camila Cuellar, Cecilia Rocha, Dr. Felipe da Silva, and Dr. Thiago Amaral, who cultivated an innate sense of family in the Department of Animal Sciences. I would also like to also thank my friends both far and near, who are too numerous to name, for always having my back during the tribulations of graduate school.

Finally, I would like to extend my deepest thanks to my family. I thank my parents, David and Michelle, for their willingness to support me and their patience through the turbulent nature of graduate school. I also thank my parents for instilling in me a love of science and the dairy cow. I thank my sister, Emma, for being one of my biggest supporters and best friends in life. I thank my grandparents, Harold and Carol, for their love and instilling in me the determination to accomplish difficult things. Last but certainly not least, I would like to give huge thank you to my fiancé, Logan Dotson. I was incredibly fortunate to meet him during my PhD. His patience and support were critical for me finishing my degree.

TABLE OF CONTENTS

page

ACKNOWLEDGMENTS 4

LIST OF TABLES 10

LIST OF ABBREVIATIONS 13

ABSTRACT 17

CHAPTER

1 LITERATURE REVIEW 19

The Role of the Immune System in Reproduction 20
History of Reproductive Immunology as it Pertains to Viviparity 20
Immune Cells Involved in Reproduction, Immune System Activation, and Inflammatory Responses 22
Immune Cell Involvement in Follicle Differentiation, Ovulation, and Luteinization 25
Maternal Recognition of Pregnancy 29
Influences of Environmental Stressors on Fertility 31
Uterine Disease in Dairy Cattle 41
Definitions and Causes of Uterine Disease in Dairy Cattle 41
Treatment and Prevention of Uterine Infections in Dairy Cattle 44
Pathogenesis and Pathophysiology of Uterine Disease Associated Infertility in Dairy Cows 48
Molecular and Cellular Response to Uterine Infection in the Endometrium 49
Hypothalamic-Pituitary-Gonadal Axis Signaling 51
Molecular and Cellular Responses to Infections Within the Ovary 52
Ovulation, Luteinization, and the Production of Progesterone 56
Ovarian Folliculogenesis and Granulosa Cell Maturation 56
Luteinization and Progesterone Synthesis 60
Experimental Models of Induced Inflammation 65
Objectives for this Program of Study 68

2 PATERNAL HIGH GAIN DIET INFLUENCES BLASTOCYST FORMATION FOLLOWING IN VITRO FERTILIZATION IN BOVINE* 72

Summary 72
Introduction 73
Materials and Methods 75
Animals, Experimental Design, and Diet Description 75
Semen Collection and Evaluation 76
Flow Cytometry 78
In Vitro Production of Bovine Embryos 79

Immunofluorescence and Cell Counting 79
RNA Isolation and Real-Time RT-Polymerase Chain Reaction 80
Statistical Analyses 81
Results 82
High Gain Diet Increased Growth and Adiposity of Bulls 82
High Gain Diet Had Minimal Effect on Spermatozoa Parameters 83
Bulls Fed a High Gain Diet Have Reduced Capacity to Develop Blastocyst Stage Embryos After In Vitro Fertilization and Embryo Culture 84
Semen of Bulls Fed a High Gain Diet Does Not Affect Blastocyst Cell Allocation or Expression of Genes Associated with Blastocyst Quality 85
Discussion 85
Acknowledgements of Chapter 2 91

3 BOVINE UTERINE DISEASE IS ASSOCIATED WITH SHORT- AND LONG-TERM PERTURBATIONS TO OVARIAN FUNCTION 101

Summary 101
Introduction 102
Materials and Methods 104
Ethics Statement 104
Study 1 Design: Assessing the Association Between Spontaneous Postpartum Uterine Disease and First Estrous Cycle Ovarian Function 105
Study 2 Design: Effects of Induced Endometritis on Long Term Corpus Luteum Function 107
Statistical Analysis 109
Results 110
Enrolled Cow Production, Reproduction, and Health Characteristics 110
Health Information of Ovulatory Cows 111
Associations Between Metritis and Postpartum Ovarian Dynamics and Function 112
Association Between Endometritis and Postpartum Ovarian Dynamics and Function 113
Effects of Induced Endometritis on Corpus Luteum Gene Expression 113
Discussion 114

4 EXPOSURE OF BOVINE GRANULOSA CELLS TO LIPOPOLYSACCHARIDE REDUCES PROGESTERONE SECRETION DURING LUTEINIZATION 133

Summary 133
Introduction 134
Materials and Methods 135
Granulosa Cell Isolation, Culture and LPS Challenge 135
In Vitro Luteinization of Cultured Granulosa Cells 137
Quantification of Estradiol and Progesterone in Supernatants 138
RNA Isolation and Real Time Polymerase Chain Reaction 138
Live Cell Fluorescence Microscopy of Mitochondria and Lipid 139
Cellular Respirometry and Mitochondrial Stress Test 140

Total Cellular Cholesterol and Cholesterol Uptake Quantification 141
Statistical Analysis 143
Results 144
Lipopolysaccharide Treatment Increases Expression of Inflammatory Mediators and Reduces Estradiol Accumulation 144
In Vitro Luteinization Increase Cellular Progesterone Secretion..... 144
Treatment of Granulosa Cells to LPS Reduces Subsequent Progesterone Synthesis During Luteinization 144
Luteinization of Granulosa Cells Increases Cellular Respiration 145
Treatment of Granulosa Cells with LPS Reduces Lipid Droplets and Mitochondria Density During Luteinization 146
Treatment of Granulosa Cells with LPS Reduces Cholesterol Uptake During Luteinization 147
Discussion 148

5 THE EFFECTS OF INDUCED ENDOMETRITIS ON OOCYTE DEVELOPMENTAL COMPETENCE AND ENDOMETRIAL GENE EXPRESSION 166

Summary 166
Introduction..... 167
Materials and Methods 169
Experimental Protocol and Establishment of Uterine Infection 170
Propagation of Pathogenic *E. coli* and *T. pyogenes* for Intrauterine Infusion. 171
Evaluation of Uterine Infection 172
Oocyte Recovery and In Vitro Fertilization..... 173
Collection of Endometrial Samples for RNAseq 175
Quantification of Peripheral Progesterone 175
RNA Extraction 176
Real Time RT-PCR 177
Library Construction and Sequencing..... 177
Read Mapping and Differential Gene Expression Analysis 178
Pathway Analysis of Differentially Expressed Genes 178
Statistical Analysis 179
Results 180
Effects of Intrauterine Infusion 180
Effect of Bacteria Infusion on Oocyte Recovery and Blastocyst Development..... 180
Effect of Uterine Infection on the Endometrial Transcriptome 181
Discussion 183

6 OVERALL DISCUSSION AND CONCLUSIONS 205

APPENDIX

A SUPPLEMENTAL FIGURES..... 218

B SUPPLEMENTAL TABLES 221

LIST OF REFERENCES 243

BIOGRAPHICAL SKETCH 270

LIST OF TABLES

Table		page
2-1	Primer sequences used for real-time RT-PCR.	92
2-2	Body weight and carcass ultrasound of bulls fed a high gain diet.	93
2-3	Impact of treatment on computer assisted sperm analyses and flow cytometry response variables for fresh and frozen-thawed semen.	94
2-4	Effect of treatment on fresh sperm morphology.	94
3-1	Descriptive characteristics of all enrolled cows with metritis or no metritis.	121
3-2	Descriptive characteristics of all enrolled cows with endometritis or no endometritis.	122
3-3	Relative expression of all detected genes in the corpus luteum after intrauterine infusion of bacteria.	123
5-1	Primer sequences uses for real time RT-PCR.	190
5-2	Summary of read mapping for endometrial samples collected forty-one days after the intrauterine infusion of bacteria or PBS control.	191
5-3	Most abundantly expressed endometrial genes regardless of treatment.	192
5-4	Greatest differentially expressed endometrial genes following the intrauterine infusion of bacteria.	193
5-5	Top predicted canonical pathways identified within the endometrium following infusion of bacteria based on adjusted *P*-value and z-score.	194
5-6	Predicted molecular networks of differentially expressed endometrial genes following intrauterine infusion of bacteria.	195
5-7	Predicted upstream regulators of differentially expressed endometrial genes following intrauterine infusion of bacteria.	198
B-1	Primers sequences used for real time PCR analysis of luteal tissue segregated according to molecular function.	221
B-2	Differentially expressed genes of the endometrium after intrauterine infusion of *E. coli* and *T. pyogenes.*	226
B-3	Predicted canonical pathways altered within the endometrium following intrauterine infusion of *E. coli* and *T. pyogenes.*	232

LIST OF FIGURES

Figure		page
1-1	A conceptual model of the cellular and molecular effects of uterine infection and bacterial components on female reproductive physiology.	70
1-2	A conceptual model of the molecular and cellular processes underpinning steroidogenesis and differentiation of ovarian cells.	71
2-1	Experimental model	96
2-2	Dietary intervention influenced sperm quality	97
2-3	Effect of sire diet on IVF outcomes.	98
2-4	Effect of sire diet on IVF-derived blastocyst cell number	99
2-5	Effect of sire diet on IVF-derived blastocyst gene expression	100
3-1	Experimental models	126
3-2	Health characteristics of all enrolled cows.	127
3-3	Health characteristics of ovulatory cows	128
3-4	Associations between metritis and endometritis on ovulation dynamics	129
3-5	Association between metritis and ovarian dynamics during the first postpartum estrous cycle	130
3-6	Association between endometritis and ovarian dynamics during the first postpartum estrous cycle	131
3-7	Long-term effects of uterine infection on corpus luteum function and gene expression	132
4-1	Experimental model..	156
4-2	Acute response of granulosa cells to LPS.	157
4-3	Effect of granulosa cell treatment with LPS on progesterone synthesis during luteinization.	158
4-4	Effect of granulosa cell treatment with LPS on expression of steroidogenic machinery during luteinization.	159
4-5	Effect of LPS treatment on cellular respiration.	160

4-6 Effect of granulosa cell treatment with LPS on lipid droplet and mitochondria density during luteinization. 162

4-7 Effect of granulosa cell treatment with LPS on cholesterol uptake during luteinization. 163

4-8 Effect of granulosa cell treatment with LPS total cellular cholesterol during luteinization. 164

4-9 Conceptual model for the carryover effects of LPS on granulosa cells during luteinization. 165

5-1 Experimental model. 199

5-2 Efficacy of intrauterine infusion. 200

5-3 Effect of intrauterine infusion of bacteria on acute endometrial gene expression.. 201

5-4 Effect of intrauterine infusion of bacteria on oocyte quality and developmental competence following in vitro fertilization and embryo culture. 202

5-5 Differentially expressed genes of the endometrium following infusion of bacteria.. 203

5-6 Top canonical pathways of the endometrium following infusion of bacteria. 204

A-1 Flow cytometry scatter plots..... 218

A-2 Effect of granulosa cell treatment with LPS or MβCD on cellular respiration during luteinization. 219

A-3 Principal component analysis of endometrial transcript reads acquired from endometrium after infusion of pathogenic bacteria.. 220

LIST OF ABBREVIATIONS

BSA	Bovine serum albumin
cAMP	Cyclic adenosine monophosphate
cDNA	Complementary DNA
CFU	Colony forming units
CL	Corpus luteum
COC	Cumulus oocyte complex
CpG	5' - C-phosphate- G- 3'
CXCL8	C-X-C motif chemokine ligand 8
CYP17A1	Cytochrome P450 family 17 subfamily A member 1
CYP19A1	Cytochrome P450 family 19 subfamily A member 1
DAMP	Damage associated molecular pattern
DIM	Days in milk
DMI	Dry matter intake
DNA	Deoxyribonucleic acid
DPBS	Dulbecco's phosphate buffered saline
DPR	Daughter pregnancy rate
E2	17-B estradiol
ELISA	Enzyme-linked immunosorbent assay
ER	Endoplasmic reticulum
FCS	Fetal calf serum
FDR	False discovery rate
FSH	Follicle stimulating hormone
FSHR	Follicle stimulating hormone receptor
GAPDH	Glyceraldehyde 3-phosphate dehydrogenase

GnRH	Gonadotropin-releasing hormone
GPCR	G-protein coupled receptor
GV	Germinal vesicle
HDL	High density lipoprotein
HEPES	4-(2-hydroxyethly)-1-piperazineethanesulfonic acid
HFD	High fat diets
HMGCR	3-hydroxy-3-methyl-glutaryl-coenzyme A reductase
HPG	Hypothalamic-pituitary-gonadal
HSD3B1	Hydroxy-delta-5-steroid dehydrogenase
HSL	Hormone sensitive lipase
i.m.	Intramuscular
IFN	Interferon
IFNG	Interferon gamma
IFNT	Interferon tau
IGF1	Insulin-like growth factor 1
IL	Interleukin
IL6	Interleukin 6
IMM	Inner mitochondrial membrane
ISG	Interferon-stimulated gene
ISGs	Interferon stimulated genes
ITS	Insulin-transferrin-selenium
IVC	In vitro culture
IVF	In vitro fertilization
LB	Luria-Bertani broth
LDL	Low density lipoprotein

LH	Luteinizing hormone
LHCGR	Luteinizing hormone cognate receptor
LPS	Lipopolysaccharide
MAMs	Mitochondria-associated membranes
MAPK	Mitogen-activated protein kinase
MHC	Major histocompatibility complex
MII	Metaphase II
MIQE	Minimum information for publication of quantitative real-time PCR experiments
NCBI	National Center for Biotechnology Information
NFKB	Nuclear factor kappa light polypeptide gene enhancer in B- cells
NK	Natural Killer
OMM	Outer mitochondrial membrane
oPT-1	Ovine trophoblast protein one
P4	Progesterone
P450scc	Cytochrome P450 side-chain cleavage
PAMP	Pathogen associated molecular pattern
PBS	Phosphate buffered saline
PCR	Polymerase chain reaction
PG	Prostaglandin
PGF2α	Prostaglandin F (2alpha)
PGN	Peptidoglycan
PKA	Protein Kinase A
PLC	Phospholipase C
PMN	Polymorphonuclear
PPR	Pattern recognition receptor

PTA	Predicted transmitting ability
RPL19	60S ribosomal protein L19
RT-PCR	Real-time polymerase chain reaction
SAS	Statistical analysis system
SCR	Sire conception rate
spp	Species plurimae
SPSS	Statistical package for the social sciences
SR-B1	Scavenger receptor type B class 1
STAR	Steroidogenic acute regulatory protein
TBS	Tris buffered saline
TGF	Transforming growth factor
Th	T helper
THI	Temperature humidity index
TLR	Toll-like receptor
TMR	Total mixed ration
TNF	Tumor necrosis factor
TNF	Tumor necrosis factor
TNF-α	Tumor necrosis factor-alpha
TNFR	Tumor necrosis factor receptor

Abstract of Dissertation Presented to the Graduate School
of the University of Florida in Partial Fulfillment of the
Requirements for the Degree of Doctor of Philosophy

INVESTIGATING THE NEXUS BETWEEN INFLAMMATION AND FERTILITY IN CATTLE

By

Zachary Kent Seekford

May 2024

Chair: John J. Bromfield
Major: Animal Sciences

Fertility of cattle is a cornerstone to profitability on both dairy and beef operations. Environmental factors including diet or infection reduce fertility of males and females, ultimately diminishing the likelihood of pregnancy. This dissertation investigates the interactions between two different physiological states and the corresponding effects on male or female reproductive tissues. I hypothesized that 1) paternal overnutrition would reduce the ability of spermatozoa to support early embryonic development, and 2) uterine diseases would alter ovarian and endometrial function, reducing the success for pregnancy.

To test the first hypothesis, bulls were fed a control diet or a high-gain diet for 74 d (Chapter-2). Semen was evaluated using in vitro fertilization to assess embryo development. Feeding bulls a high-gain diet produced sperm with a reduced capacity to develop blastocyst stage embryos.

To test the second hypothesis, I measured follicle and corpus luteum growth, and plasma steroid hormones during the first postpartum estrous cycle of cows with or without uterine disease (Chapter-3). Follicle growth, corpus luteum growth and steroidogenesis were reduced in a manner coincident with uterine disease. To

investigate the mechanisms by which uterine disease alters luteal function (Chapter-4), I show that lipopolysaccharide treatment of granulosa cells reduces progesterone synthesis during luteinization due to perturbed cholesterol availability and mitochondrial density. Lastly, I induced endometritis in nonlactating cows using an intrauterine infusion of pathogenic bacteria to evaluate oocyte and endometrial quality after disease resolution (Chapter-5). Infusion of bacteria had no effect on blastocyst development of oocytes submitted to in vitro fertilization compared to controls. Endometrial tissue collected 41 d after bacterial infusion on d 16 of the estrous cycle had altered gene expression associated with glutathione mediated detoxification, pathogen induced cytokine storm signaling, and neutrophil degranulation. Together, these data demonstrate both immediate and carryover effects of uterine disease on ovarian and endometrial function.

In summary, different environmental factors can negatively affect fertility in cattle. This dissertation shows that paternal overnutrition reduces male fertility and that uterine diseases modulate ovarian and endometrial function required for pregnancy success. Collectively, these studies provide insight into the roles of environmental factors on fertility outcomes.

CHAPTER 1
LITERATURE REVIEW

Infertility is estimated to affect up to 15% of couples globally, with nearly 186 million individuals impacted (Boivin et al., 2007, Mascarenhas et al., 2012). The field of human fertility research is broad and encompasses many aspects of both male and female physiology, which makes targeting questions to address the future of infertility quite difficult. In 2021, a large, rationalized list of the top research priorities related to infertility was generated (Duffy et al., 2021). After organizing and categorizing individual research questions generated by healthcare professionals, researchers, and people experiencing fertility problems, a common question arose concerning the intersection between individual reproductive fitness and the influence of their environment. As a result, a growing body of research has been developed to interrogate the relationships and consequences of environmental stressors on both male and female fertility in humans.

Cattle also have compromised fertility associated with environmental stressors and serve as a model species for biomedical and fertility research (Walsh et al., 2011). Additionally, fertility of dairy cattle is a cornerstone to profitability and efficiency within the dairy industry (Britt, 1985). In 2006, the average value of a new pregnancy was estimated at $278 in lactating Holstein cows (De Vries, 2006). However, the expense of a pregnancy loss was estimated to be $555 with the cost increasing as gestation progressed. In the context of dairy production systems, the greater the number of days in which cows are not pregnant post-calving is costly (De Vries, 2006). As such, it is critical to investigate stressors that can influence fertility success and failure, measured as pregnancy and more importantly the live birth of a healthy calf. Stressors such as

temperature, parental nutrition, vaccination status, and the exposure of an individual to environmental pathogens can all alter immune responses and influence fertility in both males and females (De Kruif, 1978). Additionally, the exposure to stressors can disrupt fertility at the level of the gamete, preimplantation embryo, and later in gestation, while the timing of exposure to stressors may also have long-term implications long after the stressor has been resolved. Thus, the mechanisms by which stressors affect fertility long-term need to be investigated. The intention of this dissertation is to address some potential molecular, cellular, and physiological consequences of environmental stressors on fertility in dairy cattle.

The Role of the Immune System in Reproduction

History of Reproductive Immunology as it Pertains to Viviparity

The field of reproductive immunology is credited to Sir Peter Medawar and his studies and observations investigating transplantation biology, dizygotic twins in cattle and postulating the idea of immunologic tolerance. Concurrently, there were seminal experiments conducted earlier in cattle. Indeed, one of the first observations in cattle describing fetal immune tolerance was conducted by Ray Owen at the University of Wisconsin (Owen, 1945). This study published in *Science* observed that there were differences in blood antigens of twin calves of different sex that were sired by two different bulls, and concluded that the calves had exchanged cells during fetal life likely through placental vascular anastomosis. The persistence of these antigens in genetically dissimilar animals suggested that a mechanism of immunological tolerance between half siblings exists. Later, in 1951, the results of skin grafting experiments between monozygotic and dizygotic twin calves confirmed that grafts between both twin types were tolerated while grafts interchanged between animals of other degrees of

genetic diversity were rapidly destroyed (Anderson et al., 1951). These observations ultimately led Medawar to speculate about the phenomena by which fetal allografts were tolerated by the maternal immune system, deemed immunological tolerance (Medawar, 1953, Medawar, 1961). Indeed, Medawar postulated on the immunological paradox of pregnancy and hypothesized three mechanisms for the fetus to avoid recognition by the maternal immune system throughout the nine months of gestation. Firstly, that the placenta forms an anatomical barrier between the dam and fetus preventing allorecognition by the maternal immune system; secondly, that the early pregnancy is antigenically immature and undetectable by the maternal immune system; and lastly that the mother becomes immunologically inert during pregnancy (Medawar, 1953, Medawar, 1961).

Since Medawar's observations using skin grafts, it has been realized that immune cells play critical roles in various aspects of reproductive processes. Indeed, the immune system is involved whether directly or indirectly at nearly every step that is critical for reproductive success, and thus the field of reproductive immunology has expanded greatly. Central to the field of reproductive immunology is the inherent aspect that mammals have acquired a vertebrate immune system, which identifies self from non-self. While in the context of normal physiological response, this delineation is critical for detection and elimination of foreign invaders such as bacteria, viruses, or damaged cells; this characteristic of the immune system raises a unique phenomenon under the circumstances of pregnancy whereby the mother must appropriately respond to the semi-allogeneic embryo (Ott, 2020). Furthermore, the immune system is critical in regulating tissues homeostasis, hemostasis, and angiogenesis, all of which are vital for

reproductive success (Ott, 2019, 2020). The female reproductive tract is host to many immune cell types, and many hormones derived from the hypothalamic-pituitary-gonadal (HPG) axis can modulate both the innate and acquired immune systems. Thus, this section will discuss various stages of immune cell involvement in reproductive processes.

Immune Cells Involved in Reproduction, Immune System Activation, and Inflammatory Responses

The cells of the bovine immune system participate in a multitude of cellular interactions between each other and tissue cells via cell surface proteins and secreted molecules (Ott, 2019, 2020). There are populations of immune cells that have specific functions as they relate to protection of the host. Furthermore, there is integration of these different cell types in functions of the reproductive tract. The immune system contains two different arms that are delineated by their function.

The first arm, which is evolutionarily conserved in the animal kingdom, is the innate immune system. The cells of the innate immune system originate from a common myeloid progenitor, contain phagocytic capabilities, and mediate the rapid clearance of pathogens and damaged or infected cells using hydrolytic enzymes. The innate immune system utilizes mechanisms of non-specific pathogen recognition to protect against microbial infection and tissue damage. The recognition of pathogen associated molecular patterns (PAMPs), or damage associated molecular patterns (DAMPs) is mediated through pattern recognition receptors (PRRs) on the host cell. The Toll-like receptor (TLR) and Nod-like receptor families are two of the most well studied PRRs. The binding of PAMPs to their corresponding PRR is unique in that ligands common to different species of bacteria can successfully activate their corresponding receptor and

initiate a cellular response which ultimately increases the secretion of inflammatory mediators and aids in the recruitment of other professional cells of the immune system. Hallmark to an infection or tissue injury are the indications of inflammation such as redness, heat, swelling, pain, and loss of function (Sheldon et al., 2014).

Granulocytes, which includes neutrophils, basophils, and eosinophils are among the most abundant leukocyte classifications in peripheral blood. Neutrophils respond rapidly at the site of infection to clear pathogens through phagocytic enzymes and bactericidal proteins. Upon arrival and initial clearance of pathogens, neutrophils coordinate the movement of adaptive immune cells via cell signaling molecules (chemokines) to the location of pathogens for further 'education' of the adaptive immune system (see below). Cytokines are cell signaling molecules produced by immune and non-immune cells that further regulate the activation, inhibition, and cellular movement of immune cells. Monocytes circulate in the periphery until signaled into tissues where they undergo differentiation to macrophages and dendritic cells. In the bovine, there are a variety of monocytes that differ with respect to their size, granularity, nuclear morphology and function, with the largest subset of monocytes being classical monocytes (Hussen et al., 2013). Macrophages which are appropriately named "big eaters," phagocytize pathogens at the site of infection and recruit other immune cells to the site of infection. Additionally, macrophages regulate the degree of inflammation to prevent unnecessary tissue damage through the production of interleukin (IL) 10 and IL4 (Hussen and Schuberth, 2017). Dendritic cells which localize in mucosal tissues engulf particles from their surroundings and upon activation, leave the resident tissue via the lymphatic system and accumulate in the draining lymph nodes.

A key function of both macrophages and dendritic cells is their ability to present foreign antigens to thymus derived (T cells) and bone marrow derived (B cells) lymphocytes through the process of antigen presentation. The presentation of antigens to lymphocyte cells begins the incorporation of the second arm of the immune system. The lymphoid or adaptive immune system is established during fetal development and trained throughout postnatal life to allow the immune system to differentiate self from foreign antigens. The adaptive immune system is critical for the development of immune cell memory, which imbues the animal with the ability to recognize foreign pathogens following a prior exposure and elicit a rapid, robust second response to a previously encountered pathogen. The professional antigen presenting cells from the innate immune system utilize major histocompatibility complex (MHC) class II molecules to display foreign antigens for recognition by cells of the adaptive immune system. Conversely, nonimmune cells display self-antigen on their cell surface using MHC class I to regulate the activation of immune cells involved in viral infection and cell damage.

The adaptive immune system contains specialized T cells, B cells, and natural killer (NK) cells. These T, B, and NK cells are activated when presented with foreign antigen and can be directed to take on a unique phenotype that changes their response to pathogens according to the cytokine environment present at the time of activation (Lippolis, 2008). In simplistic terms, T cells can differentiate into either T helper (Th) 1, Th2, Th17, or T regulatory (Treg) cells depending on the signals present at the time of antigen presentation. Cytokine signals from macrophages, including IL10 and IL4 inhibit the development of a pro-inflammatory Th1 phenotype and promote Th2 anti-inflammatory and Treg phenotypes that regulate inflammatory responses to prevent

unnecessary tissue damage during inflammation. Activation of B cells by foreign antigens initiates proliferation and synthesis of immunoglobulins targeted to specific pathogen associated antigens which opsonize pathogens for phagocytic clearance (Prieto and Felippe, 2017).

Immune Cell Involvement in Follicle Differentiation, Ovulation, and Luteinization

Follicular development and the process of ovulation have previously been described as inflammatory events. Espey in 1980 proposed that around the time of ovulation, the ovary follows a cycle of cellular inflammation, ovulatory follicle rupture, and then tissue repair (Espey, 1980). More recently it has become clear that the process of ovulation also includes the innate immune system due to the involvement of the PRR system. Around the time of ovulation, follicles become highly vascularized, produce large amounts of prostaglandins, and synthesize a hyaluronan rich matrix similar to that observed during tissue inflammation and wound repair (Richards et al., 2008). Around the time of the luteinizing hormone (LH) surge, leukocytes rapidly invade the ovulatory follicle which was previously devoid of hematopoietic immune cells (Murdoch and Steadman, 1991, Murdoch and McCormick, 1993, Brannstrom et al., 1994, Watanabe et al., 1997, Penny et al., 1999). The infiltration of immune cells into the pre-ovulatory follicle and subsequent corpus luteum (CL) appear to follow three phases (Fair, 2015). Firstly, mast cells infiltrate the theca layer and degranulate prior to the LH surge (Nakamura et al., 1987). Secondly, an influx of eosinophilic and neutrophilic granulocytes and T-lymphocytes occurs, whereas the final stage of invasion involves the movement of phagocytic monocytes into the follicle (Murdoch and Steadman, 1991). These changes in leukocyte populations are attributed to the elevated concentrations of chemoattractants produced by the developing follicle.

These post-LH mediated changes to immune cell populations are coincident with the deterioration of the basement membrane between the theca and granulosa cells, and the secretion of granulosa cell specific acute inflammatory factors (Dieleman et al., 1983, Richards et al., 2008, Walsh et al., 2012). It has been hypothesized that the increase in follicle secretion of inflammatory signals activates the ovarian innate immune system such that various proteins and cell death signals engage TLRs and act as ‘alarmins’ to initiate physiological functions related to ovulation and luteinization. Indeed, oxidized low density lipoprotein acts as a crucial alarmin when binding to TLR4 and is critical in the pre-ovulatory inflammatory cascade (Takeda and Akira, 2005).

The corpus hemorrhagicum which arises from the collapsed post-ovulatory follicle morphologically resembles a fresh wound; however, it is a heterogenous mixture of cell types that not only includes the steroidogenic luteal cells, but also vascular endothelial cells, fibroblasts, and various types of immune cells (Abdulrahman and Fair, 2019). While the vast majority of literature pertaining to immune cell interactions with the CL are targeted at the role of immune cells in luteal regression; granulocytes, neutrophils, macrophages and eosinophils also invade the naïve CL at the time of ovulation and as vascularization progresses (Fair, 2015). It is estimated that approximately 53% of the cell populations inside the mature bovine CL are macrophages (Parry et al., 1980, O'Shea, 1987). Interestingly, when macrophages are depleted using a *Cd11b-Dtr* mouse model, corpus luteum development is altered and embryonic implantation is arrested because of reduced progesterone (Care et al., 2014). This change in luteal and steroid phenotype was directly related to increased expression of inflammation and apoptosis genes *Ptgs2* and *Hif1a,* and reduced

expression of steroidogenesis genes *Star, Cyp11a1,* and *Hsd3b1* (Care et al., 2014). This mouse model also revealed that macrophage depletion changed the luteal microvascular network due to inappropriate juxtaposition of macrophages to endothelial cells and reduced expression of vascular endothelial growth factors such as *Vegfa, Vegfb, Vegfc, and Figf* (Care et al., 2014). There is very little evidence to suggest the involvement of T lymphocytes in the repair of the ovulatory site or early luteinization in the bovine (Abdulrahman and Fair, 2019). The expression of MHC molecules on the surface of luteal cells is dynamic (Pate, 1996). Bovine luteal cells isolated from a day 6 CL express high levels of MHC class I, but expression of MHC class II is low; however, by day 10, the expression of MHC class II was approximately 80% which may suggest the critical function of interactions between immune cells and other cells within the CL (Pate, 1996).

In addition to direct cell-to-cell interactions, immune and luteal cells communicate using secreted molecules (Pate, 1996). Localized macrophages provide sources of both tumor necrosis factor (TNF) and tumor necrosis factor receptor (TNFR) to the corpus luteum (Fair, 2015). The actions of TNF on the lifespan of the CL are conflicted within the literature. Some reports conclude that TNF acts to stimulate the secretion of various prostaglandins (PG) such as PGF2α, PGE2, and PG12 and that secretion of PGE2 regulates the luteotropic vascularization of the CL (Okuda et al., 1999, Fair, 2015). However, other reports have demonstrated that concentrations of TNF and interferon (IFN) γ are greater in the regressing CL compared to the other stages of the estrous cycle as indicated by consistent levels of IFNγ mRNA throughout the estrous cycle (Townson and Pate, 1996). Cultured bovine luteal cells treated with IFNγ or TNF inhibit

LH-stimulated progesterone production, increase prostaglandin synthesis, upregulate MHC class I and II, and initiate cell death, suggesting a role for TNF in luteal regression (Fairchild and Pate, 1989, Pate et al., 2010). Other cytokines produced by immune cells or luteal cells that are implicated in CL function include IL1α, IL1β, IL6, transforming growth factor beta 1 (TGFB1), macrophage migration inhibitory factor, and osteopontin (Pate et al., 2010).

Immune regulation is critical for the complete regression of the CL, which must occur if no pregnancy is recognized by the maternal system to allow for new follicular development to occur. Luteolysis is characterized by apoptosis of luteal cells and vascular regression of endothelial cells, triggered by increased signaling of uterine PGF2α (Abdulrahman and Fair, 2019). The corpus luteum acutely responds to the direct effects of PGF2α by decreasing progesterone secretion and inhibiting the mRNA expression of *STAR* and *HSD3B1* which are critical to produce progesterone (Tsai and Wiltbank, 1998, Atli et al., 2018). The actions of PGF2α also target endothelial cells to induce angiolysis and vasoconstriction, thus reducing the amount of oxygen and nutrients available to the CL (Abdulrahman and Fair, 2019). In cattle, T-lymphocytes rapidly increase just prior to the onset of luteolysis with 45% being $CD8^+$ cytotoxic T-cells, 25% $CD4^+$ T helper cells, and 30% gamma delta ($\gamma\delta^+$) T cells (Penny et al., 1999, Cannon et al., 2003, Poole and Pate, 2012). As luteal regression progresses, progesterone concentrations decrease resulting in macrophage and T-cell activation causing an increased production of TNF and IFN, which likely regulate apoptosis and ovarian tissue remodeling (Fair, 2015). Treatment of porcine luteal cells with IL6

drastically reduced progesterone synthesis and the expression of *IL6* mRNA was increased in regressing CL compared to the functional CL (Okuda et al., 1999).

Maternal Recognition of Pregnancy

The implications of Medawar's early work are that inappropriate immune dialogue or immune incompatibility between the conceptus and the endometrium may lead to rejection of the conceptus and pregnancy failure; however, the complete absence of dialogue does not permit for maternal recognition of pregnancy which must occur to support the pregnancy throughout gestation. The phrase, "maternal recognition of pregnancy," is attributed to Roger V. Short (Short, 1969). The notion of maternal recognition of pregnancy stimulated thoughts about how the embryo of early pregnancy was capable of signaling to the mother to ensure maintenance of the corpus luteum beyond the normal length of the estrous or menstrual cycle (Geisert et al., 2015).

The fundamental principle of maternal recognition of pregnancy is that the conceptus must block the luteolytic cascade that normally occurs and allow for a return to cyclicity and another attempt at pregnancy. The original evidence from Rowson and Moor in 1967 that the conceptus secreted a substance that could block luteolysis was produced following daily intrauterine infusion of day 14 or 15 ovine embryo homogenate. Infusion of embryo homogenate could prevent luteolysis and extended the life of the CL by 25 days (Rowson and Moor, 1967). Following this discovery, it was determined that the embryo derived signal that blocked luteolysis was inactivated by heat and proteases, and later named trophoblastin (Martal et al., 1979). Around the same time, an experiment collected sheep conceptuses and cultured them with radiolabeled amino acids and assayed the conditioned medium via gel filtration chromatography to detect proteins synthesized de novo by the conceptus (Wilson et al.,

1979). The results from this experiment discovered a low-molecular weight radiolabeled protein named ovine trophoblast protein one (oPT-1) (Wilson et al., 1979, Godkin et al., 1982). A series of later experiments, again in sheep, determined that both trophoblastin and oPT-1 were the same molecule and corresponded with embryo gene expression that occurred at the same time as attachment of the trophectoderm to the luminal epithelium (Ashworth and Bazer, 1989). Cloning and sequencing experiments of the oTP-1 gene revealed that it was a member of the Type I IFN alpha family of proteins, named IFN-tau (IFNT) which has been shown to be the pregnancy recognition factor in ruminants (Imakawa et al., 1987, Stewart et al., 1987).

The embryonic trophoblast secretes IFNT beginning at the blastocyst stage and continues to increase synthesis with conceptus elongation (Garrett et al., 1988, Roberts et al., 1993, Mann et al., 2006). The secretion of IFNT from the conceptus peaks just prior to attachment to the uterine epithelium and diminishes thereafter (Bartol et al., 1985, Roberts et al., 1993). The discovery that the pregnancy recognition factor in ruminants was an interferon was surprising given that members of this cytokine family serve as antiviral cytokines (Mathew et al., 2022). Interestingly, at least one or more insertion and rearrangement events have occurred within the *IFNT* promoter and enhancer elements which replace the pathogen signal recognition sites with trophectoderm-specific DNA elements that are exclusive to the trophectoderm layer of the conceptus (Ealy and Wooldridge, 2017). Furthermore, conceptus derived signals begin to drive immune responses towards tolerance and facilitate the endometrial immune cell secretion of cytokines that promote placental growth representing a shift in the Th1-Th2 balance (Wegmann et al., 1993, Oliveira et al., 2013). For example, there

are marked increases in the populations of NK cells, macrophages, and dendritic cells during early pregnancy in dairy heifers (Oliveira and Hansen, 2009, Kamat et al., 2016, Vasudevan et al., 2017). In addition to the changes to endometrial immune cell populations as identified by flow cytometry, there are consistent upregulation of genes related to immune function identified in the transcriptome of the endometrium during early pregnancy that are likely in response to maternal recognition of pregnancy (Gray et al., 2006, Bauersachs et al., 2009, Cerri et al., 2012, Mathew et al., 2019, Dickson et al., 2022a).

The actions of IFNT during pregnancy on the endometrium as an agent to prevent luteolysis are mediated through the binding of IFNT to the IFN receptor to prevent pulsatile release of PGF2α from the epithelium of the endometrium. Under cyclic, non-pregnant conditions, the endometrial luminal epithelium responds to circulating oxytocin via the oxytocin receptor and secretes pulses of PGF2α that initiates CL regression (Lamming et al., 1995, Wathes and Lamming, 1995). However, when a cow is pregnant, IFNT prevents the upregulation of the oxytocin receptor preventing the oxytocin induced secretion of PGF2α. In addition to the gene regulatory effects relating to CL maintenance, IFNT can stimulate the expression of IFN-stimulated genes (ISGs) in various cells. The detection of ISGs in peripheral blood mononuclear cells during pregnancy indicates that there are systemic effects of pregnancy on the circulating immune system.

Influences of Environmental Stressors on Fertility

A wide spectrum of stressors not directly involved with the reproductive tract can influence fertility. Stressors such as infections and inflammation both within the reproductive tract such as metritis (to be discussed later) and distant from the

reproductive tract (mastitis and laminitis), heat stress, metabolic disorders, and genetics can negatively impact reproductive outcomes. Indeed, fertility decreases, and pregnancy loss increases in cows diagnosed with one or more diseases within 60 days postpartum (Santos et al., 2011).

Inflammation outside the reproductive tract, such as mastitis is associated with reductions in fertility. Mastitis is an infection of the mammary gland typically by bacteria that results in clinical symptoms such as decreased milk production, increased abundance of leukocytes in milk, increased body temperature, and red, warm, swollen mammary quarters (Hansen et al., 2004). Mastitis between artificial insemination and the time of pregnancy diagnosis has been associated with increased days to first service, days open, and services per conception (Schrick et al., 2001). Similarly, mastitis prior to AI is associated with increased services per conception when compared to cows without mastitis or with mastitis diagnosed after AI (Schrick et al., 2001). Experimental evidence in sheep has demonstrated that immune activation resulting from immunization to bacterial components associated with mastitis reduces pregnancy rate (Holásková et al., 2004). Ewes were allocated to receive one of four treatments: immunization with bacterial components, immunization with heat killed bacteria, or no immunization controls. All ewes had estrous cycles synchronized and submitted to breeding with fertile rams. On day 5 after breeding, all immunized ewes, and half of the control ewes were intravenously challenged with bacterial components and pregnancy was assessed 42 days after breeding. Ewes receiving only the challenge after breeding experienced an 8% reduction in pregnancy rate compared to control; however, when ewes were immunized prior to bacterial component challenge, pregnancy rates were

reduced by 17% and 26% for ewes immunized with heat killed cells and bacterial components, respectively (Holásková et al., 2004). These data indicate that pregnancy outcomes are negatively related to repeated challenge of bacterial components associated with mastitis. Furthermore, the ovarian reserve appears to be sensitive to mastitis infections. For example, oocytes collected from cows with naturally occurring mastitis and submitted to in vitro fertilization (IVF) had reduced blastocyst formation compared to cows without mastitis (Roth et al., 2013). This observation was supported by experimental evidence which demonstrated that oocytes derived from cows that received either an intramammary infusion of Gram-negative endotoxin or Gram-positive toxin had reduced cleavage and blastocyst formation compared to healthy controls (Asaf et al., 2014). Furthermore, the blastocysts derived from Gram-positive challenged cows had increased apoptosis and *PTGS2* expression compared to controls (Asaf et al., 2014). Proposed mechanisms facilitating mastitis driven subfertility include hyperthermia disrupting oocyte maturation and embryonic development, alterations in uterine function because of divergent cytokine secretion, and impairment of the HPG axis (Hansen et al., 2004).

Another environmental stressor influencing reproductive efficiency in cattle is thermal stress. Global surface temperatures have risen approximately 0.2ºC per decade over the last 30 years (Hansen et al., 2006). The temperature humidity index (THI) is widely used to assess the magnitude of heat stress on animal performance. This index accounts for both environmental temperature and relative humidity. Most mammals have body temperatures between 35 and 39ºC and are maintained within a narrow range above environmental temperatures by generating and dissipating metabolic heat

(Takahashi, 2012). Alterations in environmental conditions can upset the balance that regulates body temperature (Takahashi, 2012). As such, THI above 68 can result in physiological signs of mild heat stress in lactating dairy cows (Zimbelman et al., 2009). Further elevation of THI causes increased body temperature, reduced milk production, decreased growth and impaired fertility in cattle and negatively affects both sexes (Takahashi, 2012). Cows experiencing thermal stress in hotter months have increased pregnancy loss and require more services per conception compared to cooler cows in months of lower temperature and humidity (Badinga et al., 1985).

Many proposed mechanisms of thermal stress mediated reproductive failure have been investigated. In dairy cows, heat stress affects endocrine function, oocyte maturation, embryonic development and the interaction between the conceptus and uterus. It has been demonstrated that heat stress reduces the duration and intensity of estrus as well as the number of mounting events (Gwazdauskas et al., 1981, Pennington et al., 1985, Younas et al., 1993). Indeed, it has been demonstrated that Holstein cows exposed to heat stress during estrous synchronization have reduced follicular diameter and follicular fluid volume compared to cows provided shade (Badinga et al., 1993). In a different study, cows provided with shade during hotter months display altered follicular development and dominance during periods of heat stress compared to cooler months (Badinga et al., 1994). Elevated ambient temperatures decrease the number and developmental competence of oocytes following IVF in dairy cows, suggesting that heat stress is negatively impacting ovarian and oocyte function (Hansen et al., 2001, Roth, 2008). While exposure of GV stage oocytes to hyperthermic conditions of 41ºC did not impair GV breakdown; this heat

stress reduces progression to MII and blastocyst development (Payton et al., 2004). Furthermore, heat stress exposure between estrus and insemination disrupts embryonic development that culminates in an increased proportion of abnormal embryos (Ealy et al., 1993). When conceptuses were isolated from the uterus of cows exposed to hyperthermic conditions conceptus weight is decreased (Biggers et al., 1987, Geisert et al., 1988). Additionally, maternal hypothermia alters uterine protein abundance and results in increased synthesis of trophoblastic proteins, indicating that heat stress during the earliest phases of gestation may alter the growth and secretory activity of the conceptus and contribute to reduced fertility (Geisert et al., 1988). In males heat stress also results in deleterious effects on fertility. In mammals, the testes are suspended within the scrotum outside the body and maintained between 2 and 8ºC below core body temperature. This reduced temperature is essential for normal spermatogenesis. In bulls, testicular hyperthermia of 40ºC for 12 hours resulted in detrimental effects to testicular function and spermatogenesis (Skinner and Louw, 1966). These thermal effects on the testes translate directly to reduced semen quality during the summer months (Meyerhoeffer et al., 1985). Thus, thermal stress affects both female and male reproductive outcomes through various mechanisms and can negatively contribute to the likelihood of reproductive success in cattle.

Nutrition, metabolic status, and reproductive outcomes are intimately related in mammals. The influence of nutrition on fertility can be either direct or indirect (Robinson et al., 2006). The direct effects of nutrition on reproduction are attributed to the abundance of specific nutrients essential for oocyte and spermatozoa development, ovulation, fertilization, embryonic development, and establishment and maintenance of

pregnancy (Robinson et al., 2006). Indirectly, nutrition impacts the circulating concentrations of hormones and nutrient sensitive-metabolites required for success in various reproductive tissues (Robinson et al., 2006). Furthermore, nutritional status significantly influences the timing of puberty attainment in heifers (Amstalden et al., 2014). The current understanding for puberty attainment involves a marked increase in high-frequency releases of gonadotrophin releasing hormone (GnRH) and subsequent LH pulses (Day et al., 1984). For this to occur, a shift in the balance of signals regulating GnRH secretion must occur whereby the excitatory signals stimulating GnRH secretion must exceed the inhibitory inputs that decrease pulsatility (Amstalden et al., 2014). Nutrition influences the neuronal signaling within the hypothalamus via estradiol-receptive neurons that directly regulate the secretory activity of GnRH neurons (Amstalden et al., 2014). Different nutritional statuses result in the secretion of orexigenic peptide, neuropeptide Y and anorexigenic peptide derived from proopiomelanocortin, melanocyte-stimulating hormone α (Amstalden et al., 2014). These peptides are believed to be the major afferent pathways that transmit nutritional signals to GnRH neurons within the hypothalamus (Amstalden et al., 2014). Indeed, the effects of nutrition on the HPG axis are critical in the attainment of sexual maturity; however, the effects of nutrition also extend beyond sexual maturity to directly influence ovarian function and oocyte competence.

High-yielding dairy cows experience an excessive negative energy balance during early lactation to maintain milk production which coincides with a critical window of development of oocytes required to establish the subsequent pregnancy (Robinson et al., 2006). In lactating cows, most of the glucose being produced by the liver is utilized

for the synthesis of lactose to support milk production resulting in a transient insulin resistance during the early postpartum period (Ebner, 1978). The follicle containing the oocyte is not exempt from the effects of postpartum nutritional challenges. It has been demonstrated that follicular fluid composition is associated with nutritional changes in serum concentrations of metabolites that reflect the energy, protein, and mineral status of the cow (Leroy et al., 2004). Glucose is essential for adequate maturation of the oocyte, cumulus cell expansion, embryo cleavage, and subsequent blastocyst development (Bisinotto et al., 2018). Experiments that matured bovine oocytes in glucose concentrations comparable with follicular fluid concentrations observed in cows experiencing ketosis resulted in reduced cleavage and proportion of embryos developing to the blastocyst stage (Leroy et al., 2006). Additionally, during the postpartum period high-yielding dairy cows experience an extensive mobilization of fat that culminates in the release of high amounts of non-esterified fatty acids (NEFA) into the blood (Bisinotto et al., 2018). The concentrations of NEFA in follicular fluid are comparable to those detected in serum (Leroy et al., 2005). Furthermore, maturation of oocytes in the presence of palmitic and stearic acids resulted in increased apoptosis and necrosis of cumulus cells, reduced fertilization, decreased zygotic cleavage and blastocyst formation (Leroy et al., 2005). Thus, it is suggested that the oocyte is vulnerable to changes in the biochemical composition of the follicular microenvironment which may contribute to diminished embryonic development and overall reductions in fertility of dairy cows experiencing metabolic stress.

Nutrition is also critical for male fertility. Like the female, metabolic hormones play integral roles in sexual development of the bull and are crucial in stimulating GnRH

pulsatility (Kenny and Byrne, 2018). Feeding young bulls a high-energy diet beginning at 8 weeks of age for approximately 6 months was sufficient to increase LH secretion, peripheral testosterone concentrations, testicular size and epididymal weight when compared to controls (Harstine et al., 2015). In another study, dairy bulls were fed a high, medium or low nutrition diets based on energy and protein levels until 31 weeks of age at which point they all were fed a medium-nutrition diet until 72 weeks of age (Dance et al., 2015). The authors discovered that bulls fed a high nutrition diet were younger at puberty and had larger testes throughout the entire experimental period when compared to bulls fed a low nutrition diet. It was also revealed that bulls fed a high nutrition diet had a more substantial early rise in LH and had elevated concentrations of insulin-like growth factor 1 (IGF-1) when compared to bulls fed the low nutrition diet, suggesting that IGF-1 has a role in regulating early gonadotropin rise and reproductive development (Dance et al., 2015). Thus, early life dietary availability and nutritional status can potentially modulate future reproductive success of bulls.

Spermatogenesis in the bull is approximately 54 days (Saunders, 2003, Staub and Johnson, 2018) and is susceptible to the influences of nutrition (Robinson et al., 2006). Under-nutrition of bulls results in reduced sperm motility, increased morphological defects, altered spermatogenesis and ultimately reduced fertility (Harrison et al., 2022). As previously discussed, the testes must be maintained 2 to 8ºC cooler than core body temperature for normal spermatogenesis to occur. Experiments that fed elevated levels of dietary energy resulted in increased scrotal fatness and concurrent increases in scrotal temperature (Coulter et al., 1997). Bulls fed a higher energy level had decreased percentages of morphologically normal and progressively

linear motile sperm when compared to control bulls, indicating that dietary driven thermal dysregulation of the testes can affect semen quality (Coulter et al., 1997). There is also evidence that accelerated early life nutrition can alter sperm DNA methylation post-puberty (Perrier et al., 2020). Male Holstein-Friesian calves were assigned to a high or moderate plane of nutrition for the first 24 weeks of age and then all bulls were assigned to a moderate dietary inclusion until puberty. Ejaculates collected at 15 and 16 months of age were submitted to reduced representation bisulfite sequencing to ascertain the methylation status of spermatozoa. The authors revealed that there were 580 differentially methylated CpGs between the high and moderate fed bulls with the high fed bulls having hypermethylation in endogenous retrotransposons, introns, and intergenic regions (Perrier et al., 2020). The authors also determined that genes involved in spermatogenesis, Sertoli cell function, and the HPG axis were differentially methylated in ejaculates collected at 15 months of age, reflective of the earlier time of puberty onset in the high fed bulls (Perrier et al., 2020). In mice, dietary induced obesity alters sperm cell chromatin configuration, increases reactive oxygen species, and alters the epigenome (Houfflyn et al., 2017). Furthermore, embryos sired by dietary-induced obese mice have reduced cleavage rates, development to the eight-cell stage, blastocyst formation, and pregnancy rates compared to embryos sired by mice fed a control diet (Ghanayem et al., 2010, Mitchell et al., 2011).

The genetic composition of animals also plays a key role in the likelihood of reproductive success and overall breed fertility. Prior to incorporation of fertility traits into dairy cattle selection indices, breeding strategies focused heavily on production traits which ultimately resulted in declines of reproductive performance (Hansen et al.,

1983, Ma et al., 2019). Fertility traits generally have low heritability, but there is a clear antagonistic relationship between highly heritable milk production and fertility traits (Hansen et al., 1983, Peñagaricano and Khatib, 2012). Fertility traits are often difficult to measure accurately because they are greatly affected by management decisions on farm that are highly correlated with conception and pregnancy rates (Ma et al., 2019). Genomic evaluations coupled with genome wide association studies have revealed vast genomic regions of diverse traits that present candidate genes to improve fertility (Ma et al., 2019). Indeed, when eight genome wide association studies comparing fertility traits were compiled together it was revealed that a quantitative trait locus on chromosome 18 is significantly associated with fertility traits such as conception to calving, calving ease, and direct calf survival (Ma et al., 2019). Additionally, genome wide association studies have made associations between sire conception rate and single nucleotide polymorphisms that are positively linked with bull fertility (Peñagaricano et al., 2012). While genome wide association studies for fertility traits tend to be underpowered, the available data and studies have allowed for the association of specific loci to fertility traits for future investigation with the aims of improving fertility.

In conclusion, many stressors in both males and females can affect fertility. Although many stressors in the context of cattle have been explored, others require further investigation to determine mechanisms of action. Indeed, one of the stressors which requires further investigation are the mechanisms leading to reduced fertility following uterine infection.

Uterine Disease in Dairy Cattle

Definitions and Causes of Uterine Disease in Dairy Cattle

While various stressors distant to the reproductive tract can negatively impact the likelihood of pregnancy success, pathologies within the reproductive tract also impact fertility. After calving the bovine uterus is highly susceptible to exposure to bacteria and the risk of uterine diseases is elevated during the transition period. There is inconsistency amongst researchers, veterinarians, farmers, and within the literature pertaining to the definitions of uterine infection, disease, and bacterial driven uterine inflammation in cattle (Sheldon et al., 2009; Lima, 2020). Microbial infiltration of the postpartum uterus is ubiquitous (Sheldon and Dobson, 2004). Parturition results in the female reproductive tract being exposed to the environment such that up to 90% of postpartum dairy cows have bacteria in the upper reproductive tract (Elliott et al., 1968; Griffin et al., 1974; Sheldon et al., 2002). Inflammation of the postpartum uterus is normal and critical for tissue involution and repair. However, the regulation of inflammation is important in maintaining the balance between repair and diseased states (Kelly et al., 2019; Sheldon et al., 2019; LeBlanc, 2023). Despite uterine infiltration of bacteria in most cows following parturition, only a subset of cows will go on to develop infections of the uterus.

The vast majority of uterine diseases following parturition are as a result of bacterial infections. Two of the most frequent bacterial species associated with uterine disease are Gram-negative *Escherichia coli* and Gram-positive *Trueperella pyogenes* while *Streptococcus* spp., *Staphylococcus* spp., and *Bacillus* spp. are also consistently identified from the uterus of healthy cows (Sheldon et al., 2009; Hertl et al., 2010; Gilbert and Santos, 2016, Galvão et al., 2019). A major limitation of these culture-

dependent studies is highlighted by the fact that many bacterial species do not propagate in culture (Galvão et al., 2019). In 2010 the reliance on culture-dependent species determination was replaced with PCR to explore the microbiome and revealed that *E. coli* infection predisposed cows to further infection with *Fusobacterium necrophorum* and *T. pyogenes*, which drastically increased the risk of development of uterine disease (Galvão et al., 2019). The characterization of the uterine microbiome using metagenomic sequencing has revealed that other bacterial species that were previously unidentified because of the inherent difficulty with bacterial culturing are associated with the development of uterine disease, including *Bacteroides pyogenes, Porphyromonas levii,* and *Helcococcus ovis* (Galvão et al., 2019).

Uterine diseases are clinically defined as puerperal metritis, clinical endometritis, subclinical endometritis, and pyometra (Sheldon et al., 2006). The prevalence of uterine diseases in the postpartum period is between 20-40% for metritis, 15-30% for clinical endometritis, and approximately 30% for subclinical endometritis (Sheldon and Dobson, 2004, Sheldon et al., 2006, LeBlanc, 2008, Sheldon et al., 2009, Pinedo et al., 2020). Uterine diseases in the postpartum period are characterized both by the presentation of symptoms and according to the time postpartum that symptoms arise (Sheldon et al., 2006). Puerperal metritis is a severe infection of the uterus that affects all layers of tissue and is diagnosed within the first 7 to 21 days postpartum (Sheldon and Dobson, 2004, Sheldon et al., 2006, LeBlanc, 2008). Metritis is characterized by enlargement of the uterus with a watery, necrotic fluid and is often accompanied with putrid discharge, fever, and other systemic symptoms such as depressed appetite and milk production (Paisley et al., 1986, Sheldon and Dobson, 2004, Földi et al., 2006, Sheldon et al.,

2006). Damage to the uterus caused by dystocia, retained fetal membranes, twinning, and the presence of a dead calf increase the likelihood of metritis (Opsomer et al., 2000, Kim and Kang, 2003, LeBlanc, 2008, Sheldon et al., 2009, Potter et al., 2010). Despite the similarities in color of vaginal discharge, metritis is distinct from uterine lochia, the latter being the typical discharge, which is normal during the process of uterine involution (LeBlanc, 2008). Metritis is estimated to cost between $240 and $884 per case and results in projected reductions of $900 million a year in profitability for U.S. dairy producers attributed primarily to treatment costs, reproductive failure, and replacement animals (Pérez-Báez et al., 2021).

While less severe with respect to immediate mortality risk, endometritis poses different challenges. Endometritis is detected after 2 to 8 weeks postpartum and is identified by the presence of viscous white or off-white mucopurulent vaginal discharge (Sheldon et al., 2006, LeBlanc, 2008). Histologically, endometritis affects fewer layers of the uterine wall than metritis but is evident by the disruption of the endometrial epithelium, infiltration of immune cells, accumulation of lymphocytes, and stromal edema (Bonnett et al., 1993, Bondurant, 1999, LeBlanc, 2008). Dystocia, twins, retained placenta, or previous diagnosis of metritis increase the likelihood that a cow will be diagnosed with clinical endometritis (LeBlanc et al., 2002, LeBlanc, 2008). Additionally, subclinical endometritis is characterized by chronic inflammation of the endometrium without clinical signs of disease. The detection of subclinical endometritis is determined by endometrial cytology (Sheldon et al., 2006). While the classification of subclinical endometritis varies in the literature, the presence of ≥ 18% neutrophils between 20-33

days postpartum or ≥ 10% neutrophils between 34-47 days postpartum is considered symptomatic of subclinical endometritis (Kasimanickam et al., 2004).

Treatment and Prevention of Uterine Infections in Dairy Cattle

The primary objectives for treating uterine diseases are improving cow health and welfare and maintaining reproductive performance after disease resolution. While the self-cure rate of uterine disease can be as high as 77%, it is understood that treatment should be administered to mitigate negative impacts on cow welfare and other cow performance parameters (LeBlanc, 2008). Furthermore, the results and interpretation of clinical intervention can depend on how animals are diagnosed and the definition of cure or recovery (Steffan et al., 1984, Knutti et al., 2000, Dhaliwal et al., 2001, LeBlanc et al., 2002, Chenault et al., 2004). Treatment of uterine disease has traditionally included antimicrobials in response to diagnosis and the United States currently only has three approved antibiotics for the treatment of uterine diseases. Ceftiofur crystalline-free acid (Excede, Zoetis), ceftiofur hydrochloride (Excenel, Zoetis), and oxytetracyclines (Liquamycin LA-200, Zoetis) are the only approved antimicrobials for the treatment of uterine disease in the United States; however, their efficacy in maintaining fertility after disease resolution is unclear. Alternative treatment strategies have been investigated in response to the growing threat of antimicrobial resistance ultimately intending to reduce the amount of antimicrobials used to dairy cows (Lima, 2020). These therapies have been utilized to try and reduce the proliferation of bacteria within the uterus or improve the ability of the uterus to immunomodulate against pathogens. Thus, these therapies have been described for the treatment or prevention of metritis, clinical endometritis, and subclinical endometritis (Lima, 2020).

One of the earliest treatment alternatives of uterine disease was to utilize PGF2α analogues. The use of prostaglandins to treat endometritis yields contradictory results (Haimerl et al., 2018). A large experimental study conducted in north central Florida sought to use PGF2α as a therapy to reduce the prevalence of subclinical endometritis and improve pregnancy per artificial insemination (Lima et al., 2013). Cows were enrolled at 25 ± 3 days in milk and were randomly allocated to remain as untreated controls or receive either a single dose of PGF2α at 39 ± 3 or two doses of PGF2α at 25 ± 3 days in milk and 39 ± 3 days in milk followed by synchronization and insemination at 75 ± 3 days in milk. There was a 6.8% reduction in the prevalence of subclinical endometritis at 32 ± 3 days in milk when cows received two doses of PGF2α; however, the effect disappeared at 46 ± 3 days in milk and 14% of the cows still had subclinical endometritis. There was no effect of one or two treatments of PGF2α on pregnancy per AI or the incidence of pregnancy loss between 32 and 60 days of gestation, indicating that PGF2α was unable to improve uterine health, pregnancy per artificial insemination, or pregnancy loss (Lima et al., 2013). Furthermore, data from a meta-analysis investigating the efficacy of treatment for endometritis with PGF2α as measured by the calving to first service interval and calving to conception interval found that there were no effects of PGF2α on either response (Haimerl et al., 2018).

Other alternative strategies to antibiotics were to investigate the possible utility of intrauterine infusions of various compounds such as chitosan microparticles, essential oils, bacteriophage cocktails, or ozone (Lima, 2020). Chitosan microparticles synthesized from chitin are a linear polysaccharide that have a broad-spectrum of antimicrobial activity (Jeon et al., 2014). When infused at the day of calving to prevent

metritis, cows that received chitosan microparticles had reduced incidence of metritis 7 days postpartum compared to control cows; however, there was no differences in the rate of metritis at 4, 10, or 14 days postpartum (Daetz et al., 2016). Chitosan microparticles have also been studied to aid in the cure of metritis. When chitosan microparticles were infused at the time of metritis diagnosis and compared to cows who received an infusion of ceftiofur crystalline-free acid or untreated control; surprisingly, cows that received the microparticle infusion had impaired milk yield, reduced survival and fertility compared to untreated controls (de Oliveira et al., 2020). One study compared the ability of an organic essential oil containing carvacrol, which is a monoterpenic phenol produced by aromatic plants such as oregano, with an intrauterine infusion of iodine povidone to cure metritis (Pinedo et al., 2015). The results from this study indicated that cows treated with the essential oil had a reduced incidence of metritis both 6 and 14 days after the first treatment and an increased odds of pregnancy at the time of AI, 150 days, and 300 days postpartum compared to cows treated with iodine povidone (Pinedo et al., 2015).

Furthermore, ozone has been explored as a possible treatment of subclinical endometritis because ozone inhibits infectious organisms and limits anti-inflammatory responses by inhibiting proinflammatory cytokines via the stimulation of immunosuppressive cytokines IL10 and TNFB1 (Lima, 2020). A small study sought to explore the effects of ozone infusion on the incidence of subclinical endometritis and compared the infusion group with untreated controls (Escandón et al., 2020). The results indicated that ozone infusion reduced the incidence of subclinical endometritis by 10-fold and increased the first service conception rate by 33.8 percent. The results

from this study, however, likely need to be replicated because the researchers only included 40 cows per treatment group. Lastly, other strategies targeted at uterine immunomodulation to cure endometritis include intrauterine infusion of lipopolysaccharide (LPS) or IL8. In a large experiment which infused either saline or one of two doses of LPS into the uterus of lactating cows 35 ± 6 days postpartum found that the intrauterine treatment of 150 μg of LPS improved the likelihood of pregnancy compared to cows treated with saline; however, pregnancy rates were not restored to levels comparable to cows without endometritis (Moraes et al., 2017). Furthermore, infusion with recombinant bovine IL8 reduced the incidence of puerperal metritis in multiparous cows (Zinicola et al., 2019).

Another proposed preventative for metritis was to utilize vaccinations against metritis pathogens (Machado et al., 2014, Freick et al., 2017, Meira Jr et al., 2020). One study utilized a vaccine administered either intravaginally or subcutaneously that contained different combinations of major virulence factors such as *fimH, IktA,* or *Plo* and/or whole inactivate *E. coli, F. necrophorum* and *T. pyogenes* that are representative of some of the bacteria known to cause metritis (Machado et al., 2014). In this study, three different formulations of vaccine were utilized and were administered 60 days before expected calving with a booster 30 days following the initial dose of vaccine. Subcutaneous vaccination resulted in an effective immunization strategy as measured by serological IgG concentrations. The vaccine formulation that contained both virulence factors and whole inactivated cells had the greatest effect by reducing metritis incidence by 16.5% compared to unvaccinated cows (Machado et al., 2014). Another study which sought to develop a herd-specific vaccine containing inactivated *T.*

pyogenes, E. coli, S. uberis, Bacteroides, and *Peptostreptococcus* species obtained from metritis cows (Freick et al., 2017). This study, which vaccinated late gestation heifers six weeks prior to calving with a booster three weeks later, failed to reduce the incidence of metritis following parturition compared to unvaccinated heifers (Freick et al., 2017). A third clinical trial randomized and immunized heifers with a subcutaneous injection of either control aluminum hydroxide, inactivated bacteria and bacterial subunits, inactivated bacteria, or bacterial subunits at 240 ± 3 days of gestation (Meira Jr et al., 2020). Immunization reduced the incidence of puerperal metritis by 5.8 percent, reduced the total vaginal bacterial load of *F. necrophorum* at 9 days postpartum and increased reproductive performance compared to control. In conclusion, the use of vaccines to reduce the incidence of metritis after calving is reported to have mixed effects, therefore, further research optimizing the virulence factor and timing of vaccination are required to improve efficacy.

Pathogenesis and Pathophysiology of Uterine Disease Associated Infertility in Dairy Cows

The pathogenesis and pathophysiology of uterine disease is multifaceted. Despite the creativity and innovation that has been developed to treat both disease and the underlying inflammation or use of antimicrobials, fertility in cows with uterine disease remains lower compared to their disease-free counterparts. Indeed, it has been well characterized from multiple large, multisite studies that uterine diseases is associated with reduced pregnancy rates, increased pregnancy loss, and increased time to conception (Borsberry and Dobson, 1989, Ribeiro et al., 2016, Pinedo et al., 2017, Carvalho et al., 2019, Merenda et al., 2021, Pérez-Báez et al., 2021). Thus, it becomes plausible that uterine disease and pathogenic components of bacteria that cause

inflammation lead to disruption of many cellular and molecular compartments of the reproductive and fertility cycle, representing potential targets for improving disease induced subfertility. While the causes of disease associated subfertility are not known they likely include effects on the endometrium, ovary and HPG axis (**Figure 1-1**). This section will highlight the molecular, cellular, and physiological responses caused by uterine diseases in the female reproductive tract of dairy cattle. A conceptual model of the cellular and molecular effects of uterine infection and bacterial components on female reproductive physiology are presented in Figure 1-1.

Molecular and Cellular Response to Uterine Infection in the Endometrium

Parturition leads to severe disruption of the protective endometrial epithelial barrier and the dilation of the cervix that permits bacteria to gain access to the uterine environment. Ultimately this results in the reproductive tract experiencing significant inflammation and damage following infection by pathogenic bacteria (Herath et al., 2009, Chapwanya et al., 2012, Bromfield et al., 2015). Many cell types, including endometrial epithelial and stromal cells and hematopoietic immune cells rapidly respond to conserved PAMPs by increasing secretions of PGE2, IL1, IL6 and IL8, promoting cellular inflammation (Herath et al., 2006, Davies et al., 2008, Cronin et al., 2012, Turner et al., 2014). Amos and colleagues demonstrated that endometrial cells are uniquely susceptible to damage by pyolysin, the from pore-forming toxin produced by *T. pyogenes* (Amos et al., 2014). Indeed, there are clear consequences of uterine disease on endometrial function. In 2016 an experiment in north-central Florida characterized adverse postpartum health events within the first 42 days after calving from more than 5,000 cows and assessed the pregnancy outcomes following the first service (Ribeiro et al., 2016). This study revealed that regardless of whether or not a cow received artificial

insemination or an embryo transfer from a healthy donor, the frequency of pregnancy at day 45 and calving was reduced if animals were diagnosed with metritis or retained placenta (Ribeiro et al., 2016). Furthermore, day 15 and 16 conceptuses were smaller and produced less IFNT in cows that previously had uterine disease compared to cows without disease (Ribeiro et al., 2016). The authors suggest that the inability of embryo transfer to rescue pregnancy rates is indicative of compromised uterine function because embryo transfer bypasses potential fertilization errors and early embryonic mortality and is reflective of the ineptitude of the uterus to potentiate pregnancy.

Several studies have also investigated changes to the molecular signature of the endometrium in response to uterine infections. Microarray analysis of cows with clinical and subclinical endometritis 50 days postpartum revealed that despite the resolution of disease, pathways related to the immune system, cell adhesion, apoptosis, cell signaling, and chemotaxis were altered compared to healthy animals (Salilew-Wondim et al., 2016). The miRNA profiles are also altered in cows with endometritis (Salilew-Wondim et al., 2016). Interestingly, subclinical endometritis affects the transcriptome profiles of different portions of the endometrial glands, lumen, and stroma of dairy cows (Pereira et al., 2022). The infusion of *E. coli* and *T. pyogenes* into the uterus of virgin heifers resulted in changes to the transcriptome of the caruncular endometrium, intercaruncular endometrium, isthmus and ampulla of the oviduct three months after the infusion of bacteria (Horlock et al., 2020). The top canonical pathways altered in caruncular and intercaruncular endometrium following bacterial infusion were related to cellular development, cell growth and proliferation and hematological system development and function (Horlock et al., 2020). Dickson and colleagues also showed

that the endometrial response to pregnancy in cows that were previously exposed to bacterial infusion altered the expression of genes related to iNOS, TLR, and IL7 signaling pathways (Dickson et al., 2022a). Additionally, the infusion of *E. coli* and *T. pyogenes* in lactating cows altered the metabolomic composition of histotroph such that pathways linked to phospholipid synthesis, cellular energy production, and the Warburg effect were dysregulated(Husnain et al., 2023). Strong evidence suggests that the endometrium is affected both short and long-term following uterine disease and these changes to molecular function may be associated with subfertility following disease resolution (**Figure 1-1**).

Hypothalamic-Pituitary-Gonadal Axis Signaling

The HPG axis is central to reproductive success, and Gram-negative LPS has been demonstrated to perturb the delicate signaling that regulates the axis. Sheep challenged with intravenous LPS have depressed pulsatile GnRH release from the hypothalamus into the hypophyseal portal system compared to saline controls (Battaglia et al., 1997). In the same study, sheep treated with LPS had lower mean LH concentrations and LH pulse amplitude compared to sheep receiving saline (Battaglia et al., 1997). Further, low doses of LPS infused intravenously into ewes blocked LH pulses without inhibiting endogenous GnRH pulses (Battaglia et al., 2000). Similarly, in heifers that received an intrauterine infusion of *E. coli* LPS prior to ovulation, the concentrations of LH remained at baseline values and ovulation was impaired (Peter et al., 1989). However, in a separate study, when LPS was infused into the uterus of nulliparous heifers, there were no effects on the concentrations of FSH or LH (Sheldon et al., 2002, Williams et al., 2008). Changes to the HPG axis in animals experiencing uterine

infection or endotoxic challenge may contribute to reduced fertility compared to healthy animals (**Figure 1-1**).

Molecular and Cellular Responses to Infections Within the Ovary

In addition to the effects of uterine disease, bacterial infusion or LPS challenge on endometrial function, the study from Ribeiro in 2016 also revealed that embryonic quality and development was reduced in cows that had previous uterine disease (Ribeiro et al., 2016). This study supported the hypothesis that uterine disease may be impacting the follicle or oocyte; however, because the authors assessed embryonic quality from in vivo derived embryos, the reduced quality in this study may reflect effects of disease on both the oocyte and the endometrium. Interestingly, LPS has direct effects on the oocyte such that exposure of bovine oocytes to LPS during in vitro maturation increases the frequency of meiotic failure and reduces the embryo development following fertilization (Soto et al., 2003, Bromfield and Sheldon, 2011). In an experiment in which cows received an intrauterine infusion of *E. coli* and *T. pyogenes* recovered oocytes had a reduced capacity to develop morula stage embryos compared to controls (Dickson et al., 2020). Furthermore, when *E. coli* and *T. pyogenes* were infused into the uterus of heifers and oocytes were collected 4- and 60-days later there were distinct changes to the oocyte transcriptome between bacteria and control infused heifers (Piersanti et al., 2020). The transcriptional changes that were identified were not shared between oocytes collected from the earlier and later timepoints, indicating that oocytes in earlier stages of folliculogenesis may be susceptible to uterine inflammation (Piersanti et al., 2020).

Observational studies have been conducted to investigate possible association between uterine disease, uterine pathogen load, and ovarian function following

parturition. Cows with uterine infection or higher pathogen loads have been reported to have slower follicular growth and reduced peripheral estradiol compared to healthy cows (Sheldon et al., 2002, Williams et al., 2007). Further, intrauterine infusion of LPS delayed follicle ovulation compared to cows receiving saline (Williams et al., 2008). While the changes in follicular growth may be attributed to acute response to infection and result in systemic changes to peripheral physiology; it is interesting to note that LPS accumulates in follicular fluid and is positively correlated with the severity of uterine inflammation (Herath et al., 2007). In vitro LPS exposure to bovine ovarian cortex accelerates activation of primordial follicles which is associated with the loss of primordial follicle PTEN and FOXO3 translocation into the cytoplasm (Bromfield and Sheldon, 2011). This further supports the hypothesis that ovarian follicles of various stages of development may be susceptible to inflammation (**Figure 1-1**).

The steroidogenic granulosa cells within the follicle express all 10 TLRs and respond to various PAMPs such as LPS, lipoteichoic acid, peptidoglycan, and Pam3cSK4 by increasing the secretion of proinflammatory molecules including IL6 and IL8 (Herath et al., 2007, Bromfield and Sheldon, 2011). The stimulation of granulosa cells with LPS activates the TLR4 signaling pathway and results in rapid phosphorylation of TLR signaling components p38 and ERK, ultimately increasing the expression of *IL6* and *CXCL8*, which is blocked when TLR4 is inhibited by small interfering RNAs (Bromfield and Sheldon, 2011). The consequences of granulosa cell inflammation results in reduced secretion of estradiol, decreased expression of *CYP19A1*, and reduced abundance of aromatase (Herath et al., 2007, Bromfield and Sheldon, 2011, Dickson et al., 2022b). Additionally, intrauterine infusion of *E. coli* and *T.*

pyogenes or spontaneous metritis alters the transcriptome of antral follicle granulosa cells long after the resolution of infection (Piersanti et al., 2019a, Horlock et al., 2020). The authors indicate the significance of this finding by highlighting that the sampled granulosa cells would have been preantral follicles at the time of infection (Horlock et al., 2020).

While the effects of uterine disease and LPS on the follicle are relatively well established; the effects of either uterine disease or LPS on the corpus luteum that develops after ovulation are less clear. Clinical data suggests that cows with uterine disease have extended luteal phases (Opsomer et al., 2000, Sheldon et al., 2002, Williams et al., 2007). In vitro evidence suggests that endometrial prostaglandin synthesis may play a role in perturbed luteal function of cows after disease resolution. Endometrial explants treated with LPS increased secretion of PGE2 but not PGF2α, indicating that endometrial inflammation may result in a prostaglandin switch that leads to increased abundance of luteotropic PGE2 and down regulates the secretion of luteolytic PGF2α (Herath et al., 2009). Early observational studies which investigated the association between uterine pathogen load and corpus luteum size and function revealed that cows with higher pathogen load had reduced corpus luteum diameter and plasma progesterone than cows with lower abundance of uterine pathogens (Sheldon et al., 2002, Williams et al., 2007). A study from Japan which characterized the long-term effects of metritis on luteal function in 47 lactating cows revealed that cows with metritis had smaller corpora lutea in the first estrous following parturition compared to healthy cows but had no difference in the concentration of plasma progesterone (Strüve et al., 2013). This study also described that cows with metritis had no difference in luteal size,

progesterone, or steroidogenic gene expression in the second or fourth estrous cycles postpartum (Strüve et al., 2013). Furthermore, a large study which followed more than 400 cows following parturition identified that there is an association between clinical disease and reduced plasma progesterone (Bruinjé et al., 2023). This observational study also identified a tendency for reduced progesterone on day 8 following parturition in cows that had purulent vaginal discharge compared to healthy cows (Bruinjé et al., 2023). The hypothesis that uterine disease or bacterial components can compromise luteal function was further supported when preovulatory intravenous infusions of LPS reduced corpus luteum diameter and plasma progesterone following ovulation (Lüttgenau et al., 2016). These observations, however, contrast with other evidence which indicates that cows with either clinical or subclinical endometritis have no reductions in plasma progesterone (Molina-Coto et al., 2020).

The corpus luteum is comprised of multiple cell types and expresses all 10 TLRs throughout the estrous cycle and pregnancy (Gadsby et al., 2017). The expression of TLR1, TLR2, TLR4, and TLR6 increases during later stages of luteal life near the time of luteolysis (Lüttgenau et al., 2016a, Gadsby et al., 2017, Atli et al., 2018). The intrauterine infusion of LPS 10 days after ovulation increases the luteal expression of *TLR2, TLR4, IL1A, IL1B, HSD20A, and PTGES* indicating that the corpus luteum alters synthesis of inflammatory mediators and prostaglandins. Further, the expression of *PTGFR, STAR,* and *HSD3B* were all reduced in cows receiving LPS infusion indicating that LPS has direct effects on the steroidogenic function of the corpus luteum (Lüttgenau et al., 2016). Interestingly, the effects of TLR ligands on luteal cell steroidogenesis in vitro are unclear. Luteal cells isolated from slaughterhouse corpora

lutea and subsequently treated with LPS have increased secretion of progesterone compared to control cells (Grant et al., 2007). However, when granulosa or theca cells are exposed to LPS and allowed to luteinize, the secretion of progesterone is reduced in treated theca cells, but not granulosa cells (Shimizu et al., 2016). This reduction in progesterone was attributed to reduced abundance of steroid acute regulatory protein (STAR) and 3β-hydroxysteroid dehydrogenase Δ^{5-4} isomerase (HSD3B) proteins, but not altered gene expression, indicating that post-transcriptional or post-translational modifications are mediating the steroidogenic capacity of these cells (Shimizu et al., 2016).

The effects of uterine disease and inflammatory components on granulosa cells have been well defined, which indicates that cows with uterine disease have reduced follicular development and reduced estradiol secretion. However, this phenotype leaves a gap in knowledge to characterize and interrogate the potential carryover effects of follicular inflammation on the function of the subsequent corpus luteum. Impaired corpus luteum function could have significant implications for the capacity of cows with uterine disease to successfully prepare for and support the early pregnancy. Thus, it is essential to understand the cellular and molecular components that are integral in normal follicular and luteal growth, development, and function to begin interrogating potential implications of pathological or inflammatory states in cows with uterine disease.

Ovulation, Luteinization, and the Production of Progesterone

Ovarian Folliculogenesis and Granulosa Cell Maturation

The follicle is a dynamic ovarian structure that contains the oocyte surrounded by somatic granulosa cells. Female mammals are born with a finite number of oocytes

which is established around the time of birth (Mandl and Zuckerman, 1951, Zuckerman, 1951). Indeed, in mammals such as humans and the bovine, the first follicles are formed during embryonic life, while in other species including rodents, follicles are formed shortly after birth (Aerts and Bols, 2010). These first follicles are called primordial follicles, which contain an oocyte surrounded by a single, flattened layer of pre-granulosa cells (Hirshfield, 1991, 1992, 1997). Formation of the primordial follicle in cattle occurs approximately 140 days after conception, or halfway through gestation (Russe, 1983). In cattle, it is estimated that the ovary contains 150,000 primordial follicles at the time of birth and the number decreases to approximately 3,000 by 15 to 20 years of age (Erickson, 1966). After activation, primordial follicles will undergo specific growth that results in the formation of a primary follicle. The oocyte of primary follicles increases in size compared to that of a primordial follicle; the zona pellucida begins to form around the oocyte and the granulosa cells lining the follicle take on a cuboidal morphology (Hirshfield, 1997).

After the primary follicular stage, the follicle will begin to accumulate multiple layers of granulosa cells that encase the oocyte and a single layer of theca cells toward the basement membrane of the follicle and is now referred to as a secondary follicle (Hirshfield, 1997). A hallmark molecular change takes place at the secondary follicle stage whereby the follicle becomes sensitive to gonadotrophins and begins to express the FSH receptor (FSHR) thus beginning steroidogenesis (Hirshfield, 1997). Upon binding of FSH to the FSHR, the heterotrimeric G proteins disassociate to activate an intracellular signaling cascade through adenylate cyclase stimulation, cyclic AMP

synthesis, and protein kinase A activation (Sayers and Hanyaloglu, 2018). Activation of the FSHR stimulates granulosa cell proliferation and steroidogenesis.

The next stage of follicular development is the tertiary or antral follicle and is identified by the formation of a fluid filled antrum within the population of granulosa cells. Follicular fluid fills the antrum which likely arises from filtered blood and serves to bathe both the granulosa cells and oocyte in nutrients and signaling factors (Romero-Arredondo and Seidel Jr, 1994, Ali et al., 2004). After formation of the antrum, granulosa cells can be defined as either cumulus granulosa cells which directly surround the oocyte or mural granulosa cells which surround the basement membrane of the follicle. The final stage of follicular development is the dominant, pre-ovulatory or Graafian stage follicle which is primed to ovulate and release the oocyte (Hirshfield, 1997). Follicle recruitment begins after the formation of the primordial follicle which permits the formation of antral follicles even during fetal life and continues until depletion of the ovary (Russe, 1983). In the cow, the timing of development from a primordial to preovulatory follicle is estimated to be 80-100 days (Britt, 2008).

In 1960 growth of antral follicles in cattle was proposed to follow two waves of follicular activity throughout the estrous cycle (Rajakoski, 1960). However, in 1983, a study which characterized the changes in steroid concentrations and gonadotropin receptors of follicular fluid in nonovulatory follicles concluded that the bovine ovary undergoes two periods of follicular growth and atresia between days 3-13 of the estrous cycle, until a follicle acquires dominance and continues growth in a third wave of follicle development (Ireland and Roche, 1983). The period of accelerated follicle growth is called diameter deviation (Sartori et al., 2001). The understanding of follicle dynamics

was significantly improved with the development of transrectal ultrasonography of the ovary (Pierson et al., 1988).

Final growth and maturation of the follicle is dependent upon increased LH pulsatility acting upon theca cells to provide androgen substrate for aromatization into 17β-estradiol by granulosa cells (**Figure 1-2**). Simultaneously, FSH increases the enzymatic activity of aromatase in granulosa cells, maximizing estradiol synthesis (Richards et al., 1987). This mutually coordinated role of both theca and granulosa cell physiology lent itself to the formation of the two cell-two gonadotrophin theory (Fortune, 1986, Fortune and Quirk, 1988). In this model, both granulosa cells and theca cells express cytochrome P450 side-chain cleavage (P450scc), which enzymatically cleaves the side chain of cholesterol to form 21-carbon progestins and is the rate limiting step in the conversion of cholesterol into steroid hormones. However, despite this shared expression of P450scc, granulosa cells express FSHR while theca cells express LH receptor (LHCGR) (Bao and Garverick, 1998). The binding of LH to the LHR in theca cells initiates the activation of cytochrome P450 17α-hydroxylase which converts progestins into androstenedione, while granulosa cells do not produce androgens even when supplemented with progestin precursors (Fortune, 1986). Furthermore, follicular isolates containing both granulosa and theca cells produced more androstenedione than independent cultures of theca cells (Fortune, 1986). Thus, it was concluded that theca cells produce androstenedione which is then aromatized by cytochrome P450arom (P450arom) in granulosa cells into 17β-estradiol (Bao and Garverick, 1998). During later follicular development, 17β-estradiol and FSH act synergistically to increase the expression of LHCGR on the membrane of granulosa cells. A conceptual model of

the molecular and cellular processes underpinning steroidogenesis and differentiation of ovarian cells is depicted in Figure 1-2.

Ovarian function is the critical feedback that occurs between the hypothalamus, the pituitary, and the ovary. Hypothalamic GnRH stimulates the anterior pituitary to release FSH and LH in different manners depending on the day of the estrous cycle. For example, as the dominant follicle grows and produces greater concentrations of estradiol near the time of ovulation, 17β-estradiol exerts positive feedback on the preoptic area of the hypothalamus to produce more GnRH leading to a surge of LH from the anterior pituitary (Padmanabhan et al., 1978, Kesner et al., 1981). The LH surge induces changes to gene expression of granulosa cells such that within 6 hours after LH stimulation, granulosa cells change their molecular functions from cell division, development and proliferation to vascularization and lipid synthesis; indicating the cells are preparing for ovulation (Gilbert et al., 2011). Granulosa cell molecular function continues to change until 22 hours after the LH surge where molecular profiles indicate the granulosa cells are active in processes such as protein localization and intracellular transport (Gilbert et al., 2011). Thus, these changes to granulosa cell gene expression are indicative of their cellular differentiation into luteal cells around the time of ovulation (**Figure 1-2**).

Luteinization and Progesterone Synthesis

The steroidogenic cells found in the CL of cattle fall into two distinct categories dependent upon their size and morphological characteristics (Bishop et al., 2022). ‘Small luteal cells’ are typically between 12 and 23 μm in diameter and contain elongated mitochondria and cup shaped nuclei (Weber et al., 1987). ‘Large luteal cells’ are typically greater than 23 μm in diameter and contain swollen mitochondria, with a

centrally located, round nucleus (Weber et al., 1987, Fields et al., 1992, Fields and Fields, 1996, Bishop et al., 2022). It is widely accepted that large luteal cells produce greater amounts of progesterone than their small luteal cell counterparts. Early histological assessments determined that large luteal cells were luteinized granulosa cells. Interestingly, when monoclonal antibodies were generated against either granulosa or theca cells from BALB/c mice and used to immunolocalize specific cell types in the heifer CL, it was further supported that large luteal cells were of granulosa origin and small luteal cells were of theca origin (Alila et al., 1989). The differentiation of follicular cells into steroidogenic luteal cells is facilitated by the actions of LH. Evidence from hypophysectomized sheep demonstrated that removal of the pituitary on day 5 of the estrous cycle reduced luteal growth and the secretion of progesterone compared to sham-hypophysectomized sheep, while administering exogenous LH was sufficient to restore luteal size and progesterone production (Kaltenbach et al., 1968, Farin et al., 1990). Upon LH binding the LHCGR, adenylyl cyclase increases intracellular cAMP, activates PKA, and phosphorylation of PKA substrates that lead to stimulation of steroidogenesis (Przygrodzka et al., 2021). Similarly, LH can lead to activation of phospholipase C resulting in increased intracellular calcium and activation of mitogen-activated protein kinases (MAPK) (Przygrodzka et al., 2021). The binding of LH also has implications for the molecular function of the differentiating cells, whereby the stimulation of PKA triggers increased expression of proteolytic, angiogenic, and proinflammatory transcripts that promote tissue remodeling and formation of vessels for adequate steroidogenesis (Przygrodzka et al., 2021). This coordinated increase in gene expression during luteinization is concomitant with reduced expression of factors

involved in estradiol synthesis (*CYP19A1*), gonadotropin receptors (*FSHR* and *LHCGR*) and cell cycle (*CDK1, CDK2, CDKN2*) (Przygrodzka et al., 2021).

In addition to the changes in molecular function of luteal cells upon LH stimulation, there are also drastic morphological changes that occur during the process of luteinization. For example, as both granulosa and luteal cells undergo luteinization, there is an increase in the amount of Golgi elements, endoplasmic reticulum, lysosomes, eosinophilic granules, and lipid droplets (Channing and Crisp, 1972). Of these organelles, the lipid droplets have garnered the most attention in the context of steroidogenic luteal cells. Lipid droplets are intracellular hubs for storage of neutral lipids such as cholesterol esters and triglycerides (Przygrodzka et al., 2021). Lipid droplets are coated in proteins that function to stabilize the droplet and permit interactions with other proteins for incorporation or removal of lipids from the lipid droplet core and facilitate the trafficking and connection with other organelles (Fujimoto and Parton, 2011). Bovine luteal cells contain greater numbers of lipid droplets than most other tissue cell types that are enriched with triglycerides that can be used for steroid synthesis (Talbott et al., 2020). Luteal lipid droplets also have a greater abundance of essential proteins that regulate the process of steroidogenesis such as STAR, CYP11A1, and HSD3B (Przygrodzka et al., 2021). The lipid droplets of luteal cells are regulated by both luteotropic and luteolytic hormones. For example, LH mobilizes lipid droplet cholesterol stores while luteolytic PGF2α causes triglycerides to increase (Ellsworth and Armstrong, 1973, Heath et al., 1983, Waterman, 1988). This regulation of stored cholesterol or triglycerides is critical for the production of progesterone.

In addition to the cellular and molecular changes that are mediated by LH binding to the LHCGR of early luteal cells, there are also changes to the biochemical and biosynthetic properties of the steroidogenic machinery required to produce copious amounts of progesterone. Central to the process of luteinization is the preparation for drastic increases in de novo steroidogenesis and the bioconversion of cholesterol into pregnenolone (Wiltbank et al., 1989, Carroll et al., 1992). Cholesterol bound to high density lipoprotein (HDL) is presumed to be the primary source of cholesterol utilized for progesterone production in the bovine CL because the concentrations of HDL are 8- to 10-fold greater than low density lipoprotein (LDL) in bovine serum, and HDL represents approximately 90% of the total cholesterol in the circulating periphery of cattle (Takahashi et al., 2021). Uptake of extracellular cholesterol is mediated through both the LDL-receptor and the scavenger receptor type B class 1 (SR-B1) in luteal cells (Lopez and McLean, 1999, Sekar and Veldhuis, 2004). Upon binding of HDL to the SR-B1 protein on the cell surface, cholesterol esters are internalized without lysosomal degradation of the HDL such that the HDL can be recycled (Shen et al., 2018). Once cholesterol enters the cell it can either be used immediately for steroidogenesis or undergo esterification with long-chain fatty acids, such as triglycerides, and stored as cholesterol esters in lipid droplets (Niswender, 2002). When stimulated by LH, the intracellular PKA stimulation leads to phosphorylation of hormone sensitive lipase (HSL) at both Ser563 and Ser660 and promotes the hydrolytic cleavage of diacylglycerol, triacylglycerol, and cholesterol from lipid droplets (Cordle et al., 1986, Plewes et al., 2020). Luteal cells can also synthesize cholesterol *de novo* via the mevalonate pathway such that acetyl-CoA is transformed into mevalonate under the regulation of 3-hydroxy-

3-methyl-glutaryl-coenzyme A reductase (HMGCR) (Faust et al., 1980, Reverchon et al., 2014). Following either *de novo* synthesis or hydrolytic release of cholesterol from lipid droplets, free cholesterol is trafficked to the mitochondria via different elements of the cell cytoskeleton such as actin, tubulin, and intermediary filaments and sterol carrier proteins for synthesis of steroid hormone (Gwynne and Condon, 1982, Nagy and Freeman, 1990, Niswender, 2002, Shen et al., 2018).

While mitochondria are traditionally considered for their roles in synthesizing ATP, these dynamic organelles are also critical in the regulation of steroidogenesis in luteal cells. In steroidogenic cell types, the mitochondria form a specialized microdomain with the endoplasmic reticulum which is the cellular organelle critical in protein folding, lipid metabolism, and calcium homeostasis. These mitochondrial-endoplasmic reticulum microdomains are termed mitochondria-associated membranes (MAMs) and are integral in cell signaling and scaffolding for proteins within luteal cells (Przygrodzka et al., 2021). This network of MAMs facilitates the movement of both stored and *de novo* cholesterol from the endoplasmic reticulum to the outer mitochondrial membrane (OMM). Key regulatory enzymes in the biosynthetic pathway for progesterone such as STAR and CYP11A1 are nuclear encoded and contain mitochondrial targeting sequences that upon transcription and translation in the endoplasmic reticulum lead to the trafficking and insertion into the inner mitochondrial membrane (IMM). For example, STAR is translated into a 37 kDa protein with a specific mitochondrial targeting sequence that can be differentially phosphorylated and is post-translationally modified to be inserted into the OMM with most of the protein facing the matrix to facilitate cholesterol movement to the IMM (Niswender, 2002). The enzymatic

activity of STAR is critical in trafficking hydrophobic cholesterol into the IMM and represents the rate-limiting step in progesterone synthesis and is a point for acute hormonal control of luteal cell progesterone biosynthesis (Niswender, 2002, Plewes et al., 2020). Upon cholesterol entry into the mitochondria, two essential enzymatic reactions must occur. The enzymatic complex P450scc which resides on the IMM catalyzes the conversion of cholesterol to pregnenolone by enzymatically removing the cholesterol sidechain (Farkash et al., 1986). The P450scc complex contains three proteins FDX1, FDXR, and CYP11A1 (Davis and LaVoie, 2019). The resulting pregnenolone is then converted into the final form of progesterone via the enzymatic activity of HSD3B. The location of the conversion of pregnenolone to progesterone is dependent upon the enzymatic isoform performing the action as there are different isoforms of HSD3B that are associated with either the mitochondria or the endoplasmic reticulum (Cherradi et al., 1994).

In summary, the steroidogenic properties of follicular granulosa cells and the subsequent luteal cells are intimately involved with signaling of the HPG axis. The cellular differentiation events and the biosynthetic pathways for both estradiol and progesterone include opportunistic steps for acute regulation of steroidogenesis that can be impacted by factors both on a cellular and organismal level. Thus, the understanding of these regulatory elements warrants further investigation.

Experimental Models of Induced Inflammation

While there are a wide variety of stressors that can induce inflammation in mammals, conducting controlled experiments to elucidate the effects of one singular environmental stimulus requires a unique approach. Indeed, many experimental models for induced inflammation exist, and herein this dissertation, two proinflammatory models

will be utilized: the induced uterine infection and the feeding of adipogenic diets. Studying spontaneous postpartum uterine infections in dairy cattle is difficult because there are often many confounding factors of disease that negatively influence the animal's physiology. The initiation of lactation combined with other peripartum diseases add confounding factors to studies investigating the mechanisms of uterine infection driven subfertility. Thus, developing models targeted towards minimizing peripheral physiological stressors will allow for targeted analysis of how infection driven inflammation can result in impaired fertility.

Models of uterine infection in cattle have existed for nearly 70 years and have permitted the study of uterine inflammation on fertility. Some of the earliest experiments infused infectious bacteria into the uteri of cows either in the follicular or luteal phases of the estrous cycle, or used ovariectomized cows supplemented with either progesterone or stilboestrol to ask questions about steroid hormones and disease susceptibility (Rowson et al., 1953). When bacteria were infused into cows in the luteal phase or ovariectomized cows receiving progesterone, pyometra developed within two days, while cows in estrus or ovariectomized cows receiving stilboestrol had no purulent exudate (Rowson et al., 1953). These early studies demonstrated how the endocrine milieu can impact the development of uterine infection in cattle.

When specific bacterial species such as *F. necrophorum*, *Bacteriodes melaninogenicus* or *Actinomyces pyogenes* (now *T. pyogenes*) were infused into the uteri, pyometra and uterine inflammation were induced (Silva et al., 2023). Other studies that isolated purulent exudate from the uteri of cows with chronic pyometra and transferred this exudate into recipient cows resulted in reduced estrous cycle lengths

and increases in endometrial inflammation (Gallagher and Ball, 1980). The culmination of these findings led to the development of a combined infection model whereby exogenous progesterone is administered to mimic the luteal phase, the endometrium is scarified to damage the mucosal layer similar to that observed after parturition, and a cocktail of both pathogenic *E. coli* and *T. pyogenes* isolated from a cow with metritis is infused into the uterus of heifers to induce a uterine infection which presents symptoms similar to clinical endometritis (Piersanti et al., 2019b).

The prevalence of chronic overnutrition and obesity in human populations have also warranted the need for a model to study the effects of calorie rich diets on various physiological responses. High-fat or high calorie diets (HFD) are considered a significant modifiable risk factor for diseases such as diabetes and types of cancer (Duan et al., 2018). The vast majority of the dietary induced obesity models occur in mice and are fed to mimic Western-style diets that contain increased amounts of clarified butterfat, reduced amounts of starch and overall increased digestible energy compared to control diets (Fullston et al., 2013). The ingestion of HFD results in systemic, chronic low-grade inflammation (Duan et al., 2018). Indeed, inflammation develops in tissues such as the liver, adipose tissue, skeletal muscle, and intestine (Guillemot-Legris et al., 2016). Alterations to the gut microbiota are associated with chronic systemic inflammation after consumption of HFD. When germ-free mice were fed a HFD, these mice did not experience obesity or upregulation of intestinal TNFα compared to conventional mice that were also fed a HFD (Turnbaugh et al., 2009). Interestingly, when the germ-free mice had gut microbiota reconstituted from obese mice, the germ-free mice increased their body fat (Turnbaugh et al., 2009). It has also

been demonstrated that changes to the gut microbiota can activate TLR signaling pathways, ultimately leading to increased intestinal permeability to endotoxins and results in elevated translocation of LPS to the circulation (Ding et al., 2010, Kim et al., 2013). Furthermore, studies using the sheep as a model for maternal obesity have demonstrated that dietary induced inflammation causes upregulation of inflammation signaling and cytokine expression in the mid-gestation placenta (Zhu et al., 2010). Thus, feeding a HFD can induce inflammation and alter the immune environment.

Objectives for this Program of Study

While there is a broad body of literature drawing associations with environmental stressors and fertility, the mechanisms responsible for reduced fertility following environmental stressors remain to be elucidated. The overall objective of the studies reported in this dissertation are to experimentally describe and interrogate the consequences of two unique environmental stressors in relation to both male and female fertility. Using various models, the following experiments were assessed 1) the influences of paternal overnutrition on male fertility, and 2) the impacts of uterine infection on ovarian and endometrial function. After inducing moderate weight gain in bulls, paternal fertility was assessed by utilizing IVF and embryo culture (chapter 2). Next, investigations were performed to understand the effects of spontaneous, postpartum uterine disease on ovarian function and dynamics (chapter 3), and the cellular mechanisms by which progesterone production is altered following granulosa cell exposure to the bacterial component LPS (chapter 4). Lastly, the relative effects of induced uterine infection to both the oocyte and the endometrium were evaluated (chapter 5). By understanding the various impacts of environmental stressors on both

male and female fertility, future work can be targeted to develop therapeutics and intervention strategies to improve fertility in cattle.

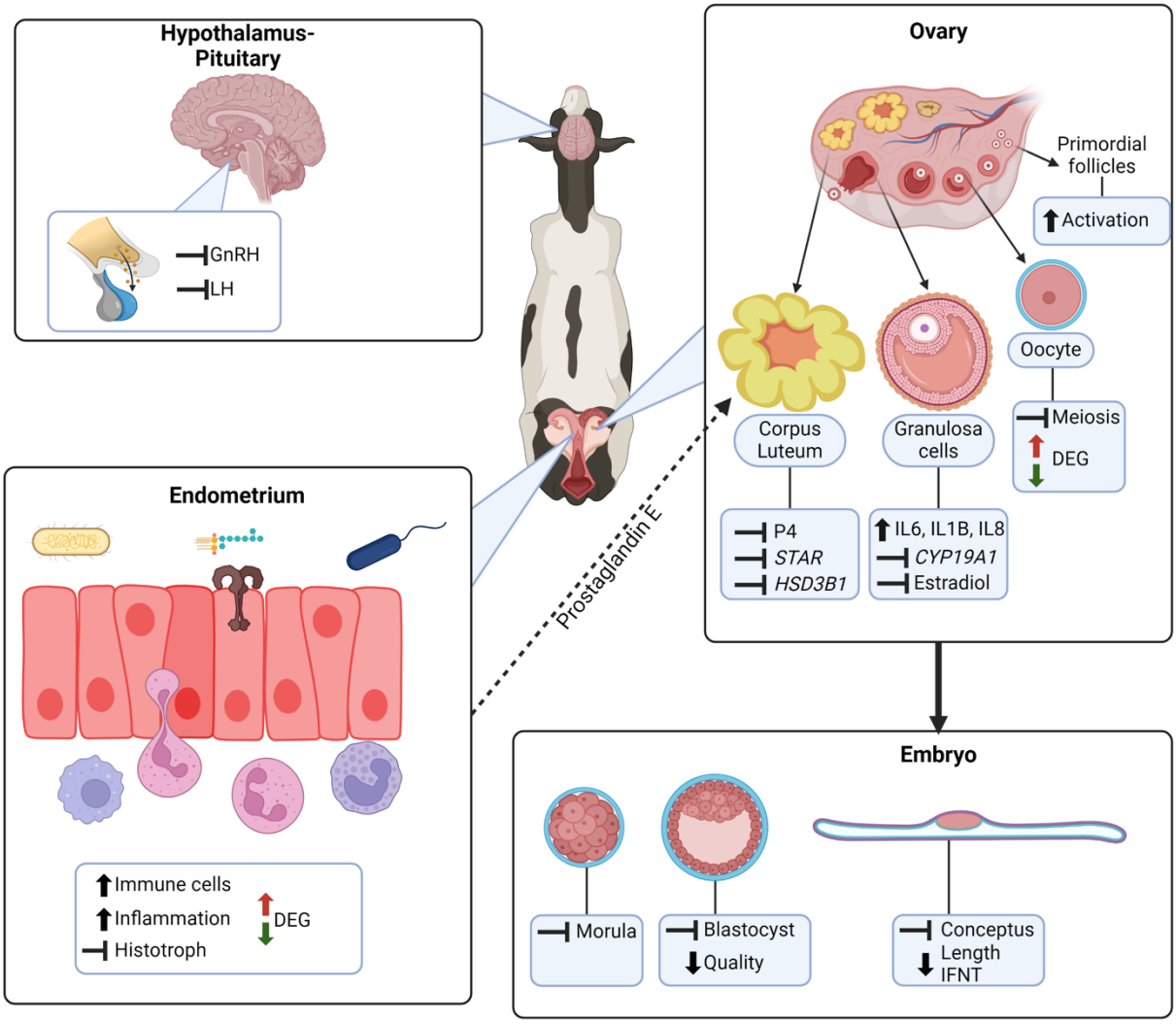

Figure 1-1. A conceptual model of the cellular and molecular effects of uterine infection and bacterial components on female reproductive physiology.

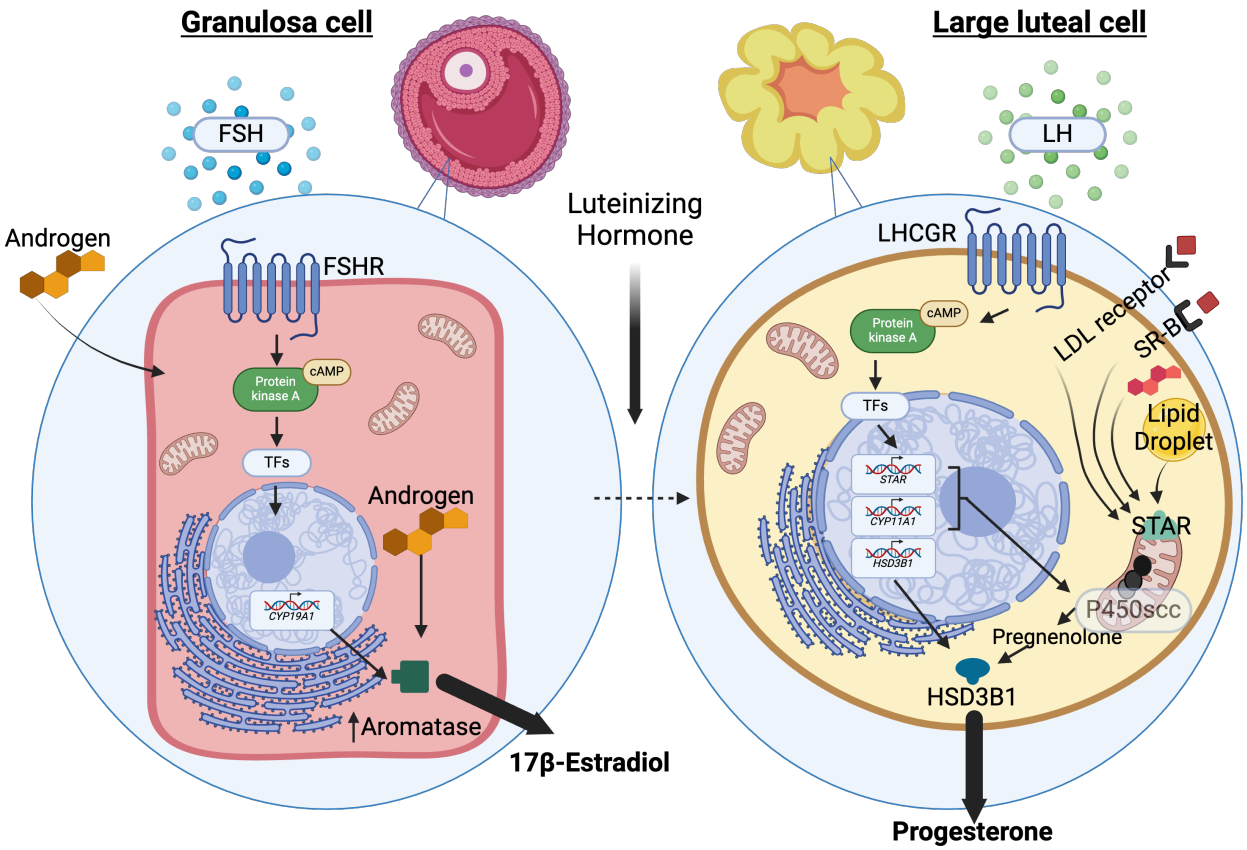

Figure 1-2. A conceptual model of the molecular and cellular processes underpinning steroidogenesis and differentiation of ovarian cells.

CHAPTER 2
PATERNAL HIGH GAIN DIET INFLUENCES BLASTOCYST FORMATION FOLLOWING IN VITRO FERTILIZATION IN BOVINE*

Summary

Bulls used in cattle production are often overfed to induce rapid growth, early puberty and increase sale price. While the negative consequences of undernutrition on bull sperm quality are known, it is unclear how a high gain diet influences embryo development. I hypothesized that semen collected from bulls fed a high gain diet would have a reduced capacity to produce blastocysts following in vitro fertilization. Eight mature bulls were stratified by body weight and fed the same diet for 67 d at either a maintenance level (0.5% body weight per day; n = 4) or a high gain rate (1.25% body weight per day; n = 4). Semen was collected by electroejaculation at the end of the feeding regimen and subjected to sperm analysis, frozen, and used for in vitro fertilization. The high gain diet increased body weight, average daily gain, and subcutaneous fat thickness compared to the maintenance diet. Sperm of high gain bulls tended to have increased early necrosis and had increased post-thaw acrosome damage compared with maintenance bulls, but diet did not affect sperm motility or morphology. Semen of high gain bulls reduced the percentage of cleaved oocytes that developed to blastocyst stage embryos. Paternal diet had no effect on the number of total or CDX2 positive cells of blastocysts, or blastocysts gene expression for markers associated with developmental capacity. Feeding bulls a high gain diet did not affect sperm morphology or motility, but increased adiposity and reduced the ability of sperm to generate blastocyst stage embryos.

---

* Work presented in this chapter was published as Seekford, et al., 2023. Bulls fed a high-gain diet decrease blastocyst formation after in vitro fertilization. Reproduction, 166, 149-159. https://doi.org/10.1530/REP-23-0006

Introduction

Increased paternal body mass index negatively impacts male fertility in multiple species and is mediated by effects on sperm biology, motility, and alterations to seminal plasma composition (Kort et al., 2006, Schjenken et al., 2021). Obesity in men is associated with increased morphological abnormalities, sperm DNA fragmentation, and altered mitochondrial membrane potential that may contribute to infertility (Campbell et al., 2015). Dietary induced obesity in rodents alters sperm chromatin configuration, increases reactive oxygen species, alters the sperm epigenome, and impairs the capacity for seminal plasma to elicit a tolerogenic immune response after mating (Houfflyn et al., 2017, Schjenken et al., 2021). In mice, embryos from dietary-induced obese males are both metabolically and morphologically different compared to embryos derived from control males. These resultant embryos have reduced cleavage rates, decreased development to the eight-cell and blastocyst stages, and alterations in the ratio of inner cell mass and trophectoderm cells compared to embryos from control males (Ghanayem et al., 2010, Mitchell et al., 2011, Binder et al., 2012), suggesting paternal diet can negatively impact embryonic development. While maternal diet has been widely associated with reproductive and postnatal outcomes, these data suggest that paternal diet also contributes to reproductive success and postnatal outcomes of offspring in rodents and possibly humans. Negative effects of paternal under-nutrition on reproductive success are relatively well characterized in cattle (Mwansa and Makarechian, 1991, AK et al., 2018). Under-nutrition of bulls results in reduced sperm motility, increased morphological defects, altered spermatogenesis, and ultimately reduced fertility (Harrison et al., 2022). Negative effects of male over nutrition on fertility have also been shown in the bovine in both observational and controlled studies

(Coulter and Kozub, 1984, Coulter et al., 1997). Bulls used for artificial insemination or live cover are generally fed to highlight enhanced growth characteristics achieved by feeding high-gain diets resulting in increased adiposity (McDonald et al., 2010). Increased fat deposition in bulls is thought to increase the adiposity of the scrotum and reduce thermoregulation of the testis, resulting in greater sperm defects and reduced fertility (Skinner, 1981, Coulter and Kozub, 1984). Young bulls with increased body weight are more likely to fail a breeding soundness examination compared with their lighter counterparts (McDonald et al., 2010). Moreover, bulls exposed to high energy diets have decreased sperm motility and increased sperm morphology defects compared with bulls fed a control diet (Coulter et al., 1997).

Post-fertilization consequences of paternal high energy diets have not been explored in the bovine; therefore, I utilized in vitro fertilization and culture of bovine embryos to evaluate the fertility of spermatozoa of mature bulls fed a high gain diet that resulted in increased adiposity. I hypothesized that semen collected from bulls fed a high gain diet would have a reduced capacity to develop blastocysts following in vitro fertilization and embryo culture. Furthermore, I hypothesized that bulls fed a high gain diet would produce blastocysts with reduced trophectoderm cell numbers and differential expression of genes associated to developmental competency. Data presented here provide evidence that mature bulls fed a high gain diet have a reduced capacity to produce embryos following in vitro fertilization in the absence of sperm motility or morphological defects that would result a bull failing a breeding soundness examination.

Materials and Methods

Animals, Experimental Design, and Diet Description

All procedures were performed under the approval and supervision of the University of Georgia's Institutional Animal Care and Use Committee, protocol number A2020-11-009-Y2-A1.

Animals were housed at the Eatonton Beef Research Unit, Eatonton GA, USA. Mature Angus and Hereford bulls (n = 9; body weight = 946 ± 85 kg; mean ± SD) were stratified by breed, age, and body weight, and randomly assigned to either a high gain (HG) diet designed to achieve an average daily gain of 1.38 kg/d, or a maintenance (MAINT) diet designed to maintain body weight. Bulls in both treatments were fed the same diet (dry matter composition of 71.5% rolled corn, 10% corn gluten, 6% soyhull pellets, 6% soybean meal, 1.8% NaCl, 0.5% urea, and 0.2% trace mineral mix [net energy for maintenance = 2.10 Mcal/kg, net energy for gain = 1.44 Mcal/kg, crude protein = 14.1%, neutral detergent fiber = 16.6%, Ca = 0.54% and P = 0.37%]) at different inclusion rates, and had ad libitum access to bermudagrass hay (*Cynodon dactylon*; net energy for maintenance = 1.02 Mcal/kg, net energy for gain = 0.45 Mcal/kg, crude protein = 10.2%, neutral detergent fiber = 71.6%). Bulls were housed in individual pens to monitor individual daily feed intake. An acclimation period began on d -7 with an inclusion of 0.25% of body weight to adapt bulls to the facilities and the proposed diet. Starting on day 0, daily dietary offerings were incrementally increased for 7 d. After the end of the adaptation (d 7), MAINT bulls received 0.5% of their body weight per day and HG bulls received 1.25% of their body weight per day for an additional 67 d providing a total divergent feeding regiment of 74 d (**Figure 2-1**). Average body weight and body condition score (BCS) (Wagner et al., 1988) were

obtained from two consecutive measurements 24 to 48 h apart at the beginning (d -7) and at the end (d 74) of the feeding regiment. Additionally, body weight and BCS were assessed on d 28 and 43, and body weight was used to adjust diet inclusion rates. Subcutaneous fat, rump fat, intramuscular fat and ribeye area were evaluated on d -7 and 74 using carcass ultrasonography (3.5 mHz linear array transducer, Aloka 500V; Corometrics Medical Systems Inc., Wallingford, CT) (Emenheiser et al., 2014). Collected data was interpreted using Beef Information Analysis Pro Plus software (Designer Genes USA, Harrison, AR) (Detweiler et al., 2019).

Semen Collection and Evaluation

Scrotal circumference was assessed with a scrotal measuring tape and semen collections were performed using programed settings of an electroejaculator (Pulsator IV, Lane Manufacturing Inc., Denver, CO) on days -7, 71 and 74. Exclusion criteria for bulls used in the evaluation included any gross genital pathology, ≤ 30% individual sperm motility, ≤ 70% morphologically normal spermatozoa, and a minimum scrotal circumference ≤ 34 cm. One bull of the nine failed to meet inclusion criteria and was excluded from the study. Twenty-four h prior to semen collections on d -7 and 71, a cleanup semen collection was performed, and semen was discarded. Semen collected at d 71 and 74 were used for semen analysis, and semen collected on d 74 was used for in vitro embryo production. Sperm morphology was evaluated in fresh semen by diluting semen 1:10 (v:v) with formalin buffered solution and evaluated using phase-contrast microscopy at 100× magnification under oil immersion. A total of 100 spermatozoa were evaluated based on the presence of primary and secondary abnormalities as previously described (Koziol and Armstrong, 2018). Sperm concentration was estimated using a densimeter (Animal Reproduction Systems Inc.,

Ontario, CA) and semen was diluted in pre-warmed commercial extender solution (OptiXcell, IMV Technologies, Brooklyn Park, MN) to a final concentration of 5×10^7 sperm/mL. Extended semen was refrigerated for at least 30 min prior to packaging in 0.5-mL French straws (cat# 005569, IMV Technologies) at 2.5×10^7 sperm/straw. Semen straws were incubated in liquid nitrogen vapor for 10 min followed by complete submersion and storage in liquid nitrogen (Robbins et al., 1976).

Sperm motility of fresh and frozen-thawed semen was evaluated using a computer-assisted semen analyzer (CASA; SpermVision Professional, Minitube of America, Verone, WI). System settings used for analysis included field depth of view = 20 µm; pixel to µm ratio = 130-100; cell area = 18-80 µm; frames acquired = 30; frame rate = 60 Hz; average orientation change cutoff static cells = 5 degrees; and distance straight line cutoff = 4.5 µm/s. Briefly, semen was loaded in a 20-µm chamber over the heated stage at 38°C and percent total motile and progressively motile spermatozoa were assessed for all cells present in seven fields with a 20× phase-contrast objective. Motility parameters evaluated included average velocity path (VAP), straight-line velocity (VSL), and curvilinear velocity (VCL).

Sperm plasma membrane integrity was analyzed using SYBR14 and propidium iodide (LIVE/DEAD kit, cat. No. L7011, Thermo Fisher Scientific, Waltham, MA). Sperm at 2.5×10^7 cells/mL were diluted 1:1 in DPBS and incubated with 100 nM SYBR14 and 9.6 µM propidium iodide. Semen samples were then incubated for 10 min at 38°C followed by fluorescence microscopy evaluation using a 40× objective. Spermatozoa were then classified as membrane intact, or membrane damaged using a built-in software within the CASA (SpermVision Professional, Minitube of America).

Flow Cytometry

Acrosome integrity was evaluated using fluorescein isothiocyanate-labeled peanut agglutin (FITC-PNA; Cat. No. F-2301-1, EY Laboratories, San Mateo, CA) and propidium iodide. A 1-mL suspension of 5×10^6 spermatozoa was incubated with 1 µL of a 1 µg/mL solution of FITC-PNA and 1 µL of a 6 µ*M* solution of propidium iodide at 38°C for 10 min followed by flow cytometry to estimate the percent of acrosome-damaged and membrane-intact spermatozoa. Apoptosis was evaluated by estimating the percentage of membrane-intact apoptotic cells using FITC-labelled Annexin V stain (Thermo Fisher Scientific). Spermatozoa were washed by centrifugation at 600 × *g* for 5 min and resuspended at 4×10^5 sperm in 1 mL of binding buffer (0.01 M HEPES, 1.4 *M* sodium chloride, 25 m*M* calcium chloride in distilled water, pH 7.4). Sperm were then incubated with 10 µL of FITC-Annexin V for 15 min at room temperature. Sperm were washed by centrifugation and resuspended in 0.5 mL in binding buffer with 0.5 µL of a 6 µ*M* solution of propidium iodide. Flow cytometry was performed using an Accuri C6 Plus (BD Biosciences, Franklin Lakes, NJ) to evaluate 10,000 events for each sample. Initial gating based on forward and side scatter identified spermatozoa and eliminated debris and somatic cells from the analysis (**Figure A-1**). The green and red signals were detected using a 5-mW blue argon laser (488 nm) and specific emission filters (535 ± 30 nm for green and 585 ± 30 nm for red). Background fluorescence was evaluated in unstained samples and used to identify positive labeled spermatozoa. Following color compensation, fluorescence emission data were collected with logarithmic amplification for green fluorescence (FITC) and red fluorescence (propidium iodide).

In Vitro Production of Bovine Embryos

A total of 2771 abattoir-derived (J.R. Simplot Company, Boise ID) cumulus oocyte complexes were incubated at 38.5℃ and matured overnight in groups of 20–25 for 22 h in four replicates. Between 186 and 396, cumulus oocyte complexes were used per bull. Subsequently, cumulus–oocyte complexes in groups of 25–30 were transferred to 4-well plates (Thermo Fisher Scientific) containing BO-IVF medium (IVF Bioscience, Falmouth, UK) and covered with mineral oil (IVF Bioscience). Thawed semen collected from each bull on day 74 was purified by density gradient centrifugation utilizing BO-SemenPrep (IVF Bioscience) and a uniform sperm suspension was diluted to a concentration of 2.0×10^6 sperm/mL. A total of 500 µL of sperm was applied to each fertilization well to yield a final concentration of 1.0×10^6 sperm/mL (day 0). Each bull was used in each of the four individual IVF replicates. Following fertilization (20 ± 2 h), oocytes were washed with BO-IVC medium (serum free with a synthetic serum replacement, supplemented with BSA; IVF Bioscience), and cumulus cells were removed by vortexing. Groups of 20–25 presumptive zygotes were transferred to 500 µL of BO-IVC medium (IVF Bioscience) and cultured for 8 days. Embryo cleavage was assessed 3 days post-fertilization and blastocyst formation was evaluated on day 7.5 post-fertilization.

Immunofluorescence and Cell Counting

A representative sample of blastocysts were selected on day 7.5 post-fertilization from all four replicates representing all eight bulls ($n = 21$ MAINT; $n = 23$ HG) and processed for differential cell counting. Briefly, embryos were fixed in 4% [w/v] paraformaldehyde (Thermo Fisher Scientific) for 15 min and washed in Tris-buffered saline with 0.1% Tween 20 (Thermo Fisher Scientific). Blastocysts were permeabilized

in 0.25% Triton X-100 (Thermo Fisher Scientific) for 20 min, washed in TBST, and blocked with 10% goat serum for 1 h at room temperature. Blastocysts were incubated with anti-CDX2 IgG1 (BioGenex Laboratories, Fremont, CA, USA; #CDX2-88) for 1 h at room temperature, washed in TBST and incubated with anti-mouse IgG-Alex488 (1:1000 dilution; Thermo Fisher Scientific) and Hoechst 33342 (Thermo Fisher Scientific) for 1 h at room temperature. Blastocysts were washed in TBST and mounted in glycerol:PBS (1:1) on glass slides. Each blastocyst was imaged using a Zeiss Axio Observer 7 (Zeiss, Jena, Germany) fitted with an Andor DSD2 Confocal Unit and Zyla Plus 4.2-megapixel camera (Oxford Instruments, Abingdon, United Kingdom) utilizing a Plan-Apochromat 40× objective lens. Optical Z-stacks were acquired for each blastocyst and the Fiji package of ImageJ (National Institutes of Health, Bethesda, MD, USA) was used to quantify total cell number, CDX2-positive cell number (trophectoderm), and CDX2-negative cell number (inner cell mass).

RNA Isolation and Real-Time RT-Polymerase Chain Reaction

Pools of blastocysts derived from all four replicates representing all eight bulls were stored in 350 µL of RLT buffer (Qiagen) at -80ºC. Total RNA was extracted from blastocysts using the RNeasy Micro Extraction Kit according to the manufacturer's instructions (Qiagen). Briefly, RLT buffer was added to Eppendorf tubes containing embryo pools and samples were vortexed for 30 seconds. Lysates were collected and homogenized using a Qiashredder column (Qiagen) before purification of total RNA using the RNAeasy MinElute spin column with DNAse treatment (Qiagen). Reverse transcription was performed utilizing the Verso Reverse Transcription cDNA synthesis kit (Thermo Fisher Scientific). Resultant cDNA underwent selective pre-amplification

using SsoAdvanced PreAmp Supermix (Bio-Rad, Hercules, CA) in combination with a pool of all primers prior to real-time RT-PCR.

Forward and reverse primers for each target were designed using the NCBI database to span exon junctions (**Table 2-1**). Amplification efficiency for each primer pair was evaluated and met MIQE guidelines ($R^2 > 0.98$ and efficiency of 90-110%) (Bustin et al., 2009). Real-time RT-PCR was performed in triplicate using a three-step protocol. Each 20 µL reaction consisted of 300 nM of each forward and reverse primer, iTaq Universal SYBR Green Master Mix (Bio-Rad) and cDNA. Amplification was performed using a Bio-Rad CFX Connect light cycle with an initial denaturation at 95℃ for 30s followed by 40 cycles of 95℃ for 5 s, 60℃ for 10 s (annealing temperature for primer pair *PTGS2* was 62℃), and a final extension at 60℃ for 30 s. A no-template pre-amplification negative control and a no-template negative control were used to confirm specific amplification for each primer pair. Relative expression for genes of interest was calculated using the $2^{-\Delta Ct}$ method relative to the geometric mean of *GAPDH, RPL19,* and *SDHA*.

Statistical Analyses

All data were analyzed using the SAS statistical package (version 9.4; SAS/STAT, SAS Inst. Inc., Cary, NC, USA). Growth and carcass response variables were analyzed using the MIXED procedure of SAS. Data were analyzed separately for each day and models included the fixed effect of treatment (MAINT *vs.* HG) and the random effect of sire.

The GLIMMIX procedure in SAS was utilized to analyze all sperm morphology, flow cytometry, and CASA response variables (with the exceptions of VCL, VAP, and

VSL) using the average responses from semen collections on d 71 and 74. Proportional data were assumed to follow a beta distribution and statistical models utilized to analyze CASA and flow cytometry response variables included the fixed effect of treatment (MAINT *vs.* HG), semen (fresh *vs*. frozen), and the interaction between treatment and semen. In addition, models for these response variables included the random effect of sire. Variables of VCL, VAP, and VSL collected by CASA were analyzed using the MIXED procedure and statistical models included the fixed effect of treatment (MAINT *vs.* HG), semen (fresh *vs.* frozen), and the interaction between treatment and semen.

Oocyte cleavage and blastocyst development were analyzed using the GLIMMIX procedure in SAS with the fixed effects of treatment (MAINT *vs.* HG), experimental replicate, and the interaction between treatment and replicate. The model accounted for the random effect of bull nested within treatment. Blastocyst gene expression and cell count data were analyzed with the MIXED procedure and included the fixed effects of treatment (MAINT *vs.* HG), experimental replicate, and the interaction between treatment and replicate.

Average velocity path and gene expression responses failed to meet the assumptions of normality and natural log transformations were performed. For all analyses, statistical significance was established at ($P \leq 0.05$), while a tendency was identified as ($P > 0.05$ and ≤ 0.10). Data are reported as least squares means and standard error of the means.

Results

High Gain Diet Increased Growth and Adiposity of Bulls

Body weight, subcutaneous fat thickness, and average daily gain (d -7 to d 74) were greater ($P \leq 0.02$) in HG bulls compared to MAINT bulls on d 74 (**Table 2-2**). Body

weight was 142.4 kg greater in HG bull compared to MAINT bulls, while subcutaneous fat thickness measured at the 12th rib was increased in HG bulls by 6.6 mm compared to MAINT bulls. Average daily gain from d -7 to d 74 was 1.95 kg/d greater in HG bulls compared to MAINT bulls. Rump fat thickness tended (P = 0.08) to be greater in HG bulls by 12.2 mm compared to MAINT bulls. These data indicate that the HG bulls had increased body weight and adiposity compared to MAINT bulls after the 74 d dietary intervention.

High Gain Diet Had Minimal Effect on Spermatozoa Parameters

Semen collected on d 71 and d 74 was analyzed by CASA and flow cytometry before and after cryopreservation. Overall, cryopreservation of sperm reduced total motility, progressive motility, VCL, and VSL and increased the proportion of immotile sperm ($P \leq 0.02$) (**Table 2-3**). Additionally, cryopreservation decreased the proportion of viable sperm ($P < 0.01$), membrane intact sperm ($P < 0.01$), and necrotic sperm ($P < 0.01$), while increasing the proportion of apoptotic sperm ($P < 0.01$) (**Table 2-3**). A treatment by semen interaction (P = 0.02) was observed for the percentage of sperm with acrosome damage (**Figure 2-2A**), where frozen-thawed semen of HG bulls had greater acrosome damage compared with fresh semen of HG bulls and frozen-thawed semen of MAINT bulls. In addition, semen of HG bulls tended (P = 0.06) to have greater acrosome damage compared with fresh semen of MAINT bulls. Bulls in the HG group tended (P = 0.09) to have an increased proportion of early apoptotic sperm compared with MAINT bulls regardless of cryopreservation (**Figure 2-2B**). There was a tendency (P = 0.09) for an interaction between treatment and semen type for the percentage of viable sperm; however, there was no difference (P = 0.14) in the percentage of viable sperm when comparing frozen-thawed semen of HG and MAINT bulls (**Figure 2-2C**).

There was no effect of diet on any response variables associated with sperm morphology of fresh semen (P = 0.40; **Table 2-4**).

Bulls Fed a High Gain Diet Have Reduced Capacity to Develop Blastocyst Stage Embryos After In Vitro Fertilization and Embryo Culture

Frozen-thawed semen was utilized for in vitro fertilization and culture of bovine oocytes. There was no effect of diet (P = 0.94) on the proportion of oocytes that were cleaved by d 3 (MAINT: 70.2 ± 5.4% *vs.* HG: 66.0 ± 5.8%; **Figure 2-3A**); however, there was an effect of replicate (P < 0.01) and an interaction between treatment and replicate (P < 0.01) on the proportion of oocytes that were cleaved by d 3. Semen of HG bulls tended to reduce the proportion of oocytes that developed to the blastocyst stage (P = 0.07) from 16.3 ± 2.2% in the MAINT group to 10.5 ± 1.6% in the HG group (**Figure 2-3B**); however, there was an effect of replicate (P < 0.01) but no interaction between treatment and replicate (P = 0.56) for the proportion of oocytes that developed to the blastocyst stage. Semen from HG bulls reduced (P = 0.01) the proportion of cleaved embryos to develop to the blastocyst stage, from 23.8 ± 1.7% in the MAINT group to 16.2 ± 1.4% in the HG group (**Figure 2-3C**). There was an effect of replicate (P < 0.01), and a tendency for an interaction between treatment and replicate (P = 0.06) for the proportion of cleaved embryos to develop to the blastocyst stage. The capacity for individual bulls to produce cleaved embryos and blastocyst stage embryos in each of the four replicates is shown in Fig. 2. Three individual replicates had very low cleavage rates, as such any replicate with a cleavage rate below 55% was removed from a secondary analysis (highlighted as red circles in **Figure 2-3**). The secondary analysis also demonstrated that semen from HG bulls had no effect on the proportion of oocytes that were cleaved by d 3 (73.5 ± 3.0% *vs.* HG: 73.20 ± 3.0%; P > 0.05) but did reduce

the proportion of oocytes that developed to the blastocyst stage (17.2 ± 1.5% *vs.* 12.2 ± 1.2%; $P = 0.04$), and the proportion of cleaved embryos to develop to the blastocyst stage (23.9 ± 1.6% *vs.* 17.1 ± 1.4%; $P = 0.01$) compared to semen from MAINT bulls.

Semen of Bulls Fed a High Gain Diet Does Not Affect Blastocyst Cell Allocation or Expression of Genes Associated with Blastocyst Quality

To evaluate if paternal diet influenced the allocation of cells to the trophectoderm or inner cell mass of blastocysts (**Figure 2-4**), regular and expanded blastocysts were evaluated at d 7.5 for the total number of blastomeres and the proportion of cells that were CDX2 positive (trophectoderm) or CDX2 negative (inner cell mass). Paternal diet had no effect on the total number of cells ($P = 0.27$) (**Figure 2-4A**), trophectoderm cells ($P = 0.20$) (**Figure 2-4B)**, inner cell mass cells ($P = 0.75$) (**Figure 2-4C**) or the ratio of trophectoderm to inner cell mass cells in blastocysts ($P = 0.19$) (**Figure 2-D**). There was no effect of replicate or the interaction between treatment and replicate ($P \geq 0.22$). Representative images of blastocysts from each treatment are depicted in **Figure 2-4E**.

To determine if paternal diet affected blastocyst expression of mRNA transcripts associated with blastocyst quality, d 7 regular and expanded blastocysts were analyzed for the expression of *DNMT3A, HSP1A1, IFNT2, IGF2R, SLC2A1, PTGS2* (**Figure 2-5**)(Tesfaye et al., 2004, Sagirkaya et al., 2006). While all transcripts were detected in each pool of blastocysts, there was no effect of paternal diet ($P \geq 0.21$), replicate ($P \geq 0.62$), or treatment by replicate interaction ($P \geq 0.14$) on blastocyst mRNA expression of any target genes analyzed.

Discussion

Fertility in cattle is multifactorial with the majority of research focused on the female to improve gamete, uterine, placental, and endocrine physiology; however, the

contribution of the sire to fertility requires a greater research focus to improve cattle reproduction. Temporary undernutrition of bulls reduces fertility (Mwansa and Makarechian, 1991) and is commonly observed during the breeding season in pasture-based systems where bulls can lose 10-15% of their body weight (Hersom and Thrift, 2009, Harrison et al., 2022). Conversely, bulls used for artificial insemination and live cover are often fed highly anabolic diets to emphasize growth related traits which are desirable to beef cattle producers (Harrison et al., 2022). Cattle fed high energy diets during the prepubertal period hasten the onset of puberty and increase availability of saleable semen (Byrne et al., 2018); however, obesity is associated with male infertility in humans and rodents (Kort et al., 2006, Campbell et al., 2015). The ramifications of a high gain diet on bull fertility remain unclear. Here, I hypothesized that feeding a high gain diet to mature bulls would reduce the fertility of sperm used for in vitro fertilization and embryo culture. Providing bulls with the high gain diet described here for 74 d effectively increased body weight, average daily gain and fat deposition compared with bulls fed a maintenance diet. There were no differences in sperm cell quality parameters related to kinematics as evaluated by CASA or morphology because of a high gain diet. The most significant changes to sperm cell membrane integrity as assessed by flow cytometry were caused by cryopreservation. Bulls fed a high gain diet did however produce 28.3% fewer blastocysts after in vitro fertilization and embryo culture compared to bulls fed a maintenance diet. In humans, increased male adiposity has been associated with decreased in vitro embryo production and post-transfer clinical pregnancy rates (Yang et al., 2016). Similarly, paternal high fat diets fed to rodents result in decrease cleavage rate, blastocyst rates, and post-transfer pregnancy

success and embryos with fewer inner cell mass and trophectoderm cells (Mitchell et al., 2011, Binder et al., 2012). In the present study, diet did not impact the allocation of either inner cell mass or trophectoderm cells, nor did diet affect blastocyst expression of genes associated with embryo quality. Collectively, these data suggest that exposing bulls to highly anabolic conditions induces changes to sperm biology and function that reduces the capacity of embryos to develop to the blastocyst stage in the absence of overt sperm cell defects, thus implying other molecular mechanisms by which paternal diet impacts embryo development.

Complete spermatogenesis from spermatogonium to spermatozoa in the bull requires 61 d, plus an approximate 10 d for epididymal transport and maturation (reviewed by Staub and Johnson)(Staub and Johnson, 2018). The dietary intervention utilized here lasted for a total of 74 d including a 7 d adaptation period, suggesting that any effect of paternal diet on sperm cells would encompass the entirety of spermatogenesis from meiosis to cellular differentiation. Intriguingly we did not observe any effects of paternal diet on sperm parameters including motility, morphology or fertilization capacity which suggests that the reduced blastocyst development is likely caused by molecular perturbations in sperm. Paternal diabetes results in reduced fertilization and blastocyst formation rates, attributed to alterations in sperm cell motility, testicular steroidogenesis, and expression of glucose transporter *SLC2A* (Kim and Moley, 2008*)*. Sperm cells collected from mice fed a high fat diet have increased reactive oxygen species, DNA damage, and reduced ability to undergo capacitation (Bakos et al., 2011). Additionally, paternal obesity contributes to dysregulated gene expression and DNA methylation patterns of resultant placenta when compared to

normal weight males (Mitchell et al., 2017). These data indicate that sperm cell epigenetic markers may be inappropriately changed because of paternal diet and could contribute to hindered embryonic development (Dobbs et al., 2013, Graf et al., 2014). Embryonic genome activation in cattle occurs at the 4-cell stage of development. Due to the observed reduction in blastocyst development and unaffected cleavage rates, it is reasonable to assume that the reduced embryo development observed may be associated with intrinsic sperm factor required after embryonic genome activation, such as the paternal epigenome or RNA. Heritability of paternal traits via non-genomic mechanisms was first described by Ng et al., when rats fed a paternal high fat diet programed the development of β-cell dysfunction in female offspring (Ng et al., 2010). Similarly, a high fat paternal diet in mice alters the expression of sperm transfer RNA-derived small RNAs (tsRNAs) that could program metabolic disorders in offspring when transferred to normal zygotes, emphasizing the non-genomic capacity of sperm to transmit heritable information to the embryo (Chen et al., 2016). The programing capacity of sperm from bulls fed a high gain diet is yet to be determined.

Fertilization occurs in more than 80% of both beef and dairy cattle after artificial insemination; however, post-fertilization developmental failure occurs in approximately 20% of pregnancies prior to d 4 of gestation (Santos et al., 2004, Wiltbank et al., 2016, Ealy and Seekford, 2019, Reese et al., 2020). Much of these early pregnancy losses have been attributed to complications in female physiology, with little emphasis on the paternal contributions to embryo development. Most dairy bulls used for artificial insemination have long pedigrees of fertility, are genomically screened for fertility traits and have robust field data to support fertility. Indeed, sire conception rate (the

probability of pregnancy from a bull compared to the average of all bulls) has been associated with in vitro and in vivo embryo production (Ward et al., 2001, Ward et al., 2002, Barceló-Fimbres et al., 2011, Ortega et al., 2018), indicating an association between field fertility phenotype and early embryonic development. Bulls used for live cover in the beef industry, however, are generally only subjected to qualitative assessment through a breeding soundness examination which estimates a bull's potential for reproduction, incorporating metrics such as sperm concentration, subjective gross motility estimates, scrotal circumference, and sperm morphology defects (Hopkins and Spitzer, 1997). None of these fertility estimates account for environmental factors that could impact fertility, such as exposure to toxicants, disease, body condition or diet. Indeed, the sperm of high gain diets in this study had sperm characteristics that would pass a traditional breeding soundness exam albeit having lower fertility in the in vitro fertilization system.

Various models have been employed to understand the contribution of the male to fertility in cattle and rodents. Androgenetic rodent embryos in which the female pronucleus is replaced by a second male pronucleus result in embryos that form a relatively normal placenta, while parthenogenetic embryos containing two female pronuclei form severely compromised placenta (Surani et al., 1986). Similarly in the bovine, parthenogenetic embryos produce a trophectoderm that expresses less *IFNT2* when compared to in vivo derived embryos on d 20 of gestation (Hirayama et al., 2014). This suggests that in the mouse and bovine, the paternal genome is critical in placental function and is likely regulated at the level of the epigenome. Furthermore, blastocysts produced by obese male mice have a reduced number of inner cell mass and

trophectoderm cells, and impaired placental growth (Mitchell et al., 2011, Binder et al., 2012). In the present study, I did not observe a difference in the number of inner cell mass, trophectoderm cells or gene expression of *IFNT2* in blastocysts derived from bulls fed a high gain diet. The effect of paternal diet on the capacity of the trophectoderm to secrete interferon tau and other pregnancy associated molecules later in gestation requires further investigation.

The model employed here used dietary manipulation of mature bulls that had already progressed through puberty and completed growth. Future investigations of dietary intervention in bulls should consider the implications of feeding a high gain diet to young, growing bulls before puberty when the testis may be more vulnerable to environmental influences. In addition, the mechanisms regarding the reduced blastocyst development after fertilization require significant investigation. It is likely that the epigenome is affected in sperm of bulls fed a high gain diet, and the extent to which this phenotype could be reversed by restricting dietary intake of bulls warrants further study. Finally, the field fertility of bulls fed a high gain diet must be evaluated. While in vitro fertilization is a proxy for bull fertility, the capacity of sperm to generate a pregnancy and produce live, healthy calves is the gold standard required to state that paternal high gain diet influences fertility.

In conclusion, a high gain diet fed to mature bulls for 74 days reduces the development of blastocysts following in vitro fertilization in the absence of overt sperm defects. These data demonstrate that paternal nutrition influences preimplantation embryonic development by non-genomic mechanisms and may contribute to the fertility of bulls used in the cattle industry.

Acknowledgements of Chapter 2

Sincere appreciation is expressed to the Eatonton Beef Research Farm personnel and the collaborators from the University of Georgia for their assistance with sample collection.

Table 2-1. Primer sequences used for real-time RT-PCR.

Gene Symbol	Primer sequence	Accession number
DNMT3A	5’ – CCATGTACCGCAAGGCTATCTA	XM_024998.68.1
	3’ – CCTGTCATGGCACATTGGAA	
GAPDH	5’ – AGGTCGGAGTGAACGGATTC	NM_001034034.2
	3’ – ATGGCGACGATGTCCACTTT	
HSPA1A	5’ – GACAAGTGCCAGGAGGTGATTT	NM_203322.3
	3’ – CAGTCTGCTGATGATGGGGTTA	
IFNT2	5’ – TCCATGAGATGCTCCAGCAGT	NM_001015511.4
	3’ – TGTTGGAGCCCAGTGCAGA	
IGF2R	5’ – CAGGTCTTGCAACTGGTGTATGA	NM_174352.2
	3’ – TTGTCCAGGGAGATCAGCATG	
PTGS2	5’ – CGTGAAAGGCTGTCCCTTTA	NM_001105323.1
	3’ – ATCTAGTCCAGAGTGGGAAGAG	
RPL19	5’ – ATGCCAACTCCCGCCAGCAGAT	NM_001040516.2
	3’ – TGTTTTTCCGGCATCGAGCCCG	
SDHA	5’ – GGAACACTGACCTGGTGGAG	NM_174178.2
	3’ – GGAACACTGACCTGGTGGAG	
SLC2A1	5’ – AGCGTCATCTTCATCCCAGC	NM_174602.2
	3’ – AGCTTCTTCAGCACGCTCTT	

Table 2-2. Body weight and carcass ultrasound of bulls fed a high gain diet[1].

	MAINT	HG	SEM	*P*-value
Body weight, kg				
Day -7	951.7	935.8	42.4	0.80
Day 28	956.5	982.0	38.1	0.65
Day 43	929.3	1,009.3	34.8	0.16
Day 74	953.0	1,095.4	34.2	0.02
ADG, kg/d[2]	0.02	1.97	0.15	< 0.01
SC fat[3], mm				
Day -7	3.8	4.6	1.0	0.54
Day 74	4.1	10.7	1.5	< 0.01
Rump fat, mm				
Day -7	4.1	6.4	2.0	0.46
Day 74	4.1	16.3	4.1	0.08
Intramuscular fat, %				
Day -7	3.48	3.72	0.30	0.54
Day 74	2.96	3.50	0.39	0.36
Ribeye area, cm^2				
Day -7	110.1	106.1	4.45	0.54
Day 74	119.9	131.2	7.94	0.35

[1]Bulls were fed a maintenance (MAINT) diet or high-gain (HG) diet for 67 d after a 7 d adaptation period.
[2]Average daily gain (ADG).
[3]Subcutaneous fat (SC)

Table 2-3. Impact of treatment on computer assisted sperm analyses and flow cytometry response variables for fresh and frozen-thawed semen[1].

	MAINT		HG			*P*-value		
	Fresh	Frozen	Fresh	Frozen	SEM	Diet	Semen[2]	Diet×Semen
Total motility, %	73.81	29.98	72.60	21.15	8.32	0.63	< 0.01	0.39
Progressive motility, %	71.58	24.39	67.38	16.28	8.58	0.53	< 0.01	0.51
Local motility, %	3.65	5.16	5.13	4.96	0.75	0.75	0.35	0.26
Immotile, %	24.66	70.13	27.37	78.88	8.23	0.58	< 0.01	0.46
VCL[3], µm/s	134.56	90.84	130.79	84.96	10.63	0.72	< 0.01	0.90
VAP[4], µm/s	5.97	3.94	4.23	3.91	0.89	0.36	0.24	0.37
VSL[5], µm/s	46.04	37.42	45.55	38.14	2.84	0.97	0.02	0.83
Membrane intact sperm, %	69.69	32.31	56.62	33.60	8.77	0.59	< 0.01	0.26
Necrotic sperm, %	0.41	0.20	0.40	0.17	0.10	0.79	< 0.01	0.72
Apoptotic sperm, %	13.18	33.18	5.23	25.05	6.99	0.17	< 0.01	0.36

[1]Bulls were fed a maintenance (MAINT) diet or high-gain (HG) diet for 67 d after a 7 d adaptation period and semen parameters were evaluated in semen collected on d 71 and 74.
[2]Parameters were evaluated in fresh semen or cryopreserved semen after thawing.
[3]Curvilinear velocity (VCL).
[4]Average velocity path (VAP).
[5]Straight-line velocity (VSL).

Table 2-4. Effect of treatment[1] on fresh sperm morphology[1,2].

	MAINT	HG	SEM	*P*-value
Normal morphology, %	68.81	75.30	5.20	0.40
Proximal droplet, %	2.30	2.26	0.99	0.57
Head defect, %	7.49	8.02	0.01	0.79
Midpiece defect, %	1.19	0.75	0.55	0.59
Acrosome defect, %	0.74	0.53	0.16	0.54
Coiled tail, %	5.24	4.09	1.63	0.62
Kinked tail, %	10.20	7.09	0.03	0.45
Detached head, %	4.08	3.09	1.56	0.63

[1]Bulls were fed a maintenance (MAINT) diet or high-gain (HG) diet for 67 d after a 7 d adaptation period.
[2]Sperm morphology analyses were performed in fresh semen from two separate collections and the average of the collections was utilized as estimate for each bull.

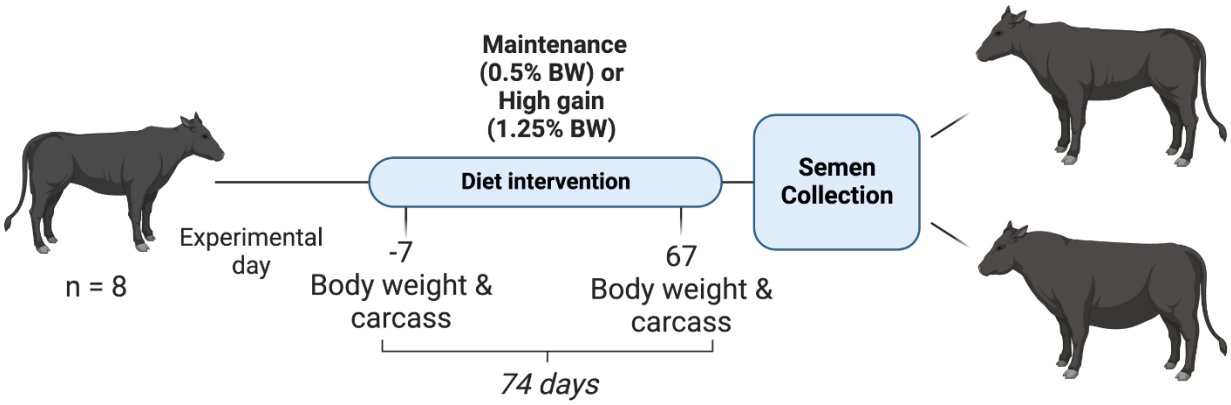

Figure 2-1. Experimental model. Mature Angus and Hereford bulls (n = 8) were stratified by breed, age, and body weight, and randomly assigned to either a high gain diet designed to achieve an average daily gain of 1.38 kg/day, or a maintenance (MAINT) diet designed to maintain body weight. Bulls in both treatments were fed the same diet at different inclusion rates and had access to Bermuda grass hay ad libitum. Bulls were housed in individual pens to monitor individual daily feed intake. An acclimation period began on d -7 and starting on day 0, daily dietary offerings were incrementally increased for 7 days. After the end of the adaptation period (d 7), maintenance bulls received 0.5% of their body weight per day and high gain bulls received 1.25% of their body weight per day for an additional 67 days providing a total divergent feeding regiment of 74 days.

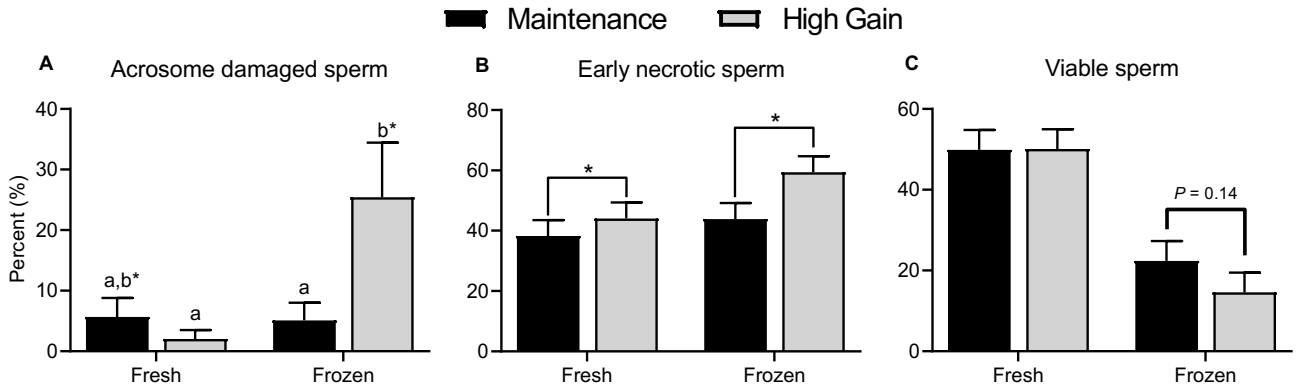

Figure 2-2. Dietary intervention influenced sperm quality. Ejaculated spermatozoa of bulls fed either a maintenance (n = 4) or high (n = 4) diet were analyzed using flow cytometry and evaluated for acrosomal integrity (A), early necrosis (B), and viability (C). Sperm were evaluated fresh or after cryopreservation and thawing (frozen). Data are presented as the least squares means ± SEM. Different superscript indicate statistical difference ($P < 0.05$) and different symbols indicate a tendency ($P < 0.10$) between high gain diet compared to control. (A) Diet: $P = 0.62$, cryopreservation: $P = 0.02$, and diet × cryopreservation: $P = 0.02$. (B) Diet: $P = 0.09$, cryopreservation: $P = 0.09$, and diet × cryopreservation: $P = 0.41$. (C) diet: $P = 0.43$, cryopreservation: $P < 0.01$, and diet × cryopreservation: $P = 0.09$.

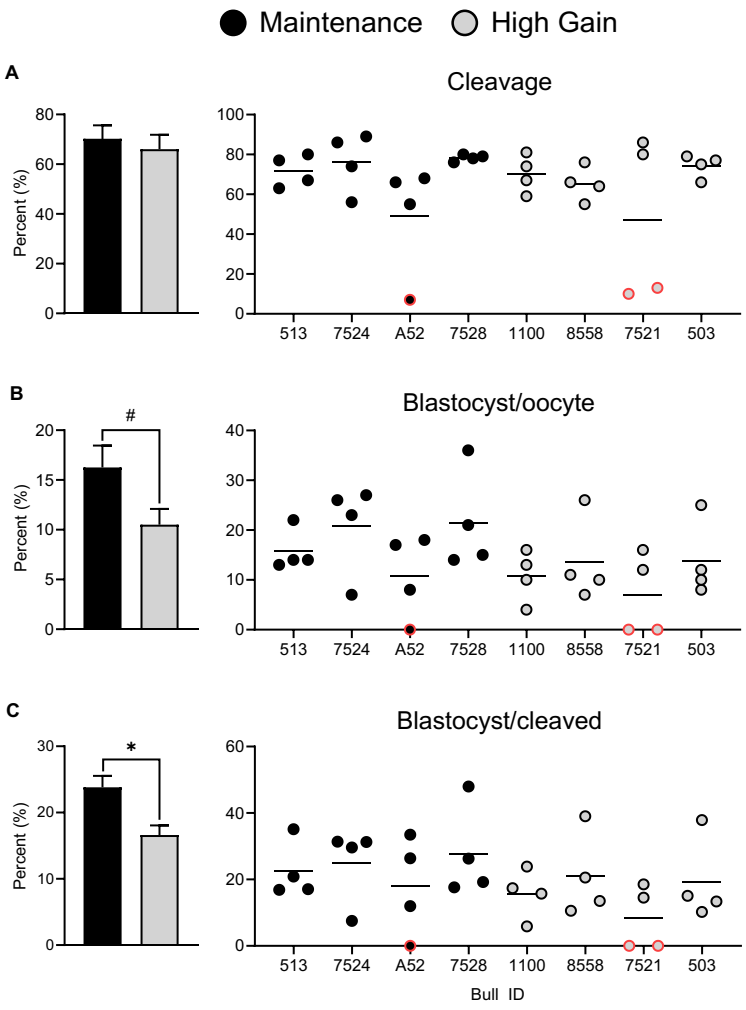

Figure 2-3. Effect of sire diet on IVF outcomes. Oocytes were fertilized in vitro with semen of bulls fed either a maintenance (n = 4) or high gain (n = 4) diet. Zygote cleavage was assessed at day 3 post-fertilization (A). The percent of oocytes (B) and cleaved oocytes (C) to form blastocysts were analyzed at d 7.5 post-fertilization. Data are presented as the least square means ± SEM for bar graphs. Individual data points represent the percentage of oocytes undergoing cleavage and forming blastocysts stratified by each sire. Individual replicates highlighted in red had cleavage less than 55% and were excluded from a secondary analysis described in the text. * indicates $P < 0.05$ and # indicates $P < 0.10$.

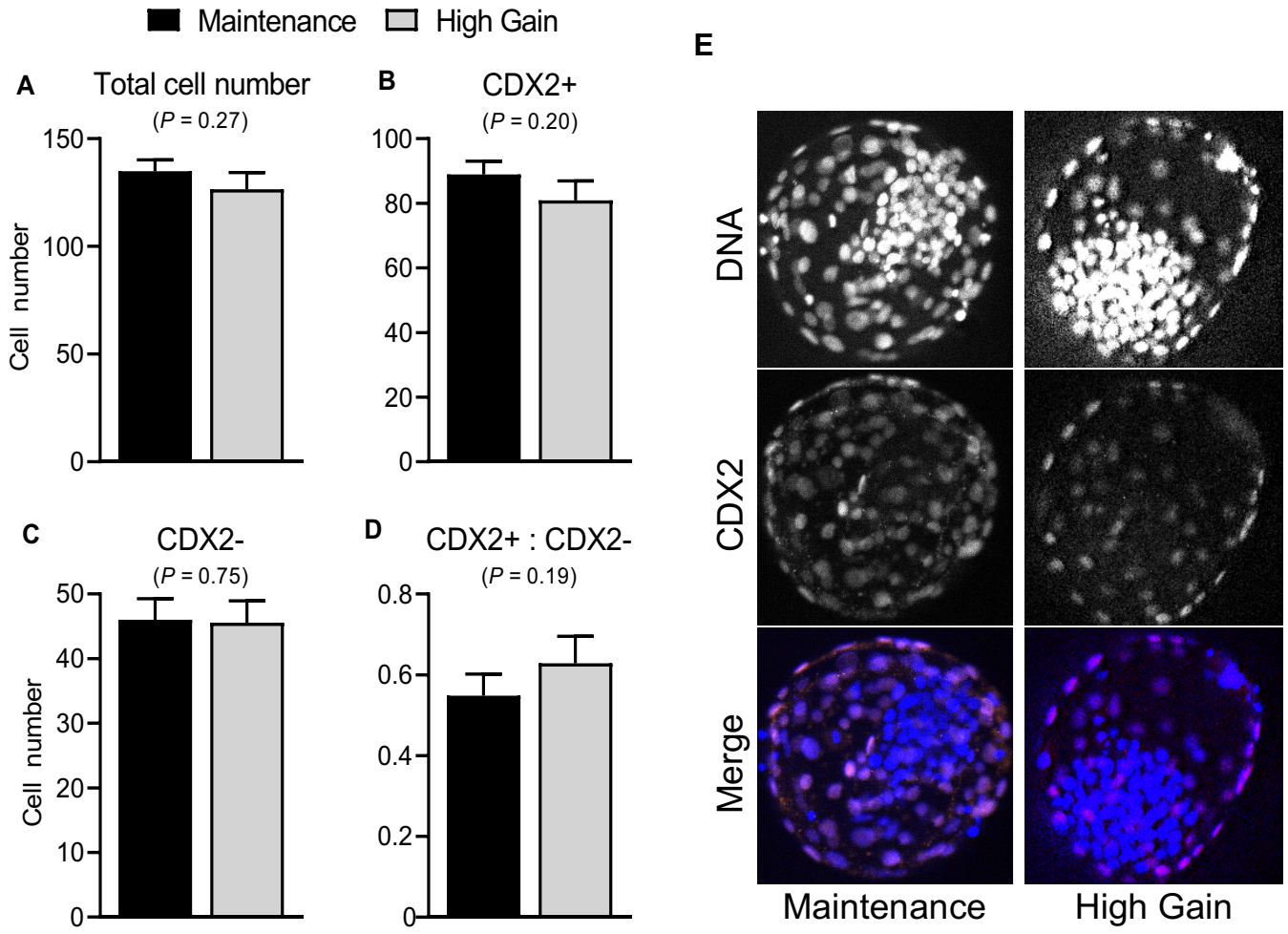

Figure 2-4. Effect of sire diet on IVF-derived blastocyst cell number. Oocytes were fertilized in vitro with semen of bulls fed either a maintenance (n = 4) or high-gain (n = 4) diet and blastocysts were evaluated for cell lineage allocation. The number of total (A), CDX2-positive (B), CDX2-negative (C) cells, and ratio of CDX2 positive to CDX2 negative cells (D) were determined by immunocytochemistry. Data are presented as least square mean ± SEM. A total of 21–23 blastocysts were evaluated per treatment representing all eight bulls. Representative images (E) of DNA, CDX2 and a merge (blue = DNA; red = CDX2) of blastocysts sired by maintenance or high gain diet bulls.

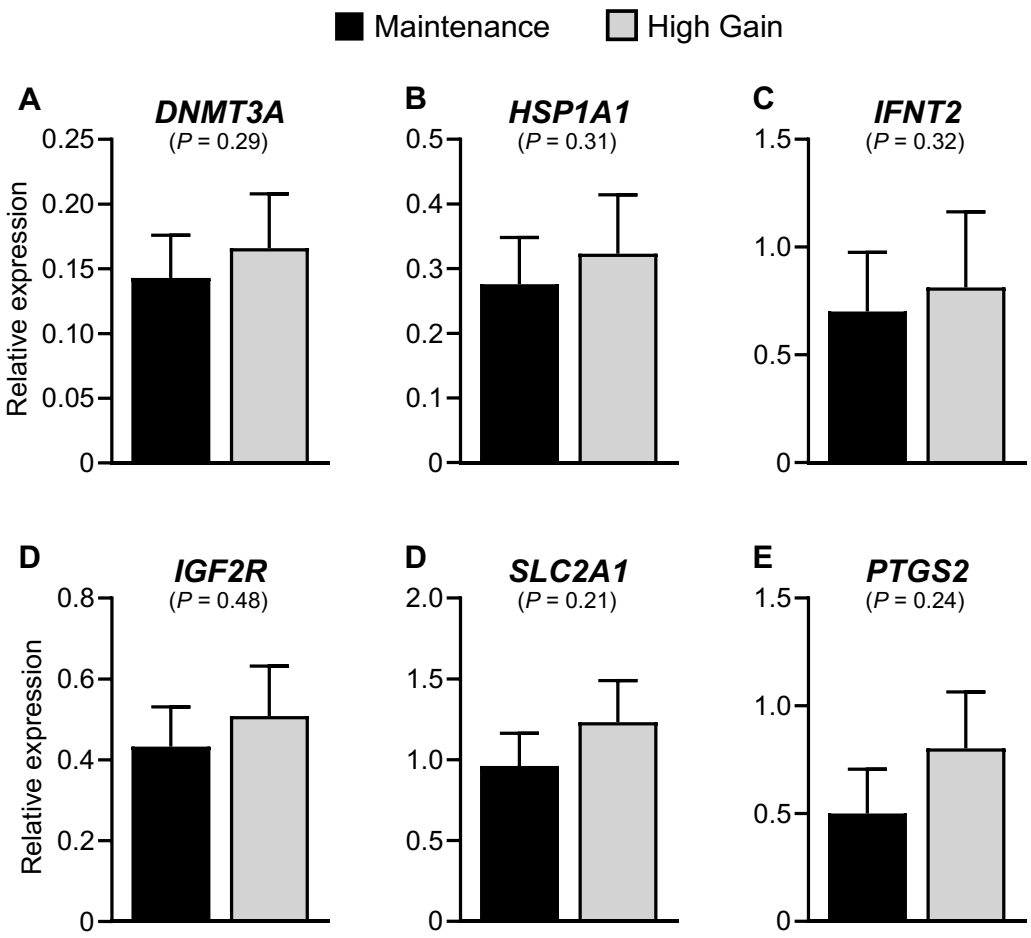

Figure 2-5. Effect of sire diet on IVF-derived blastocyst gene expression. Oocytes were fertilized in vitro with semen of bulls fed either a maintenance (n=4) or high-gain (n=4) diet and blastocyst expression of *DNTM3A* (A), *HSPA1A* (B), *IFNT2* (C), *IGF2R* (D), *SLC2A1* (E), and *PTGS2* (F) was evaluated by real time RT-PCR. Data are presented as least square mean ± SEM relative expression to the geometric mean of reference genes (*GAPDH*, *SDHA*, and *RPL19*). Each bar represents the relative gene expression from each bull in four individual IVF replicates.

CHAPTER 3
BOVINE UTERINE DISEASE IS ASSOCIATED WITH SHORT- AND LONG-TERM PERTURBATIONS TO OVARIAN FUNCTION

Summary

The objective of these studies was to investigate the effects of uterine diseases on contemporaneous and long-term ovarian dynamics and function in dairy cows. Two approaches were taken to test the hypothesis that uterine disease results in altered ovarian function. Study 1 investigated the effects of uterine disease on contemporaneous follicle and corpus luteum growth and function. Uterine health status was assessed in 17 ovulatory, primiparous, lactating Holstein cows on d 4, 7, 14, 21, and 28 postpartum by observing vaginal discharge. Animals were categorized as having uterine disease ≤ 14 d postpartum (metritis) or ≥ 15 d postpartum (endometritis). Blood collection and transrectal ultrasonography were performed daily from postpartum d 7 to 26 to evaluate estradiol and progesterone, and the size of the largest follicle and subsequent corpus luteum. There was no association between metritis or endometritis on the day of ovulation or the diameter of the preovulatory follicle. Metritis was associated with reduced follicle growth from postpartum d 7 to 16 (P = 0.002) and tended to reduce plasma estradiol concentrations (P = 0.062) compared to cows without metritis. Metritis was not associated with reduced growth of the subsequent corpus luteum from postpartum d 17 to 26 but was associated with reduce plasma progesterone (P = 0.026). Endometritis was associated with reduced corpus luteum growth (P = 0.005) from postpartum d 17 to 26 but was not associated with reduced plasma progesterone compared to cows without endometritis. Endometritis was not associated with reduced follicular growth or peripheral estradiol from d 7 to 16 postpartum. This study suggests that uterine disease is associated with

contemporaneous ovarian function, whereby the ovarian structure present at the time of disease is affected. To test the long-term effects of uterine disease on later corpus luteum function, study 2 utilized twenty-three primiparous, non-lactating, Holstein cows that received an intrauterine infusion of either pathogenic *Escherichia coli* and *Trueperella pyogenes* or saline as a control. Estrus cycles were synchronized and corpora lutea were recovered at d 16 of the estrous cycle, 146 d after infection. Gene expression for 94 genes related to corpus luteum function were analyzed by RT-PCR. Despite no effect of uterine infection on circulating progesterone 146 d after infection, genes associated with the steroid synthesis pathway (*CYP17A1, HSD3B1*), lipid metabolism (*ACAT1*), and immune function (*NCF1* and *TLR9)* were differentially expressed long after bacterial infection compared to controls. Combined, these studies suggest that uterine diseases effect contemporaneous ovarian function at the time of infection and may cause alterations to the future endocrine capacity of the ovary even after disease resolution.

Introduction

Shortly following parturition, the uterus of lactating dairy cows is exposed to a broad range of bacterial species (Galvão et al., 2019). While most cows can tolerate the presence of these bacteria, nearly 40% cows will develop uterine diseases such as metritis and endometritis (Sheldon and Dobson, 2004, LeBlanc, 2012). Uterine diseases can be characterized both by the presentation of symptoms and the time in which symptoms occur postpartum (Sheldon et al., 2006). Metritis is associated with significant financial losses for dairy herds attributed to reduced milk production, reproductive performance, and animal survival in the herd (Pérez-Báez et al., 2021).

Indeed, the reproductive performance of cows after the resolution of uterine disease is reduced compared to cows without uterine disease (Ribeiro et al., 2016). While the mechanisms of reduced reproductive performance are not clearly defined, they likely include alterations to endometrial function, hypothalamic-pituitary signaling and ovarian function.

Uterine disease or uterine infection reduces follicular growth, estradiol secretion, luteal size and circulating progesterone in the first estrous cycle following parturition (Sheldon et al., 2002, Williams et al., 2007, Williams et al., 2008, Strüve et al., 2013). Accumulation of lipopolysaccharide (LPS) in follicular fluid is positively associated with the degree of uterine inflammation in dairy cows (Herath et al., 2007), and granulosa cells express all 10 Toll like receptors that recognize pathogen associated molecular patterns, including LPS (Williams et al., 2008, Price et al., 2013). In the presence of LPS, granulosa cells initiate an innate inflammatory response, increase the synthesis of cytokines, chemokines and alter prostaglandin production. In addition, exposure of granulosa cells to LPS reduces the secretion of estradiol, likely due to a reduced expression of *CYP19A1* required for steroid synthesis (Herath et al., 2007, Williams et al., 2008, Price et al., 2013, Dickson et al., 2022b). Surprisingly, the transcriptome of granulosa cells, endometrial cells and oviduct cells are all altered three months after intrauterine infusion of pathogenic bacterial, suggesting long-term alterations to the reproductive tract that may be responsible for reduced fertility observed in cows after the resolution disease (Horlock et al., 2020). The effects of uterine disease on the function of the corpus luteum are less clear. Progesterone concentrations following artificial insemination are reduced in cows diagnosed with any prior clinical disease

including uterine disease or purulent vaginal discharge (Bruinjé et al., 2023). Repeated intrauterine infusion of LPS from the time of ovulation for 9 d reduced the size of the subsequent corpus luteum and peripheral progesterone, and altered the luteal expression of *STAR*, *HSD3B*, and *PGFR* required for progesterone synthesis (Lüttgenau et al., 2016a). Conversely, others have shown that prior endometritis does not alter peripheral progesterone following insemination (Molina-Coto et al., 2020).

The present study utilized two approaches to interrogate 1) the contemporaneous effects of metritis or endometritis on ovarian dynamics following parturition; and 2) the long-term effects of intrauterine infusion of bacteria on corpus luteum gene expression. It was hypothesized that uterine disease would 1) perturb ovarian dynamics resulting in reduced follicle and corpus luteum size and function coincident with disease, and that 2) intrauterine infusion of bacteria would alter corpus luteum gene expression five months later. Data presented here show that the size and function of the follicle and corpus luteum are perturbed at the time of uterine disease, and that intrauterine infusion of bacteria alters the expression of corpus luteum genes five months later.

Materials and Methods

Ethics Statement

All procedures utilized for these studies were approved by the University of Florida Institutional Animal Care and Use Committee under protocol numbers 202111389 and 201508884 and performed at the University of Florida Dairy Research Unit. Study 1 was conducted from June to October 2021 and study 2 was conducted from February to August 2018.

Study 1 Design: Assessing the Association Between Spontaneous Postpartum Uterine Disease and First Estrous Cycle Ovarian Function

A total of 47 primiparous, lactating Holstein cows were enrolled in this study. The study was designed as a prospective case-control study whereby all primiparous animals were enrolled at d 4 postpartum. Individuals were designated as having uterine disease or no uterine disease within a given period after calving. Between 0600 and 1100 h on d 4, 7, and 10 postpartum, animals were evaluated for ketosis, displaced abomasum, or retained placenta and positive animals were excluded from the study. Cows diagnosed with clinical metritis (fetid, watery, red-brown vaginal discharge) in the first 14 days postpartum received a subcutaneous injection of EXCEDE Ceftiofur crystalline free acid sterile suspension (Zoetis Animal Health, Parsippany, NJ, USA) at 6.6 mg/kg of body weight in the posterior aspect of the ear, followed by a second treatment 72 h after diagnosis. On d 4, 7, 14, 21, and 28 postpartum, rectal temperature, vaginal discharge, and body condition (1-5 scale) was evaluated. Vaginal mucus was assessed using an intravaginal device (Metricheck, Simcro, Hamilton New Zealand). Vaginal mucus was scored using a 5-point scale (0 = clear mucus or lochia; 1 = clear mucus or lochia with flecks of pus; 2 = mucopurulent discharge with < 50% pus; 3 = mucopurulent discharge with > 50% pus; 4 = watery, red or brown, and fetid discharge) and collected in 7 mL polystyrene Bijou containers (Thermo Fisher Scientific, Waltham, MA) and stored at -20°C (Sheldon et al., 2006). Cows were categorized as having metritis (n = 21) or no metritis (n = 26) when presenting a vaginal mucus score of 4 on days 4, 7, or 14 postpartum, and/or as having endometritis (n = 19) or no endometritis (n = 28) when presenting a vaginal mucus score of 3 or 4 on d 21 or 28 postpartum (**Figure 3-1A**).

From d 7 to d 26 postpartum, ovarian structures of each cow were assessed daily with an Ibex EVO ultrasound and linear 5-9 MHz multifrequency transducer (E.I. Medical Imaging, Loveland, CO, USA) (Williams et al., 2007). The largest follicle and corpus luteum size were measured by averaging two measurements of maximal cross-sectional length and recorded for both ovaries. Ovulation was defined as the time when a large dominant follicle was replaced with a CL on the following day. Cows were defined as anovulatory and excluded from analysis when repeated follicle growth and regression with no corpus luteum formation occurred throughout the 21-d observation period. Cows were defined as cystic and excluded from analysis when a large anovulatory follicular structure exceeded 25 mm in diameter and persisted for more than 10 d (Kesler and Garverick, 1982). Ovulatory cows were categorized as having metritis (n = 9) or no metritis (n = 8) when presenting a vaginal mucus score of 4 on days 4, 7, or 14 postpartum, and/or as having endometritis (n = 10) or no endometritis (n = 7) when presenting a vaginal mucus score of 3 or 4 on d 21 or 28 postpartum.

Blood was collected daily from d 7 to d 26 postpartum via coccygeal venipuncture into evacuated tubes containing lithium heparin (Vacutainer; 9 mL, Becton Dickinson, Franklin Lakes, NJ) and placed immediately on ice. Whole blood was centrifuged at 2,400 × *g* at room temperature to collect plasma that was aliquoted and stored at -20ºC. Plasma estradiol was measured by radioimmunoassay following ether extraction using antibody and ^{125}I-estradiol tracer from MP Biomedicals (Santa Ana, CA, USA) as previously described (Kirby et al., 1997, Perry et al., 2004). Plasma progesterone and haptoglobin were quantified using commercially available ELISAs according to the manufacturer's instructions (DRG International, Springfield Township,

NJ; Life Diagnostics, West Chester, PA). The coefficient of variations for estradiol, progesterone, and haptoglobin were 8.78%, 10.06%, and 2.79%, respectively.

Study 2 Design: Effects of Induced Endometritis on Long Term Corpus Luteum Function

Methodology and data pertaining to intrauterine infusion and disease progression have been previously reported (Dickson et al., 2020, Dickson et al., 2022a). In brief, estrous cycles of 23 non-lactating primiparous Holstein cows were synchronized prior to intrauterine infusion of vehicle medium (n = 11) or *Escherichia coli* MS499 and *Trueperella pyogenes* MS249 (n = 12) on experimental d 0 (**Figure 3-1B**). On d 110, estrous cycles of cows were synchronized using an Ovsynch protocol using PGF2α (dinoprost tromethamine; Prostamate, Bayer HealthCare, LLC, Animal Health Division, Shawnee Mission, KS) and GnRH (gonadorelin diacetate tetrahydrate; OvaCyst, Bayer), and on d 130 all cows were inseminated with 0.5 mL of commercial Holstein semen (Select Sires, Plain City, OH). Sixteen days after insemination, cows were slaughtered on d 146 and the corpus luteum was dissected with sterile forceps and scissors, maximal diameter was measured using calipers, snap frozen in liquid nitrogen and stored at -80ºC until processed for RNA extraction. No animals had clinical signs of uterine infection at the time of insemination or slaughter. One corpus luteum from the bacteria treatment was lost at the time of slaughter.

Corpus luteum tissue was thawed, resuspended in 350 µL of RLT buffer (Qiagen, Hilden, Germany) and homogenized using 2.8 mm ceramic beads (Qiagen) in a bead beater tissue homogenizer (Precellys 24; Bertin Technologies SAS, Montigny-le-Bretonneux, France). All samples were processed using two cycles of 45 s each at 6,500 rpm with 30 s interval on ice between cycles. Following homogenization, luteal

RNA was extracted using the RNeasy mini kit according to the manufacturer's instructions which included an on-column DNase digestion (Qiagen). Extracted RNA purity and concentration were evaluated using a NanoDrop 2000 spectrophotometer (Thermo Fisher Scientific). Samples had a mean 260/280 and 260/230 ratio of 2.08 ± 0.02 and 1.86 ± 0.40, respectively.

A total of 94 selected genes were quantified using the Fluidigm quantitative PCR microfluidic 96.96 dynamic array device Biomark HD system (Fluidigm Co., San Francisco, CA) and EvaGreen SYBR green chemistry (Bio-Rad, Hercules, CA). All PCR primers were designed by Fluidigm Delta Gene assays and synthesized by Fluidigm (Fluidigm Co.). The constructed gene panel (**Table B-1**) was designed to interrogate various genes associated with steroid synthesis (*CYP11A1, CYP11B1, CYP17A1, CYP19A1, FASN, HSD11B1, HSD17B10, HSD3B1, STAR*), lipid metabolism (*ACAA2, ACACA, ACAT1, ACSL1, CYP3A4, CYP4A11, HADH, POR*), corpus luteum function (*FGF2, GHR, IGF1, IGF2, IGF2R, IGFBP2, PGR*), vascularity (*FLT1, FLT3, VEGFA, VEGFB, VEGFC, VEGFD*), cell cycle (*ATM, CCNB1, CCND2, CCNE1, CDC20, CDK1, CDK2, CDKN1A, CDKN1B, PTEN, SRC, WEE1*), cell signaling (*LHCGR, MAP2K1, MAPK13, PPARA, PPARG, PRKCB, PTGER3, PTGER4, STAT1, STAT3, STAT4*), inflammation/immune signaling (*CD14, CD40, CXCL8, IFNB1, IL12A, IL1A, IL1B, IL4, IL6, IL6R, NCF1, NFKB1, NFKBIA, PTPRC, TLR1, TLR2, TLR4, TLR6, TLR9, TNF*), epigenetics (*DNMT1, DNMT3A, H2AFX, H2AFZ, HDAC1, HDAC8, TET1, TET2*), cell death (*APAF1, BAD, BAX, BCL2, CASP7, CASP9, FOXO3*), and reference genes (*ACTB, ACTA2, GAPDH, RPL19, RPS9* and *YWHAZ*). The geometric mean was calculated using the cycle threshold (Ct) of stably expressed reference genes (*ACTB,*

GAPDH, ACTA2, RPL19, RPS9) and statistical analyses were performed using the delta Ct values (Steibel et al., 2009) and data are presented as relative expression using the $2^{-\Delta Ct}$ method.

Statistical Analysis

All data were analyzed using the SAS statistical package (version 9.4; SAS/STAT, SAS Inst. Inc., Cary, NC, USA). Reproduction, production, day of ovulation, and size of ovulatory follicle data were analyzed with a generalized linear model with the fixed effects of metritis or endometritis. Vaginal mucus score, rectal temperature, haptoglobin, and body condition score were analyzed with a linear mixed model with repeated measures and compound symmetry variance-covariance structure. Fixed effects in the model included metritis, day and the interaction between metritis and day or endometritis, day and the interaction between endometritis and day. Cow within day was repeated in the analysis. Cow was included as a random effect in the model. Ovarian structure and hormone data were analyzed by ANOVA with linear mixed-effects models using the MIXED procedure of SAS. The statistical models included the fixed effects of disease (metritis *vs* no metritis, or endometritis *vs* no endometritis), day postpartum, and the interaction between disease and day. The model also included the random effect of cow nested within corresponding disease. Gene expression data was analyzed by ANOVA with a linear mixed effects model with the fixed effect of treatment and the random effect of cow nested within treatment. All genes failed to meet the assumptions of normality and the delta Ct was log transformed and checked for normality of residuals and homogeneity of variance, analyzed, and back transformed for presentation. For all analyses, statistical significance was established at $P < 0.05$, while

a tendency was identified as $P > 0.05$ and ≤ 0.10. Data are reported as least squares means and standard error of the means.

Results

Enrolled Cow Production, Reproduction, and Health Characteristics

The first objective of Study 1 was to interrogate the descriptive data of all cows (cycling, anovulatory and cystic) initially enrolled in the study (n = 47). Of the 47 cows enrolled in the study, 21.3% had metritis only (n = 10); 25.5% had endometritis only (n = 12); 34.0% had both metritis and endometritis (n = 16); and 19.1% had neither metritis nor endometritis (n = 9). Of cows diagnosed with metritis (n = 26), 46.2% had a vaginal mucus score of 4 on d 4 postpartum (n = 12); 76.9% had a vaginal mucus score of 4 on d 7 postpartum (n = 20); and 30.8% had a vaginal mucus score of 4 on 14 d postpartum (n = 8). Of cows diagnosed with endometritis (n = 28), 78.6% had a vaginal mucus score > 3 on d 21 postpartum (n = 22) and 46.4% had a vaginal mucus score > 3 on d 28 postpartum (n = 13).

There was no association between metritis (**Table 3-1**) or endometritis (**Table 3-2**) on the age at heifer conception, services per heifer conception, age at calving, or gestation length ($P > 0.10$). In the first lactation after parturition, there was no association of metritis (**Table 3-1**) or endometritis (**Table 3-2**) on days to first service or days to conception. Metritis tended ($P = 0.060$) to increase the number of services per pregnancy compared to cows with no metritis (3.15 ± 0.36 *vs.* 2.14 ± 0.40; **Table 3-1**). There was no association between endometritis and services per pregnancy compared to cows with no endometritis. There were no association of metritis or endometritis on energy corrected milk, average daily milk, total fat, or total protein (**Table 3-1** and **3-2**).

As expected, vaginal mucus score was greater ($P < 0.001$) on d 4, 7, and 14 in metritis cows compared to no metritis cows between d 7 and 28 postpartum (**Figure 3-2A**). Additionally, rectal temperature was elevated ($P = 0.040$) and body condition score was decreased ($P = 0.008$) in cows with metritis compared to cows without metritis between d 7 and 28 postpartum (**Figure 3-2B** and **3-2C**). Similarly, vaginal mucus score was greater ($P < 0.001$) in endometritis cows compared to no endometritis cows between d 7 and 28 postpartum (**Figure 3-2D**). Additionally, rectal temperature tended to be elevated ($P = 0.057$) and body condition score was decreased ($P = 0.005$) in cows with endometritis compared to cows without endometritis between d 7 and 28 postpartum (**Figure 3-2E** and **3-2F**). There was no association of either metritis or endometritis on the percentage of ovulatory, or anovulatory cows between d 7 and 28 postpartum (**Table 3-1 and 3-2**). There was an increase ($P = 0.050$) in the incidence of follicular cysts in cows with metritis compared to cows with no metritis (**Table 3-1)**. There was no association between endometritis and the percentage of follicular cysts (**Table 3-2**).

Health Information of Ovulatory Cows

The associations between uterine diseases on the descriptive data for ovulatory cows were also evaluated. Of the 17 ovulatory cows, 17.6% had metritis only (n = 3), 23.5% had endometritis only (n = 4), 35.3% had both metritis and endometritis (n = 6), and 23.5% had neither metritis nor endometritis (n = 4).

Vaginal mucus score was greater ($P < 0.001$) in metritis cows compared to no metritis cows between d 7 and 28 postpartum (**Figure 3-3A**). Additionally, rectal temperature was elevated ($P = 0.030$) in cows with metritis compared to cows without metritis between d 7 and 28 postpartum (**Figure 3-3B**), while body condition score was

not affected (P = 0.787) by metritis in ovulatory cows (**Figure 3-3C**). Circulating haptoglobin at d 7 postpartum was not statistically different (P = 0.395) in ovulatory cows with metritis compared to ovulatory cows without metritis (125.72 ± 28.49 μg/mL *vs.* 48.82 ± 30.22 μg/mL; **Figure 3-3D**).

Vaginal mucus score was greater (P = 0.023) in endometritis cows compared to no endometritis cows between d 7 and 28 postpartum (**Figure 3-3E**). Additionally, rectal temperature was not affected (P = 0.312) by endometritis (**Figure 3-EF**), while body condition score was reduced by endometritis in ovulatory cows (P < 0.001) between d 7 and 28 postpartum compared to cows with no endometritis (**Figure 3-3G**). Circulating haptoglobin at d 21 postpartum was increased 2.6-fold (P = 0.034) in ovulatory cows with endometritis compared to ovulatory cows without endometritis (39.07 μg/mL ± 25.18 *vs.* 10.84 ± 30.09 μg/mL; **Figure 3-3H**).

Associations Between Metritis and Postpartum Ovarian Dynamics and Function

To investigate the associations between metritis and ovarian function during the first estrous cycle, ovarian dynamics and function were analyzed in ovulatory cows. There was no association of metritis on the size of the ovulatory follicle (13.8 ± 1.5 mm *vs.* 13.9 ± 1.5 mm; P = 0.977) or day of ovulation (15.5 ± 1.0 d *vs.* 15.2 ± 1.0 d; P = 0.850) (**Figure 3-4A)**. Metritis was associated with reduced follicle growth (P = 0.002) between d 7 and 16 postpartum compared to cows with no metritis (**Figure 3-5A**). There was a tendency for (P = 0.062) metritis to reduce plasma estradiol between d 7 and 16 postpartum compared to cows with no metritis (**Figure 3-5B**). There was no association (P = 0.411) of metritis on corpus luteum growth between d 17 and 26 postpartum (**Figure 3-5C**). Metritis was associated with reduced (P = 0.026) plasma

progesterone between d 17 and 26 postpartum compared to cows without metritis (**Figure 3-5D**).

Association Between Endometritis and Postpartum Ovarian Dynamics and Function

Next, we sought to investigate the association of endometritis on ovarian function during the first estrous cycle of ovulatory cows. There was no association between endometritis on the size of the ovulatory follicle (14.6 ± 1.7 mm *vs.* 13.4 ± 1.3 mm; *P* = 0.586) or day of ovulation (15.3 ± 1.1 d *vs.* 15.4 ± 0.9 days; *P* = 0. 939) (**Figure 3-4B)**. Endometritis was not associated with reduced follicle growth (*P* = 0.389) or plasma estradiol (*P* = 0.151) between d 7 and 16 postpartum compared to cows without endometritis (**Figure 3-6A** and **3-6B**). In addition, endometritis was associated with reduced (*P* = 0.005) corpus luteum growth between d 17 and 26 postpartum (**Figure 3-6C**) but was not associated with reduced (*P* = 0.454) plasma progesterone (**Figure 3-6D**).

Effects of Induced Endometritis on Corpus Luteum Gene Expression

Corpus luteum size and function were evaluated on d 16 of the estrous cycle, 146 d after intrauterine infusion of pathogenic bacteria (n = 11) or saline control (n = 11). Intrauterine infusion of bacteria did not affect (*P* = 0.710) plasma progesterone (**Figure 3-7A)** or corpus luteum diameter (22.6 ± 0.8 mm *vs.* 22.5 ± 0.5 mm; *P* = 0.920) on d 16 of the estrous cycle, 146 d after intrauterine infusion. Gene expression of 94 genes related to steroid synthesis, lipid metabolism, corpus luteum function, vascularity, cell cycle, cell signaling, inflammation/immune signaling, epigenetics, and cell death were evaluated in corpus luteum tissue by Fluidigm RT-PCR (expression of five reference genes were also evaluated; **Table 3-3**) A total of eight genes (*BAD, CXCL8, CYP4A11,*

IFNB1, IL6, NFKBIA, PGK1, and *TET1*), and one housekeeper (*YWHAZ*), were not detected in any sample and excluded from analysis. Intrauterine infusion of bacteria reduced the expression of *NCF1* ($P = 0.047$) and *TLR9* ($P = 0.032$) by 29.9% and 34.8%, respectively compared to control cows (**Figure 3-7B** and **3-7C**). Expression of *CYP17A1* tended to be reduced ($P = 0.094$) in bacteria infused cows compared to controls (**Figure 3-7D**). Interestingly, intrauterine infusion of bacteria tended to increase the expression of *ACAT1* ($P = 0.096$) and *HSD3B1* ($P = 0.065$) compared to controls (**Figure 3-7E** and **3-7F**).

Discussion

The factors that result in subfertility of dairy cows after the resolution of uterine disease are multifaceted. While there are effects of uterine disease on the capacity of the endometrium to support pregnancy; there are also effects of uterine disease on ovarian physiology. Altered ovarian function could contribute to reduced future fertility. The present study investigated the contemporaneous and long-term effects of different uterine diseases on ovarian function. Here it was shown that both metritis and endometritis impact the growth of ovarian structures and concentrations of plasma steroid hormones. Interestingly, the data indicate that the time of disease primarily affects the immediate, contemporaneous ovarian structure present; metritis reduces follicle growth while endometritis that occurs later affects the corpus luteum. These data agree with other published literature which indicate that metritis can reduce the growth of the ovarian follicle and plasma estradiol of the first postpartum estrous cycle (Sheldon et al., 2002, Williams et al., 2007). Further, these new data are in agreement with previous experiments that demonstrate a negative correlation between bacterial infection of the uterus and growth and function of the corpus luteum of the first

postpartum estrous cycle (Williams et al., 2007). In addition, it is shown that induced uterine infection 146 days prior alters the expression of corpus luteum genes despite resolution of the infection. Collectively these data describe both contemporaneous and long-term effects of different uterine diseases on ovarian function in the dairy cow.

In agreement with the current findings, Williams et al. (2007) reported an association between elevated uterine *E. coli* and *Arcanobacterium pyogenes* (now *T. pyogenes*) at d 7 postpartum and impaired follicle growth and plasma estradiol between d 7 and 16 postpartum (Williams et al., 2007). The presence of *E. coli* in the uterus of cows with uterine inflammation is positively associated with increased LPS accumulation in follicular fluid during the first estrous cycle (Herath et al., 2007). The processes of ovulation and luteinization are directly linked to changes in the peripheral endocrine milieu such that signals from the hypothalamus interact with ovarian derived signals in both positive and negative feedback loops to regulate ovarian dynamics. Some in vivo evidence indicates there are reductions to the pulsatile release of hypothalamic GnRH and pituitary LH following intravenous LPS challenge (Peter et al., 1989, Battaglia et al., 1997). However, when LPS is infused directly into the uterus of heifers, there was no effect on the concentrations of peripheral LH (Sheldon et al., 2002, Williams et al., 2008). Additionally, there have not been detected differences in the concentrations of plasma FSH in cows with uterine bacterial contamination or following intrauterine infusion of LPS (Sheldon et al., 2002, Williams et al., 2008). It is unclear if the changes to ovarian dynamics are directly linked to reductions in peripheral concentrations of gonadotropins or indirect effects of uterine inflammation and infection on the ovary.

Bovine granulosa cells express Toll-like receptor 4 and are sensitive to LPS stimulation, in that upon LPS treatment granulosa cells increase the synthesis of inflammatory mediators (Bromfield and Sheldon, 2011, Price et al., 2013). Indeed, LPS has direct effects on the steroidogenic function of granulosa cells whereby LPS stimulation reduces the capacity of granulosa cells to synthesize estradiol in vitro, while downregulating the expression of *CYP19A1* and aromatase (Price et al., 2013, Dickson et al., 2022b). The mechanisms by which LPS reduces aromatase in granulosa cells has not been resolved. Interestingly, the effects of metritis on follicle growth and plasma estradiol observed here did not carry over and impact the growth of the subsequent corpus luteum; however, subsequent plasma progesterone between d 17 and 26 postpartum was reduced in cows that had metritis. This is in agreement with Williams, 2007 in which cows with elevated uterine *E. coli* on d 7 postpartum had reduced plasma progesterone between d 17 and 26 postpartum (Williams et al., 2007). Thus, it is important to further investigate the mechanisms by which metritis impacts corpus luteum function after the resolution of disease.

In parallel, the work presented here also investigated the effect of endometritis on corpus luteum growth and function during active disease. As expected, endometritis that occurred after the growth of the follicle of the first estrous cycle had no effect on follicle growth or plasma estradiol; however, endometritis that occurred at the same time as corpus luteum development did reduce corpus luteum growth, but surprisingly not plasma progesterone. Similar to granulosa cells, luteal cells express the entire family of Toll-like receptors throughout the luteal period (Gadsby et al., 2017). Intrauterine infusion of *E. coli* LPS on d 9.5 during the luteal phase reduces corpus luteum growth,

plasma progesterone and induced premature luteolysis due to increased endometrial synthesis of PGF2α (Lüttgenau et al., 2016a). In parallel, a single intravenous infusion of LPS on d 10 of the estrous cycle increased the expression of corpus luteum *TLR2*, *TLR4*, *IL1A*, *IL1B*, *HSD20A*, and *PTGES*, suggesting that luteal tissue is capable of experiencing localized inflammation to alter steroidogenic function (Lüttgenau et al., 2016b). Similarly, corpora lutea from cows with endometritis had reduced weight and progesterone content compared to cows free of endometrial inflammation (Mohammed et al., 2020). The authors attribute the reduced progesterone content to altered abundance of CYP11A, HSD3B, and STAR proteins; however, there were also reductions in vascularity and pericytes of corpora lutea from cows with endometritis (Mohammed et al., 2020). This study also revealed that luteal endothelial cell networks were reduced following treatment with either LPS or a TLR4 agonist due to increased endothelial cells apoptosis (Mohammed et al., 2020). Bruinjé et al. in 2023 demonstrated that progesterone 8 d after insemination was reduced in cows with clinical disease, and there was a tendency for a reduction in cows with purulent vaginal discharge indicative of endometritis (Bruinjé et al., 2023). Further, intravenous infusion of 0.5 µg/kg of LPS on d 10 of the estrous cycle reduced the size of the corpus luteum and decreased luteal blood flow by 34% within 3 hours of infusion (Herzog et al., 2012). This response to LPS is rapid such that within 30 minutes of LPS infusion the concentrations of plasma prostaglandin F metabolites increased by 10-fold (9.2 ng/mL *vs.* 0.8 ng/mL) and within 1 hour the concentrations of PGE was doubled (3.61 ng/mL *vs.* 1.98 ng/mL) compared to controls (Herzog et al., 2012). In vitro studies have demonstrated that endometrial epithelial cells exposed to LPS switch their secretion of

luteolytic PGF2α to increase the secretion of luteotropic PGE2, which may help explain how uterine infection could modulate the function of the corpus luteum indirectly (Herath et al., 2009). The switch in endometrial prostaglandin production is hypothesized to contribute to extended luteal phases observed in some cows with uterine disease (Herath et al., 2009).

The long-term effects of uterine disease on various tissues of the reproductive tract have been previously investigated. Granulosa cells isolated from preovulatory follicles of cows 6 weeks after the resolution of spontaneous metritis differentially express 177 genes involved in immune function, cell-cell communication, cell cycle, and cellular metabolism (Piersanti et al., 2019). Similarly, Horlock and colleagues assessed the transcriptome of various reproductive tract tissues three months after the intrauterine infusion of pathogenic *E. coli* and *T. pyogenes* into virgin heifers (Horlock et al., 2020). They describe 89 differentially expressed genes in granulosa cells of antral follicles, and that granulosa cells had the greatest number of predicted upstream regulators of gene expression compared to uterine and oviduct tissues. The authors speculated that observed changes to granulosa cells were likely initiated when follicles were at the pre-antral stage of development during infection (Horlock et al., 2020). The long-term effects of uterine disease on the corpus luteum have not been extensively investigated. Strüve et al. (2013) investigated the effects of metritis on the corpus luteum during the first four estrous cycles after calving and found that metritis reduced corpus luteum size only in the first estrous cycle following parturition, but had no effect on plasma progesterone (Strüve et al., 2013). The data presented here indicate that while plasma progesterone is not different 146 days after intrauterine infusion of

bacteria, expression of genes related to corpus luteum function were differentially expressed. One gene that was downregulated in luteal tissue of cows infused with bacteria, *NCF1,* encodes for neutrophil cytosolic factor 1 which is a subunit of the NADPH oxidase complex and contributes to phagocytic activity and balancing oxidative stress. The abundance of NCF1 protein was shown to be upregulated in porcine granulosa cells that were undergoing atresia compared to healthy follicles (Shan et al., 2021). The downregulation of *NCF1* observed here may indicate that processes related to normal regulation of oxidative status may be perturbed in corpora lutea of cows previously infected with bacteria. Similarly, the expression of *TLR9* was downregulated in luteal tissue of cows infused with bacteria. Toll-like receptor 9 is a member of the TLR family of receptors involved in pathogen recognition. Interestingly, the activation of one TLR family member can modulate the gene expression of other TLRs (Nhu et al., 2006). An experiment using bovine granulosa cells demonstrated that exposure to Pam3CSK (a synthetic TLR2 agonist) reduced the expression of *TLR9* after 3 h (Price, 2013). The authors suggested that the downregulation of *TLR9* is likely in direct response to the activation of TLR2 (Price et al., 2013). It is therefore interesting to ponder the potential long-term mediators of innate immune function following an initial inflammatory insult.

Cows with uterine disease have a greater frequency of pregnancy loss compared to cows without uterine disease, such that pregnancy rates at 45 d and to calving are reduced in cows with prior uterine disease whether receiving embryo transfer or artificial insemination (Ribeiro et al., 2016). This observation suggests that uterine disease has a long-term impact on the capacity of the uterus to support a pregnancy. However, there are also apparent changes to ovarian cells in cows with uterine disease that could

perpetuate subfertility. Indeed, the transcriptome of oocytes is changed both 4 and 60 d following intrauterine infusion of *E. coli* and *T. pyogenes* compared to saline infused heifers (Piersanti et al., 2020). These molecular changes could be responsible for the reduced capacity of oocytes from bacteria infused cows to develop into morula following in vitro fertilization (Dickson et al., 2020). Furthermore, treatment of cumulus oocyte complexes with LPS during in vitro maturation increases the frequency of meiotic failure and reduces oocyte developmental competence compared to controls (Soto et al., 2003, Bromfield and Sheldon, 2011). There are also implications for reduced progesterone synthesis by the corpus luteum in causing subfertility, such that progesterone is critical in modulating endometrial gene expression and the uterine luminal metabolome in preparation for pregnancy (Forde et al., 2010, Martins et al., 2022, Silva et al., 2023).

In conclusion, uterine disease affects the growth and function of ovarian structures present at the time of disease; such that metritis reduces follicle growth and plasma estradiol while endometritis reduces corpus luteum growth. In addition, these data also demonstrate the long-term effects of induced endometritis on the expression of genes related to corpus luteum function after the resolution of disease. Collectively these studies suggest that uterine diseases throughout the lifespan of the cow may impact ovarian function that could be associated with reduced fertility observed in cows following uterine disease resolution.

Table 3-1. Descriptive characteristics of all enrolled cows with metritis or without metritis[1].

Response	No metritis (n = 21)	Metritis (n = 26)	*P*-value
Age at conception when heifer (mo)	14.28 ± 0.42	13.63 ± 0.38	0.26
Services per conception when heifer	1.62 ± 0.18	1.62 ± 0.16	0.99
Age at calving (mo)	23.40 ± 0.42	22.75 ± 0.38	0.25
Gestation length (d)	273.8 ± 0.9	273.2 ± 0.8	0.63
Male calf (%)	57.1 ± 0.1	42.3 ± 0.1	0.32
Days to first service (d)	76.5 ± 1.0	77.1 ± 0.8	0.63
Days to conception (d)	124.0 ± 12.5	142.3 ± 10.5	0.27
Services per pregnancy	2.14 ± 0.40	3.15 ± 0.36	0.06
305 ME[2]	13,865 ± 850	13,268 ± 763	0.60
ECM[3]	10,257 ± 1,027	12,472 ± 923	0.12
Average daily ECM	33.37 ± 1.64	35.22 ± 1.48	0.41
Total fat (kg)	378.55 ± 40.01	445.68 ± 35.95	0.22
Total protein (kg)	310.80 ± 31.77	368.62 ± 28.55	0.18
Average daily milk (kg)	30.44 ± 1.69	33.46 ± 1.52	0.19
Ovulatory, n/n (%)	8/21 (38.1%)	9/26 (34.6%)	0.81
Anovulatory, n/n (%)	12/21 (57.1%)	10/26 (38.4%)	0.21
Cystic, n/n (%)	1/21 (4.8%)	7/26 (26.9%)	0.05

[1] Vaginal mucus was evaluated and cows were categorized as having either metritis (≤ 14 d, score = 4) or no metritis (≤ 14 d, score ≤ 3);
[2] ME = Mature Equivalent.
[3] ECM = Energy Corrected Milk.

Table 3-2. Descriptive characteristics of all enrolled cows with endometritis or without endometritis[1].

Response	No Endometritis (n = 19)	Endometritis (n = 28)	*P*-value
Age at conception when heifer (mo)	14.37 ± 0.44	13.61 ± 0.36	0.19
Services per conception when heifer	1.68 ± 0.18	1.57 ± 0.15	0.64
Age at calving (mo)	23.5 ± 0.4	22.7 ± 0.4	0.19
Gestation length (d)	273.6 ± 0.9	273.4 ± 0.8	0.85
Male calf (%)	57.9 ± 0.12	42.8 ± 0.09	0.32
Days to first service (d)	75.7 ± 0.9	77.7 ± 0.8	0.12
Days to conception (d)	123.4 ± 12.9	141.9 ± 10.3	0.27
Services per pregnancy	2.37 ± 0.43	2.93 ± 0.35	0.32
305 ME [2]	13,234 ± 907	13,740 ± 736	0.66
ECM[3]	10,961 ± 1,106	11,836 ± 911	0.54
Average daily ECM	35.38 ± 1.73	33.73 ± 1.42	0.46
Total fat (kg)	397.46 ± 42.63	428.05 ± 35.12	0.58
Total protein (kg)	321.53 ± 33.83	357.21 ± 27.86	0.42
Average daily milk (kg)	33.04 ± 1.8	31.48 ± 1.49	0.51
Ovulatory, n/n (%)	7/19 (36.8%)	10/28 (35.7%)	0.94
Anovulatory, n/n (%)	8/19 (42.1%)	14/28 (50.0%)	0.60
Cystic, n/n (%)	4/19 (19.0%)	4/28 (14.3%)	0.56

[1] Vaginal mucus was evaluated and cows were categorized as having either endometritis (15 d ≥, score ≥ 3) or no endometritis (15 d ≥, score ≤ 2);
[2] ME = Mature Equivalent.
[3] ECM = Energy Corrected Milk.

Table 3-3. Relative expression of all detected genes in the corpus luteum after intrauterine infusion of bacteria[1].

Gene	Vehicle (n = 11)	Bacteria (n = 11)	*P* - value
ACAA2	0.155 ± 0.143	0.050 ± 0.038	0.54
ACACA	0.873 ± 0.853	0.271 ± 0.208	0.78
ACAT1	1.919 ± 0.996	23.730 ± 13.835	0.10
ACSL1	2.298 ± 2.193	0.436 ± 0.284	0.82
APAF1	6.471 ± 5.310	0.011 ± 0.010	0.11
ATM	0.063 ± 0.053	0.165 ± 0.099	0.64
BAX	0.272 ± 0.237	0.387 ± 0.293	0.58
BCL2	18.932 ± 18.605	3.167 ± 2.581	0.85
CASP7	9.196 ± 9.158	0.494 ± 0.269	0.52
CASP9	0.091 ± 0.061	0.013 ± 0.006	0.86
CCNB1	1.927 ± 1.328	0.236 ± 0.228	0.35
CCND2	3.189 ± 3.163	0.348 ± 0.205	0.94
CCNE1	0.008 ± 0.005	0.077 ± 0.071	0.63
CD14	0.366 ± 0.175	4.414 ± 3.286	0.88
CD40	3.491 ± 3.333	1.694 ± 1.113	0.99
CDC20	0.857 ± 0.774	2.279 ± 0.974	0.14
CDK1	1.644 ± 1.411	0.010 ± 0.004	0.44
CDK2	1.525 ± 1.130	0.093 ± 0.044	0.93
CDKN1A	0.187 ± 0.112	0.195 ± 0.187	0.83
CDKN1B	13.427 ± 13.170	2.582 ± 1.731	0.46
CYP11A1	497.126 ± 481.105	87.538 ± 63.798	0.78
CYP11B1	0.905 ± 0.878	0.435 ± 0.330	0.77
CYP17A1	0.103 ± 0.091	0.001 ± 0.000	0.09
CYP19A1	0.065 ± 0.053	0.371 ± 0.279	0.52
CYP3A4	0.125 ± 0.063	1.442 ± 1.313	0.78
DNMT1	0.086 ± 0.050	0.011 ± 0.005	0.11
DNMT3A	0.254 ± 0.136	1.270 ± 0.996	0.76
FASN	60.916 ± 59.302	0.423 ± 0.253	0.24
FGF2	0.178 ± 0.154	0.110 ± 0.067	0.75
FLT1	1.791 ± 1.673	1.445 ± 1.398	0.34
FLT3LG	2.732 ± 2.729	0.594 ± 0.591	0.50
FOXO3	5.913 ± 5.602	1.221 ± 1.211	0.47
GHR	1.756 ± 1.243	0.738 ± 0.388	0.72
H2AFX	5.889 ± 3.242	0.477 ± 0.272	0.74
H2AFZ	5.413 ± 4.840	0.212 ± 0.160	0.21
HADH	0.043 ± 0.029	0.113 ± 0.064	0.63

Table 3-3. Continued

Gene	Vehicle (n = 11)	Bacteria (n = 11)	*P* - Value
HDAC1	0.745 ± 0.510	6.975 ± 4.415	0.58
HDAC8	0.887 ± 0.830	0.732 ± 0.480	0.82
HSD11B1	0.672 ± 0.665	0.216 ± 0.121	0.76
HSD17B10	2.721 ± 1.461	34.497 ± 19.352	0.71
HSD3B1	1.037 ± 0.587	6.142 ± 3.001	0.01
IGF1	6.688 ± 4.440	1.121 ± 0.745	0.98
IGF2	3.015 ± 1.623	2.514 ± 1.859	0.29
IGF2R	21.584 ± 21.368	3.547 ± 3.106	0.56
IGFBP2	4.861 ± 3.354	0.747 ± 0.421	0.93
IL12A	5.583 ± 5.098	0.437 ± 0.239	0.81
IL1A	0.693 ± 0.650	0.074 ± 0.051	0.49
IL1B	0.824 ± 0.686	0.178 ± 0.118	0.68
IL4	0.347 ± 0.218	0.499 ± 0.430	0.70
IL6R	1.117 ± 0.430	4.900 ± 2.901	0.97
LHCGR	0.837 ± 0.391	6.862 ± 4.013	0.63
MAP2K1	0.192 ± 0.145	0.152 ± 0.089	0.96
MAPK13	1.574 ± 1.077	0.896 ± 0.739	0.99
NCF1	1.244 ± 0.558	0.339 ± 0.247	0.01
NFKB1	6.391 ± 5.302	0.446 ± 0.421	0.40
PGR	0.672 ± 0.321	4.334 ± 2.392	0.55
POR	108.730 ± 108.297	16.650 ± 10.830	0.51
PPARA	0.046 ± 0.026	0.174 ± 0.127	0.70
PPARG	0.080 ± 0.042	0.027 ± 0.012	0.64
PRKCB	7.471 ± 7.042	5.342 ± 3.353	0.62
PTEN	0.076 ± 0.051	0.015 ± 0.004	0.55
PTGER3	0.910 ± 0.467	1.042 ± 0.530	0.79
PTGER4	1.721 ± 1.225	0.673 ± 0.473	0.80
PTPRC	2.618 ± 2.076	0.334 ± 0.284	0.94
SRC	135.873 ± 135.544	4.002 ± 2.368	0.72
STAR	443.645 ± 424.870	109.986 ± 51.235	0.97
STAT1	0.215 ± 0.155	0.062 ± 0.036	0.32
STAT3	3.832 ± 3.643	1.653 ± 1.162	0.34
STAT4	6.621 ± 4.544	0.842 ± 0.684	0.89
TET2	0.017 ± 0.014	0.685 ± 0.434	0.28
TLR1	12.328 ± 10.104	2.590 ± 1.526	0.28
TLR2	1.327 ± 1.073	0.470 ± 0.342	0.54
TLR4	0.446 ± 0.378	0.491 ± 0.271	0.68
TLR6	0.458 ± 0.336	0.106 ± 0.063	0.60

Table 3-3. Continued

Gene	Vehicle (n = 11)	Bacteria (n = 11)	*P* - Value
TLR9	0.119 ± 0.074	0.041 ± 0.041	0.03
TNF	0.063 ± 0.035	0.104 ± 0.101	0.22
VEGFA	125.246 ± 114.022	22.836 ± 10.153	0.56
VEGFB	3.870 ± 3.830	0.810 ± 0.504	0.32
VEGFC	4.086 ± 1.769	1.563 ± 0.917	0.33
VEGFD	0.079 ± 0.072	0.099 ± 0.048	0.83
WEE1	0.085 ± 0.039	0.023 ± 0.010	0.39

[1] Gene expression data are presented as the mean relative expression ± SEM calculated using the $2^{-\Delta Ct}$ method.

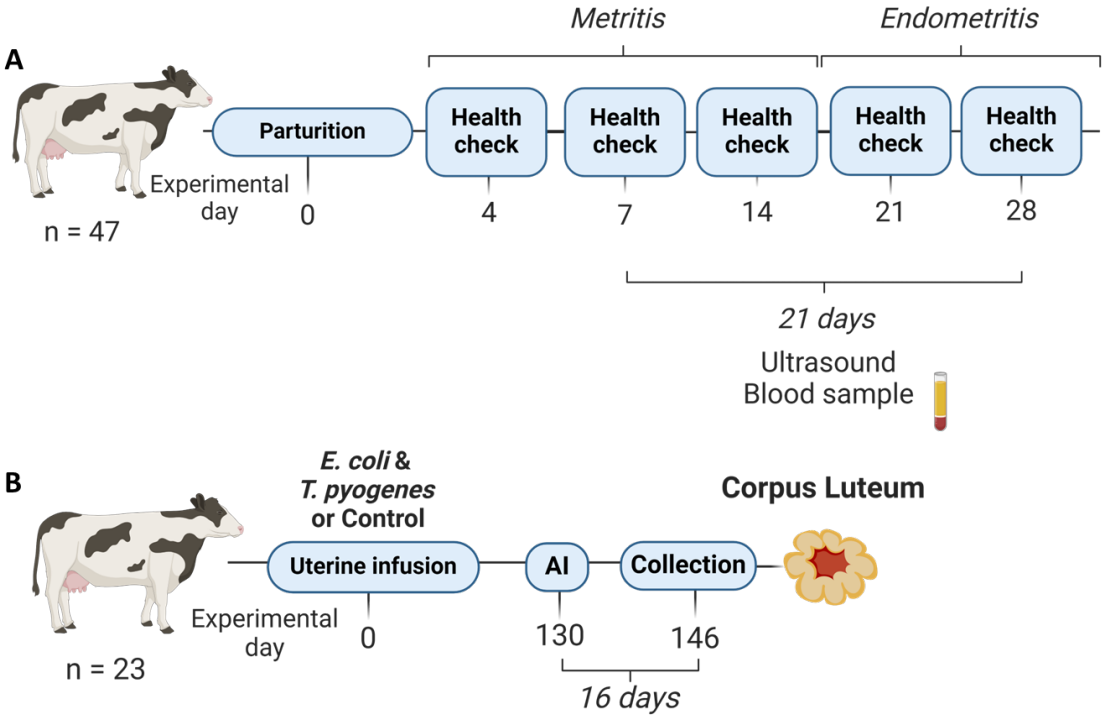

Figure 3-1. Experimental models. Study 1 (A) utilized 47 primiparous lactating Holstein cows enrolled on the day of parturition. Health evaluations were conducted 4, 7, 14, 21, and 28 d postpartum. Daily ultrasonography and blood sampling began on d 7 postpartum and continued until d 28 postpartum. Cows were categorized as having metritis when presenting a vaginal mucus score of 4 on days 4, 7, or 14 postpartum, and/or as having endometritis when presenting a vaginal mucus score ≥ 3 on d 21 or 28 postpartum. Study 2 (B) utilized 23 nonlactating primiparous Holstein cows that received an intrauterine infusion of either *E. coli* and *T. pyogenes* or saline as a control on experimental d 0. Estrous cycles were synchronized, and cows were inseminated on d 130. Animals were sacrificed on d 146 and corpora lutea were collected for subsequent analysis.

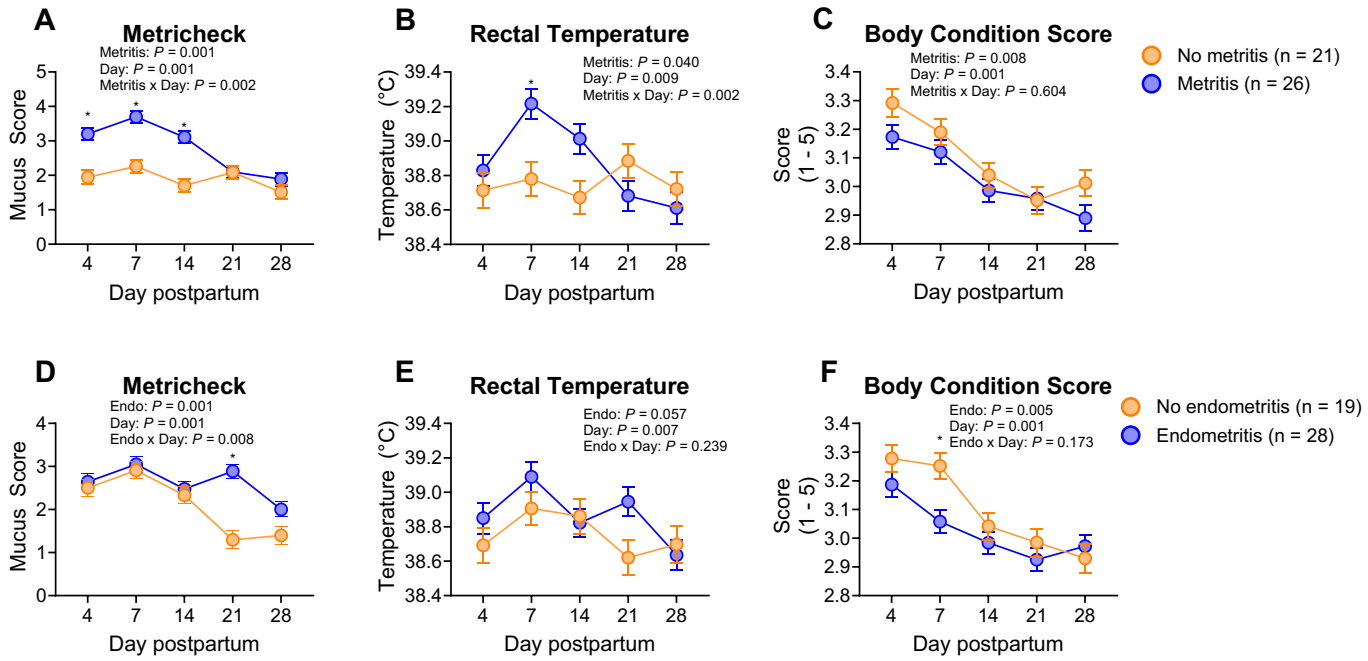

Figure 3-2. Health characteristics of all enrolled cows. Individual health assessments including vaginal mucus score (A and D), rectal temperature (B and E), and body condition score (C and F) were conducted on 4, 7, 14, 21, and 28 d postpartum for all enrolled cows regardless of ovulatory status. Health status of cows was categorized according to vaginal mucus scores; metritis (A-C) was categorized as a vaginal mucus score of 4 on d 4, 7 or 14 postpartum, while endometritis (D-F) was categorized as a vaginal mucus score ≥ 3 on d 21 or 28 postpartum. Data are presented as the least squares means ± SEM.

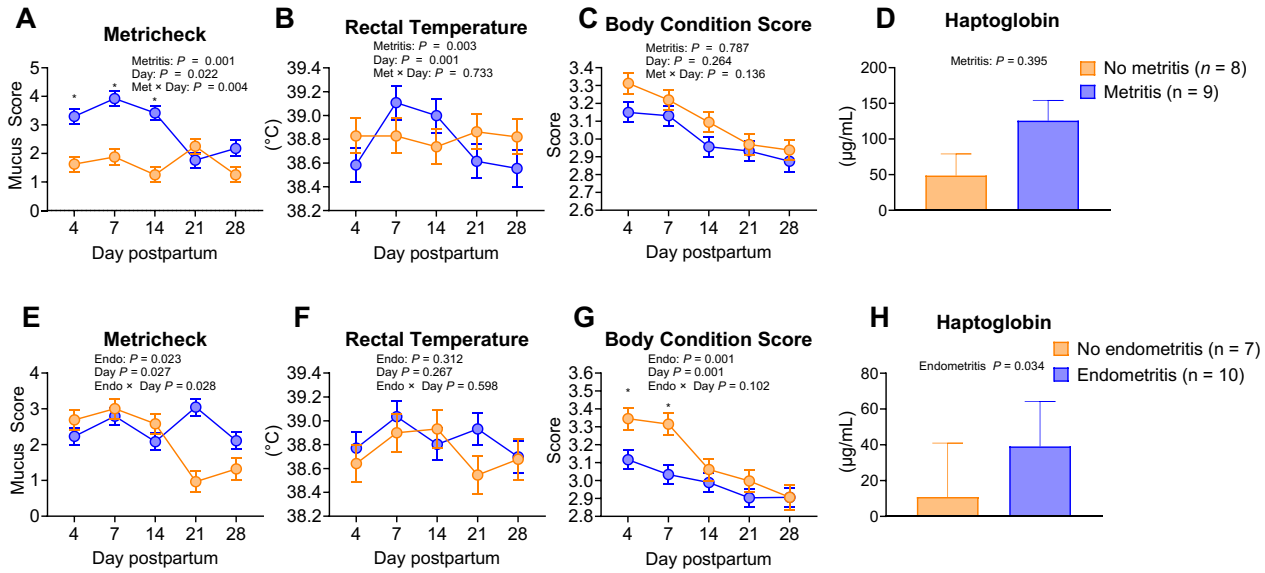

Figure 3-3. Health characteristics of ovulatory cows. Individual health assessments including vaginal mucus score (A and D), rectal temperature (B and E), and body condition score (C and F) were conducted on 4, 7, 14, 21, and 28 d postpartum for all ovulatory cows (n = 17). Plasma haptoglobin was quantified on d 7 and 21 postpartum (D and H). Health status of cows was categorized according to vaginal mucus scores; metritis (A-D) was categorized as a vaginal mucus score of 4 on d 4, 7 or 14 postpartum, while endometritis (E-H) was categorized as a vaginal mucus score ≥ 3 on d 21 or 28 postpartum. Data are presented as the least squares means ± SEM.

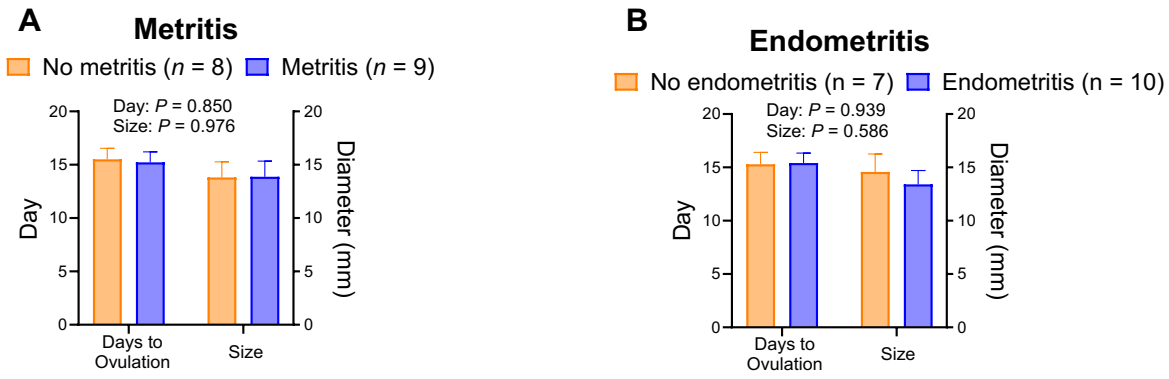

Figure 3-4. Associations between metritis and endometritis on ovulation dynamics. The effect of metritis (A) and endometritis (B) on the day of ovulation and size of the ovulatory follicle was evaluated for ovulatory cows (n = 17). Day of ovulation was defined as the day when a large dominant follicle was replaced with a CL on the following day. Size of the ovulatory follicle was defined as the measurement of the follicle immediately before ovulation. Data are presented as the least squares means ± SEM.

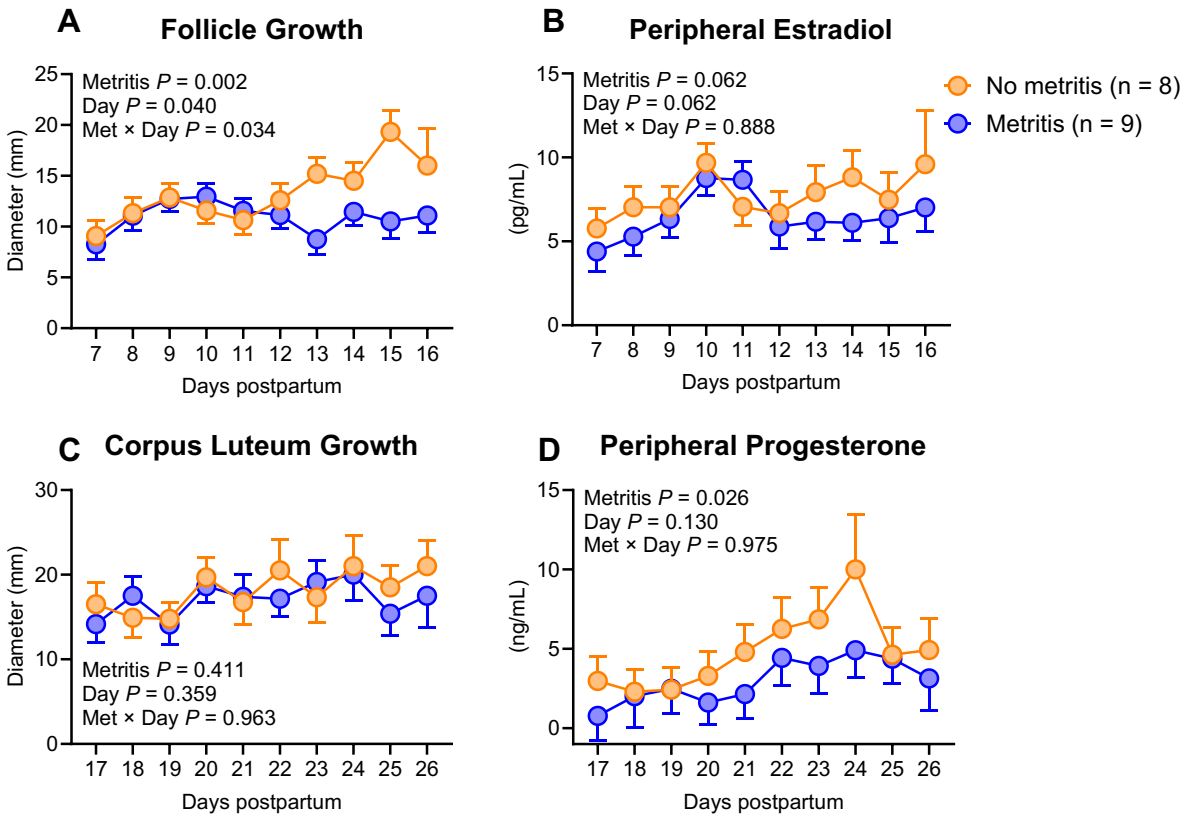

Figure 3-5. Association between metritis and ovarian dynamics during the first postpartum estrous cycle. Ovulatory cows were categorized as having metritis (n = 9) or no metritis (n = 8). Follicle (A) growth from d 7 to 16 postpartum and corpus luteum (C) growth from d 17 to 26 postpartum was measured by transrectal ultrasonography for ovulatory cows. Concentrations of plasma estradiol (B) from d 7 to 16 postpartum and progesterone (D) from d 17 to 26 postpartum were quantified by ELISA. Data are presented as the least squares means ± SEM.

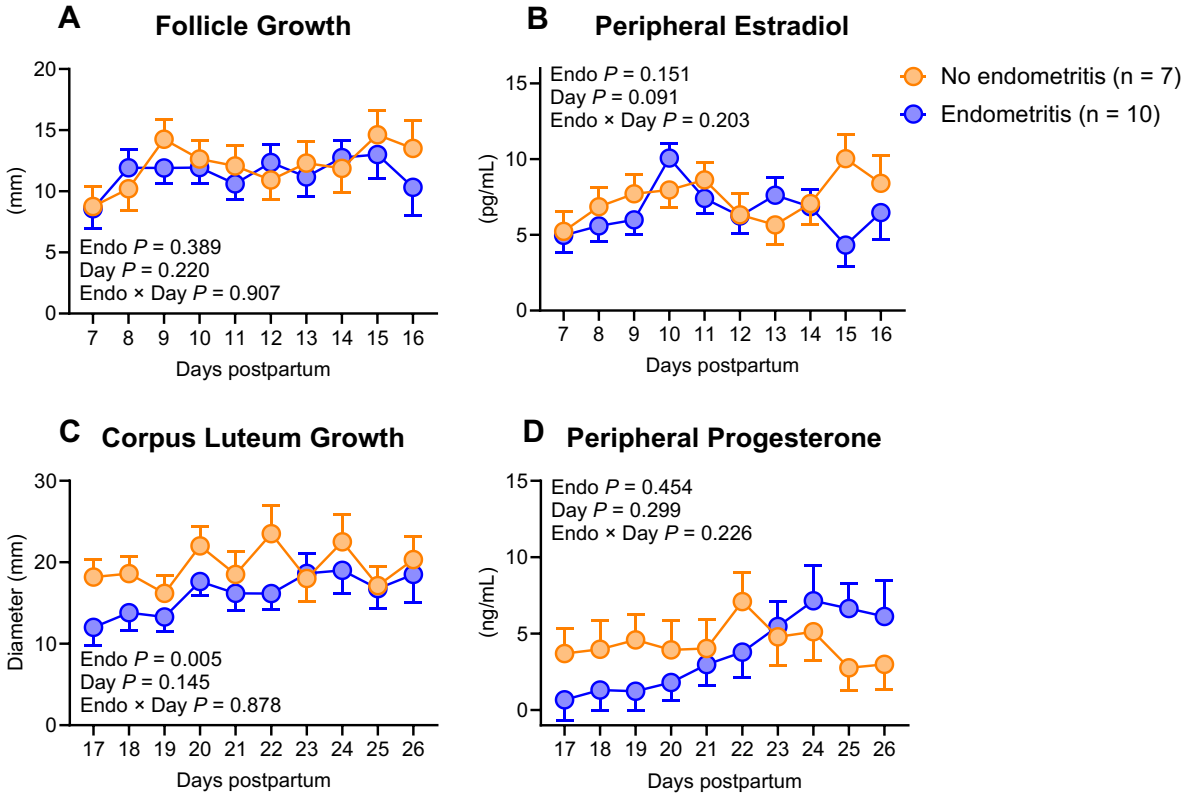

Figure 3-6. Association between endometritis and ovarian dynamics during the first postpartum estrous cycle. Ovulatory cows were categorized as having endometritis (n = 10) or no endometritis (n = 7). Follicle (A) growth from d 7 to 16 postpartum and corpus luteum (C) growth from d 17 to 26 postpartum was measured by transrectal ultrasonography for ovulatory cows. Concentrations of plasma estradiol (B) from d 7 to 16 postpartum and progesterone (D) from d 17 to 26 postpartum were quantified by ELISA. Data are presented as the least squares means ± SEM.

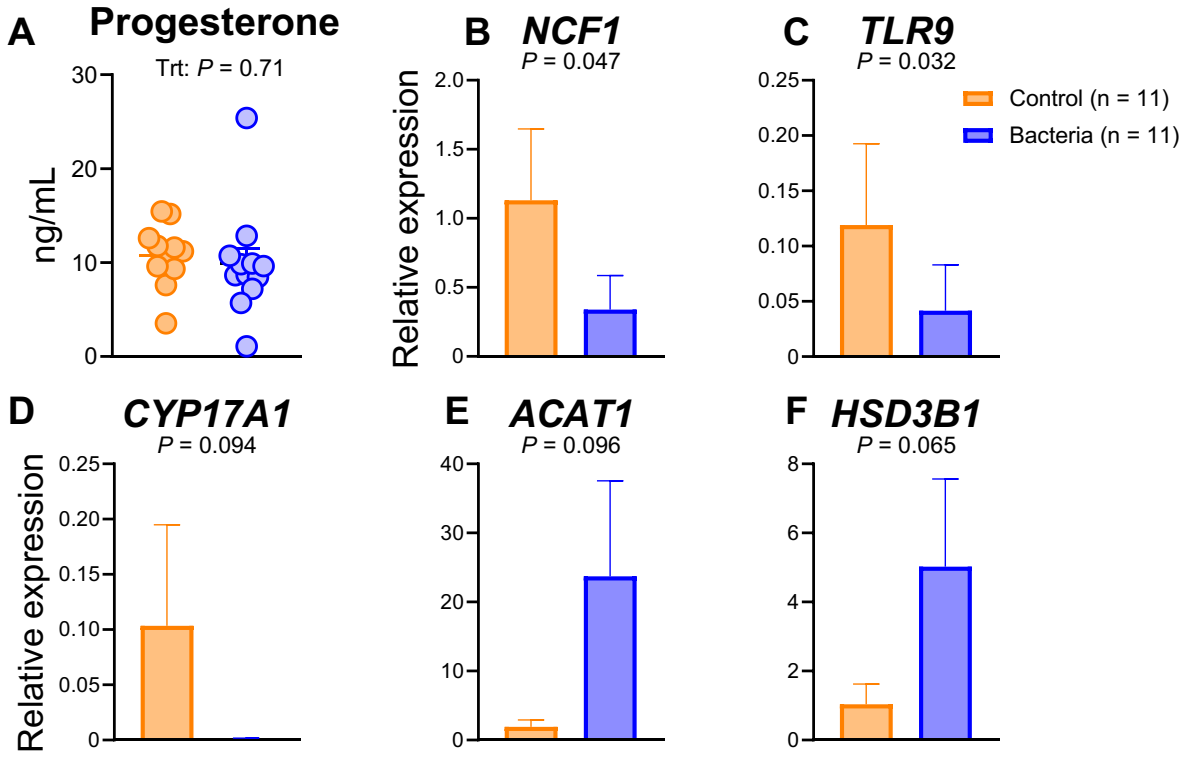

Figure 3-7. Long-term effects of uterine infection on corpus luteum function and gene expression. Study 2 utilized nonlactating primiparous Holstein cows that received an intrauterine infusion of *E. coli* and *T. pyogenes* (n = 12) or saline as a control (n = 11). Cows were slaughtered on d 16 of the estrous cycle, 146 d after infection. Plasma progesterone (A) was quantified on the day of slaughter by commercial ELISA. Gene expression of luteal tissue was evaluated by Fluidigm quantitative PCR microfluidic. One corpus luteum from a bacteria infused cow was lost at the time of slaughter. Genes related to immune function (*NCF1* and *TLR9*) (B and C), and lipid metabolism (*CYP17A1, ACAT1,* and *HSD3B1*) (D, E, and F) were differentially expressed in cows previously receiving bacterial infusion. Progesterone data is presented as the least squares means ± SEM and gene expression data are presented as the mean relative expression ± SEM.

CHAPTER 4
EXPOSURE OF BOVINE GRANULOSA CELLS TO LIPOPOLYSACCHARIDE REDUCES PROGESTERONE SECRETION DURING LUTEINIZATION

Summary

The mammalian ovary nurtures the development of female gametes and produces the steroid hormones estrogen and progesterone which are indispensable for reproductive function. Bacterial infections in the uterus of dairy cows result in decreased fecundity despite resolution of the infection. Uterine disease in dairy cows is caused by pathogenic bacteria, including Gram-negative *Escherichia coli* and is associated with lipopolysaccharide accumulation in follicular fluid that initiates granulosa cell inflammation via the Toll-like receptor 4 pathway. Follicle growth and plasma estradiol is reduced in cows with uterine disease, and treatment of bovine granulosa cells with lipopolysaccharide reduces *CYP19A1* expression and estradiol synthesis. It is unclear if the effects of lipopolysaccharide on the steroidogenic capacity of granulosa cells persist in cells during luteinization. We hypothesized that lipopolysaccharide treatment of granulosa cells would alter the steroidogenic capacity of cells during luteinization. Herein, I demonstrate that exposure of granulosa cells to lipopolysaccharide reduces the synthesis of progesterone by cells during luteinization. In attempt to determine the mechanisms of altered progesterone synthesis, I show that exposure of granulosa cells to lipopolysaccharide does not alter the expression of luteal cell *STAR* or *HSD3B1* required for progesterone synthesis. However, I show that exposure of granulosa cells to lipopolysaccharide reduces intracellular lipid droplets and cholesterol uptake during luteinization required for progesterone synthesis, suggesting a potential mechanisms of altered steroidogenesis. Collectively, these findings show that granulosa cell exposure to lipopolysaccharide reduces progesterone synthesis during luteinization due to altered

cholesterol and mitochondrial function. Perturbations to granulosa cell physiology may have prolonged effects on ovarian function that contribute to reduced fecundity of cows after uterine disease.

Introduction

It is not known exactly how bacterial infections of the uterus reduces fertility in dairy cows (Sheldon and Dobson, 2004). Uterine diseases in dairy cattle are associated with increased intrauterine and intrafollicular concentrations of lipopolysaccharide (LPS) (Herath et al., 2007, Herath et al., 2009). Bovine granulosa cells express the entire family of Toll-like receptors (TLR), including TLR4 (Price et al., 2013). Lipopolysaccharide originating from Gram-negative bacteria including pathogenic *Escherichia coli* activates TLR4 and initiates an innate inflammatory response by increasing phosphorylation of mitogen-activated protein kinases and p38/ERK which stimulates the secretion of inflammatory mediators such as IL1α, IL1β, IL6, and IL8 (Bromfield and Sheldon, 2011, Price et al., 2013). In cows with uterine disease, follicular growth and plasma estradiol concentrations are reduced (Sheldon et al., 2002, Williams et al., 2007). The exposure of cultured granulosa cells to LPS reduces the secretion of estradiol, abundance of aromatase and transcription of *CYP19A1* (Herath et al., 2007, Price et al., 2013, Dickson et al., 2022b). Interestingly, granulosa cells exhibit prolonged alterations to the transcriptome long after the resolution of disease, indicating that follicles of various developmental stages may be sensitive to uterine disease (Horlock et al., 2020, Piersanti et al., 2020).

While uterine disease and LPS affect follicle and granulosa cell function; it remains unclear whether there are changes to subsequent luteal function following ovulation. Some reports indicate that cows with uterine disease and cows with

increased pathogen loads have reduced corpus luteum size and progesterone secretion compared to uterine disease-free counterparts (Sheldon et al., 2002, Williams et al., 2007, Strüve et al., 2013). Furthermore, repeated intrauterine infusions of LPS prior to ovulation reduces corpus luteum cross sectional area, reduces peripheral progesterone concentrations and reduces luteal tissue expression of *STAR*, *PTGFR*, and *HSD3B* (Lüttgenau et al., 2016a). It has been speculated that granulosa cell exposure to cytokines, growth factors, gonadotropins, or steroids could impact granulosa cell physiology that are then carried over into subsequent luteal cells after differentiation, ultimately affecting corpus luteum function and capacity to support pregnancy (Abedel-Majed et al., 2019). Herein, I tested the hypothesis that granulosa cell exposure to LPS would alter the progesterone synthesis of resultant luteal cells. Data presented here demonstrate that granulosa cell exposure to LPS reduces progesterone production of large luteal cells during luteinization that is associated with reduced intracellular lipid accumulation and mitochondrial function.

Materials and Methods

Granulosa Cell Isolation, Culture and LPS Challenge

All materials were purchased from Thermo Fisher Scientific (Waltham, MA) unless otherwise stated. The experiment was conducted as a randomized complete block design with repeated measurements. Each 6 well plate contained an individual treatment which represented the experimental unit. Wells were passaged and maintained as individual experimental units throughout the culture period.

The isolation of granulosa cells was performed as previously described with minor modifications (Bromfield and Sheldon, 2011, Price et al., 2013, Dickson et al., 2022b, Horlock et al., 2022). Bovine ovaries were collected from a local abattoir and

transported to the laboratory for use within 6 h of collection. Ovaries were transported at 22°C in 0.9% saline containing 1% penicillin and streptomycin. Upon arrival, ovaries were washed three times in warm (38.5°C) saline containing 1% (w/v) penicillin/streptomycin.

Between 10 and 15 ovaries were processed together and represented a biological replicate. Small and medium diameter follicles (2-8 mm) were slashed with a scalpel blade and rinsed in collection medium as part of an oocyte recovery protocol. Collection medium containing both cumulus oocyte complexes and mural granulosa cells was filtered using a sterile 100 µm cell strainer to remove cumulus oocyte complexes and tissue debris. The subsequent filtrate was then passed through a sterile 40 µm filter for isolation of granulosa cells. Granulosa cells remaining in the filter were rinsed with complete base cell culture medium, containing a final concentration of 10% fetal calf serum, 1% insulin-transferrin-sodium selenite (ITS) (10 mg/L human recombinant insulin, 5.5 mg/L human recombinant transferrin, 6.7 µg/L selenious acid), 1% penicillin/streptomycin (50 IU/mL penicillin and 50 µg/mL streptomycin), and 1% GlutaMAX (2 mM L-alanyl-L-glutamine dipeptide in 0.85% NaCl). The isolated cell suspension was centrifuged at 500 × *g* for 10 min. Any contaminating red blood cells were lysed by the addition of 900 µL of cell culture grade H_2O, immediately followed by the addition of 100 µL of sterile 10× phosphate buffered saline (PBS). Cells were then washed with calcium and magnesium free Dulbecco's PBS by centrifugation at 500 × *g* for 10 min. The cell pellet was then resuspended in 1 mL of complete culture medium containing 100 U/mL hyaluronidase and vortexed for 10 s every 3 min for 10 min. Cells were then washed in complete cell culture medium by centrifugation at 500 × *g* for 10

min. Cell concentrations were adjusted to 1.5 × 10^6 cells/mL and plated in 6 well tissue culture plates in 2 mL of complete cell culture medium and cultured at 38.5ºC with 5% CO_2 in humidified air.

After 24 hours of initial culture, adherent granulosa cells were washed in warm PBS immediately prior to the application of treatments. All treatments were applied using complete treatment medium (phenol red-free Medium 199; 10% charcoal-stripped FCS (v/v); 1% ITS (v/v); 1% penicillin/streptomycin (50 IU/mL penicillin and 50 µg/mL streptomycin) (v/v); 1% GlutaMAX (v/v); 1 ng/mL porcine follicle stimulating hormone (v/v); and 1 µM androstenedione (v/v). Granulosa cells were exposed to treatment medium alone or treatment medium containing ultrapure LPS (*E. coli* 0111-B4; tlrl-3pelps) in ten-fold increasing concentrations from 10^2 to 10^4 ng/mL for 24 h.

In Vitro Luteinization of Cultured Granulosa Cells

The luteinization of granulosa cells was performed as previously described (Meidan et al., 1990) with some modifications (**Figure 4-1**). In brief, granulosa cells were collected and treated with LPS or medium alone for 24 h as above. After the initial 24 h exposure to treatment, a sample of conditioned medium was collected and stored at -80ºC. Adherent cells were then rinsed with warmed PBS and incubated with 0.25% trypsin-EDTA for 10 minutes at 38.5ºC in humidified air. The cell suspension was then collected and washed with complete base cell culture medium (as above). Cells were centrifuged at 500 × *g* for 10 min. Cell concentrations were adjusted to 1.5 × 10^6 cells/mL and re-plated in 6 well tissue culture plates in 2 mL of luteinization medium (complete base cell culture medium with the addition of 1% FCS (v/v); 2 µg/mL bovine insulin, and 10 µM forskolin) and cultured at 38.5ºC with 5% CO_2 in humidified air for 48 h. Cells were passaged every 48 hours for 9 d and re-plated at 1.5 × 10^6 cells/ mL. At

each passage, a sample of cells and supernatant was collected and stored at -80ºC. A timeline of the experimental procedure is depicted in **Figure 4-1**.

Quantification of Estradiol and Progesterone in Supernatants

The primary experiment to assess steroid hormone production was repeated using 6 independent biological replicates. Estradiol and progesterone accumulation in supernatants was measured by enzyme immunoassay (Estradiol and Progesterone ELISA, DRG International) according to the manufacturer's instructions, and was previously validated for cell culture supernatants (Bromfield and Sheldon, 2013, Price et al., 2013). Supernatants were diluted (1:100) in standard zero buffer and run in parallel with a provided standard curve. All samples were run in duplicate and measured on a Biotek Synergy HT microplate reader (Agilent, Winooski, VT). The intra-assay coefficient of variation was 12.5% and 16.3 % and the inter-assay coefficient of variation were 9.1 % and 9.0% for estradiol and progesterone, respectively.

RNA Isolation and Real Time Polymerase Chain Reaction

Total RNA was isolated from granulosa and luteal cells using the RNeasy Mini kit (Qiagen) according to the manufacturer's instructions. Quality and quantity of RNA was assessed by an ultraviolet-visible spectrophotometer (Nanodrop 2000, Thermo Fisher Scientific). Total RNA was isolated from cells at the time of cell isolation prior to plating, after the initial treatment, and at each passage of luteal-like cells. Reverse transcription was performed with 1 µg of RNA using the Verso cDNA synthesis kit. Primers for PCR were designed using the NCBI database and are detailed in **Table 4-1**. All primers were validated to ensure they met the MIQE guidelines of $R^2 > 0.98$ and efficiency of 90-110% (Bustin et al., 2009). Each 20 µL reaction consisted of 300 nM of each forward and reverse primer, iTaq Universal SYBR Green Master Mix and cDNA. Amplification

was performed using a Bio-Rad CFX Connect light cycle with an initial denaturation at 95ºC for 30 s followed by 40 cycles of 95ºC for 5 s, 60ºC for 10 s, and a final extension at 60 ºC for 30 s (annealing temperature for *HSD3B1* and *STAR* primers were 54ºC and 55.7ºC , respectively). A no-template negative control which replaced cDNA with water was used to confirm specific amplification for each primer pair. Relative expression for genes of interest was calculated using the $2^{-\Delta Ct}$ method relative to the geometric mean of *GAPDH* and *RPL19.*

Live Cell Fluorescence Microscopy of Mitochondria and Lipid

Granulosa cells from three independent biological replicates were isolated as described above. Cells were plated in 12.5 cm^2 vented tissue culture flasks or 4-chamber, glass bottom 35 mm dishes at a concentration of 1.5×10^5 cells/mL and allowed to adhere for 24 h at 38.5ºC. After an initial 24 h attachment period, non-adherent cells were aspirated from the culture medium and treatment medium was applied (complete treatment medium alone or complete treatment medium containing 10^3 ng/mL LPS). After the 24 h treatment period, treatment medium was removed and cells in the 4-chamber dishes were incubated in complete base medium containing 50 nM MitoTracker Red CMXRos, 1 µM BODIPY 493/503, and 1 µg/mL Hoechst 33342 for 30 min. Cells were then washed with PBS and replaced with complete base medium containing 20 mM HEPES. Cells were maintained on a slide warmer at 38.5ºC shielded from light and immediately imaged using a Zeiss Axio Observer 7 fitted with an Andor DSD2 Spinning Disk Confocal Unit and Zyla Plus 4.2-megapixel camera using a Plan-Apochromat 40 × objective lens. Seven independent fields of view were quantified for each biological replicate and treatment. Mitochondrial and lipid staining were quantified using ImageJ by defining the region of interest around the cell border and measuring

the mean fluorescence intensity for each cell. At each 48 h timepoint after treatment, cells were passaged from flasks and replated at 1.5×10^6 cells/mL for continuous culture and a subset of cells were plated directly into 4-chamber dishes at a concentration of 1.5×10^5 cells/mL in complete luteinization medium for subsequent imaging.

Cellular Respirometry and Mitochondrial Stress Test

Granulosa cells were collected in complete base medium as described above and cultured for an initial 24 h. After the 24 h of culture, non-adherent cells were aspirated from the culture medium, and adherent granulosa cells were washed in warm PBS. Adherent granulosa cells were incubated with 0.25% trypsin-EDTA for 10 min at 38.5ºC in humidified air. Granulosa cells were treated with complete treatment medium alone, complete treatment medium containing LPS in ten-fold increasing concentrations from 10^2 to 10^4 ng/mL, or complete treatment medium containing 1 mM of methyl-β-cyclodextrin for 24 h. Cells utilized for d 1 post-treatment respirometry were resuspended to a final concentration of 7.5×10^4 cells/well and seeded in 80 µL per well into an Agilent XFe96 Spheroid Microplate and cultured for 24 h with treatment. Cells being utilized for continuous culture were suspended to a final concentration of 1.5×10^6 cells/mL and plated in 12.5 cm^2 vented tissue culture flasks. All cells were exposed to treatment for 24 h. After the 24 h treatment period, treatment medium was removed, and cells seeded in the Agilent XFe96 Spheroid Microplate for respirometry were rinsed with 80 µL of warm PBS and 80 µL of Seahorse XF DMEM (Agilent) was added prior to assay. Cells for continuous culture were rinsed with warmed PBS and passaged into a new Agilent XFe96 Spheroid Microplate at 7.5×10^4 cells/well and seeded in 80 µL per

well for the subsequent day analysis and a new 12.5 cm^2 vented tissue culture flask at 1.5 × 10^6 cells/mL every 24 h for 9 days in luteinization medium.

Total Cellular Cholesterol and Cholesterol Uptake Quantification

Total cellular cholesterol was quantified using the Amplex Red Cholesterol Assay kit as previously described (Horlock et al., 2022). Briefly, granulosa cells were collected and plated at 1.5 × 10^6 cells/mL in 6 well plates and treated with complete treatment medium alone, complete treatment medium containing LPS in ten-fold increasing concentrations from 10^2 to 10^4 ng/mL, or complete treatment medium containing 1 mM of methyl-β-cyclodextrin for 24 h. Following 24 h treatment, cells were passaged as above and cultured in luteinization medium at a final seeding density of 1.5 × 10^6 cells/mL. Following replating, 3.0 x 10^5 total cells were aliquoted into a 1.5 mL Eppendorf tube and centrifuged at 500 × *g* for 10 minutes. Supernatant was removed, and the cell pellet was washed twice with warm PBS by centrifugation. Cell pellets were collected in 200 µL of cholesterol assay buffer and stored at -80°C until further processing. Upon thawing, cells were lysed by passing through a 20-gauge needle ten times using a 2 mL syringe, and lysates were diluted (1:5) in cholesterol assay buffer. The assay included a 10 µM H_2O_2 positive control, and empty wells with only assay buffer as a negative control. Estimated values were adjusted for the residual fluorescence calculated in the negative control wells. Plates were measured using a Biotek Synergy HT microplate reader. The intra-assay coefficient of variation was 12.56% and the inter-assay coefficient of variation was 2.59%. Total cellular protein was estimated using the Pierce BCA Protein Assay according to manufacturer's recommendations. Briefly, 25 µL of cell lysate used for total cellular cholesterol

quantification were mixed with 200 µL of working reagent (1:50 dilution) in a 96-well plate and incubated at 37ºC for 30 min and allowed to cool to room temperature. Absorbance was measured at 562 nm. The intra-assay coefficient of variation was 6.85% and the inter-assay coefficient of variation was 20.4%.

Cellular uptake of cholesterol was measured using a pulse of TopFluor fluorescent cholesterol (Avanti Polar Lipids, Alabaster, AL). Cells were collected and treated as previously described (control medium alone or 10^3 ng/mL of LPS). Following treatment, cells were passaged and seeded in 200 µL at a concentration of 1.5×10^5 cells/mL in 8-well Falcon culture slides for 24 h. Fresh medium containing 5 µM TopFluor was applied to cells and returned to the incubator for 1 h. Following the pulse, cells were washed twice with warm PBS and fixed with 4% PFA for 15 min at room temperature. Following fixation, cells were rinsed twice with PBS. Fixed cells were permeabilized for 15 min at room temperature with PBS containing 0.01% Triton-X 100 and 1% BSA and counterstained with 100 nM Phalloidin Alexa Fluor 568 and 1 µg/mL Hoechst 33342 for 30 min. Slides were coverslipped with 200 µL of PBS and imaged using a Zeiss Axio Observer 7 fitted with an Andor DSD2 Spinning Disk Confocal Unit and Zyla Plus 4.2-megapixel camera using a Plan-Apochromat 40× objective lens. Five independent fields of view were quantified for each biological replicate and treatment at each time point. Due to the abundance of cholesterol uptake during luteinization, the camera exposure was reduced for each d to optimize imaging (270 ms 1 d post-treatment to 48.5 ms 9 d post-treatment). The same collection parameters were utilized for all treatments at each given time point. Cholesterol uptake was quantified using ImageJ by defining the region of interest around the cell border and measuring the

mean fluorescence intensity of each cell. Final mean fluorescence values were back transformed by dividing the estimated mean fluorescence intensity by the camera exposure to reflect the increase in cholesterol uptake by the cells.

Statistical Analysis

All statistical analysis were performed using the SAS statistical package (version 9.4; SAS/STAT, SAS Inst. Inc., Cary, NC, USA). For the primary experiment, orthogonal polynomial contrast statements for each dose of LPS were determined using the IML procedure in SAS to make pairwise comparisons for each dose. Supernatant progesterone, gene expression, cell number, respirometry, and total cell cholesterol throughout the culture period were analyzed using the MIXED procedure in SAS with repeated measures. The model included the fixed effects of treatment, day, and interaction between treatment and day, while also accounting for the random effect of replicate nested within treatment to prevent pseudoreplication. Replicate was repeated throughout the analysis. A subsequent analysis was performed for respirometry responses whereby the dose of LPS was removed and the main effect of type of treatment (control, LPS, or methyl-β-cyclodextrin), day, and treatment by day interactions were tested. Cellular fluorescence data were analyzed using the MIXED procedure and the model accounted for the fixed effects of treatment, day, and the interaction between treatment and day. Data for expression of inflammatory genes (*CXCL8 and IL6*) and estradiol were analyzed separately for day 2, representing the 24 h period after the application of LPS using the MIXED procedure in SAS. The model accounted for the fixed effect of treatment and the random effect of observation nested within treatment. Progesterone and gene expression responses failed to meet the assumptions of normality and were transformed in SAS using the Box-Cox procedure

(Box and Cox, 1964) from a macro. Statistical significance was set at $P \leq 0.05$ and interactions between $P \leq 0.10$ and $P \geq 0.05$. Graphs were made using GraphPad Prism v9 (San Diego, CA) and depict least squares means ± standard error of the mean.

Results

Lipopolysaccharide Treatment Increases Expression of Inflammatory Mediators and Reduces Estradiol Accumulation

Exposure of granulosa cells to 10^2 or 10^3 ng/mL LPS increased ($P = 0.008$) the expression of *CXCL8* by 2.3 and 2.2-fold compared to control after 24 h, respectively (**Figure 4-2A)**. Exposure to 10^3 and 10^4 ng/mL LPS increased ($P < 0.001$) the expression of *IL6* by 1.60 and 1.8-fold compared to control after 24 h, respectively (**Figure 4-2B**).

Exposure of granulosa cells to LPS for 24 h reduced ($P = 0.044$) estradiol accumulation compared to control by 87.8%, 93.9%, and 93.3% for each 10-fold increase of LPS (**Figure 4-2C**). Similarly, LPS reduced ($P = 0.029$) the expression of CYP*19A1* compared to control by 58.6%, 78.2%, and 72.9% for each 10-fold increase of LPS (**Figure 4-2D**).

In Vitro Luteinization Increase Cellular Progesterone Secretion

Progesterone accumulation, cell number, and progesterone accumulation corrected for cell number increased ($P < 0.001$) from d 1 until d 9 of culture (**Figure 4-3**), suggesting cells underwent functional luteinization.

Treatment of Granulosa Cells to LPS Reduces Subsequent Progesterone Synthesis During Luteinization

The effect of granulosa cells treated with LPS on subsequent progesterone synthesis was evaluated during luteinization. Overall, treatment of granulosa cells with LPS reduced ($P = 0.001$) the accumulation of progesterone over the 9 d period of

luteinization. The effect of LPS on 48 h progesterone accumulation were most pronounced 3, 5, and 7 d after treatment with 10^3 or 10^4 ng/mL of LPS compared to control cells (**Figure 4-3A**).

The total number of cells at the end of each 48 h period was increased 5, 7 and 9 d after the start of culture compared to d 1. There was no effect of LPS (P = 0.871) on the cell number after each 48 h period (**Figure 4-3B**). When progesterone secretion was normalized to the number of cells present in the well, exposure to LPS reduced (P = 0.002) subsequent progesterone synthesis during luteinization compared to control cells. Furthermore, 10^3 and 10^4 ng/mL of LPS reduced (P = 0.002) the secretion of progesterone 3, 5, 7, and 9 d after treatment compared to control cells (**Figure 4-3C**).

To determine the possible mechanism of altered progesterone synthesis, I evaluated the gene expression of *STAR* and *HSD3B1* (**Figure 4-4**). The day of culture effected (P < 0.001) expression of both *STAR* and *HSD3B1*, where the expression of *STAR* was reduced (P = 0.032) by 516.2% at d 9 compared d 1 (**Figure 4-4A**), and the expression of *HSD3B1* was increased (P < 0.001) by 45.9%, 59.0%, 56.7, and 44.5% on d 3, 5, 7, and 9 compared to d 1 (**Figure 4-4B**). However, granulosa cell treatment with LPS did not affect the expression of *STAR* or *HSD3B1* during luteinization.

Luteinization of Granulosa Cells Increases Cellular Respiration

The Agilent Seahorse Mito Stress Test was used to evaluate if altered mitochondrial function was responsible for reduced progesterone synthesis of cells treated with LPS (**Figure 4-5**). There was no effect of LPS treatment on basal respiration (**Figure 4-5A**), proton leak (**Figure 4-5B**), maximal respiration (**Figure 4-5C**), spare respiratory capacity (**Figure 4-5D**), ATP-linked respiration (**Figure 4-5E**), or non-mitochondrial respiration (**Figure 4-5F**). However, the day of culture affected (P <

0.001) basal respiration, proton leak, maximal respiration, spare respiratory capacity, ATP-linked respiration, and non-mitochondrial respiration suggesting that luteinization altered mitochondrial function during culture.

As a positive control, granulosa cells were treated with 1 mM methyl-β-cyclodextrin (MβCD) for 24 h to deplete intracellular cholesterol (Figure A-2). Basal respiration (P = 0.066) and ATP-linked respiration (P = 0.092) respiration tended to be increased in cells treated with MβCD compared to cells treated with LPS or control. There were also interactions between MβCD and day for basal respiration (P = 0.028), maximal respiration (P = 0.012), spare respiratory capacity (P = 0.011), and ATP-coupled respiration (P = 0.024) suggesting that depleting cellular cholesterol alters mitochondrial function.

Treatment of Granulosa Cells with LPS Reduces Lipid Droplets and Mitochondria Density During Luteinization

To evaluate the effect of LPS treatment on lipid droplet and mitochondria density during luteinization cells were stained with BODIPY 493/503 and MitoTracker CMXros Red (**Figure 4-6A**). Overall, treatment of granulosa cells with LPS reduced (P < 0.001) the mean fluorescence of lipid droplets by 13.4% during luteinization (**Figure 4-6B**). Furthermore, treatment of granulosa cells with LPS reduced (P < 0.050) the staining of lipid droplets on d 1, 3, and 5 after treatment and tended (P = 0.040) to reduced lipid droplets on d 9 d after treatment compared to control. Regardless of treatment, the staining of lipid droplets on d 9 was reduced (P < 0.001) by 50.6% compared to d 1 (**Figure 4-6B**).

While there was not an overall effect of LPS treatment on mitochondrial fluorescence, LPS treated cells on d 3 after treatment show reduced (P < 0.001)

mitochondrial fluorescence compared to control cells on d 3 (**Figure 4-6C**). Regardless of treatment, there was an overall effect of day on mitochondrial fluorescence whereby cells on d 9 had an 82.8% increase ($P < 0.001$) in fluorescence compared to d 1 (**Figure 4-6C**). Overall, treatment with LPS reduced ($P = 0.001$) the ratio of lipid droplet fluorescence to mitochondrial fluorescence (**Figure 4-6D**). Specifically, the LPS reduced ($P < 0.001$) the ratio of lipid droplet fluorescence to mitochondrial fluorescence on d 1 and d 5 compared to control. In addition, regardless of treatment the ratio of lipid droplet fluorescence to mitochondrial fluorescence was reduced ($P < 0.001$) by 92.6% on 9 d compared to d 1 of culture (**Figure 4-6D**).

Treatment of Granulosa Cells with LPS Reduces Cholesterol Uptake During Luteinization

To evaluate the effect of LPS treatment on acute cholesterol uptake cells were incubated with a 1 h pulse of fluorescently labeled cholesterol during luteinization (**Figure 4-7A**). Overall there was no effect of LPS treatment on cholesterol uptake; however there was a LPS by day interaction ($P < 0.001$), whereby LPS treatment reduced cholesterol uptake on d 1 and 3 (**Figure 4-7B**). Regardless of treatment, cells dramatically increased cholesterol uptake during luteinization from d 1 to d 9, such that cholesterol uptake was increased by 3.6-fold between d 1 and d 9 ($P < 0.001$).

Total cellular cholesterol was quantified to determine the effect of LPS or MβCD treatment on both cholesterol uptake and de novo cholesterol synthesis (**Figure 4-8**). Overall, there was no effect of treatment on total cellular cholesterol (**Figure 4-8A**) or total cellular protein (**Figure 4-8B**). Finally, the concentration of cellular cholesterol was normalized on a per milligram of total cellular protein and there was no effect of treatment on normalized cholesterol during luteinization (**Figure 4-8C**).

Discussion

Subfertility of dairy cows after resolution of uterine disease is likely potentiated by a multitude of effects on various reproductive tissues, including the ovary. Uterine disease is associated with reductions in postpartum follicular growth and estradiol secretion (Sheldon et al., 2002, Williams et al., 2007). Additionally, the reduced estradiol secretion of granulosa cells following LPS challenge in vitro is well documented (Bromfield and Sheldon, 2011, Price et al., 2013, Dickson et al., 2022b). However, the direct relationship between prior follicular and granulosa cell inflammation and the steroidogenesis of the corpus luteum is unclear. Here, bovine granulosa cells were isolated from small to medium follicles and treated with LPS in vitro and encouraged to undergo luteinization. As we expected, LPS treatment increased the expression of *CXCL8* and *IL6* indicative of an inflammatory response. Furthermore, 24 h exposure of granulosa cells to LPS reduced the secretion of estradiol and the expression of *CYP19A1*.

While the molecular mechanisms leading to LPS reducing *CYP19A1* expression, aromatase abundance, and estradiol secretion in granulosa cells is unclear, this phenotype following uterine disease and LPS challenge have been repeated numerous times both in vitro and in vivo. Despite this repeatable observation on follicle and granulosa cell function, the effects of uterine disease or LPS challenge on luteal function are less clear. In observational studies, cows with active uterine disease have reduced corpus luteum diameter and peripheral progesterone (Sheldon et al., 2002, Williams et al., 2007, Strüve et al., 2013, Bruinjé et al., 2023). The effects of uterine disease or LPS on corpus luteum function in experimental settings are conflicted. Repeated intrauterine infusion of LPS reduced peripheral progesterone and luteal

expression of *STAR, HD3B1*, and *PTGFR* compared to cows receiving saline infusion (Lüttgenau et al., 2016a). Perfusion of mid-cycle corpora lutea with LPS reduced progesterone responsiveness to hCG, but was attributed to elevated levels of luteal apoptosis rather than alterations in steroidogenesis (Lüttgenau et al., 2016b). However, in synchronized lactating cows with subclinical endometritis there were no detectable differences in peripheral progesterone after insemination (Molina-Coto et al., 2020). Furthermore, the effects of LPS on luteal function have also been investigated in vitro with conflicting results. Thecal cells treated with LPS and allowed to luteinize had reduced progesterone secretion, STAR and HSD3B protein abundance compared to controls; however, the direct LPS treatment of cultured luteal cells increased the secretion of progesterone compared to control cells (Grant et al., 2007, Shimizu et al., 2016). Here, I demonstrate that treatment of granulosa cell with LPS results in carry over effects on the ability of cells to produce progesterone during the process of luteinization. While the effects we observed of LPS treatment on granulosa cell *CYP19A1* expression are consistent with those reported by others, the effects of LPS on gene expression during luteinization are less clear. I detected no effect of LPS treatment on the expression of genes critical for progesterone production or in the proliferative capacity of cells during luteinization. Given this, I next sought to investigate potential cellular mechanisms that could result in the reduced progesterone synthesis observed following LPS treatment of granulosa cells.

The process of luteinization and the synthesis of progesterone in luteal cells involves coordinated changes to the endocrine and intracellular physiology with respect to the signaling molecules, steroidogenic enzymes, cholesterol availability, and

mitochondrial activity that permit the synthesis of high levels of steroid hormone. As such, there are many possible sites in the steroidogenic pathway for acute control of progesterone synthesis. Central to progesterone biosynthesis is the canonical signaling pathway which begins with LH binding the LH receptor. The LH receptor is a G protein-coupled transmembrane receptor, which upon activation stimulates increases in cellular concentrations of cyclic adenosine monophosphate (cAMP), activation of protein kinase A (PKA), and phosphorylation of PKA targeted enzymes (Przygrodzka et al., 2021). Some in vivo evidence indicates there are reductions to the pulsatile release of GnRH and LH following intravenous LPS challenge compared to control (Peter et al., 1989, Battaglia et al., 1997). However, when LPS is infused directly into the uterus of heifers, there are no differences in the concentrations of peripheral LH compared to control heifers (Sheldon et al., 2002, Williams et al., 2008). Reduced LH in cows with uterine disease may result in impaired cell signal transduction and improper luteinization of granulosa cells following ovulation that results in altered progesterone synthesis.

Cholesterol availability is an essential requirement to produce progesterone. While *de novo* cholesterol synthesis in luteal cells occurs and is facilitated by the mevalonate pathway, the primary sources of cholesterol are derived from the blood in the forms of either high- or low-density lipoprotein cholesteryl esters (Wiltbank et al., 1989, Carroll et al., 1992a, Carroll et al., 1992b). Follicular fluid also contains more HDL cholesterol than LDL cholesterol (Horlock et al., 2022). Interestingly, cholesterol is required for bovine granulosa cells to generate an inflammatory response to LPS, where granulosa cells cultured in either serum or follicular fluid containing cholesterol increased LPS-stimulated secretion of inflammatory mediators, while depleting

cholesterol availability attenuated the LPS induced inflammatory response (Horlock et al., 2022). The siRNA inhibition of mevalonate pathway enzymes *HMCGR, FDPS,* and *FDFT1* also reduced the capacity of granulosa cells to respond to LPS treatment, demonstrating the importance of cholesterol in ovarian cell physiology beyond steroidogenesis (Horlock et al., 2022). The work presented here demonstrates that LPS treatment of granulosa cells reduces cellular uptake up exogenous cholesterol during luteinization which could be responsible for altered progesterone synthesis. This observation, however, was independent of any detectable changes in total cellular cholesterol. One possible explanation for the lack of difference in total cellular cholesterol is that luteal cells are upregulating de novo cholesterol synthesis following an LPS challenge. This speculation could be supported by the evidence demonstrated by Horlock et al., (2022) whereby attenuating the mevalonate pathway reduced the inflammatory response of granulosa cells; during luteinization the upregulation of de novo cholesterol synthesis may be a compensatory mechanism to maintain cellular homeostasis. Furthermore, cholesterol is the glue that maintains lipid rafts in cell membranes. Lipid rafts are dynamic, small floating units of protein and lipids within the bilayer of cellular membranes and are intimately involved in signal transduction and the pathogenesis of diseases (Simons and Ehehalt, 2002). Toll-like receptor 4 and other components of TLR4 signaling pathway such as CD14, heat shock proteins 70/90, and MAP kinases translocate to lipid rafts of macrophages upon stimulation with LPS (Triantafilou et al., 2002, Olsson and Sundler, 2006). Interestingly, LPS stimulation causes rapid formation and expansion of lipid rafts, sequestering cholesterol to these microdomains to favor molecular interactions during innate immune responses (Nomura

et al., 2011). It is intriguing to speculate about the implications of lipid raft formation after stimulation by LPS and whether cholesterol sequestration affects steroid biosynthesis. Ultimately these results suggest that the cholesterol inside the cell may be involved in other roles independent of steroidogenesis.

Upon receptor mediated endocytosis, intracellular cholesterol has two fates: trafficking directly to the mitochondria or storage in lipid droplets as cholesterol esters (Niswender, 2002). Bovine luteal cells contain a greater number of lipid droplets than other tissues aside from adipocytes and act as intracellular hubs for storage of neutral lipids such as cholesterol esters and triglycerides (Talbott et al., 2020, Przygrodzka et al., 2021). Activation of the LH receptor initiates downstream signaling that ultimately results in the phosphorylation of enzymes by PKA, including hormone sensitive lipase (HSL) that facilitates the hydrolytic release of cholesterol from intracellular lipid droplets (Plewes et al., 2020). A certain degree of lipolysis is required for luteal cells to produce progesterone; however, adipocytes stimulated with LPS increase lipolysis compared to controls, suggesting that lipolysis in adipocytes is facilitated by activation of both the classical pathways (when LH binds to the LH receptor) and inflammatory pathways that increase cAMP, the phosphorylation of PKA and activation of HSL (Chirivi et al., 2022). Under the inflammatory lipolytic pathway, however, the resulting activation of HSL is facilitated by the activation of MEK/ERK signaling and the impairment of Akt phosphorylation (Chirivi et al., 2022). The data presented here show that LPS treatment of granulosa cells reduces the abundance of lipid droplets during the early phases of luteinization. The reduced staining for lipids observed here may be attributed to either reduced cholesterol synthesis or increased hydrolytic cleavage of lipids from the lipid

droplets. Thus, the effects of LPS on the abundance and phosphorylation status of HSL during luteinization need to be investigated.

After the hydrolytic cleavage of cholesterol from lipid droplets, cholesterol is transported across the outer mitochondrial membrane to the inner mitochondrial membrane via the steroidogenic acute regulatory protein (STAR). Mitochondria contain the P450 side chain cleavage enzyme (CYP11A1) which catalyzes cholesterol into pregnenolone (Farkash et al., 1986). Pregnenolone is then shuttled out of the mitochondria where it is converted into progesterone by the protein 3β-HSD in the endoplasmic reticulum (Cherradi et al., 1994). Thus, mitochondria are integral in the synthesis of progesterone by luteal cells. The experiment here measured mitochondrial respiration as a proxy for mitochondrial membrane function and found that LPS treatment of granulosa cells had no effect on cellular respiration during luteinization. Interestingly, however, is that LPS treatment of granulosa cells reduced the staining for MitoTracker during luteinization. MitoTracker only accumulates in membrane permeable mitochondria and given that there were no observed differences in mitochondrial respiration it is plausible to conclude that either the size or number of mitochondria are being reduced during luteinization because of previous LPS treatment of granulosa cells. Thus, it is interesting to postulate on mechanisms that could regulate inflammation induced mitophagy or potential compensatory mechanisms by which LPS alters cellular metabolism during luteinization.

In these series of experiments, it was determined that LPS treatment of granulosa cells has many effects on the cellular function of cells during luteinization which are summarized in **Figure 4-9**. Further studies are warranted to determine

specific mechanisms relating to the reduced uptake of cholesterol and to determine if LPS treatment of granulosa cells affects the abundance of critical lipases which facilitate the hydrolytic cleavage of stored cholesterol esters from lipid droplets. Additionally, the roles of inflammation mediated mitophagy warrant investigation in the context of steroidogenic cells. Collectively, these studies suggest that inflammation of the ovarian follicle caused by uterine disease could alter the steroidogenic function of subsequent luteal cells after the resolution of disease. If uterine disease does indeed alter corpus luteum function after the resolution of uterine disease, this could in part help to explain the subfertility of cows caused by uterine disease.

Table 4-1. Primer sequences used for real time RT-PCR

Gene Symbol	Primer sequence	Accession number
ACTB	5′ – CAGAAGCACTCGTACGTGGG – 3′ 3′ – TTGGCCTTAGGGTTCAGGG – 5′	NM_173979.3
CXCL8	5′ – GCAGGTATTTGTGAAGAGAGCTG – 3′ 3′ – CACAGAACATGAGGCACTGAA – 5′	NM_173925.2
CYP19A1	5′ – CGCAAAGCCTTAGAGGATGA – 3′ 3′ – ACCATGGCGATGTACTTTCC – 5′	NM_174305.1
GAPDH	5’ – AGGTCGGAGTGAACGGATTC – 3′ 3’ – ATGGCGACGATGTCCACTTT – 5′	NM_001034034.2
HSD3B1	5’ – CACAATCTGACCGCATCGT – 3′ 3’ – GAGAAACGCTCACCAGGAAC – 5′	NM_174343.3
IL6	5′ – ATGACTTCTGCTTTCCCTACCC – 3′ 3′ – GCTGCTTTCACACTCATCATTC – 5′	NM_173923.2
RPL19	5’ – ATGCCAACTCCCGCCAGCAGAT – 3′ 3’ – TGTTTTTCCGGCATCGAGCCCG – 5′	NM_001040516.2
STAR	5′– AGAAGGGTGTCATCAGAGCG – 3′ 3′ – TGGTCCTTGAGGGACTTCCA – 5′	NM_174189.3

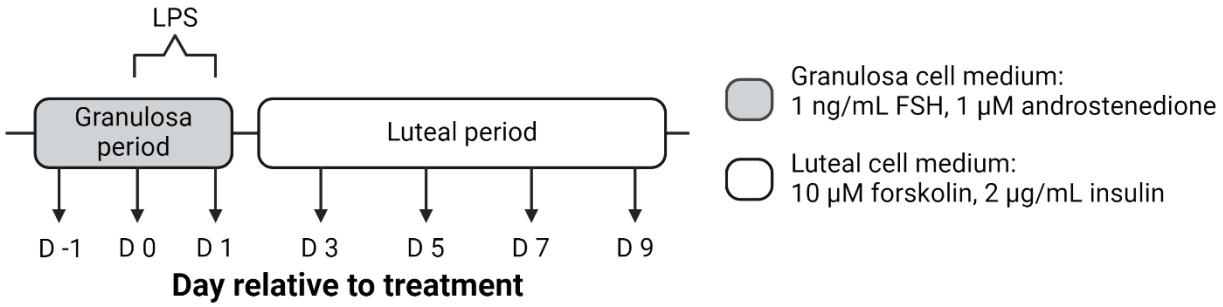

Figure 4-1. Experimental model. Bovine granulosa cells were isolated from 4-8 mm diameter follicles from abattoir derived ovaries and plated at 1.5 x 10^6 cells/mL. Granulosa cells were cultured in granulosa cell medium containing 1 ng/mL follicle stimulating hormone and 1 μM androstenedione for 24 h and then treated with 10-fold increasing doses of LPS for 24 h. On d 1 after treatment, granulosa cells were collected and replated at the same starting density of 1.5 x 10^6 cells/mL now in luteal cell medium containing 10 μM forskolin and 2 μg/mL bovine insulin. Cells were collected and sampled every 48 h for a total of 9 d, each time being replated at 1.5 x 10^6 cells/mL.

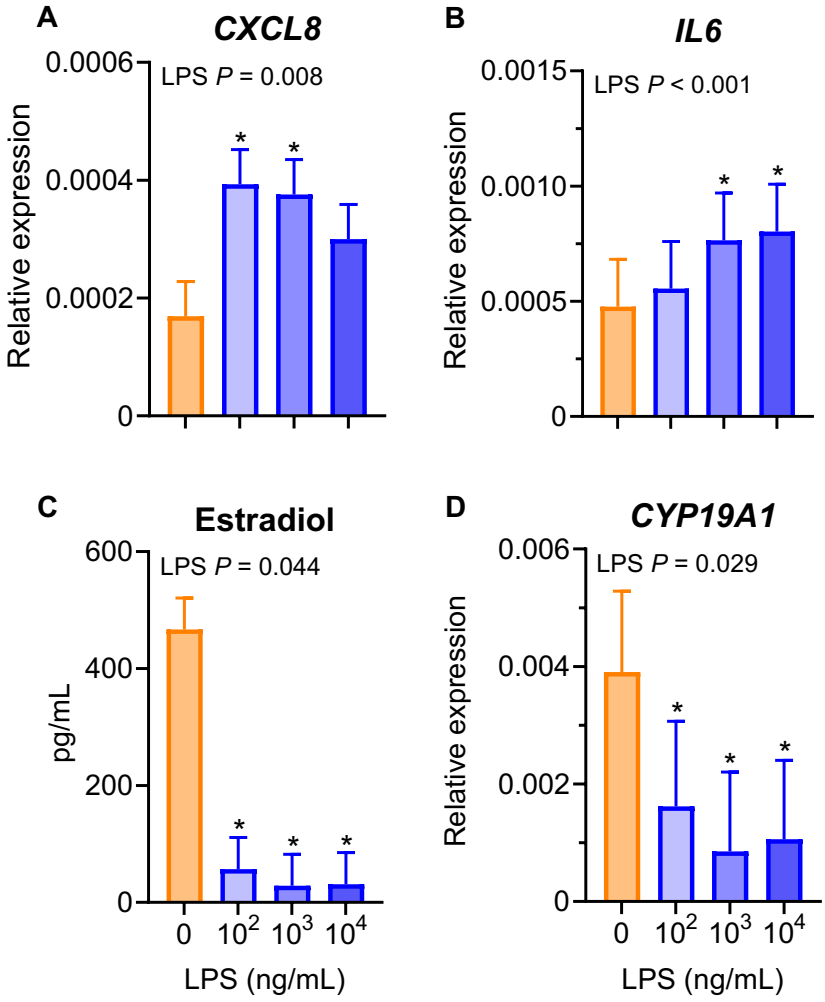

Figure 4-2. Acute response of granulosa cells to LPS**.** Bovine granulosa cells (n = 6) were treated with 10-fold increasing doses of LPS for 24 h. Following treatment, cells were collected and analyzed by RT-PCR for the expression of *CXCL8* (A), *IL6* (B) and *CYP19A1* (D). The 24 h accumulation of estradiol was quantified by ELISA (C). Data are presented as least squares means ± SEM. Asterisks indicate statistical significance ($P < 0.05$) compared to the medium alone control.

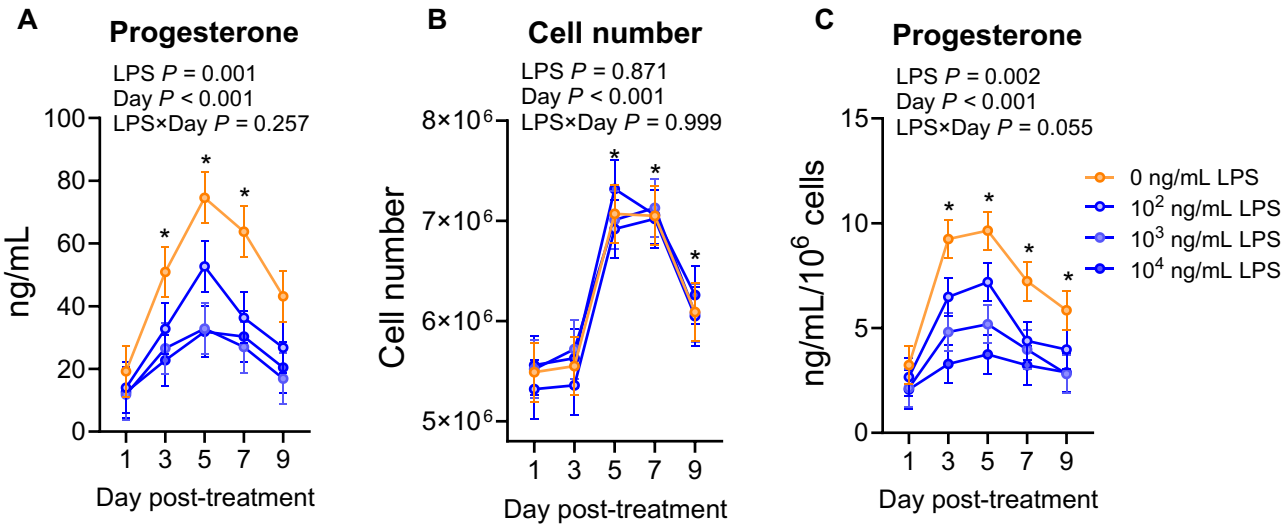

Figure 4-3. Effect of granulosa cell treatment with LPS on progesterone synthesis during luteinization. Granulosa cells (n = 6) were treated with LPS or medium alone and cultured in luteinization medium for 9 d. Progesterone accumulation was quantified every 48 h by ELISA (A). Cell number was assessed every 48 h with each passage (B) and accumulation of progesterone was normalized to cell number (C). Data are presented as least squares means ± SEM. Asterisks in panel A and C indicate statistical significance ($P < 0.05$) for the effect of LPS (10^3 and 10^4 *vs.* control). Asterisks in panel B indicate statistical significance ($P < 0.05$) for the effect of day (day 1 *vs.* day 9).

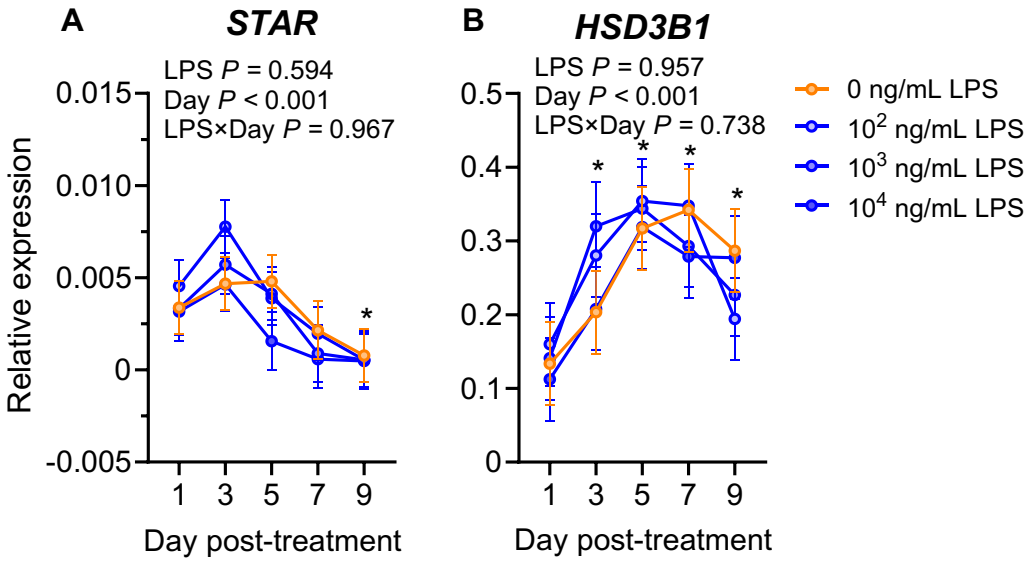

Figure 4-4. Effect of granulosa cell treatment with LPS on expression of steroidogenic machinery during luteinization. Bovine granulosa cells (n = 6) were treated with 10-fold increasing doses of LPS for 24 h. Following treatment, cells were collected every 48 h and analyzed by RT-PCR for the relative expression of *STAR* (A) and *HSD3B1* (B). Data are presented as least squares means ± SEM of the relative expression of each gene calculated using the $2^{-\Delta Ct}$ method relative to the geometric mean of *GAPDH* and *RPL19*. Asterisks indicate statistical significance ($P < 0.05$) for the effect of day (day 1 *vs.* day 9).

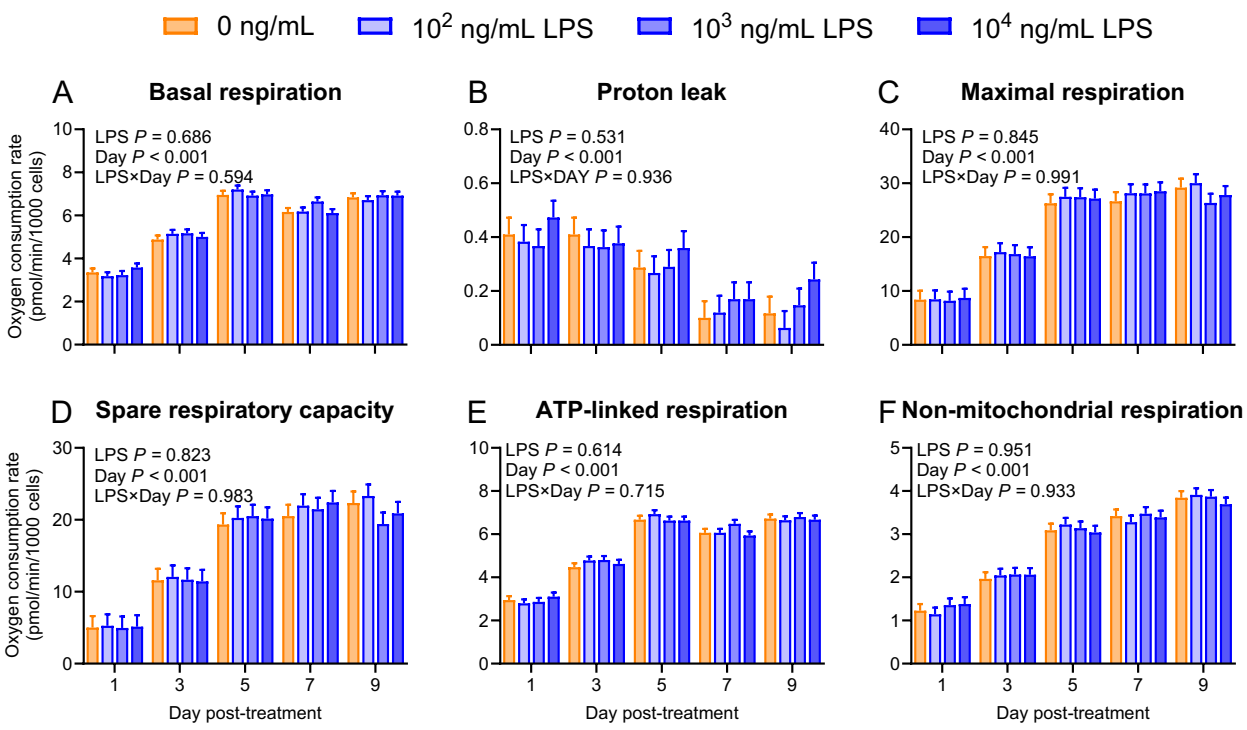

Figure 4-5. Effect of LPS treatment on cellular respiration. Bovine granulosa cells (n = 3) were treated with 10-fold increasing doses of LPS for 24 h and cellular respiration was evaluated every 48 h using the Agilent SeaHorse MitoStress Test. Basal respiration (A), proton leak (B), maximal respiration (C), spare respiratory capacity (D), ATP-linked respiration (E), and non-mitochondrial respiration (F) were measured. Data are presented as least squares means ± SEM.

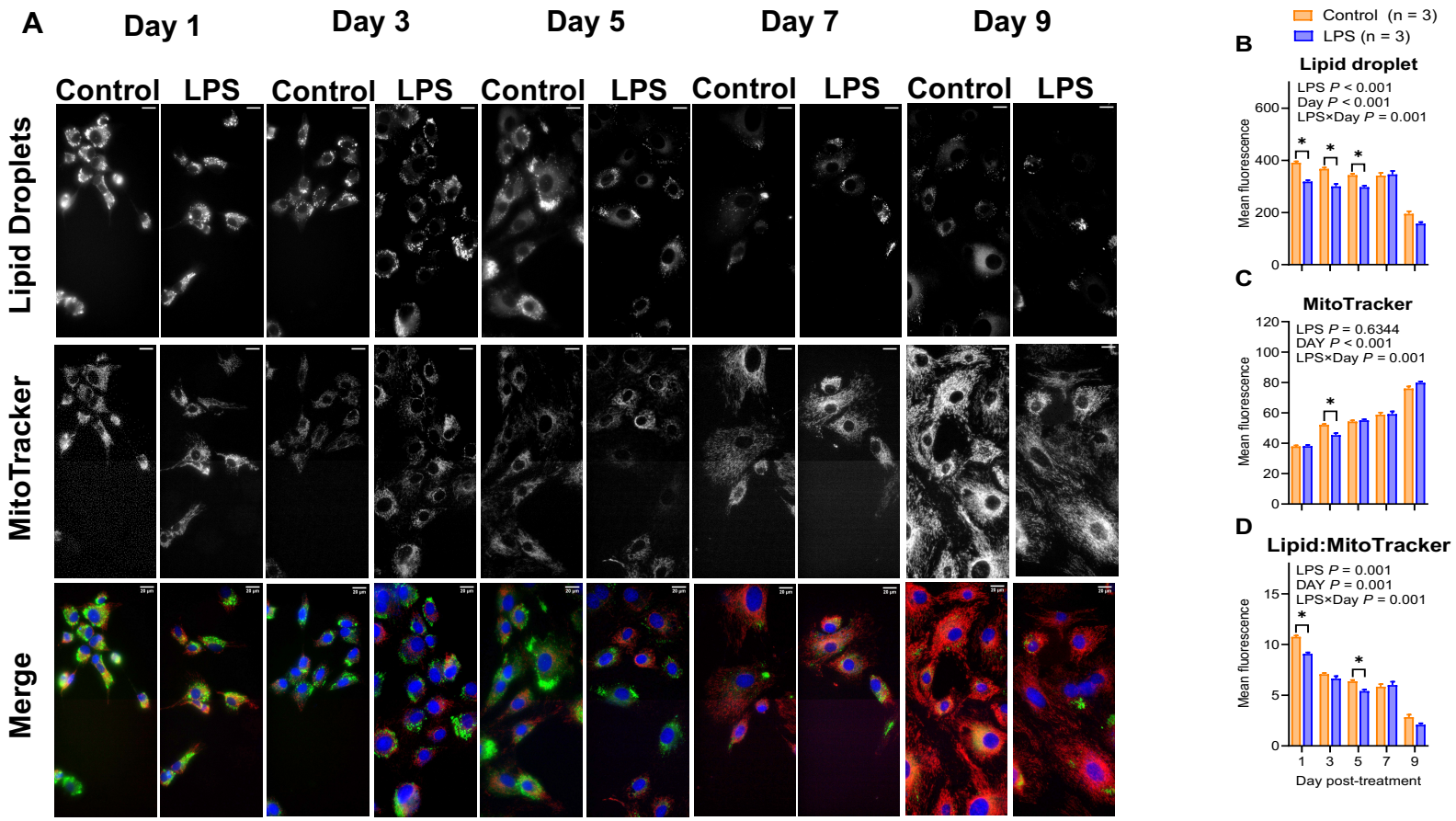

Figure 4-6. Effect of granulosa cell treatment with LPS on lipid droplet and mitochondria density during luteinization. Bovine granulosa cells (n = 3) were treated with 10^3 ng/mL of LPS for 24 h and the density of lipid droplets and mitochondria were assessed every 48 h during luteinization using BODIPY 493/503 (green) and MitoTracker CMXRos Red (red) with confocal microscopy (A). The mean fluorescence intensity per cell was measured using ImageJ for lipid droplets (B) and mitochondria (C). Furthermore, the ratio of lipid droplets to mitochondria was calculated (D). Data are presented as least squares means ± SEM. Asterisks indicate statistical significance ($P < 0.05$). Scale bar represents 20 µm.

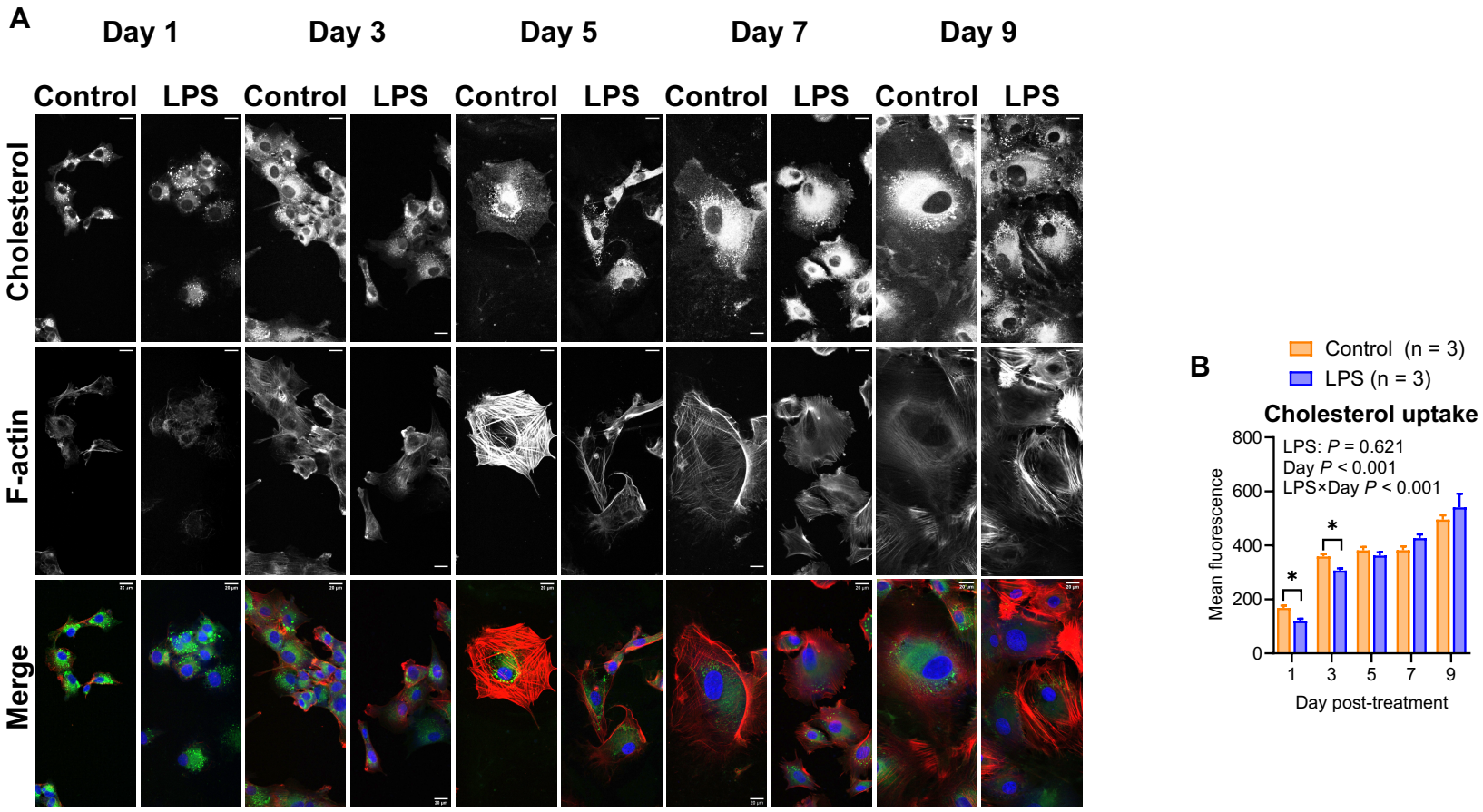

Figure 4-7. Effect of granulosa cell treatment with LPS on cholesterol uptake during luteinization. Bovine granulosa cells (n = 3) were treated with 10^3 ng/mL of LPS for 24 h and exogenous cholesterol (green) uptake was assessed every 48 h during luteinization (A). Cells were counterstained with phalloidin (red). The mean fluorescence intensity per cell was measured using ImageJ following a 1 h pulse of fluorescently labeled cholesterol during luteinization (B). Data are presented as least squares means ± SEM. Asterisks indicate statistical significance ($P < 0.05$). Scale bar represents 20 μm.

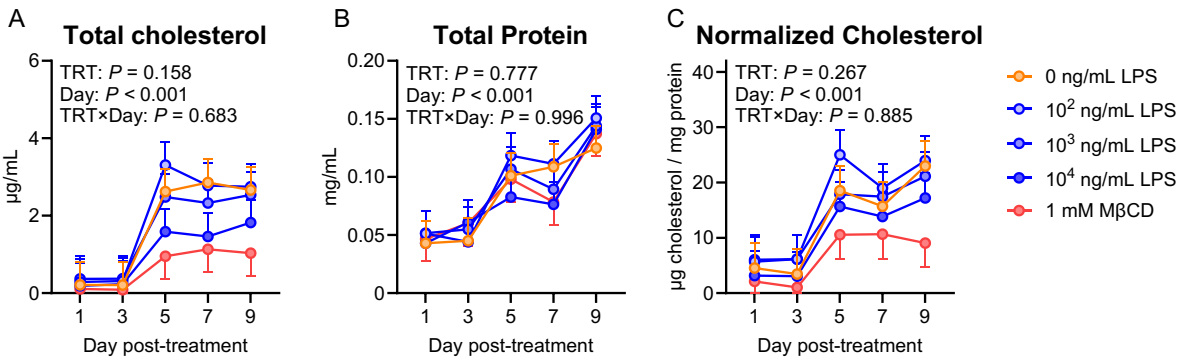

Figure 4-8. Effect of granulosa cell treatment with LPS total cellular cholesterol during luteinization. Bovine granulosa cells (n = 6) were treated with 10-fold increasing doses of LPS or 1 mM of methyl-β-cyclodextrin (MβCD) for 24 h. Total cellular cholesterol was measured every 48 h during luteinization using the Amplex Red Cholesterol Assay, which determines both unbound cellular cholesterol and cholesterol stored as cholesterol esters within lipid droplets (A). Total cellular protein was quantified with the Pierce BCA Protein Assay (B) and total cellular cholesterol was normalized to total cellular protein (C). Data are presented as least squares means ± SEM.

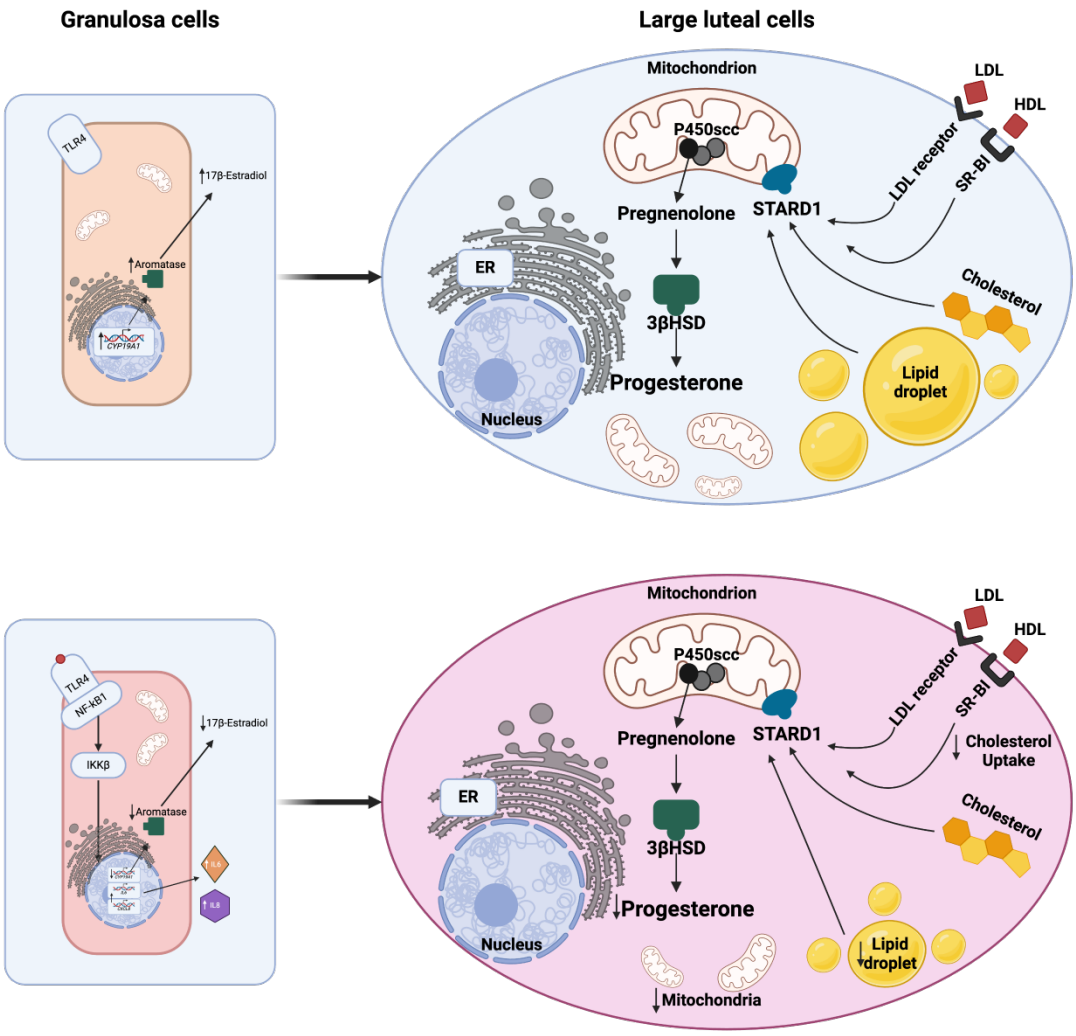

Figure 4-9. Conceptual model for the carryover effects of LPS on granulosa cells during luteinization. Granulosa cell exposure to LPS increases the expression of *CXCL8* and *IL6* and reduces the expression of *CYP19A1*. Treatment with LPS reduces granulosa cell secretion of 17β-estradiol. Granulosa cells treated with LPS secrete less progesterone during luteinization. The reduction in progesterone secretion is not attributed to differences in the expression of *STAR* or *HSD3B1*; however prior LPS treatment reduced cholesterol uptake, reduced lipid droplet accumulation, and reduced mitochondria density during luteinization helping to explain the mechanisms by which granulosa cell treatment with LPS alters steroidogenesis during luteinization.

CHAPTER 5
THE EFFECTS OF INDUCED ENDOMETRITIS ON OOCYTE DEVELOPMENTAL COMPETENCE AND ENDOMETRIAL GENE EXPRESSION

Summary

Uterine diseases occur in up to 40% of dairy cows and influence the ability of cows to become pregnant for extended periods of time after the resolution of disease. While the specific mechanisms of disease associated infertility are not known, functional changes to both the uterus and ovary are proposed targets that likely contribute to observed infertility. Here, I induced endometritis in non-lactating Holstein cows by performing an intrauterine infusion of pathogenic *Escherichia coli* and *Trueperella pyogenes*. I hypothesized that induced endometritis would 1) compromise the competence of oocytes to develop to the blastocyst stage, and 2) alter the endometrial transcriptome many weeks later at a time coincident with conceptus elongation. Cumulus oocyte complex recovered 23 d after bacteria infusion using ultrasound assisted ovum-pick up were submitted to in vitro maturation, fertilization, and embryo culture. There was no effect of induced endometritis on the total number of oocytes, or the proportion of high, mid, or low-quality oocytes recovered from donors compared to control. In addition, induced endometritis did not affect the proportion of oocyte to cleave, the proportion of oocytes to develop to blastocyst stage embryos, or the proportion of cleaved zygotes to develop to blastocyst stage embryos. Next, endometrial samples were collected 41 d after bacteria infusion at d 16 of the estrous cycle by cytobrush and submitted for RNA sequencing. A total of 203 differentially expressed genes were identified in the endometrium of cows after the infusion of bacteria compared to controls. Bacteria infusion increased the expression of Glutathione S-Transferase Alpha 3 (*GSTA3*) by 6.8 $\log_2$ fold, and decreased the

expression of Myomaker, Myoblast Fusion Factor (*MYMK)* by 3.9 $\log_2$ fold compared to controls. Functional characterization of the differentially expressed genes revealed that 54 canonical pathways and 112 predicted upstream regulators were altered following bacteria infusion. The top predicted canonical pathway effected by the infusion of bacteria was glutathione-mediated detoxification. The top three predicted upstream regulators of differentially expressed genes following bacteria infusion were interferon gamma, NFκB complex, and lipopolysaccharide. I speculate that the intrauterine infusion of pathogenic bacteria changes the transcriptional landscape at d 16 of the estrous cycle, which is a time coincident with conceptus elongation, and that these changes may diminish the endometrial capacity to support pregnancy. In conclusion, the intrauterine infusion of pathogenic bacteria had no effect on the developmental competency of oocytes to the blastocyst stage of development but did alter the endometrial transcriptome many weeks later that may perpetuate pregnancy failure. Understanding the molecular and cellular pathways altered in cows after uterine disease will allow for further development of targeted strategies to improve fertility in these cows.

Introduction

Bacterial infections of the uterus in dairy cows reduces fertility by undefined mechanisms (Sheldon and Dobson, 2004). Uterine disease in dairy cattle is associated with increased intrauterine and intrafollicular concentrations of lipopolysaccharide (Herath et al., 2007, Herath et al., 2009). It is likely that reductions in fertility after the resolution of disease are mediated by changes to both the uterus and the ovary. Indeed, the uterus is susceptible to the direct effects of uterine pathogens because parturition disrupts the protective endometrial epithelial barrier and cervical dilation permits bacterial entry to the uterine environment. The consequences of uterine contamination

and exposure to bacterial pathogen associated molecular patterns (PAMP) is rapid mobilization of neutrophils to the endometrial epithelium and increased secretions of PGE2, IL1, IL6, and IL8 (Herath et al., 2006, Davies et al., 2008, Cronin et al., 2012, Turner et al., 2014).

While immune cells work to rapidly clear infections of the uterus, the resulting inflammation has specific effects on the molecular functions of uterine tissue. Indeed, subclinical endometritis 50 d postpartum alters the endometrial transcriptome and miRNAome compared to cows without endometritis (Salilew-Wondim et al., 2016). The infusion of pathogenic *Escherichia coli* and *Trueperella pyogenes* into the uterus of virgin heifers three months prior to the time of tissue collection revealed transcriptional changes to endometrial tissues but also oviductal tissues, indicating that there are persistent changes to the reproductive tract following the resolution of infection and inflammation (Horlock et al., 2020). When a similar infection model was utilized and cows were inseminated 130 d after infusion for tissue collection on day 16 of pregnancy, it was discovered that the endometrial response to pregnancy was altered in cows previously exposed to bacterial infusion (Dickson et al., 2022). Thus, these works indicate that the endometrium is susceptible to long-term changes in gene expression, which may contribute to altered cellular and molecular functions necessary to support pregnancy.

Uterine infection also has specific effects on the cells of the ovary. Indeed, there are effects of bacterial infusion on oocyte molecular function and developmental competence. When *E. coli* and *T. pyogenes* were infused into the uterus of heifers and oocytes were collected 4- and 60-days later, there were distinct changes to the oocyte

transcriptome between bacteria and control infused heifers (Piersanti et al., 2020). The transcriptional changes that were identified were not shared between oocytes collected from the earlier and later timepoints, indicating that follicles at different stages of folliculogenesis may be differentially susceptible to uterine inflammation (Piersanti et al., 2020). In an experiment where cows received an intrauterine infusion of *E. coli* and *T. pyogenes* and had recovered oocytes submitted to IVF, oocytes recovered from bacteria infused cows had a reduced capacity to develop morula stage embryos compared to controls (Dickson et al., 2020). This change in developmental competency was most pronounced 24 d following intrauterine infusion.

Taken together, these data indicate that there are changes to both the endometrium's ability to support pregnancy and the developmental competence of the oocyte to the morula stage of development. I hypothesized that induced endometritis would 1) compromise the competence of oocytes to develop to the blastocyst stage, and 2) alter the endometrial transcriptome many weeks later at a time coincident with conceptus elongation. To address this hypothesis, I utilized an induced uterine infection model to elucidate the unique effects of bacterial infection on both the day 16 endometrium and the developmental competence of oocytes. Data presented here provide further evidence that there are long term effects of bacteria infusion on the endometrium on d 16 of the estrous cycle after the resolution of infection and inflammation.

Materials and Methods

All procedures utilized for this experiment were approved by the University of Florida Institutional Animal Care and Use Committee under the protocol number

202300000040. The experiment was conducted from May to December 2023 at the University of Florida Dairy Research Unit.

Experimental Protocol and Establishment of Uterine Infection

The establishment of uterine infections followed the protocols of Piersanti et al., (2019b) and Dickson et al., (2020) with minor modifications (**Figure 5-1**). Sixty-one primiparous non-lactating Holstein cows were enrolled in the experiment which consisted of three experimental periods. Thirty-four cows were utilized in the first two experimental periods. Period three utilized a cohort of 27 new cows and 5 cows from the two previous periods. Cow was defined as the experimental unit. The methods below were repeated for each experimental period and are depicted in **Figure 5-1**. Cows were maintained on pasture and fed a total mixed ration daily with ad libitum access to water. Cows for the first two periods were stratified by identification number once at the beginning of the experiment and randomly assigned by random number generation in Microsoft Excel to one of two infusion groups (intrauterine infusion of either PBS or bacteria). Cows retained from the first two periods retained the corresponding treatment, and the cohort of 27 new cows were randomly assigned to either infusion group as above.

Prior to the intrauterine infusion of treatment, the estrous cycle of cows were synchronized using a Double-OvSynch protocol. Briefly, cows received an i.m. injection of 100 μg GnRH gonadorelin diacetate tetrahydrate (Cystorelin, Boehringer Ingelheim, Ingelheim am Rhein, Germany) followed by i.m. injection of 25 mg prostaglandin F2α (PGF2α) (dinoprost tromethamine; Lutalyse HighCon, Zoetis, Parsippany-Troy Hills, NJ) 7 d later and GnRH after 3 and 10 d, PGF2α after 7 days and a final GnRH injection 56 h following the previous PGF2α to initiate ovulation (Souza, 2008). Uterine infusions

corresponded to 3 d after ovulation. On the day of intrauterine infusion (experimental d 0) cows received caudal epidural anesthesia of 60 mg lidocaine hydrochloride 2% (Aspen Veterinary Resources, Greely, CO) injected into the intercoccygeal intervertebral space. External genitalia were cleaned with 70% ethanol and wiped with paper towels. The lower reproductive tract was flushed twice with 1% chlorohexidine solution (Aspen Veterinary Resources) and flushed after each rinse with 0.9% saline. A Neilson catheter (450 mm; Supplies for Farmers, Lincolnshire, UK) covered with an AI chemise (IMV Technologies, Brooklyn Park, MN) was introduced transvaginally and passed through the cervix into the uterine body via rectal palpation. The chemise was broken at the cranial end of the cervix prior to entering the uterine body. Once inside the uterine body, the catheter port was palpated and rotated four times against the endometrial lining to debride the endometrium prior to the intrauterine infusion for cows receiving bacterial infusion. Uterine debridement was excluded in cows receiving a PBS infusion. Cows receiving bacterial infusion (n = 32) received 10 mL of Luria-Bertani (**LB**) broth containing 5.2 ± 1.95 × 10^7 CFU/mL *E. coli* MS499 and 10 mL of LB broth containing 3.82 ± 8.61 × 10^6 CFU/mL *T. pyogenes* MS249 followed by 10 mL of PBS to flush the catheter. Control cows (n = 29) received an intrauterine infusion of 30 mL of sterile PBS. Following intrauterine infusion, cows were housed in separate pastures within the same facility and were not permitted to comingle.

Propagation of Pathogenic *E. coli* and *T. pyogenes* for Intrauterine Infusion

Bacterial cultures were prepared as previously described (Piersanti et al., 2019b, Dickson et al., 2020). Briefly, *E. coli* MS499 was cultured from frozen glycerol stock on LB agar (Goldstone et al., 2014b). The day before intrauterine infusion, a single bacterial colony was picked from the plate and inoculated into LB broth containing 1%

tryptone, 0.5% yeast extract and 1% sodium chloride. The bacterial suspension was incubated overnight at 37ºC with gentle shaking at 200 rpm. Concurrently, *T. pyogenes* MS249 was grown from frozen glycerol stock on Trypticase Soy Blood agar at 37ºC for 48 h (Goldstone et al., 2014a). The day before infusion, a single colony was selected and inoculated into Bacto Brain Heart Infusion broth (Thermo Fisher Scientific, Waltham, MA) supplemented with 5% fetal bovine serum (Thermo Fisher Scientific) and cultured overnight at 37ºC with gentle shaking at 200 rpm. A final preparation of *E. coli* MS499 and *T. pyogenes* MS249 with a targeted final concentration of 5×10^7 CFU/mL was loaded into 10-mL syringes for infusion. Actual CFU/mL used in each replicate were calculated following the application of treatment. Syringes were loaded with sterile PBS for flushing catheters and control infusions. Inoculant and control syringes for infusion were transported to the farm on ice.

Evaluation of Uterine Infection

Rectal temperature and vaginal mucus were measured between 0700 and 1030 h on d 2, 4, and 7 relative to infusion. Vaginal mucus was assessed using an intravaginal device (Metricheck, Simcro, Hamilton New Zealand) after cleaning the external genitalia with 70% ethanol and dried with paper towels. Vaginal mucus was scored using a 5-point scale (0 = clear mucus; 1 = clear mucus with flecks of pus; 2 = mucopurulent discharge with < 50% pus; 3 = mucopurulent discharge with > 50% pus; 4 = watery, red or brown, and fetid discharge) and collected in 7 mL polystyrene Bijou containers (Thermo Fisher Scientific) and stored at -20ºC (Sheldon et al., 2006). Intravaginal devices were kept separate between treatment groups and sterilized prior to reuse for subsequent collections.

Endometrial cytobrush samples were collected on d 2 relative to infusion. Briefly, cows received caudal epidural anesthesia of 60 mg lidocaine hydrochloride 2% (Aspen Veterinary Resources) injected into the intercoccygeal intervertebral space. External genitalia were cleaned with 70% ethanol and wiped with paper towels. The cytobrush tool (Medscand Medical, Cooper Surgical, Trumball, CT) which consists of a metal sheath covered by a plastic chemise, was inserted into the vagina and passed through the cervix via rectal palpation. The plastic chemise was broken at the cranial end of the cervix and the metal sheath was retracted exposing the brush to the endometrium. The brush was rotated four times to collect endometrial cells prior to being retracted into the metal sheath and removed from the cow. The cytobrush was collected into 1.5 mL Eppendorf tubes (Eppendorf, Hamburg, Germany) containing 700 µL of RNAlater (Thermo Fisher Scientific).

Oocyte Recovery and In Vitro Fertilization

To assess the impact of endometritis on oocyte developmental competence, transvaginal ultrasound-guided ovum pick-up (OPU) was performed on a subset of cows 23 d after intrauterine infusion of either bacteria or PBS as control (control, n = 12; bacteria, n = 14). Prior to OPU, estrous cycles were synchronized using an OvSynch protocol beginning 14 d after infusion. Cows received an i.m. injection of 100 µg GnRH gonadorelin diacetate tetrahydrate (Cystorelin), followed by i.m. injection of 25 mg PGF2α (dinoprost tromethamine) 7 d later and GnRH after 56 h coincident with the time of OPU. For OPU, cows received epidural anesthesia in the intercoccygeal intervertebral space using 60 mg of lidocaine hydrochloride 2% (Aspen Veterinary). External genitalia were cleaned with 70% ethanol and wiped clean with paper towels. The vagina was rinsed once with 100 mL of 0.1% chlorhexidine solution, followed by

100 mL sterile 0.9% saline. Follicle aspirations and oocyte pickup was performed with an Ibex EVO III ultrasound with corresponding 7.5 MHz convex ultrasound probe enclosed within a plastic aspiration handle (E.I. Medical Imaging, Loveland, CO). The ultrasound probe was placed into the fornix vagina and follicles were aspirated using an 18-guage 5.5-cm needle (WTA, College Station, TX). The needle was connected to the end of a metal needle guide and connected via plastic tubing (WTA) to a 50-mL conical tube that was attached to a vacuum pump (WTA). Follicle aspirates were collected into ovum pick-up medium (IVF Bioscience, Falmouth, UK) and subsequently filtered and rinsed using an embryo flush filter (WTA). Oocytes were isolated and washed in three drops of HEPES-buffered oocyte maturation medium (IVF Biosciences) and matured in parafilm sealed polystyrene sonication tubes (Thermo Fisher Scientific) containing HEPES buffered oocyte maturation medium at 38.5ºC for 22 to 24 h in a portable incubator. Cumulus oocyte complexes were graded on a morphological scale of 1 to 4 based on the presence of granulosa cells (Grade 1: > 4 layers of granulosa cells; Grade 2: 3-4 layers of granulosa cells; Grade 3: 1-2 layers of granulosa cells; and Grade 4: denuded oocytes) (Konishi et al., 1996). All procedures for oocyte maturation, fertilization, and embryo culture were performed keeping oocytes and subsequent embryos from each donor separated in individual wells.

Following oocyte maturation, groups of 1 to 25 oocytes were transferred to 100 µL drops containing BO-IVF medium which was covered by mineral oil (IVF Bioscience). Oocytes were fertilized with sperm from the sire Monument 014HO04784 for periods 1 and 3, or Ivan 014HO4487 for period 2 (Select Sires, Plain City, OH) at a final concentration of 1×10^6 sperm/mL and placed in a humidified incubator at 38.5ºC with

6% CO_2 and balanced N_2 in air. After 11 to 12 h of fertilization, putative zygotes were washed in oocyte wash medium (IVF Biosciences) and cumulus cells were removed by vortexing for 3 min in a tube containing 1,000 IU/mL hyaluronidase and approximately 50 µL of HEPES-TALP. Presumptive zygotes from each donor were cultured in 60 µL drops containing BO-IVC medium in individual dishes in groups of 1 to 25. Embryos were assessed for cleavage 3.5 d following fertilization, and blastocyst development was assessed at d 7.5 after fertilization. Blastocysts were collected by washing three times in warmed DPBS before snap freezing in liquid nitrogen for storage at -80ºC.

Collection of Endometrial Samples for RNAseq

The estrous cycles of cows were synchronized to collect endometrial samples for sequencing by following an OvSynch protocol. Beginning 14 d after intrauterine infusion, cows received an i.m. injection of GnRH followed by PGF2α 7 d later, and finally GnRH 2 d later. Ovulation was assessed by scanning for a corpus luteum 6 d after ovulation. Endometrial cytobrush samples were collected on d 41 after infusion as above (corresponding to d 16 of the estrous cycle). The cytobrush was collected into a 1.5 mL Eppendorf tube containing 700 µL of RNAlater (Thermo Fisher Scientific).

Quantification of Peripheral Progesterone

Blood was collected 41 d after infusion (d 16 of the estrous cycle) via coccygeal venipuncture into evacuated tubes containing lithium heparin (Vacutainer; 9 mL, Becton Dickinson, Franklin Lakes, NJ) and placed immediately on ice. Whole blood was centrifuged at 2,400 × *g* at room temperature for 10 minutes to collect plasma that was aliquoted and stored at -20ºC. Plasma progesterone was quantified using a commercially available ELISA according to the manufacturer's instructions (DRG

International, Springfield Township, NJ). The intra-assay coefficient of variation for progesterone was 5.94%.

RNA Extraction

Cytobrushes stored in RNAlater (Thermo Fisher Scientific) were thawed on ice in preparation of RNA extraction. Upon thawing, the cytobrush was removed and placed into a new 1.5 mL Eppendorf tube (Eppendorf) containing 350 µL of RLT buffer (Qiagen, Hilden Germany) with sterile tweezers. The original tube containing the RNAlater solution was centrifuged at 21,380 × *g* for 7 min. Following centrifugation, the RNAlater was aspirated with a sterile Pasteur pipette (Thermo Fisher Scientific) and returned to ice. The tube containing the cytobrush and RLT buffer was vortexed for 1 min at max speed to facilitate removal of remaining cells from the brush. Following the vortex, the brush was removed with sterile tweezers and remaining cells were scraped into the tube containing the 350 µL of RLT buffer. Next, the lysate containing RLT buffer was transferred to the original tube containing the cell pellet and was further lysed by passing the lysate through an 18-gauge needle attached to a 3 mL syringe ten times. Following homogenization, endometrial RNA was purified using the RNeasy mini kit which included an on-column DNase digestion according to the manufacturer's instructions (Qiagen). For d 2 post-infusion cytobrushes, extracted RNA purity and concentration were evaluated using a NanoDrop 2000 spectrophotometer (Thermo Fisher Scientific). Samples had a mean 260/280 and 260/230 ratio of 2.02 ± 0.15 and 1.43 ± 0.63, respectively. Total RNA for sequencing was quantified, and RNA integrity and purity were assessed using an Agilent 5400 Bioanalyzer (Agilent Technologies, Santa Clara, CA). Only samples with a total RNA 28S;18S ratio ≥ 0.5 and RNA integrity number ≥ 4.5 were used for library construction.

Real Time RT-PCR

Reverse transcription was performed using the Verso cDNA synthesis kit (Thermo Fisher Scientific). All primers were designed using the National Center for Biotechnology Information database (**Table 5-1**). Amplification efficiency for each primer pair was evaluated and met MIQE guidelines of $r^2 > 0.98$ and efficiency of 90 to 110% (Bustin et al., 2009). A Bio-Rad CFX Connect light cycler (Bio-Rad, Hercules, CA) was utilized for PCR. An initial denaturation step of 95ºC for 30 s followed by 40 cycles of a two-step protocol using 95ºC for 5 s and annealing and extension at 60ºC for 30 s. The primer set for *TNF* required an annealing temperature of 62ºC. A no template control was used to determine non-specific amplification for each primer pair. The relative expression for each gene was calculated using the $2^{-\Delta Ct}$ method relative to the geometric mean of the reference genes (*ACTB* and *GAPDH*). Reference gene expression was stable across treatments and pregnancy status ($P > 0.05$).

Library Construction and Sequencing

Library preparation was conducted by Novogene Inc. (Sacramento, CA). Messenger RNA was purified from total RNA using poly-T oligo-attached magnetic beads. After fragmentation, the first strand cDNA was synthesized using random hexamer primers, followed by a second strand cDNA synthesis using either dUTP for directional library or dTTP for non-directional library. The non-directional library was ready after end repair, A-tailing, adapter ligation, size selection, amplification, and purification. The directional library was ready after end repair, A-tailing, adapter ligation, size selection, USER enzyme digestion, amplification, and purification. The library was checked with Qubit and real-time PCR for quantification and bioanalyzer for size

distribution detection. The quantified library was pooled and sequenced for pair end 150 bp reads using an Illumina NovaSeq X Plus (Illumina, San Diego, CA).

Read Mapping and Differential Gene Expression Analysis

Original data files generated from high-throughput sequencing were transformed into raw reads by CASAVA base recognition and stored in FASTQ format files. Individual reads were filtered to remove adaptors, poly-N reads, and low-quality reads from the raw data. The Q20, Q30, and GC content were calculated for the cleaned data during this step. All downstream analyses were based on the clean data with high quality reads. After data filtering, paired-end clean reads of each sample were aligned to the latest bovine reference genome (ARS-UCD2.0) using HISAT2 v2.0.5. Quantification was performed using the FeatureCounts v1.5.0-p3 to count the read numbers mapped to each gene. Differential expression analysis between bacteria infused and PBS infused cows was performed using the DESeq2 R package 1.20.0 which utilizes a model based on the negative binomial distribution. The resulting *P*-values were adjusted using the Benjamini and Hochberg's approach for controlling false discovery rate (FDR). Differential expression analysis of the two conditions was performed using the edgeR R package v3.22.5. An FDR ≤ 0.05 and $\log_2$ fold change ≥ 1 or ≤ -1 were used as the threshold to identify differentially expressed genes.

Pathway Analysis of Differentially Expressed Genes

Ingenuity Pathway Analysis (IPA) (Qiagen) was utilized to identify the potential canonical pathways, upstream regulators, and molecular networks associated with the differentially expressed genes within the endometrium altered by bacteria infusion. Only differentially expressed genes with an FDR ≤ 0.05 and $\log_2$ fold change ≥ 1 or ≤ -1 were used for analysis. Canonical pathways and upstream predictors were identified by using

a -$\log_{10}$ *P*- value > 1.3. A calculated z-score of ≥ 2 predicted activation or ≤ -2 predicted inhibition of each pathway or upstream regulators. Molecular networks affected by differentially expressed genes were determined by the network score.

Statistical Analysis

All analyses were performed using SAS statistical software v. 9.4 (SAS Institute, Cary, NC). Rectal temperature and vaginal mucus were analyzed as a repeated measurement with the MIXED procedure of SAS. The model included the fixed effects of treatment, day, and the interaction between treatment and day. In the analysis, day was repeated, and the subject was the cow nested within treatment. Gene expression, progesterone, and the number of oocytes per donor were analyzed using PROC GLM with the fixed effect of treatment. The total number of oocytes for each treatment (bacteria *vs*. control) were analyzed with a chi-square test. Analysis of reference genes (*ACTB* and *GAPDH*) was conducted using the Ct values for each sample while expression of inflammatory mediators (*CXCL8, IL1B, IL6,* and *TNF*) was conducted on the relative expression. Oocyte quality and in vitro fertilization outcomes were analyzed using the GLIMMIX procedure with the fixed effect of treatment and the random effect of experimental period. For transcriptome analysis, differentially expressed genes were identified in cows infused with bacteria compared to PBS control using an FDR ≤ 0.05 and $\log_2$FC ≥ 1 or ≤ -1. A heat map of differentially expressed genes was assembled using average linkage clustering and Pearson correlation distance. Statistical significance was set at $P \leq 0.05$.

Results

Effects of Intrauterine Infusion

There was no effect of bacteria infusion on rectal temperature (P = 0.314) compared to control (**Figure 5-2A**). Regardless of treatment, cows had lower rectal temperature 7 d after infusion compared to 2 d after infusion (P = 0.001) (**Figure 5-2A**). Overall, bacteria infusion increased vaginal mucus score (P = 0.016) compared to controls (**Figure 5-2B**). Regardless of treatment, vaginal mucus score was lower (P = 0.002) 7 d after infusion compared to 2 d after infusion (**Figure 5-2B**).

The expression of inflammatory genes within the endometrium was quantified 2 d after infusion. The relative expression of endometrial *CXCL8* was 4.99-fold greater (P = 0.018) after bacteria infusion compared to controls (**Figure 5-3A**). Similarly, the relative expression of *IL1B* was 3.19-fold greater (P = 0.049) after bacteria infusion compared to controls (**Figure 5-3B**). There was no effect of bacteria infusion on the expression of endometrial *IL6* or *TNF* (**Figure 5-3C and D**).

Effect of Bacteria Infusion on Oocyte Recovery and Blastocyst Development

The total number of oocytes collected from all donors 23 d after treatment was 379 for vehicle and 271 for bacteria. There was no effect of bacteria infusion (P = 0.103) on the number of oocytes collected per donor (21 ± 2 *vs*. 16 ± 2; bacteria *vs.* control), or on the grade of cumulus oocyte complexes collected with the majority of cumulus oocyte complexes at grade 2 (**Figure 5-4A**). There was no effect of bacteria infusion on the proportion of oocytes that became cleaved zygotes (35.7 ± 7.6% *vs.* 32.7 ± 7.2%), the proportion of oocytes to form blastocyst stage embryos (8.9 ± 2.6% *vs.* 10.0 ± 2.6%) or the proportion of cleaved zygotes to form blastocyst stage embryos (26.4 ± 7.1% *vs.* 25.0 ± 6.5%) compared to controls (**Figure 5-4B**).

Effect of Uterine Infection on the Endometrial Transcriptome

There was no effect of bacteria infusion on plasma progesterone concentrations on d 16 of the estrous cycle, 41 d after infusion (7.86 ± 3.43 *vs.* 9.36 ± 2.59 ng/mL). The 10 endometrial samples (PBS control, n = 3; bacteria, n = 7) collected on d 16 of the estrous cycle, 41 d after infusion, produced a total of 456,188,862 high quality reads after sequencing and read processing that were used for analysis of the transcriptome (**Table 5-2**). An average of 91.5% high quality reads were aligned to the reference genome resulting in the detection of 22,960 unique transcripts in the endometrium. The most abundant endometrial genes identified based on total read counts included *COX1*, *GRP*, and *EEF1A1* and are further described in (**Table 5-3**). Principal component analysis using the expression of all transcripts in endometrial samples from bacteria *vs.* control samples explains 42.6% and 14.9% of the variance observed (Figure A-3).

A total of 203 differentially expressed genes were identified in endometrial samples of cows 41 d after bacteria infusion on d 16 of the estrous cycle compared to controls (FDR ≤ 0.05 and $\log_2$ fold change ≥ 1 or ≤ -1; **Figure 5-5A**, Table B-2). Of the 203 differentially expressed genes identified, 167 genes were upregulated, and 36 genes were downregulated in endometrial samples after bacteria infusion (**Figure 5-5A**). The five genes with the greatest increase in expression after bacteria infusion were *GSTA3, PVALB, JAKMIP2, FOLH1B,* and *TCF23* (**Table 5-4**). The five genes with the greatest decrease in expression after bacteria infusion were *MYMK, LOC104974498, CDRT1, KIAA0408,* and *SLC45A2* (**Table 5-4**). A heatmap shows the uniform expression of the 203 differentially expressed genes amongst the individual cows (**Figure 5-5B**).

The differentially expressed genes were analyzed to identify canonical pathways affected after bacteria infusion. A total of 54 canonical pathways were predicted to be affected in endometrial samples 41 d after bacteria infusion, on d 16 of the estrous cycle compared to controls (Table B-3). Of these 54 pathways, 15 pathways based only on a *P*-value < 0.05 are depicted in **Figure 5-6**, with 6 of these significant pathways having a calculated z-score that predicts activation status are described in **Table 5-5**. The most significant canonical pathways identified in the endometrium (regardless of a calculated z-score) following bacterial infusion include 1) glutathione-mediated detoxification, 2) taurine biosynthesis, 3) glutathione redox reactions I, 4) α-adrenergic signaling, 5) cardiac conduction and 6) LPS/IL-1 mediated inhibition of RXR function (Table B-3).

Using the 203 differentially expressed genes, thirteen gene networks were identified in the endometrium following bacteria infusion (**Table 5-6**). The top three identified gene networks in the endometrium after bacteria infusion include 1) cancer, cellular movement, nervous system development and function 2) cell-to-cell signaling and interaction, cellular compromise, post-translational modification and 3) carbohydrate metabolism, organ development, organ morphology (**Table 5-6**).

Using the 203 differentially expressed genes, a total of 112 predicted upstream regulators of differentially expressed genes were identified (**Table B-4**). The top 10 predicted upstream regulators of differentially expressed genes with a predictive z-score for activation status (z-score ≥ 2 or ≤ -2) are depicted in **Table 5-7**, which include (activated status) interferon gamma, nuclear factor kappa B complex, lipopolysaccharide, tumor necrosis factor, and hypoxia inducible factor 1 A; and (inhibited status) the PI3-kinase inhibitor LY294002, the inhibitor of HIF1A regulated

genes CITED2, the JNK inhibitor SP600125, the prolyl hydroxylase enzymes EGLN, and the RNase enzyme RNASEH2B.

Discussion

Uterine disease affects approximately 40% of lactating cows within the first three weeks after calving (Sheldon, 2006). The fertility of cows with uterine disease following the resolution of disease, however, is compromised. These reductions in fertility are likely mediated through changes to various reproductive tissues such as the ovary and endometrium. Here I utilized an induced infection model and hypothesized that intrauterine infusion of pathogenic *E. coli* and *T. pyogenes* would reduce the development of oocytes to the blastocyst stage and would alter the endometrial transcriptome on d 16 of the estrous cycle – a time corresponding to conceptus elongation. In this study, bacteria infusion had acutely elevated vaginal mucus scores and increased endometrial expression of inflammatory mediators *CXCL8* and *IL1B* compared to control cows, indicating the successful induction of endometrial inflammation. While oocytes developmental competence was not affected by prior bacteria infusion, the endometrial transcriptome was altered 41 d after infusion on d 16 of the estrous cycle.

There are clear effects of uterine disease and bacterial infection on ovarian function. Indeed, the transcriptome of oocytes and granulosa cells collected several months following the resolution of disease are altered compared to control cows (Piersanti et al., 2019a, Horlock et al., 2020, Piersanti et al., 2020). Furthermore, the developmental competence of oocytes to develop morula stage embryos following intrauterine infusion of bacteria is reduced (Dickson et al., 2020). The reduction in oocyte development was independent of changes to cleavage and was most

pronounced 24 d following bacterial infusion. Dickson et al., (2020) elected to collect morula on d 6 following fertilization rather than allow embryos to progress to the blastocyst stage. Therefore, I chose to evaluate the developmental competence of oocytes to reach the blastocyst stage of development in the current study. Here, there was no effect of bacteria infusion on the number of oocytes recovered per donor, the proportion of zygotes to undergo cleavage, the proportion of oocytes to develop to the blastocyst stage of development or the proportion of cleaved zygotes to develop to the blastocyst stage. The absence of differences in the development to the blastocyst stage contrasts with Dickson et. al., (2020) whereby the authors elected to end the in vitro culture on d 6 post-fertilization at the morula stage of development. Therefore, it is possible that the experiment conducted here lacked the power to detect a difference in blastocyst formation and requires attention in future studies.

As previously discussed, there are persistent changes to the uterus following disease resolution which may contribute to pregnancy failure. Indeed, cows diagnosed with uterine disease within the first 42 d after calving had lower frequency of pregnancy at 45 d, lower frequency of calving, and increased frequency of pregnancy loss after either artificial insemination or embryo transfer compared to healthy herd mates (Ribeiro et al., 2016). This series of experiments indicated that the change in fertility after disease is likely attributed to alterations in the ability of the uterus to support pregnancy due to the lack of difference between pregnancy outcomes of cows receiving artificial insemination or embryo transfer, which bypasses the potential for early embryonic mortality occurring within the first week of gestation. Furthermore, previous studies have shown that the molecular signature of the uterus is compromised following uterine

disease, whereby alterations to the transcriptome have been detected in various anatomical regions such as the ampulla, isthmus, and endometrium; and these changes are persistent for extended periods of times following the resolution of disease (Salilew-Wondim et al., 2016, Horlock et al., 2020, Dickson et al., 2022).

In this study, RNA sequencing was used to elucidate the effects of uterine inflammation 41 d prior on the endometrial transcriptome at d 16 of the estrous cycle, which is coincident with the time of conceptus elongation. Regardless of treatment, the top two highest expressed genes within the endometrium on d 16 of the estrous cycle were *COX1* and *GRP*. The gene *COX1* codes for cytochrome c oxidase subunit 1 and is critical in the biosynthesis of prostaglandins. The COX enzymes (1 and 2) facilitate the conversion of arachidonic acid (representing the rate limiting step in the pathway) into functional prostaglandin intermediaries which are further acted upon by prostaglandin synthase enzymes to yield functional prostaglandins (Sih et al., 1971, Miyamoto et al., 1976). In ruminants, the endometrium produces high concentrations of prostaglandins F and E around the time of conceptus elongation (Thatcher et al., 1995). In ruminants, PGF2α is the luteolytic molecule which causes the corpus luteum to regress when embryonic signals are not detected, while prostaglandin E2 is thought to be involved in maternal recognition of pregnancy and luteal support (Thatcher et al., 1995, Arosh et al., 2002). The second most abundant gene detected within the endometrium regardless of treatment was *GRP* which codes for gastrin-releasing peptide. Immunoreactive GRP is highly abundant within the bovine endometrium throughout the estrous cycle, but the abundance increases from proestrus to diestrus and is suggested to be an important molecule for endometrial remodeling to support blastocyst

development and embryonic implantation (Budipitojo et al., 2003). Taken together, the high relative expression of both a key regulator in prostaglandin synthesis and gastrin-releasing peptide are suggestive that the samples submitted for sequencing were of endometrial epithelial origin and indicative of samples collected at d 16 of the estrous cycle.

When evaluating the differentially expressed genes within the endometrium following bacteria infusion, it was revealed that *GSTA3* (increased) and *MYMK* (decreased) had the greatest difference from control samples. The gene *GSTA3* codes for glutathione transferase A3 which is a member of the alpha class glutathione S-transferase isoenzymes that act to detoxify electrophilic decomposition products produced by reactive oxygen species, and metabolism of xenobiotics mediated through glutathione conjugation with electrophilic compounds (Hayes and McLellan, 1999, Ilic et al., 2010). The expression of *GSTA3* was increased by 6.8-$\log_2$ fold in the endometrium of cows after bacteria infusion compared to control. In an experiment which characterized cows as repeat breeders, the expression of endometrial *GSTA3* was increased by 19.2-fold compared to cows characterized as non-repeat breeders on d 15 of the estrous cycle (Hayashi et al., 2017). Furthermore, when GSTA3 was localized using immunohistochemistry, it was revealed that the protein localized to the luminal and glandular epithelial cells of the endometrium and was significantly more abundant in the repeat breeders compared to non-repeat breeders cows (Hayashi et al., 2017). Thus, given the association between GSTA3 localization in the endometrium of repeat breeder cows, it is possible that this molecule could be playing a role in subfertility of cows with prior uterine disease.

The gene *MYMK* codes for the protein myomaker, myoblast fusion factor and is involved in myoblast fusion. The expression of *MYMK* was decreased by 3.9-$\log_2$ fold in the endometrium after bacteria infusion compared to control. While *MYMK* is canonically associated with myotubule formation in the context of muscle development, the physiological process of myotubule fusion is a classical cell-cell fusion event. Cell-cell fusion events are crucial, and tightly regulated as evidenced by the number of cell types that remain mononucleated (Rochlin et al., 2010). Therefore, the subset of cell types which permit fusion in unique tissue types are proposed to be integral for tissue homeostasis and development of organisms (Rochlin et al., 2010). The function of cell-cell fusion serves to provide a gain of function characteristic that mononucleated cells cannot perform. In ruminants which have evolved to utilize a synepitheliochorial placenta, the connection between the embryonic trophectoderm and maternal endometrium possess hallmark characteristics of a cell-cell fusion event. For example, the ruminant trophectoderm contains cells that are capable of migrating through chorionic tight junctions and fusing with uterine epithelial cells to generate populations of multinucleated trophoblast cells (Wooding, 1992, 2022, Seo et al., 2024). Therefore, it is interesting to speculate on the implications of downregulated expression of a key mediator in cell-cell fusion in the context of the endometrium on d 16 of the estrous cycle when the bovine conceptus is beginning a period of rapid elongation in preparation for implantation.

The differentially expressed genes identified in the endometrium following bacteria infusion were submitted to functional analysis. The differentially expressed genes following bacteria infusion resulted in 54 canonical pathways predicted to be

altered after bacteria infusion. Of these canonical pathways, two pathways were related to immune signaling 1) pathogen induced cytokine storm signaling and 2) neutrophil degranulation. Interestingly, neutrophil movement and function is associated with the peripartum uterine immune status and the development of uterine disease. Neutrophil degranulation is important for neutralization of identified pathogens or damaged cells within the periphery of the organism (Liew and Kubes, 2019). In the context of uterine disease, neutrophils are the first immune cells which work to clear the bacterial infection. The analysis of differentially expressed genes also permitted the detection of a large number of upstream regulators predicted to regulate gene expression of the endometrium following bacteria infusion. In particular, the top three predicted upstream regulators of gene expression were 1) interferon gamma, 2) NFκB complex, and 3) lipopolysaccharide. Each of these predicted upstream regulators were also predicted to be activators of the identified differentially expressed genes. Indeed, lipopolysaccharide which originates from Gram negative bacteria such as *E. coli* is known to activate Toll-like receptor 4 on bovine endometrial epithelial cells and initiate an inflammatory response mediated through the NFκB pathway (Cronin et al., 2012). Given that the animals received an intrauterine infusion of both *E. coli* and *T. pyogenes*, it was interesting to report lipopolysaccharide as a predicted upstream regulator of differentially expressed genes which may suggest that lipopolysaccharide lingered in the uterine tissues long after the resolution of clinical symptoms in these cows.

In conclusion, we determined that there was no effect of intrauterine infusion on blastocyst formation but there were specific changes to the endometrial transcriptome following infection resolution around the time of conceptus elongation. This analysis

permitted the identification of a large set of differentially expressed genes within the endometrium following bacteria infusion. Furthermore, these genes were functionally annotated to a unique set of pathways and upstream regulators associated with previous endometritis and endometrial function. Further investigations into the identified genes and pathways are required to identify potential mechanisms of subfertility mediated by bacterial infection. The ability to characterize these pathways may permit intervention strategies for improvement of fertility outcomes in cows with uterine disease.

Table 5-1. Primer sequences uses for real time RT-PCR.

Gene Symbol	Primer sequence	Accession number
ACTB	5’ – TTGGCCTTAGGGTTCAGGG 3’ – CAGAAGCACTCGTACGTGGG	NM_173979.3
CXCL8	5’ – GCAGGTATTTGTGAAGAGAGCTG 3’ – CACAGAACATGAGGCACTGAA	NM_173925.2
GAPDH	5’ – AGGTCGGAGTGAACGGATTC 3’ – ATGGCGACGATGTCCACTTT	NM_001034034.2
IL1B	5’ – CTTCATTGCCCAGGTTTCTG 3’ – CAGGTGTTGGATGCAGCTCT	NM_174093.1
IL6	5’ – ATGACTTCTGCTTTCCCTACCC 3’ – GCTGCTTTCACACTCATCATTC	NM_173923.2
TNF	5’ – CACATACCCTGCCACAAGGC 3’ – CTGGGGACTGCTCTTCCCTCT	NM_173966.3

Table 5-2. Summary of read mapping for endometrial samples collected 41 days after the intrauterine infusion of bacteria or PBS control.

Sample ID	Treatment	RIN[1]	Raw Reads	Clean Reads	Mapped Reads	Mapped Reads (%)
A3	PBS	8.8	42,971,766	40,452,279	39,350,701	91.57%
A7	PBS	5.4	40,350,376	38,133,070	37,269,565	92.36%
A10	PBS	6.5	44,958,136	42,404,817	41,390,434	92.06%
A1	Bacteria	5.8	42,084,550	39,656,797	38,455,435	91.38%
A2	Bacteria	6.5	52,573,762	49,567,961	47,941,382	91.19%
A6	Bacteria	6.6	47,002,832	44,537,607	43,123,926	91.75%
A8	Bacteria	4.7	39,093,158	36,714,712	35,523,102	90.87%
A9	Bacteria	6.9	53,070,238	49,577,090	47,902,099	90.26%
A11	Bacteria	5.6	50,899,476	48,220,025	46,902,340	92.15%
A12	Bacteria	6.0	43,184,568	40,178,958	38,917,047	90.12%

[1]RIN = RNA integrity number.

Table 5-3. Most abundantly expressed endometrial genes regardless of treatment.

Gene symbol	Total read count	Type	Description
COX1	3,484,555	Protein-coding	Cytochrome c oxidase subunit 1
GRP	2,020,161	Protein-coding	Gastrin releasing peptide
EEF1A1	1,985,187	Protein-coding	Eukaryotic translation elongation factor 1 alpha 1
TPT1	1,308,402	Protein-coding	Tumor protein translationally-controlled 1
COX3	1,278,791	Protein-coding	Cytochrome c oxidase subunit 3
LTF	1,087,224	Protein-coding	Lactotransferrin
RPS2	971,208	Protein-coding	Ribosomal protein S2
COX2	842,481	Protein-coding	Cytochrome c oxidase subunit 2
ATP6	841,929	Protein-coding	ATP synthase subunit a
RPLP0	787,054	Protein-coding	Ribosomal protein lateral stalk subunit P0
LOC112444681	710,850	pseudogene	Protein TAR1
CYTB	697,838	Protein-coding	Cytochrome b
KEH36_r01	690,021	rRNA	L-rRNA
RPSA	678,485	Protein-coding	Ribosomal protein SA
LOC100850808	670,374	Protein-coding	Elafin-like

Table 5-4. Greatest differentially expressed endometrial genes following the intrauterine infusion of bacteria[1].

Symbol	Description	Log_2 fold change	FDR[2]
GSTA3	Protein-coding	6.81404	0.00170
PVALB	Protein-coding	6.57539	0.00059
JAKMIP2	Protein-coding	5.85417	2.11×10^{-10}
FOLH1B	Protein-coding	5.50617	0.01602
TCF23	Protein-coding	5.06216	0.03885
MYMK	Protein-coding	-3.92949	0.02346
LOC104974498	lncRNA	-3.42736	0.01688
CDRT1	Protein-coding	-3.23372	0.00081
KIAA0408	Protein-coding	-3.18754	0.00396
SLC45A2	Protein-coding	-2.18734	0.04810

[1]Differential analysis between bacteria infused and PBS infused cows was performed using the DESeq2 R package.
[2]Resulting *P*-values were adjusted using the Benjamini and Hochberg's approach for controlling false discovery rate. An FDR ≤ 0.05 and log_2 fold change ≥ 1 or ≤ -1 were used as the threshold to identify differentially expressed genes.

Table 5-5. Top predicted canonical pathways identified within the endometrium following infusion of bacteria based on adjusted *P*-value and z-score.

Canonical pathway	*P*-value ($-\log_{10}$)	z-score[1]	Differentially expressed genes in the pathway
Glutathione-mediated detoxification	6.35	2.236	*ANPEP*, *GSTA4*, *GSTM1*, *GSTM3*, *GSTT3*, *PTGES*
Cardiac conduction	2.46	2.236	*CALM1*, *CES1*, *FXYD1*, *KCNJ2*, *KCNK2*
Potassium channels	2.07	2	*KCNAB1*, *KCNJ2*, *KCNK2*, *KCNQ5*
Xenobiotic metabolism CAR signaling pathway	1.75	2.236	*CHST12*, *FMO1*, *FMO3*, *GSTM1*, *GSTM3*
Pathogen induced cytokine storm signaling pathway	1.59	2.646	*CCL28*, *CXCL10*, *CXCL6*, *GPR15LG*, *GSDMD*, *IRF1*, *PYCARD*
Neutrophil degranulation	1.49	2.828	*ANPEP*, *GSDMD*, *PGLYRP1*, *PIGR*, *PLAC8*, *PYCARD*, *PYGL*, *TUBB4B*

[1]z-score: indicates the predicted activation or inhibition status, where a z-score ≥ 2 indicates activation, or ≤ -2 which indicates inhibition.

Table 5-6. Predicted molecular networks of differentially expressed endometrial genes following intrauterine infusion of bacteria.

Gene network[1]	Score[2]	Molecules in network
Cancer, cellular movement, nervous system development and function	50	*ADCY, ADGRG7, ADRA2A, ADRB, ALCAM, ASPHD2, AZGP1, BEX2, C5AR2, CHST12, CITED4, EFEMP1, FMO3, LDLRAD1, LMO4, LPIN1, LYPD3, MALL, NFkB, NLRX1, PEPCK, PPP4R4, SERPINE2, SLC15A2, SLC22A4, SSBP4*
Cell-to-cell signaling and interaction, cellular compromise, post-translational modification	47	*DUSP6, EPHX2, EYA2, FCGBP, FXYD1, GDAP1, GJB7, GNAZ, KRT23, NRARP, PPP1R1B, PRC2, PTPN20, PTPRM, RARRES2, TCEAL1, TCHH, TFF3, TTC3, VTCN1, ZNF503*
Carbohydrate metabolism, organ development, organ morphology	37	*ADCY7, CRABP1, CSF3, FSH, IGFBP5, JDP2, KCNJ2, KRT14, LDHD, MYMK, NPL, PARP, PHGDH, PTCH1, PVALB, SHROOM4, SIX1, SPATS2L, SVIL, TP73, TSH, TSHZ3*
Cardiovascular disease, organismal injury and abnormalities, tissue morphology	32	*ABCG1, CDC42EP5, CES1, COX7A1, CSRP2, DAB1, ERK1/2, FOXA2, GPX2, GSTM1, GSTM3, HDL, KCNQ5, LDL, PDLIM2, PRKD, PTGES, RND3, TCF23*
Amino acid metabolism, protein synthesis, small molecule biochemistry	32	*AMPK, CDO1, EIF4EBP1, ERK, FAM171A1, FMO1, GMNN, HSP70, HSP90 IRX3, KCNK2, MTBP, N6AMT1, NFIA, PGLYRP1, PI3K, PKA, PMP22, PP2A, PRKAA, RAB11FIP2, Raf, RASIP1, ROR2, RUNX3, SESN1, WNT*
Embryonic development, organ development, organismal development	32	*APP, BCAT2, Bmyc, CCDC190, CCDC88C, CCND1, CFAP299, CORO6, CRACR2B, CTNNB1, DMRT2, ECI1, ELAVL2, GT1, GPR137B, GSKIP, HEATR5A, HSBP1L1, KCNAB1, LURAP1L, PTCSC3, PVALB, SCEL, SLCO2B1, TIGD1, TMA7, TNIP2, TRUB1, TSPAN12, UBXN10, UPB1, ZAR1L, ZNF385B, ZNF462*

Table 5-6. Continued.

Gene network[1]	Score[2]	Molecules in network
Cell death and survival, embryonic development, reproductive system development and function	32	*BPIFB2, C8G, CGNL1, CHST9, EGFR, EIF1AY, FANCD2, FMO1, FUT6, GPX2, HMGN2, HNF4A, HYAL3, KLHL40, LRATD1, MACROD1, MATN1, MATN4, miR-140-3p NCMAP, PARP1, PEPD, PVALB, QTRT2, RECQL4, SIGLEC10, SLC43A1, SLC45A2, STAC3, TIMM23B, TTC6, WHRN, ZNF106*
Cellular movement, infectious diseases, organismal injury and abnormalities	22	*ASGR1, ASGR2, BATF2, CCL28, CD3, CTSL, CXCL10, CXCL6, EGLN, GPR15LG, IFN, IFNG IL1, IL12 IL35, IFNA, Jnk, PIGR, PYCARD, PYGL, SEC14L3, SELENBP1, TLR,TNF*
Cell-mediated immune response, humoral immune response, protein synthesis	20	*CALC, CCDC113, CCDC68, CD3 DUOX1, DYNLT1, EFHC2, FOXP3, IFI44, IL13, IL2, IRF3, JAKMIP2, LAG3, MBOAT1, NEURL1B, NR3C1, PDLIM2, PLAC8, PLAGL2, PLEKHH1, RFTN1, RNASE3, Smad2/3, TEX36, TNFRSF25, TNFRSF4, UMOD, UNC13D, ZBTB37, ZNF395*
Cancer, organismal injury and abnormalities, tumor morphology	18	*ABHD3, ARMCX6, CCDC160, CCDC88B, CFAP157, ERICH2, ETNK2, FOXO1, HRK, IL7R, LPO, LRRC8D, MMRN2, MUC4, MYD88, NKAIN1, PLA2G2C, PLA2G2F, PLA2G4E, PXMP2, RNF152, SIT1, SLFN12, TNF, TSC1, TUBB4B, UNC13D*
Cellular assembly and organization, cellular function and maintenance, hematological system development and function	18	*AACS, ACADSB, ACSM1, ARMCX2, CALM1, COX8A, DHX34, DUS1L, HPS6, KTI12, LYPLAL1, MOCS2, MUNC18, NAA35, NAV2, NTNG1, PC, PLEKHA4, POLDIP2, QTRT2, SDHAF3, SPIRE1, STX10, STX4, STXBP6, TIMM23B, TOP3B, TRMT5, TRNT1, TSFM, YRDC, ZC3H7B, ZNF236*
Hematological system development and function, lymphoid tissue structure and development, tissue morphology	12	*CD81, CK2, IRF1, MAP2K1/2, NFKB, NT5E, RNF24, SGPL1, SLC16A7, SRC, STAT5a/b, TCR*
Carbohydrate metabolism, cellular assembly and organization, cellular compromise	2	*CFAP144, SFTPA1*

[1]Enriched gene networks identified by Ingenuity Pathway Analysis using differentially expressed genes only.

[2]Network score is derived from a *P*-value and indicates the likelihood of the genes in a network being found together due to random chance. A network score of 2 or greater gives a 99% confidence the network and genes are not being generated by random chance alone.

Table 5-7. Predicted upstream regulators of differentially expressed endometrial genes following intrauterine infusion of bacteria.

Upstream Regulator	Biotype	Activation status	z – score[1]	*P*-value	Target molecules differentially expressed in dataset
IFNG	Cytokine	Activated	3.113	0.0015	*ADCY7, ADRA2A, AZGP1, BATF2, C15orf48, CCL28, CRABP1, CSF3, CXCL10, CXCL6, ELAVL2, GSDMD, IFI44, IRF1, KRT14, PHGDH, PIGR, PPP1R1B, PTGES, RUNX3, SGPL1, SIX1, TP73*
NFκB (complex)	Complex	Activated	2.899	0.0229	*ABCG1, ADRA2A, BEX2, CITED4, CSF3, CXCL10, CXCL6, IRF1, PTGES, SLC22A4*
Lipopolysaccharide	Chemical drug	Activated	2.749	3.78×10^{-5}	*ABCG1, ADRA2A, ALCAM, ARMCX6, AZGP1, CALM1, CD81, COX7A1, CSF3, CTSL, CXCL10, CXCL6, EPHX2, FOXA2, GSDMD, IFI44, IGFBP5, IRF1, JDP2, LMO4, LORICRIN, LPIN1, NRARP, PC, PGLYRP1, PIGR, PLAC8, PLEKHA4, PTCH1, PTGES, PYCARD, RND3, RNF24, RUNX3, S100A4, SERPINE2, SESN1, SSBP4, TUBB4B*
TNF	Cytokine	Activated	2.667	1.17×10^{-6}	*ADCY7, ALCAM, ANPEP, ASGR1, C15orf48, CCL28, CDC42EP5, CDO1, CSF3, CTSL, CXCL10, CXCL6, DUSP6, FMO1, GSDMD, GSTA4, IGFBP5, IRF1, KCNJ2, KRT23, MALL, NLRX1, NRARP, PC, PGLYRP1, PHGDH, PIGR, PTGES, PXMP2, PYCARD, RARRES2, RND3, SERPINE2, SGPL1, SLC22A4, SVIL, TCHH*
HIF1A	Transcription regulator	Activated	2.609	0.0127	*COX8A, CXCL10, EIF4EBP1, GSTM3, IGFBP5, KRT14, NRARP, NT5E, PLAC8, PYGL*
LY294002	Chemical drug	Inhibited	-2.884	0.0011	*ANPEP, CSF3, CXCL10, CXCL6, DUSP6, GMNN, GSTA4, GSTM3, IGFBP5, IRF1, LMO4, RND3*
CITED2	Transcription regulator	Inhibited	-2.401	0.0063	*ARMCX6, C15orf48, CXCL10, IFI44, IRF1, PLAC8*
SP600125	Chemical drug	Inhibited	-2.357	0.0475	*CHST12, CSF3, CXCL10, CXCL6, PTGES, SGPL1*
EGLN	Group	Inhibited	-2.236	0.0066	*CCL28, CSRP2, EIF4EBP1, PYGL, SELENBP1*
RNASEH2B	Other	Inhibited	-2.219	0.0002	*CTSL, CXCL10, GSDMD, IFI44, IRF1, PYCARD*

[1]z-score: indicates the predicted activation or inhibition status, where a z-score ≥ 2 indicates activation, or ≤ -2 which indicates inhibition.

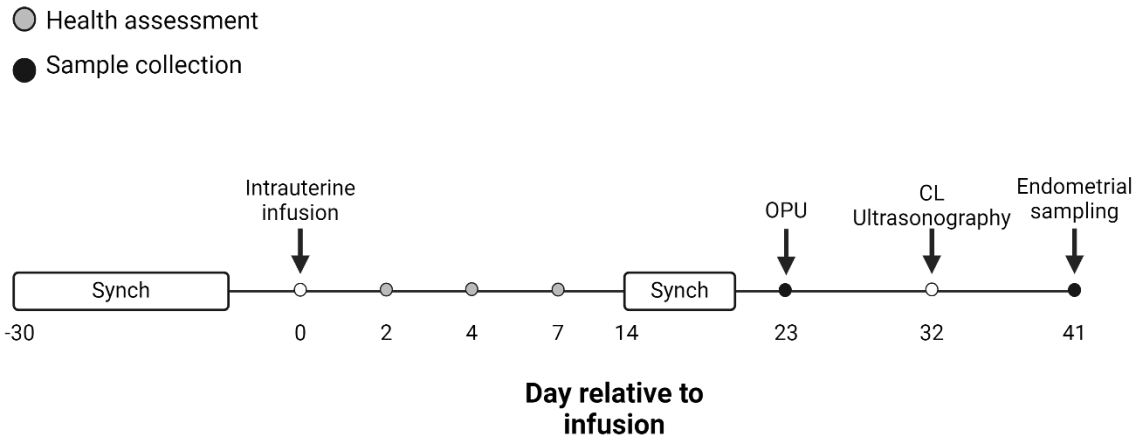

Figure 5-1. Experimental model. Estrous cycles were synchronized with gonadotrophin releasing hormone and prostaglandin F2α prior to receiving an intrauterine infusion of either PBS as control (n = 29) or pathogenic *E. coli* and *T. pyogenes* (n = 32). Health assessments were conducted 2, 4, and 7 d after infusion. Following infusion, estrous cycles were synchronized beginning 14 d after infusion and ovum pick up (OPU) was conducted 23 d after infusion. Endometrial samples were collected by cytobrush 41 d after infusion on d 16 of the estrous cycle.

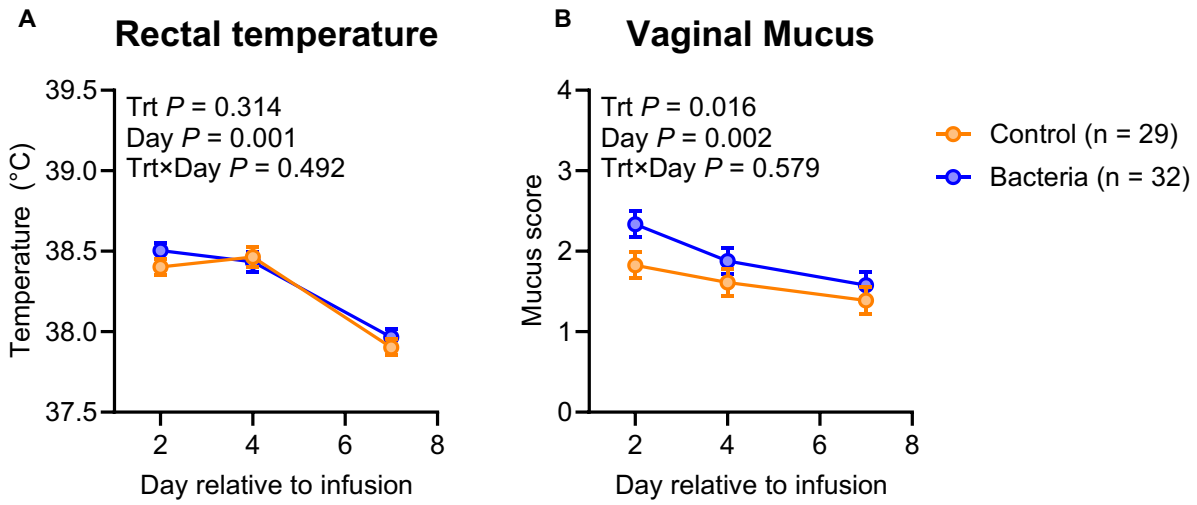

Figure 5-2. Efficacy of intrauterine infusion. Rectal temperature (A) and vaginal mucus (B) were measured on d 2, 4, and 7 after infusion of *E. coli* and *T. pyogenes* (n = 32) or PBS control (n = 29). Rectal temperature and vaginal mucus were analyzed by repeated measures analysis using a generalized linear mixed model which included the fixed effects of treatment (bacteria *vs.* saline), day, and the interaction between treatment and day. Data are presented as the least squares means ± SEM.

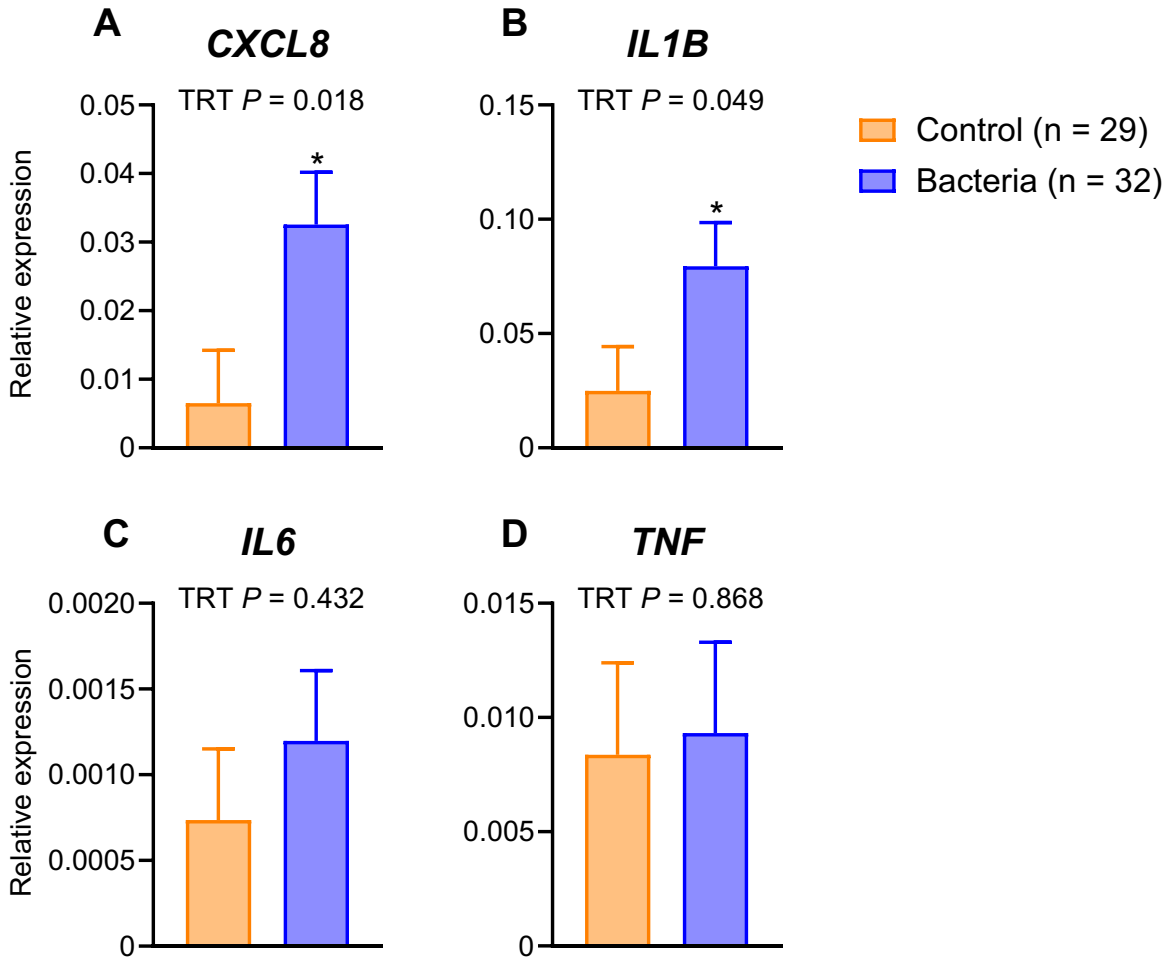

Figure 5-3. Effect of intrauterine infusion of bacteria on acute endometrial gene expression. Endometrial samples were collected via cytobrush 2 d after infusion of *E. coli* and *T. pyogenes* (n = 32) or PBS control (n = 29) and submitted to real time RT-PCR to measure expression of *CXCL8* (A), *IL1B* (B), *IL6* (C), and *TNF* (D). Gene expression was analyzed using a generalized linear model using treatment (bacteria *vs*. saline) as a fixed effect. Data are presented as the least squares means ± SEM of the expression relative to the geometric mean of the reference genes *ACTB* and *GAPDH*.

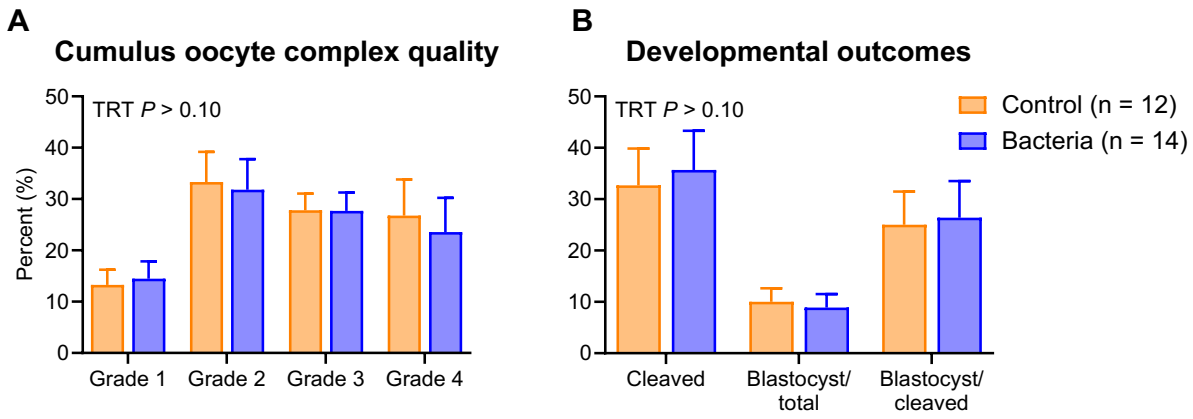

Figure 5-4. Effect of intrauterine infusion of bacteria on oocyte quality and developmental competence following in vitro fertilization and embryo culture. Cumulus oocyte complexes were collected via ultrasound guided ovum pick-up 23 d after intrauterine infusion of *E. coli* and *T. pyogenes* (n = 14) or PBS control (n = 12). Pooled oocytes from each donor were maintained as an individual replicate throughout fertilization and culture. The proportion of COC grades (A) and developmental outcomes (B) are presented. The data were analyzed with the GLIMMIX procedure using the fixed effect of treatment (bacteria *vs.* control) and random effect of experimental period. Data are presented as the least squares means ± SEM.

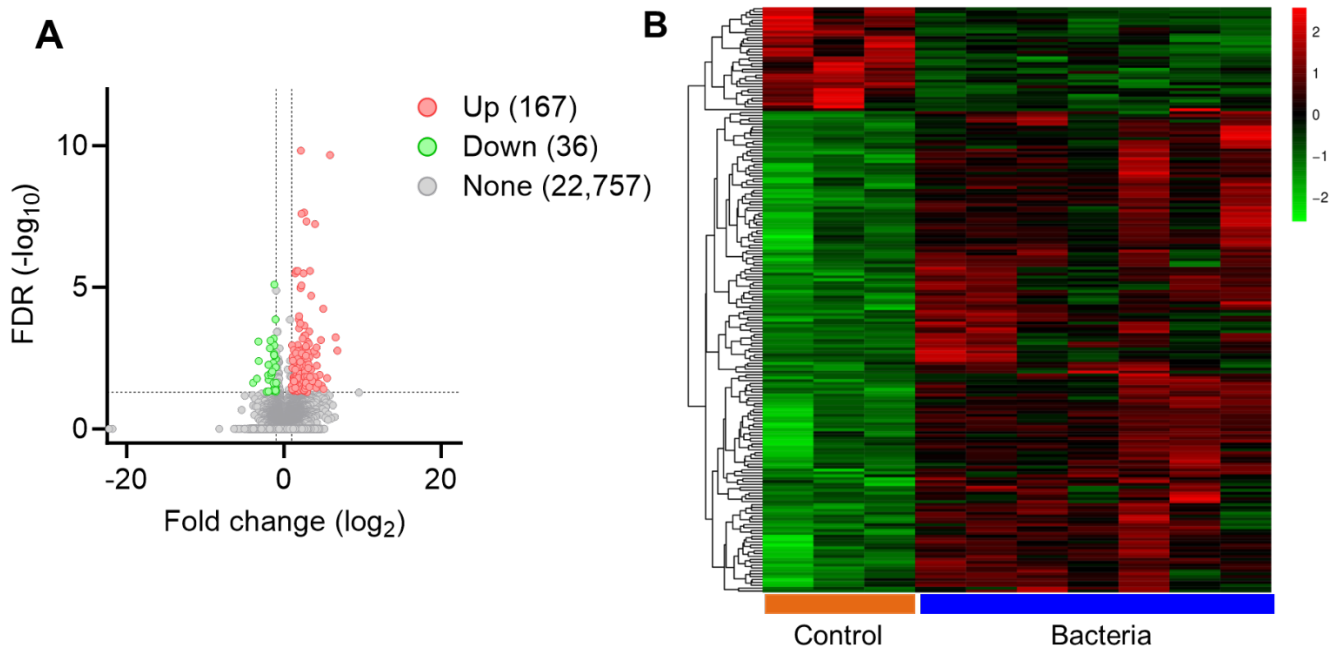

Figure 5-5. Differentially expressed genes of the endometrium following infusion of bacteria. Differentially expressed genes were identified in the endometrium 41 d after the infusion of *E. coli* and *T. pyogenes* (n = 7) or PBS control (n = 3) on d 16 of the estrous cycle. The volcano plot (A) displays the distribution of all genes after sequencing, with differentially expressed genes (FDR < 0.05 and $\log_2$ fold change > 1 or < -1) presented in red (increased) or green (decreased) compared to PBS controls. A heat map (B) of differentially expressed genes used average linkage clustering and Pearson correlation distance and shows each differentially expressed genes as a single row and each column represents an individual sample.

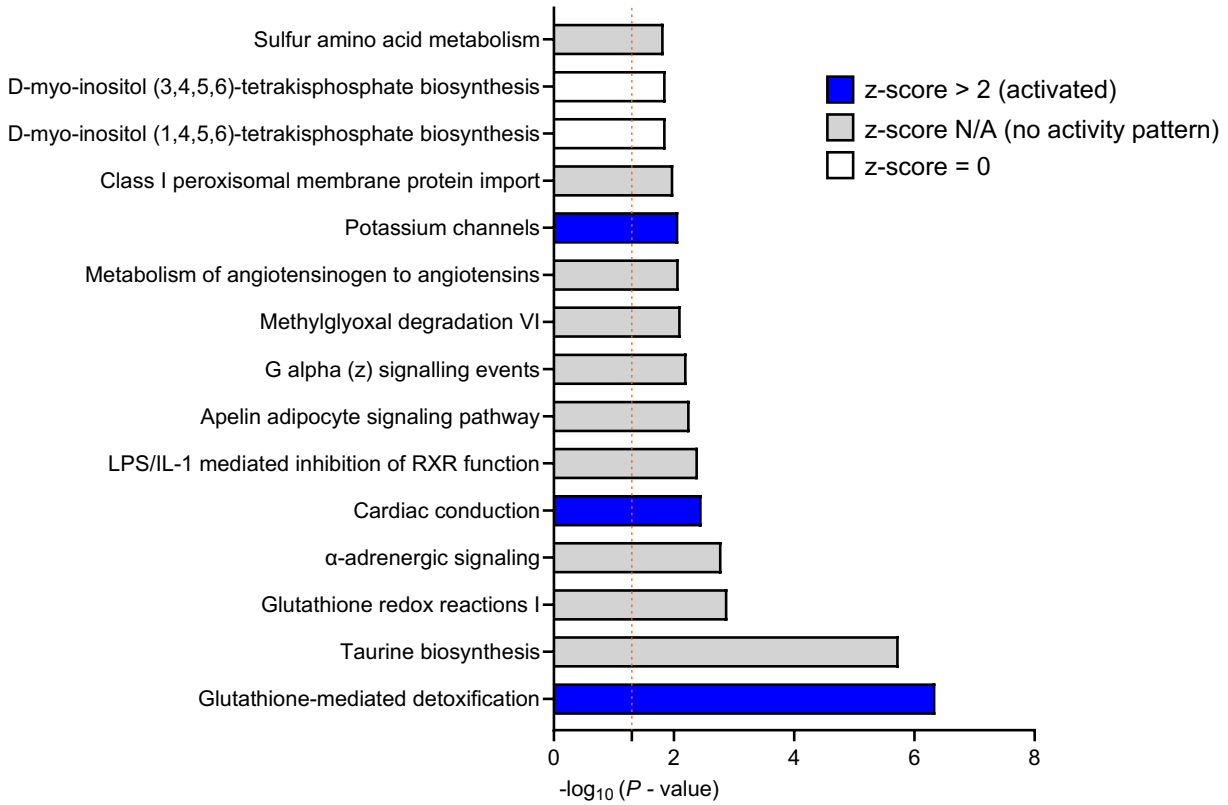

Figure 5-6. Top canonical pathways of the endometrium following infusion of bacteria. Canonical pathways were determined by using differentially expressed genes identified in the endometrium 41 d after the infusion of *E. coli* and *T. pyogenes* (n = 7) or PBS control (n = 3) on d 16 of the estrous cycle. Presented here are the 15 most significant canonical pathways of all 54 pathways based on *P*-value. Grey bars represent canonical pathways where a z-score could not be calculated, blue bars represent pathways where the z-score predicts an activated status (z-score > 2), and white bars represent pathways where the z-score could not predict the status (z-score = 0). A full list of affected canonical pathways can be found in Table B-3

CHAPTER 6
OVERALL DISCUSSION AND CONCLUSIONS

Fertility in cattle is central to profitability on both dairy and beef operations (Wathes et al., 2014). Different environmental stressors such as diet or uterine infection can reduce fertility of both males and females, ultimately diminishing the likelihood of pregnancy and successful production of offspring (Walsh et al., 2011, Singh et al., 2018). While males and females differ with respect to the cellular, molecular, and tissue dialogue required to produce functional gametes; the cumulative result is that these gametes from both parents must be competent enough to allow for fertilization and embryonic development. After these early events, the focus shifts to highlight the roles of embryonic genome activation and the maternal endometrium in supporting pregnancy continuation. Thus, aberrations to normal physiological processes in either parent can compromise the likelihood of pregnancy success. The overall objective of the studies reported here was to investigate mechanisms linking physiological stressors that could result in inflammation with potential fertility outcomes in cattle. Specifically, I hypothesized that paternal overnutrition would compromise embryonic development (Chapter 2), uterine disease would impact ovarian function (Chapter 3), lipopolysaccharide (LPS) treatment of granulosa cell would have carryover effects on progesterone synthesis during luteinization (Chapter 4), and that induced endometritis would compromise blastocyst development and alter the endometrial transcriptome coincident with the time of conceptus elongation (Chapter 5).

Bulls used for natural or artificial insemination are generally fed to highlight enhanced growth characteristics achieved by feeding high-gain diets, ultimately increasing adiposity (McDonald et al., 2010). Increased fat deposition in bulls is thought

to increase the adiposity of the scrotum and reduce thermoregulation of the testis, resulting in greater incidence of sperm defects and reduced fertility (Skinner, 1981, Coulter and Kozub, 1984). Indeed, negative effects of bull overnutrition on fertility have been demonstrated in both observational and experimental settings (Coulter and Kozub, 1984, Coulter et al., 1997). Nevertheless, post-fertilization consequences of paternal high gain diets have not been explored in the bovine. Therefore, I hypothesized that paternal overnutrition would compromise embryonic development. To investigate my first hypothesis, bulls were fed a high gain diet to induce moderate weight gain. This dietary intervention model was sufficient to increase adiposity compared to bulls fed a maintenance diet. Semen was collected from bulls 74 d after the start of the dietary treatment which is enough time to encompass the entirety of spermatogenesis in the bull. The semen collected from bulls fed the high gain diet was morphologically normal compared to bulls fed the maintenance diet. This observation was important because these bulls did pass routine semen quality assessments and breeding soundness exam. Next, the collected semen was utilized for in vitro fertilization to assess its capacity to generate blastocyst stage embryos. The data revealed that there was no effect of dietary treatment on the capacity of sperm cells to fertilize oocytes, suggesting that intrinsic sperm biology was intact. However, on d 7.5 after IVF it was realized that bulls fed the high gain diet produced fewer blastocyst stage embryos, indicative of early embryonic failure. Collectively the results presented here (Chapter 2) suggest that dietary intervention is likely changing aspects of sperm cell molecular function which perpetuates early embryonic failure. The work conducted here suggests that bull

management strategies commonly implemented may have negative effects on fertility and thus warrant attention for future feeding recommendations.

While the experiment conducted here is descriptive in nature, it is interesting to propose mechanisms mediating the changes in embryonic development following feeding a high gain diet in bulls. Sperm cells collected from mice fed a high fat diet have increased reactive oxygen species, DNA damage, and reduced ability to undergo capacitation (Bakos et al., 2011). Paternal obesity also contributes to dysregulated gene expression and DNA methylation patterns of the resultant placenta when compared to normal weight males (Mitchell et al., 2017). Therefore, it is possible that sperm cell epigenetic markers may be inappropriately changed following consumption of an anabolic diet, and these changes may contribute to either embryonic failure or changed postnatal phenotypes. This postulation is supported by evidence in rats whereby offspring sired by rats fed a high fat diet had β-cell dysfunction in female offspring (Ng et al., 2010). The epigenetic programming capacity of sperm from bulls fed a high gain diet remains to be determined, particularly in the context of embryonic genome activation and embryonic mortality.

Interestingly, consumption of high fat diets in humans and mice results in chronic low-grade inflammation, such that tissues like the liver and adipose tissue have a greater abundance of inflammatory signals (Guillemot-Legris et al., 2016, Duan et al., 2018). While in the experiment conducted here neither systemic or testicular specific markers of inflammation were measured, it is interesting to consider the role of inflammation in paternal fertility. Indeed, the hypothesis that paternal diet results in an inflammatory condition has been tested in rats (Suleiman et al., 2020). Suleiman et al.,

fed rats a high-fat diet that increased body weight, elevated levels of serum cholesterol, triglyceride and LDL and lowered HDL compared to controls (Suleiman et al., 2020). Further, the rats fed the high fat diet had elevated expression of pro-inflammatory markers *Il1b*, *Nfkb, Nos2,* and *Tnf* compared to rats fed a control diet (Suleiman et al., 2020). Furthermore, the expression of pro-apoptotic markers (p53, Bax, capsase-9, caspase-8, and caspase-3) were significantly increased in the testis of rats fed the high-fat diet compared to the control (Suleiman et al., 2020). While this study indicates that a link between dietary induced inflammation and the testis exists, this study failed to investigate the roles of inflammation on fertility. Thus, the role and physiological impact of dietary induced inflammatory signaling within the testis on fertility remains to be elucidated.

Next, various models were employed to test my second hypothesis that uterine infections affect ovarian and uterine function in dairy cows. Previous work has shown associations between uterine pathogen load and ovarian structure growth and corresponding plasma estradiol and progesterone (Sheldon et al., 2002b, Williams et al., 2007). Using an observational study of lactating primiparous Holstein cows, I investigated the effects of either metritis or endometritis on follicle and corpus luteum growth and steroidogenesis during the first estrous cycle after parturition. I found that metritis and endometritis had contemporaneous effects on the corresponding ovarian structure, such that metritis reduced the growth of the follicle and secretion of estradiol, while endometritis reduced the secretion of progesterone during the luteal phase of the estrous cycle. Other works have shown that repeated intrauterine infusion of LPS reduced the size of the corpus luteum and secretion of progesterone compared to

controls, but that this reduction was likely due to apoptosis of the luteal tissue rather than differences in steroidogenic output (Lüttgenau et al., 2016a, Lüttgenau et al., 2016b). Furthermore, a large observational study revealed that cows with metritis have lower progesterone compared to cows without metritis (Bruinjé et al., 2023). The work conducted in this chapter suggests that cows with uterine disease have changes to the endocrine milieu after calving, which may have implications on an animals ability to become pregnant.

Critical to the implications of this chapter is the understanding that this study tracked the ovarian and endocrine dynamics of the first estrous cycle postpartum. In the context of dairy management, the ovarian events followed within this chapter occur well before the expiration of the voluntary waiting period (defined as the time between parturition and the time where a cow is first eligible for insemination), which typically is 49 to 87 d after calving (Inchaisri et al., 2011). Nonetheless, the roles of steroid hormone priming of the reproductive tract are of significant interest because sex steroid concentrations can modulate endometrial function and fertility in cattle (Silva et al., 2023). A study in lactating dairy cows demonstrated that follicle development occurring under low concentrations of progesterone results in reduced fertility compared to cows with higher progesterone (Bisinotto et al., 2010). Indeed, elevated levels of progesterone prior to ovulation result in differential gene expression of the endometrial luminal epithelium where genes related to the innate immune system are upregulated while genes related to extracellular matrix remodeling and differentiation/activation of macrophages were downregulated (Silva et al., 2023). Given this, it is interesting to consider the implications of reduced progesterone during the first estrous cycle in cows

with uterine disease on the ability of these cows to become pregnant due to modifications to prior ovarian function.

Similarly, the association between preovulatory estradiol and fertility have been investigated. Many studies have demonstrated that preovulatory estradiol concentrations are positively associated with pregnancy outcomes (Lopes et al., 2007, Jinks et al., 2013, Perry et al., 2020). These changes in fertility are likely also attributable to changes in endometrial gene expression whereby cows with elevated levels of estradiol prior to ovulation have greater expression of estrogen receptor alpha, inhibin beta A, and uterine milk protein precursor compared to cows with lower levels of estradiol prior to ovulation (Perry et al., 2020). In the context of the experiment conducted in chapter 2, cows with metritis have lower concentrations of estradiol compared to cows without metritis, therefore, the reduction in estradiol may have effects on subsequent endometrial function. Furthermore, it is possible that changes in peripheral estradiol concentrations may have effects on hypothalamic-pituitary-gonadal signaling for subsequent cycles. The physiological rise in estradiol during proestrus is required to initiate the preovulatory surge of luteinizing hormone (Chenault et al., 1975). In an experiment where estradiol concentrations were controlled prior to luteolysis, it was revealed that cows that received higher doses of estradiol had an earlier LH surge compared to cows without estradiol supplementation (Stumpf et al., 1991). Taken together, these studies suggest that reduced preovulatory estradiol may have implications for subsequent fertility. For cows with metritis, reduced peripheral estradiol may have carryover effects on later fertility after the voluntary waiting period.

Given the evidence from Sheldon et al. (2002) and Williams et al. (2007), suggesting that follicle and luteal growth are compromised in cows with uterine disease, I next utilized an in vitro cell culture approach to investigate the potential carryover effects of LPS treatment of granulosa cells on steroidogenesis during luteinization. High levels of LPS are reported to accumulate within follicular fluid in cows with uterine disease (Herath et al., 2007, Piersanti et al., 2019a). In this experiment, I utilized primary granulosa cell culture and found that consistent with the literature, LPS treatment of granulosa cells increases the expression of inflammatory mediators *CXCL8* and *IL6* and reduces the secretion of estradiol. Furthermore, I found that LPS treatment of granulosa cells reduces the expression of *CYP19A1,* which codes for the enzyme aromatase and is responsible for the aromatization of androgens into estradiol. Following treatment with LPS, cells were encouraged to luteinize in the absence of direct LPS treatment. During luteinization, it was revealed that progesterone secretion was decreased if granulosa cells were treated with LPS compared to controls, indicative of a negative carryover effect of prior inflammation. This change in function during luteinization was independent of changes to gene expression of factors important in steroidogenesis. The potential mechanisms facilitating this change in progesterone were assessed and it was revealed that the uptake and storage of neutral lipids which potentially could be used for steroidogenesis was altered following granulosa cell LPS treatment. Additionally, the density of mitochondria were reduced if cells were previously exposed to LPS. This work indicates that in the absence of other physiological challenges, LPS treatment of granulosa cells has a carryover effect on steroidogenic capacity during luteinization.

Combined with the data presented in this chapter, it is worth postulating on the potential implications of altered early granulosa cell physiology on subsequent luteal function. Transcriptomic analyses have demonstrated that granulosa cells from pre-antral follicles are susceptible to bacterial infection, and that the changes to the molecular function of these granulosa cells can persist for months after the resolution of disease (Piersanti et al., 2019a, Horlock et al., 2020). Within the context of the experiment conducted here, prior granulosa cell LPS treatment resulted in aberrations to cellular cholesterol and mitochondria during luteinization. Growing evidence suggests that cholesterol metabolism acts as a molecular switch to control inflammation (Cardoso and Perucha, 2021). Activation of TLR signaling leads to reduced cholesterol efflux, ultimately resulting in further cholesterol accumulation and the amplification of inflammatory response (Tall and Yvan-Charvet, 2015). Therefore, the reduced cholesterol uptake and storage of lipid droplets observed during the early stages of luteinization may be a cellular compensatory mechanism to mitigate persistent inflammation. Similarly, the present study observed reductions in mitochondrial density during the early stages of luteinization. Mitochondrial damage was reported in murine macrophages following LPS stimulation, and that PTEN-induced putative kinase 1 (PINK1) accumulated on damaged mitochondria to promotes mitophagy (Wang et al., 2019). Therefore, it is interesting to consider the roles of mitophagy in the context of steroidogenic cells, which are highly dependent on mitochondrial function to perform the cellular task of steroid biosynthesis.

Despite the evidence that granulosa cell molecular phenotype is changed, the exact duration for which uterine disease impacts ovarian cells remains unknown. While

it is logical to make associations between disease and contemporaneous ovarian function, evidence from the literature indicates that even primordial follicles within the bovine ovary are sensitive to LPS (Bromfield and Sheldon, 2011). Therefore, the question arises of how inflammation perpetuates a potential carryover effect following uterine disease. One possibility is that LPS changes the epigenetic landscape of early follicles, which may have implications for granulosa cell function during later stages of follicular development. Indeed, pretreatment of buffalo granulosa cells with a histone deacetylase inhibitor, Trichostatin A, attenuated LPS induced pro-inflammatory cytokine gene expression and NFκB translocation into the nucleus thus rescuing the inhibitory effects of LPS on *CYP19A1* expression and estradiol secretion (Mehta et al., 2015). Thus, the impacts of uterine disease and bacterial components on the molecular function of ovarian cells could be prolonged and may depend on factors such as the severity of uterine disease, the physiological state of the cell (i.e., stage of development), and the effectiveness of treatment in resolving active infection and clearing inflammation. Collectively, perturbations to granulosa function may have implications on subsequent luteal function following a later ovulation. While it is apparent that cows with uterine disease are not completely infertile, the nuanced modifications to the steroidogenic capacity of ovarian cells may perpetuate the subfertility phenotype observed in cows following uterine disease.

Lastly, I utilized an induced infection model to investigate the effects of intrauterine infusion of pathogenic bacteria on oocyte development to the blastocyst stage and the endometrial transcriptome on day 16 of the estrous cycle which is coincident with the time of conceptus elongation. Previous work has shown that oocyte

development to the morula stage of development is reduced following intrauterine infusion of bacteria (Dickson et al., 2020). Here, I demonstrate that bacteria infusion had no effect on the quality of oocytes or capacity of oocytes to develop to the blastocyst stage of development. However, the current study and that of Dickson et al., (2020) were different in terms of assessing the stage of embryo development, the degree of inflammation caused by intrauterine infusion of bacteria, timing of oocyte collection and the basal success of in vitro fertilization and embryo culture. All of these factors may have contributed to the discrepancy observed between the two studies and I would suggest that these experiments be repeated in a larger cohort to derive a more definitive data set.

The endometrium responds to pregnancy by altering the expression of genes within the transcriptome (Forde et al., 2010, Mathew et al., 2019). Similarly, uterine disease alters the transcriptome of the uterus following spontaneous and induced infection (Salilew-Wondim et al., 2016, Horlock et al., 2020, Dickson et al., 2022a). Combined, it was revealed that uterine disease alters the transcriptomic response to pregnancy, such that the expression of genes following infection are divergent from cows without uterine disease (Dickson et al., 2022a). While other studies have investigated the effects of uterine disease and pregnancy on the transcriptome of the endometrium, the study conducted here sought to explore the transcriptome of the non-pregnant endometrium at the time a conceptus would be elongating under pregnant conditions. As expected, the transcriptome of the endometrium was different 41 d after bacteria infusion on d 16 of the estrous cycle.

The top pathway predicted to be altered following bacteria infusion was related to glutathione-mediated detoxification, which has roles in balancing reactive oxygen species. An experiment which evaluated systemic levels of oxidative stress in cows with metritis found that cows with metritis had greater systemic levels of oxidative stress, compared to healthy cows (Chandrappa et al., 2023). Similarly, LPS stimulation of primary bovine endometrial epithelial cells increased the production of oxidative stress markers and inflammatory factors (Cui et al., 2023). Together, these data suggest that oxidative stress and the potential cellular roles of glutathione-mediated detoxification may warrant exploration following inflammatory stimulus. The top up-regulated gene identified in the endometrium following bacteria infection was *GSTA3,* which codes for glutathione S-transferase alpha 3. The function of GSTA3 has been described in humans to catalyze double-bond isomerization of androstenedione and pregnenedione to testosterone and progesterone, respectively (Johansson and Mannervik, 2001). The expression and immunohistochemical localization GSTA3 were significantly increased in the d 15 endometrium of cows classified as repeat breeders, compared to cows that were classified as not repeat breeders (Hayashi et al., 2017). Taken together, the increased expression of *GSTA3* in the endometrium of cows with uterine disease may be parallel to cows with a subfertility phenotype, and the role of this enzyme needs to be explored further. Conversely, the expression of *MYMK,* which is involved in cell-cell fusion, was the most significantly down-regulated gene in the endometrium following bacteria infusion. The gene *MYMK* codes for myomaker myoblast fusion factor and could be involved in facilitating the fusion of trophoblast cells to the maternal endometrium.

The work conducted here identified gene targets and pathways altered following the infusion of bacteria within the d 16 non-pregnant endometrium. This work provides insight into the transcriptional changes occurring after the infusion of bacteria, and allows for an estimation of the baseline changes occurring within the endometrium in the absence of pregnancy signals, which are known to modulate the endometrial transcriptome. This work provides opportunities for further investigation into novel mechanisms facilitating subfertility in cows with uterine disease. For example, a critical step in functionally exploring the findings here would be to characterize the abundance of GSTA3 within the endometrium following uterine disease. If the abundance of this protein is also associated with the incidence of uterine disease, further investigation would be needed to determine the localized function within the endometrium prior to developing targeted strategies for possible pharmaceutical intervention that could modulate GSTA3 or its downstream products.

In summary, I provide experimental evidence that environmental stressors such as paternal diet and uterine infection can compromise fertility in cattle. Paternal overnutrition has implications not only within the scope of the cattle industries, but also in human health. I also found that uterine infections have distinct effects on the endometrium at a time that would be coincident with the time of conceptus elongation, and the ovary such that the steroidogenic cells of the ovary are compromised during an inflammatory challenge. Studies contained within this dissertation highlight the importance of investigating how environmental factors can influence both male and female reproductive physiology. The approaches utilized here permit a deeper understanding of both the phenotypes associated with environmental perturbations and

insight into the mechanisms leading to compromised cellular function in the ovary. Collectively, these finding provide evidence for future research endeavors to unravel a phenotype of fertility and make improvements for cattle reproduction.

APPENDIX A
SUPPLEMENTAL FIGURES

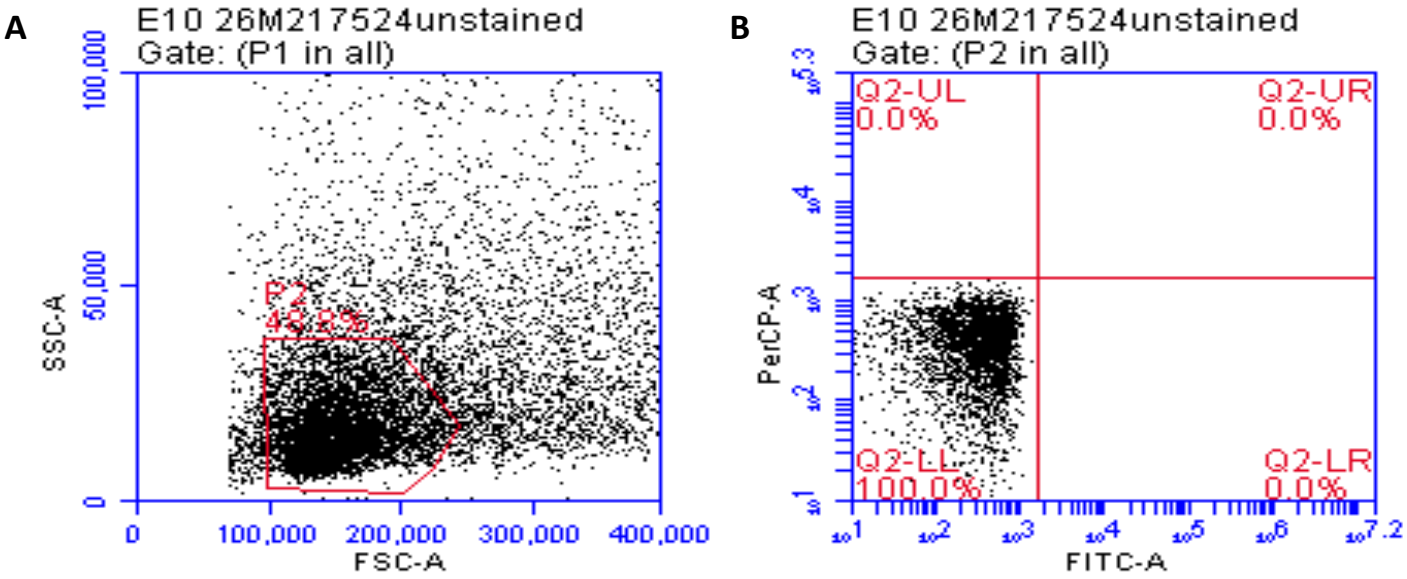

Figure A-1. Flow cytometry scatter plots. The gating strategy for sperm selection based was on distribution of forward and side scatter (A). Unstained sperm cells were used to demonstrate the control/background fluorescence of the PerCP-A and FITC signals used to determine acrosome damage and sperm cell apoptosis (B).

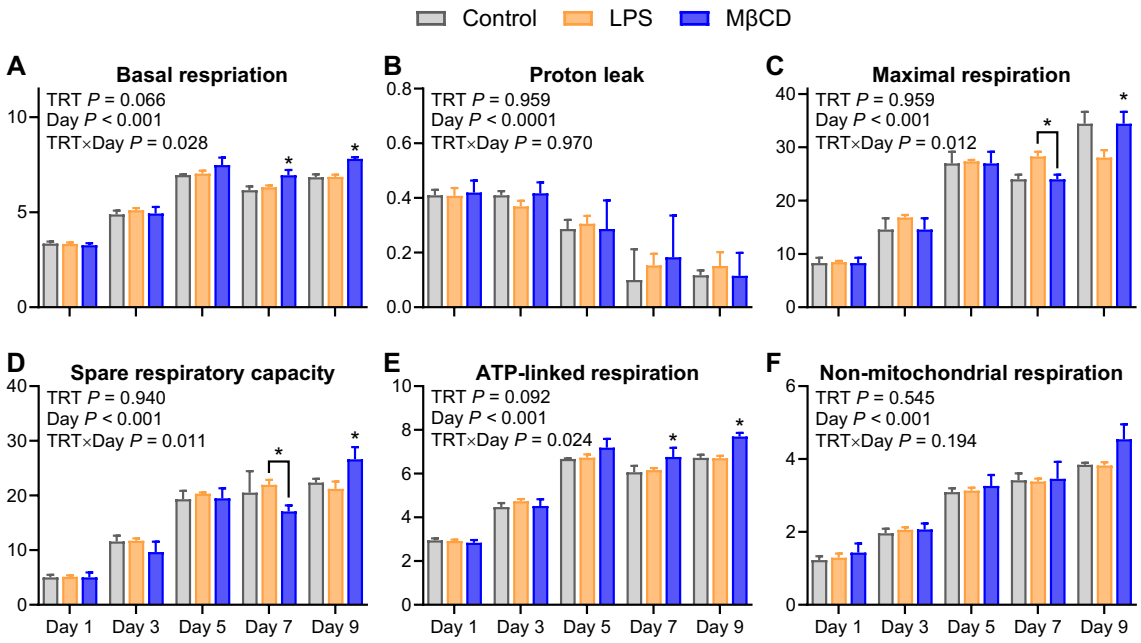

Figure A-2. Effect of granulosa cell treatment with LPS or MβCD on cellular respiration during luteinization. Bovine granulosa cells (n = 3) were treated with 10^3 ng/mL LPS for 24 h or 1mM methyl-β-cyclodextrin (MβCD) and cellular respiration was evaluated every 48 h using the Agilent SeaHorse MitoStress Test. Basal respiration (A), proton leak (B), maximal respiration (C), spare respiratory capacity (D), ATP-linked respiration (E), and non-mitochondrial respiration (F) were measured. Data are presented as least squares means ± SEM.

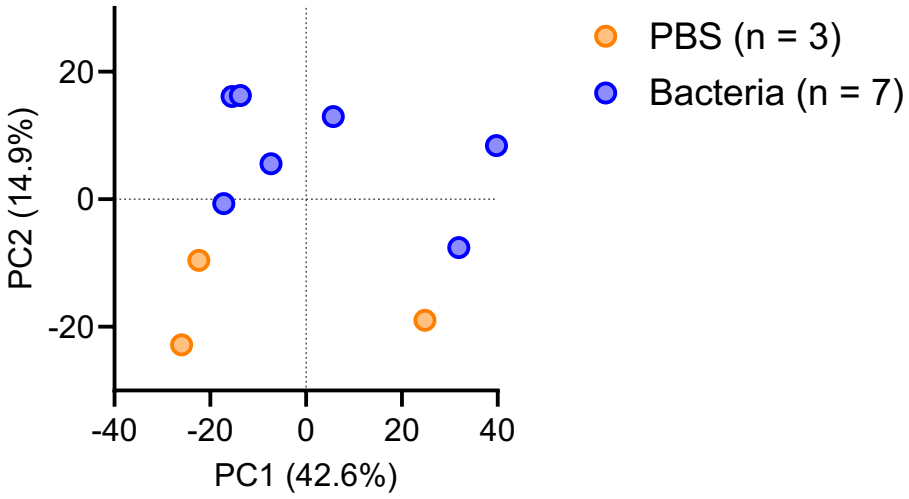

Figure A-3. Principal component analysis of endometrial transcript reads acquired from endometrium after infusion of pathogenic bacteria. Cows were estrous synchronized beginning 14 d after infusion and endometrial samples were collected 41 d after infusion, corresponding to 16 d after ovulation. Endometrial samples were submitted to RNA sequencing analysis. Read counts for all transcripts were subjected to principal component analysis. Principal component (PC1) and principal component 2 (PC2) explain 42.6% and 14.9% of the total variance, respectively.

APPENDIX B
SUPPLEMENTAL TABLES

Table B-1. Primers sequences used for real time PCR analysis of luteal tissue segregated according to molecular function.

Gene symbol	Primer sequence	Accession number
Housekeeping		
ACTA2	5’ – AAGGCCAACCGGGAGAAA 3’– ACCGCCTGAATAGCCACATA	NM_001034502.1
ACTB	5’ – TGGCACCCAGCACAATGAA 3’– GCCAATCCACACGGAGTACTT	NM_173979.3
GAPDH	5’ – AACGGGAAGCTCGTCATCAA 3’– ACATACTCAGCACCAGCATCA	NM_001034034.2
RPL19	5’ – GCCGGCTGCTTAGACGATA 3’– AACACGTTACCCTTCACCTTCA	NM_001040516.1
RPS9	5’ – GCCTCGACCAAGAGCTGAA 3’– GAATTTGACCCTCCAGACCTCA	NM_001101152.2
Cell Cycle		
ATM	5’ – TGCTTGCTGTTGTGGACTAC 3’– CCAGCCAGAAAGCATCATCA	XM_005215785.3
CCNB1	5’ – TTTAGTCTGGGTCGCCCTCTA 3’– GGCCAGAGTATGTAGCTCAACA	NM_001045872.1
CCND2	5’ – CTCCTGGCAAAGATCACCAAC 3’– TATTCAGCAGCACCACCTCA	NM_001076372.1
CCNE1	5’ – GGGGCTTGTTCAGGAGATGAA 3’– GACACAATGGTCAGGGGACTTA	NM_001192776.1
CDC20	5’ – GGTTCCTCTGCAGACCTTCA 3’– TTGGACTGCCAGGGACAC	NM_001082436.2
CDK1	5’ – CTATCCCTCCTGGTCAGTTCA 3’– GTCCCTGTGGAGAACTCTTCTA	NM_174016.2
CDK2	5’ – TTTTGGGGTCCCTGTTCGTAC 3’– TGCAGCCCAGAAGGATTTCC	NM_001014934.1
CDKN1A	5’ – TCCTGCACCCTCGTGAC 3’– AGTCTGCGTTTGGAGTGGTA	NM_001098958.2
CDKN1B	5’ –CAGTGCCCTGGGATAAGGAA 3’– GCGTCTGCTCCACTGAAC	NM_001100346.1
PTEN	5’ – GCCAACCGATACTTTTCTCCA 3’– GCCTCTGGATTTGATGACTCC	NM_001319898.1
SRC	5’ –AACTCCTCGGACACAGTCAC 3’– CATAGTCATAGAGGGCCACGAA	NM_001110804.2
WEE1	5’ –CCGGGGCTTGAGGTATATTCA 3’– GAGGCAGCATTTGGGATTGAA	NM_001101205.1
Cell Death		

Table B-1. Continued

Gene symbol	Primer sequence	Accession number
APAF1	5’ – TGGTCTGCTGATGGTGCTAA 3’– AACAGGCCACTGGAGTGAA	NM_001191507.1
BAD	5’ – GGGTCAGGGGCCTCATTA 3’– TTCCTGCTCACTCTGCTCAA	NM_001035459.1
BAX	5’ – CGGGTTGTCGCCCTTTTCTA 3’– GCCCATGATGGTCCTGATCAA	NM_173894.1
BCL2	5’ – ATGTGTGTGGAGAGCGTCAA 3’– GGTTCAGGTACTCGGTCATCC	NM_001166486.1
CASP7	5’ – ACCGGTCCTCTTTTGTCTCA 3’– GGGGATGTTGACTGATTTCCC	XM_002698509.3
CASP9	5’ –TCACTGTGAGGACCTTCAGAC 3’– GCCCGGCATCTGTTTGTAAA	NM_001205504.2
FOXO3	5’ – GCGTGCCCTACTTCAAGGATA 3’– GTGACAGGTTGTGCCGGATA	NM_001206083.1
Cell Signaling		
LHCGR	5’ – AAGCACAGCAAGGAGACCAA 3’– TAATCCCAGCCACTCAGTTCAC	NM_174061.1
MAP2K1	5’ – CGCAGAGAGAGCAGATTTGAA 3’– AGAGCCAACCTGCAAAATCC	NM_001130752.1
MAPK13	5’ – CGTGTCCCTGACGCACATA 3’– TTCTTGATGGCCACCTTCTCC	NM_001014947.1
PPARA	5’ – GACAAAGCCTCTGGCTACCA 3’– CTTCAGCCGAATCGTTCTCCTA	NM_001034036.1
PPARG	5’ – CTTGCTGTGGGGATGTCTCA 3’– ATCTCCGCTAACAGCTTCTCC	NM_181024.2
PRKCB	5’ –GAATGGTGGTGACCTCATGTAC 3’– TGGCAATTTCTGCAGCGTAA	NM_174587.1
PTGER3	5’ – CCCTGGGTTTATCTGCTGCTA 3’– ACCCTCCGTGTCTAGTCCATA	NM_181032.1
PTGER4	5’ – TTCATCGACTGGACCACCAA 3’– CGAGGATGAGGAAGGAACTGAA	NM_174589.2
STAT1	5’ –ATGCTGGTGCCAGAACTAA 3’– TGGCACAACTGGGTTTCA	NM_001077900.1
STAT3	5’ – GGTGTCAGATCACATGGGCTAA 3’– TGATGTTGTCCAGCCAGACC	NM_001012671.2
STAT4	5’ – GCACATCTGCTAGAAAGAGTCAC 3’– CATGCATGGCTGTCGTTCAA	NM_001083692.2
Corpus Luteum Function		
FGF2	5’ – GCTTCTTCCTGCGCATCC 3’– CCCCTCTCTCTTCTGCTTGAA	NM_174056.3
GHR	5’ – GATGAACCCATCTGCATGTGAA 3’– ACTGCTAGCCCAAGTATTCCA	NM_176608.1

Table B-1. Continued

Gene symbol	Primer sequence	Accession number
IGF1	5’ – GAGTTGGTGGATGCTCTCCA 3’– GACTGCTCGAGCCATACCC	NM_001077828.1
IGF2	5’ – AGGGATGTGTCTGCCTCTAC 3’– TGGACTGCTTCCAGATGTCA	NM_174087.3
IGF2R	5’ – GGCAGATTCCACTCAAGTCA 3’– AGATCAAGGTGAGGTCTCCA	NM_174352.2
IGFBP2	5’ – ACAAGCATGGCCTGTACAAC 3’– GTTCACACACCAGCACTCC	NM_174555.1
PGR	5’ – GACTCCGAGCCCAAGGAC 3’– TCCTCCTCCTCCTTGATCTTCA	NM_001205356.1
Epigenetics		
DNMT1	5’ – AGAGACGTCGAGTTACATCCA 3’– GTGTTCCTGGTCTTACTCTTCC	NM_182651.2
DNMT3A	5’ – TCTTCGCCAACAACCATGAC 3’– GGATGGGCTTCCTCTTCTCA	NM_001206502.1
H2AFX	5’ – GCTACAGCTCGGTGCTTAGAA 3’– TCCCAGGACGAAATGAAGCAA	NM_001079780.2
H2AFZ	5’ – AGCCATCCTGGAGTACCTCA 3’– GTGACGAGGGGTAATACGCTTTA	NM_174809.2
HDAC1	5’ – ATGTCCGAGTACAGCAAGCA 3’– CAGAACTCAAACAGGCCATCAAA	NM_001037444.2
HDAC8	5’ – GCCTTCAGTTTCACCTCCAA 3’– GGCCAACATCAGACACATCA	NM_001076231.2
TET1	5’ – CTCTAATGGGTGTCCAGTTGCTA 3’– TACGCTGTCGAACCAGACAA	XM_010820679.1
TET2	5’ – CACTCTTATGGCACCAACGTAC 3’– ACTCTGGTGCTCTGTGTTCA	XM_005198583.2
Inflammation		
CD14	5’ – CCGTTGTGTCTGCAACTTCA 3’– ACGGCAACCATACACTGAAC	NM_174008.1
CD40	5’ – GAAAAGGCCTGGTGGAACAA 3’– GTCCTCATCCGACTCTGGAA	NM_001105611.2
CXCL8	5’ – GTTGCTCTCTTGGCAGCTTT 3’– TGGCATCGAAGTTCTGTACTCA	NM_173925.2
IFNB1	5’ – TGCCTGAGGAGATGAAGCAA 3’– AGATGTGCTGGAGCATCTCA	NM_174350.1
IL12A	5’ – CTGAGGGCTGTCAGCAACA 3’– TCTCCTCAGAAGTGCAGGAGTA	NM_174355.2
IL1A	5’ – TCCCTGACCTCTTTGAAGACC 3’-GAGAGAGGTGGTCAATTTCAGAAC	NM_174092.1
IL1B	5’ – TGTGTGCTGAAGGCTCTCC 3’– CCTTGCACAAAGCTCATGCA	NM_174093.1
IL4	5’ – AATTCCTGGGCGGACTTGAC 3’– TTGTGCTCGTCTTGGCTTCA	NM_173921.2

Table B-1. Continued

Gene symbol	Primer sequence	Accession number
IL6	5’ – TAAGCGCATGGTCGACAAAA 3’– TCTCCTTGCTGCTTTCACAC	NM_173923.2
IL6R	5’ – CCCTAGGATTTGACGGCTACAA 3’– TTCTGTCCACGGCACTGAC	NM_001110785.3
NCF1	5’ – CCTCCTGGGCTTCGAGAA 3’– AGACAGGTCCTGCCATTTCA	NM_174119.4
NFKB1	5’ – TGGCAGCTCTTCTCAAAGCA 3’– AGGAGTCATCCAGGTCGTACA	NM_001076409.1
NFKBIA	5’ – CTGGCCTTCCTCAACTTCCA 3’– TCAGCGATTTCTGGCTGGTTA	NM_001045868.1
PTPRC	5’ – CGTGTGAGCCTCCATTTGAA 3’– ATCTTCCACGCAGTCTACCA	NM_001206523.1
TLR1	5’ – CATTTGATGCCCTGCCCATA 3’– TAACTGTGTGGCACTCAACC	NM_001046504.1
TLR2	5’ – CTGCTGCGTTGGTTTGGATA 3’– CCATGCTGTCCACAAAGCA	NM_174197.2
TLR4	5’ – ATCCTCTCCTGCCTGAGAAC 3’– AGCTCCATGCACTGGTAACTA	NM_174198.6
TLR6	5’ – GGCAACTTGACCCAACTGAA 3’– GTGCAAGTGAGCAATGGGTA	NM_001001159.1
TLR9	5’ – AACCTGCCCGCCAGAC 3’– GCCTGCACCAGGAGAGAAA	NM_183081.1
TNF	5’ – CAAGTAACAAGCCGGTAGCC 3’– GGCATTGGCATACGAGTCC	NM_173966.3
Lipid Metabolism		
ACAA2	5’ – TGTCGTCGTAGGCAATGTCA 3’– GATTCCCACACGCAAACCAA	NM_001035342.2
ACACA	5’ – GCTAACTCAACTCAGCAAGACC 3’– GGATGGCAAATGGGAAGCAA	NM_174224.2
ACAT1	5’ – GAGCTGTTTCTCTTGGACATCC 3’– GCTTCAGTGCATGAGCCAAA	NM_001046075.1
ACSL1	5’ – GGAAGAGCCAACAGACAGAA 3’– GTAGTTCCACTGGTGAAGCA	NM_001076085.1
CYP3A4	5’ – TGCAGGAGGAGATTGATGCA 3’– CCACCATGTCAAGGTACTCCA	NM_001099367.1
CYP4A11	5’ – TGGTCTACGACCCTGACTACA 3’– AGGGCTTTACGAATCTGTGGATA	NM_001077908.1
HADH	5’ – GGTGGAGGCCATTGTAGAGAA 3’– GAGGAAGTGTTGCTGGCAAA	NM_001046334.1
POR	5’ – GACTTCTACGACTGGCTCCA 3’– GTCTTGTTCCCAAGGGCAAA	NM_001035390.1
Steroid Synthesis		
CYP11A1	5’ – CTGGCATCTCCACAAAGACC 3’– GGTTAAGCCAGCCATTGTCA	NM_176644.2

Table B-1. Continued

Gene symbol	Primer sequence	Accession number
CYP11B1	5’ – CCAGCCCTGCAGAAGTACA 3’– CAGCACCCTCGCCTTCA	NM_174638.3
CYP17A1	5’ – TCAGAGAAGTGCTCCGAATCC 3’– CAACGTCTGTGCCTTTGTCA	NM_174304.2
CYP19A1	5’ – GGCAAGCTCTCCTTCTCAAA 3’– TCCATGGCATCTTTCAAGTCC	NM_174305.1
FASN	5’ – GCCCCTACTTCCAAGGTATCC 3’– GTCACCCAGTTGTCCTTCCA	NM_001012669.1
HSD11B1	5’ – CCATGCTGAAGCAGACCAAC 3’– CGCAGCAACAAGTGGACAA	NM_001123032.1
HSD17B10	5’ – ATGGGTATCCGGGTGATGAC 3’– CCAGGAAGTTGCGCACTTTA	NM_174334.3
HSD3B1	5’ – GACCAGAAGTTCGGGAGGAA 3’– TTCAGGCACTGCTCATCCA	NM_174343.3
STAR	5’ – CCCCAGCTGCGTGGATTAA 3’– TCGCTGTAGAGAGGGTCTTCC	NM_174189.3
Vascularity and Angiogenesis		
FLT1	5’ – CATGTGAAAAGCGGGCAAAC 3’– AGGCCTCATAGTGATGAATCCC	NM_001191132.4
FLT3LG	5’ – AACTGCTGGAGGATGTCAACA 3’– AAGCGAAGACAGCTGGGAA	NM_181030.2
VEGFA	5’ – CTTTTGGGAAGCCCGACAAA 3’– TCTGTCCATTTGACTCGGGAA	NM_001316955.1
VEGFB	5’ – TGGGCAGCACCAAGTCC 3’– ACACTGGCTGTGTTCTTCCA	NM_174487.2
VEGFC	5’ – GTGCATGAACACCAGCACAA 3’– CCTTGAGAGAGAGGCACTGTA	NM_174488.2
VEGFD	5’ – TGCAGGGCTCCAGTTATGAA 3’– TCTGCTGCTCAGATCGTTCTA	NM_001101043.2
HSD3B1	5’ – GACCAGAAGTTCGGGAGGAA 3’– TTCAGGCACTGCTCATCCA	NM_174343.3

Table B-2. Differentially expressed genes of the endometrium after intrauterine infusion of *E. coli* and *T. pyogenes.*

Gene	Description	Log_2FC[1]	FDR
ABCG1	ATP binding cassette subfamily G member 1	1.509	0.0227
ACSM1	Acyl-CoA synthetase medium chain family member	2.633	0.0299
ADCY7	Adenylate cyclase 7	-1.308	0.0434
ADGRG7	Adhesion G protein-coupled receptor G7	3.616	0.0202
ADRA2A	Adrenoceptor alpha 2A	1.903	0.0189
ALCAM	Activated leukocyte cell adhesion molecule	1.277	0.0323
ANPEP	Alanyl aminopeptidase	2.871	0.0235
ARMCX2	Armadillo repeat containing 2C X-linked 2	1.884	0.0154
ARMCX6	armadillo repeat containing X-linked 6	1.937	0.0041
ASGR1	Asialoglycoprotein receptor 1	2.727	0.0005
ASGR2	Asialoglycoprotein receptor 2	1.523	0.0021
ASPHD2	Aspartate beta-hydroxylase domain containing 2	2.066	0.0425
AZGP1	Alpha-2-glycoprotein 1	1.384	0.0042
BATF2	Basic leucine zipper ATF-like transcription factor 2	2.994	0.0039
BCAT2	Branched chain amino acid transaminase 2	2.078	0.0169
BEX2	Brain expressed X-linked 2	1.109	0.0029
BPIFB2	BPI fold containing family B member 2	4.796	0.0293
C10H15orf48	Chromosome 10 C15orf48	2.065	0.0202
C16H1orf21	Chromosome 16 C1orf21	1.939	0.0003
C28H10orf99	Chromosome 28 C10orf99	3.841	0.0017
C3H1orf54	Chromosome 3 C1orf54	2.351	0.0378
C3H1orf87	Chromosome 3 C1orf87	2.233	0.0221
C5AR2	Complement component 5a receptor 2	3.082	0.0019
C9H6orf163	Chromosome 9 C6orf163	2.398	0.0006
CALM	Calmodulin	1.036	0.0011
CCDC113	Coiled-coil domain containing 113	2.355	0.0421
CCDC160	Coiled-coil domain containing 160	2.259	0.0272
CCDC190	Coiled-coil domain containing 190	2.586	2.26×10^{-8}
CCDC68	Coiled-coil domain containing 68	2.132	1.07×10^{-5}
CCL28	C-C motif chemokine ligand 28	1.843	0.0365
CD81	CD81 Molecule	1.494	0.0269
CDC42EP5	CDC42 effector protein 5	2.198	0.0255
CDO1	Cysteine dioxygenase type 1	2.856	4.65×10^{-8}
CDRT1	CMT1A duplicated region transcript 1	-3.234	0.0008
CES1	Carboxylesterase 1	3.455	1.99×10^{-5}
CFAP157	Cilia and flagella associated protein 157	2.795	0.0237
CFAP299	Cilia and flagella associated protein 299	2.495	0.0425
CGNL1	Cingulin like 1	-1.961	0.0054
CHST12	Carbohydrate sulfotransferase 12	1.295	0.0208

Table B-2. Continued

Gene	Description	Log_2FC[1]	FDR
CHST9	Carbohydrate sulfotransferase 9	2.392	0.0157
CITED4	Cbp/p300 interacting transactivator with Glu/Asp rich carboxy-terminal domain 4	2.001	0.0039
COX7A1	Cytochrome c oxidase subunit 7A1	2.390	0.0023
COX8B	Cytochrome c oxidase subunit VIII-H	3.176	0.0221
CRABP1	Cellular retinoic acid binding protein 1	3.165	0.0010
CRACR2B	Calcium release activated channel regulator 2B	1.553	2.64×10^{-6}
CSF3	Colony stimulating factor 3	3.244	0.0030
CSRP2	Cysteine and glycine rich protein 2	2.066	0.0214
CT83	Cancer/testis antigen 83	2.301	0.0150
CTSL	Cathepsin L	3.445	0.0215
CXCL10	C-X-C motif chemokine ligand 10	2.506	0.0067
DAB1	DAB Adaptor Protein 1	2.384	0.0401
DMRT2	Doublesex and mab-3 related transcription factor 2	2.736	0.0366
DUSP6	Dual specificity phosphatase 6	-1.026	0.0034
EFEMP1	EGF containing fibulin extracellular matrix protein 1	3.006	0.0008
EIF4EBP1	Eukaryotic translation initiation factor 4E binding protein 1	1.270	0.0452
ELAVL2	ELAV like RNA binding protein 2	-1.965	0.0473
EPHX2	Epoxide hydrolase 2	1.450	3.18×10^{-6}
ERICH2	Glutamate rich 2	2.298	0.0272
ETNK2	Ethanolamine kinase 2	1.978	0.0026
EYA2	EYA transcriptional coactivator and phosphatase 2	1.538	0.0405
FAM171A1	Family with sequence similarity 171 member A1	1.523	0.0284
FAM183A	Family with sequence similarity 183 member A	2.456	0.0378
FAM216B	Family with sequence similarity 216 member B	2.520	0.0277
FAM84A	Family with sequence similarity 84 member A	1.852	0.0130
FCGBP	Fc fragment of IgG binding protein	1.483	0.0357
FMO1	Flavin containing monooxygenase 1	4.694	0.0007
FMO3	Flavin containing monooxygenase 3	2.870	0.0012
FOLH1B	Folate hydrolase 1B	5.506	0.0160
FOXA2	Forkhead box A2	1.960	0.0020
FXYD1	FXYD domain containing ion transport regulator 1	1.763	0.0034
GDAP1	Ganglioside induced differentiation associated protein 1	-1.080	0.0442
GJB7	Gap junction protein beta 7	4.166	0.0058
GMNN	Geminin	1.790	0.0011

Table B-2. Continued

Gene	Description	Log_2FC[1]	FDR
GNAZ	G protein subunit alpha z	1.910	0.0069
GPX2	Glutathione peroxidase 2	2.485	0.0017
GSDMD	Gasdermin D	1.769	2.64×10^{-6}
GSTA3	Glutathione S-transferase	6.814	0.0017
GSTM1	Glutathione S-transferase M1	1.159	0.0030
GSTM3	Glutathione S-transferase mu 3	1.324	0.0243
GSTT2	Glutathione S-transferase theta 2	2.338	0.0148
HSBP1L1	Heat shock factor binding protein 1 like 1	1.636	0.0126
IFI44	Interferon induced protein 44	4.125	0.0349
IGFBP5	Insulin like growth factor binding protein 5	2.219	0.0390
IRX3	Iroquois homeobox 3	2.569	0.0452
JAKMIP2	Janus kinase and microtubule interacting protein 2	5.854	2.11×10^{-10}
JDP2	Jun dimerization protein 2	2.142	1.49×10^{-10}
KCNAB1	Potassium voltage-gated channel subfamily A member regulatory beta subunit 1	3.236	0.0330
KCNJ2	Potassium voltage-gated channel subfamily J member 2	2.656	0.0289
KCNK2	Potassium two pore domain channel subfamily K member 2	2.932	0.0197
KCNQ5	Potassium voltage-gated channel subfamily Q member 5	3.329	2.64×10^{-6}
KIAA0408	KIAA0408	-3.188	0.0040
KLHL40	Kelch like family member 40	2.265	0.0022
KRT14	Keratin 14	2.775	0.0127
KRT23	Keratin 23	3.950	5.83×10^{-8}
LDHD	Lactate dehydrogenase D	1.441	0.0349
LDLRAD1	Low density lipoprotein receptor class A domain containing 1	2.592	0.0002
LMO4	LIM domain only 4	1.288	0.0388
LOC100847175	C-X-C motif chemokine 15	2.949	0.0494
LOC100848263	Schlafen family member 12	-1.601	0.0130
LOC100848933	Uncharacterized LOC100848933	2.537	0.0427
LOC101903604	Uncharacterized LOC101903604	-1.254	0.0432
LOC101905219	Uncharacterized LOC101905219	1.662	0.0160
LOC104973929	Uncharacterized LOC104973929	-1.259	0.0025
LOC104974498	Uncharacterized LOC104974498	-3.427	0.0169
LOC104975027	Uncharacterized LOC104975027	-1.618	0.0104
LOC104975666	Uncharacterized LOC104975666	3.892	0.0145
LOC107132617	Uncharacterized LOC107132617	1.313	0.0145
LOC112442284	Uncharacterized LOC112442284	2.622	0.0202

Table B-2. Continued

Gene	Description	Log_2FC[1]	FDR
LOC112443013	Uncharacterized LOC112443013	3.085	0.0070
LOC112444909	Translation machinery-associated protein 7	-1.483	0.0093
LOC112446364	Uncharacterized LOC112446364	2.691	0.0079
LOC508916	Carboxylesterase 1	4.141	0.0023
LOC787803	40S ribosomal protein S23	5.013	5.65×10^{-5}
LOR	Loricrin	4.369	0.0245
LPIN1	Lipin 1	-1.290	0.0006
LURAP1L	Leucine rich adaptor protein 1 like	1.685	0.0223
LYPD3	LY6/PLAUR domain containing 3	1.452	0.0079
MACROD1	MACRO domain containing 1	1.601	0.0148
MALL	Mal T cell differentiation protein like	1.932	0.0001
MATN4	Matrilin 4	2.432	0.0060
MBOAT1	Membrane bound O-acyltransferase domain containing 1	2.094	0.0002
MMRN2	Multimerin 2	-1.260	0.0022
MTBP	MDM2 binding protein	1.545	0.0369
MYMK	Myomaker myoblast fusion factor	-3.929	0.0235
N6AMT1	N-6 adenine-specific DNA methyltransferase 1	1.055	0.0401
NAV2	Neuron navigator 2	-1.274	0.0388
NCMAP	Non-compact myelin associated protein	3.668	0.0293
NEURL1B	Neuralized E3 ubiquitin protein ligase 1B	3.475	0.0080
NFIA	Nuclear factor I A	1.105	0.0418
NKAIN1	Sodium/potassium transporting ATPase interacting 1	2.936	0.0146
NLRX1	NLR family member X1	-1.002	0.0237
NPL	N-acetylneuraminate pyruvate lyase	-1.932	0.0186
NRARP	NOTCH regulated ankyrin repeat protein	2.572	0.0279
NT5E	5'-nucleotidase ecto	2.148	9.68×10^{-6}
NTNG1	Netrin G1	-1.796	0.0014
PC	Pyruvate carboxylase	1.203	0.0149
PDLIM2	PDZ and LIM domain 2	1.494	0.0150
PGLYRP1	Peptidoglycan recognition protein 1	2.663	0.0144
PHGDH	Phosphoglycerate dehydrogenase	1.738	0.0365
PHGR1	Proline/histidine/glycine-rich 1	4.543	0.0123
PIGR	Polymeric immunoglobulin receptor	1.759	0.0177
PLA2G2C	Phospholipase A2 group IIC	3.126	0.0052
PLAC8	Placenta-specific 8	2.466	0.0295
PLAC8	Placenta-specific 8	4.083	0.0148
PLEKHA4	Pleckstrin homology domain containing A4	2.799	0.0298
PLEKHH1	Pleckstrin homology	-1.033	0.0066
PPP1R1B	Protein phosphatase 1 regulatory inhibitor subunit 1B	2.493	3.18×10^{-6}

Table B-2. Continued

Gene	Description	Log_2FC[1]	FDR
PPP4R4	Protein phosphatase 4 regulatory subunit 4	2.785	0.0026
PTCH1	Patched 1	-1.180	0.0347
PTGES	Prostaglandin E synthase	2.670	0.0101
PTPN20	Protein tyrosine phosphatase	-2.019	0.0127
PTPRM	Protein tyrosine phosphatase	-1.072	0.0001
PVALB	Parvalbumin	6.575	0.0006
PXMP2	Peroxisomal membrane protein 2	1.003	0.0307
PYCARD	PYD and CARD domain containing	2.217	2.53×10^{-8}
PYGL	Glycogen phosphorylase L	1.612	0.0086
RAB11FIP2	RAB11 family interacting protein 2	-1.342	0.0243
RARRES2	Retinoic acid receptor responder 2	1.974	0.0412
RASIP1	Ras interacting protein 1	1.327	0.0154
RND3	Rho family GTPase 3	1.861	0.0243
RNF24	Ring finger protein 24	-1.081	0.0340
ROR2	Receptor tyrosine kinase like orphan receptor 2	1.664	0.0243
RUNX3	Runt related transcription factor 3	1.694	0.0130
S100A4	S100 calcium binding protein A4	2.354	0.0016
SCEL	Sciellin	2.580	0.0144
SEC14L3	SEC14 like lipid binding 3	2.836	0.0056
SELENBP1	Selenium binding protein 1	1.903	0.0001
SERPINE2	Serpin family E member 2	2.615	0.0005
SESN1	Sestrin 1	-1.233	0.0026
SGPL1	Sphingosine-1-phosphate lyase 1	-1.378	0.0047
SHROOM4	Shroom family member 4	-1.209	0.0011
SIGLEC10	Sialic acid binding Ig like lectin 10	2.538	0.0208
SIX1	SIX homeobox 1	2.171	0.0405
SLC15A2	Solute carrier family 15 member 2	2.088	0.0043
SLC16A7	Solute carrier family 16 member 7	2.811	0.0012
SLC22A4	Solute carrier family 22 member 4	1.974	0.0017
SLC45A2	Solute carrier family 45 member 2	-2.187	0.0481
SPATS2L	Spermatogenesis associated serine rich 2 like	1.342	0.0278
SSBP4	Single stranded DNA binding protein 4	1.696	0.0186
STAC3	SH3 and cysteine rich domain 3	-1.722	0.0008
STX10	Syntaxin 10	1.267	0.0016
STXBP6	Syntaxin binding protein 6	2.432	0.0232
SVIL	Supervillin	-1.162	0.0256
TCEAL1	Transcription elongation factor A like 1	1.132	0.0039
TCF23	Transcription factor 23	5.062	0.0388
TCHH	Trichohyalin	2.051	0.0295
TEX36	Testis expressed 36	3.207	0.0004
TFF3	Trefoil factor 3	2.722	0.0235
TP73	Tumor protein p73	1.664	0.0245

Table B-2. Continued

Gene	Description	Log_2FC[1]	FDR
TSHZ3	Teashirt zinc finger homeobox 3	2.037	0.0114
TTC3	Tetratricopeptide repeat domain 3	-1.452	0.0452
TTC6	Tetratricopeptide repeat domain 6	2.570	0.0423
TUBA1D	Tubulin	1.726	0.0456
TUBB4B	Tubulin beta 4B class IVb	1.075	0.0070
UBXN10	UBX domain protein 10	1.727	0.0452
UPB1	Beta-ureidopropionase 1	4.136	0.0013
VTCN1	V-set domain containing T cell activation inhibitor 1	3.337	0.0144
WHRN	Whirlin	1.218	0.0197
ZAR1L	Zygote arrest 1 like	-1.014	0.0412
ZBTB37	Zinc finger and BTB domain containing 37	-1.033	0.0486
ZNF385B	Zinc finger protein 385B	2.228	8.63×10^{-6}
ZNF462	Zinc finger protein 462	-1.229	7.88×10^{-6}
ZNF503	Zinc finger protein 503	1.756	0.0018

Table B-3. Predicted canonical pathways altered within the endometrium following intrauterine infusion of *E. coli* and *T. pyogenes.*

Canonical pathway	*P*-value ($-Log_{10}$)	z-score	Differentially expressed genes in the pathway
Glutathione-mediated detoxification	6.4	2.236	*ANPEP, GSTA4, GSTM1, GSTM3, GSTT3, PTGES*
Taurine biosynthesis	5.7	N/A	*CDO1, FMO1, FMO3*
Glutathione redox reactions I	2.9	N/A	*GPX2, GSTM1, PTGES*
α-Adrenergic signaling	2.8	N/A	*ADCY7, ADRA2A, CALM1, GNAZ, PYGL*
Cardiac conduction	2.5	2.236	*CALM1, CES1, FXYD1, KCNJ2, KCNK2*
LPS/IL-1 mediated inhibition of RXR function	2.4	N/A	*ABCG1, ACSM1, CHST12, FMO1, FMO3, GSTM1, GSTM3*
Apelin adipocyte signaling pathway	2.3	N/A	*ADCY7, GPX2, GSTM1, PTGES*
G alpha (z) signaling events	2.2	N/A	*ADCY7, ADRA2A, GNAZ*
Methylglyoxal degradation VI	2.1	N/A	*LDHD*
Metabolism of angiotensinogen to angiotensins	2.1	N/A	*ANPEP, CES1*
Potassium channels	2.1	2	*KCNAB1, KCNJ2, KCNK2, KCNQ5*
Class I peroxisomal membrane protein import	2.0	N/A	*GDAP1, PXMP2*
D-myo-inositol (1,4,5,6)-tetrakisphosphate biosynthesis	1.9	0	*DUSP6, EPHX2, PPP1R1B, PTPN20, PTPRM*
D-myo-inositol (3,4,5,6)-tetrakisphosphate biosynthesis	1.9	0	*DUSP6, EPHX2, PPP1R1B, PTPN20, PTPRM*
Sulfur amino acid metabolism	1.8	N/A	*CDO1, FMO1*
Glycogen metabolism	1.8	N/A	*CALM1, PYGL*
Protein Kinase A Signaling	1.8	1.134	*ADCY7, CALM1, DUSP6, EYA2, PPP1R1B, PTCH1, PTPRM, PYGL*

Table B-3. Continued

Canonical pathway	*P*-value ($-Log_{10}$)	z-score	Differentially expressed genes in the pathway
G alpha (i) signaling events	1.8	1.633	*ADCY7, ADRA2A, CCL28, CXCL10, CXCL6, GNAZ*
Granulocyte adhesion and diapedesis	1.8	N/A	*CCL28, CSF3, CXCL10, CXCL6, GPR15LG*
3-phosphoinositide degradation	1.8	0	*DUSP6, EPHX2, PPP1R1B, PTPN20, PTPRM*
Xenobiotic metabolism CAR signaling pathway	1.8	2.236	*CHST12, FMO1, FMO3, GSTM1, GSTM3*
Pyroptosis	1.7	N/A	*GSDMD, IRF1*
D-myo-inositol-5-phosphate metabolism	1.7	0	*DUSP6, EPHX2, PPP1R1B, PTPN20, PTPRM*
Nucleotide catabolism	1.7	N/A	*NT5E, UPB1*
Melanin biosynthesis	1.6	N/A	*SLC45A2*
Uracil degradation II (Reductive)	1.6	N/A	*UPB1*
Serine biosynthesis	1.6	N/A	*PHGDH*
Thymine degradation	1.6	N/A	*UPB1*
3-phosphoinositide biosynthesis	1.6	0	*DUSP6, EPHX2, PPP1R1B, PTPN20, PTPRM*
Asparagine N-linked glycosylation	1.6	N/A	*ASGR1, ASGR2*
RHO GTPases activate IQGAPs	1.6	N/A	*CALM1, TUBB4B*
Pathogen induced cytokine storm signaling pathway	1.6	2.646	*CCL28, CXCL10, CXCL6, GPR15LG, GSDMD, IRF1, PYCARD*
Xenobiotic metabolism signaling	1.6	N/A	*CES1, CHST12, FMO1, FMO3, GSTM1, GSTM3*
L-cysteine degradation I	1.5	N/A	*CDO1*
TP53 regulates metabolic genes	1.5	N/A	*COX8A, GPX2, SESN1*
Neutrophil degranulation	1.5	2.828	*ANPEP, GSDMD, PGLYRP1, PIGR, PLAC8, PYCARD, PYGL, TUBB4B*

Table B-3. Continued

Canonical pathway	*P*-value ($-Log_{10}$)	z-score	Differentially expressed genes in the pathway
Opioid signaling	1.5	N/A	*ADCY7, CALM1, PPP1R1B*
Aryl hydrocarbon receptor signaling	1.5	N/A	*GSTM1, GSTM3, NFIA, TP73*
Superpathway of inositol phosphate compounds	1.4	0	*DUSP6, EPHX2, PPP1R1B, PTPN20, PTPRM*
Reelin signaling pathway	1.4	N/A	*DAB1*
Superpathway of serine and glycine biosynthesis I	1.4	N/A	*PHGDH*
DAG and IP3 signaling	1.4	N/A	*ADCY7, CALM1*
Glycerophospholipid biosynthesis	1.4	N/A	*ETNK2, LPIN1, MBOAT1*
Vasopressin regulates renal water homeostasis via Aquaporins	1.4	N/A	*ADCY7, RAB11FIP2*
UDP-N-acetyl-D-glucosamine biosynthesis II	1.3	N/A	*FMO3*
Arachidonic acid metabolism	1.3	N/A	*EPHX2, GPX2*
Interleukin-10 signaling	1.3	N/A	*CSF3, CXCL10*
GPER1 signaling	1.3	N/A	*ADCY7, GNAZ*
Coronavirus replication pathway	1.3	N/A	*CTSL, TUBB4B*
Role of IL-17F in allergic inflammatory airway diseases	1.3	N/A	*CXCL10, CXCL6*
iNOS Signaling	1.3	N/A	*CALM1, IRF1*
Mitochondrial dysfunction	1.3	-1.633	*CALM1, COX7A1, COX8A, GPX2, GSTM1, PTGES*
Cardiac hypertrophy signaling	1.3	1	*ADCY7, ADRA2A, CALM1, GNAZ, RND3*

Table B-4. Predicted upstream regulators of gene expression within the endometrium following an intrauterine infusion of *E. coli* and *T. pyogenes*.

Upstream Regulator	Biotype	z-score	*P*-value	Target molecules differentially expressed in dataset
IFNG	Cytokine	3.113	0.0015	*ADCY7, ADRA2A, AZGP1, BATF2, C15orf48, CCL28, CRABP1, CSF3, CXCL10, CXCL6, ELAVL2, GSDMD, IFI44, IRF1, KRT14, PHGDH, PIGR, PPP1R1B, PTGES, RUNX3, SGPL1, SIX1, TP73*
NFkB (complex)	Complex	2.899	0.0229	*ABCG1, ADRA2A, BEX2, CITED4, CSF3, CXCL10, CXCL6, IRF1, PTGES, SLC22A4*
Lipopolysaccharide	Chemical drug	2.749	3.78×10^{-5}	*ABCG1, ADRA2A, ALCAM, ARMCX6, AZGP1, CALM1, CD81, COX7A1, CSF3, CTSL, CXCL10, CXCL6, EPHX2, FOXA2, GSDMD, IFI44, IGFBP5, IRF1, JDP2, LMO4, LORICRIN, LPIN1, NRARP, PC, PGLYRP1, PIGR, PLAC8, PLEKHA4, PTCH1, PTGES, PYCARD, RND3, RNF24, RUNX3, S100A4, SERPINE2, SESN1, SSBP4, TUBB4B*
TNF	Cytokine	2.667	1.17×10^{-6}	*ADCY7, ALCAM, ANPEP, ASGR1, C15orf48, CCL28, CDC42EP5, CDO1, CSF3, CTSL, CXCL10, CXCL6, DUSP6, FMO1, GSDMD, GSTA4, IGFBP5, IRF1, KCNJ2, KRT23, MALL, NLRX1, NRARP, PC, PGLYRP1, PHGDH, PIGR, PTGES, PXMP2, PYCARD, RARRES2, RND3, SERPINE2, SGPL1, SLC22A4, SVIL, TCHH*
HIF1A	Transcription regulator	2.609	0.0127	*COX8A, CXCL10, EIF4EBP1, GSTM3, IGFBP5, KRT14, NRARP, NT5E, PLAC8, PYGL*
EZH2	transcription regulator	2.607	0.0245	*C15orf48, CSF3, CXCL10, JDP2, LORICRIN, PTGES, S100A4, SGPL1*
APP	Other	2.462	0.0033	*ABCG1, CRABP1, CSF3, CXCL10, CXCL6, FXYD1, Gsta4, GSTM3, IGFBP5, IRF1, LMO4, PVALB, PYCARD, RNF24, TP73, TUBB4B*
TLR9	Transmembrane receptor	2.415	0.0095	*CSF3, CXCL10, CXCL6, IRF1, PYCARD, SGPL1*

Table B-4. Continued

Upstream Regulator	Biotype	z-score	*P*-value	Target molecules differentially expressed in dataset
IL1A	Cytokine	2.402	0.0147	*CSF3, CXCL10, CXCL6, IGFBP5, IRF1, PTGES*
OSM	Cytokine	2.391	0.0015	*ABCG1, CSF3, CTSL, CXCL10, CXCL6, EIF4EBP1, FAM171A1, IRF1, LORICRIN, PIGR, PTGES, PYGL*
RELA	Transcription regulator	2.388	0.0320	*ALCAM, BEX2, CXCL10, CXCL6, IRF1, PTGES, SERPINE2, TP73*
STAT3	Transcription regulator	2.386	0.0189	*BEX2, CSF3, CTSL, CXCL10, CXCL6, IFI44, IGFBP5, IRF1, NT5E, SERPINE2, TFF3, VTCN1*
TLR4	Transmembrane receptor	2.381	0.0363	*CSF3, CXCL10, CXCL6, IRF1, LMO4, PTGES, SGPL1*
FGF2	Growth factor	2.373	0.0353	*ANPEP, CSF3, CTSL, CXCL6, DUSP6, IGFBP5, MACROD1, S100A4*
IL6	Cytokine	2.244	0.0237	*ANPEP, CES1, CXCL10, CXCL6, DUSP6, Gsta4, IGFBP5, IRF1, KRT14, MACROD1, PTGES, VTCN1*
Dimethyl n-oxalyl-glycine	Chemical reagent	2.236	0.0262	*CCL28, CSRP2, EIF4EBP1, IGFBP5, PYGL*
KLF4	Transcription regulator	2.224	0.0400	*ALCAM, CCL28, EFEMP1, IRX3, KRT14, LORICRIN*
Salmonella enterica serotype abortus equi lipopolysaccharide	Chemical toxicant	2.219	0.0078	*CSF3, IRF1, KCNJ2, PLAC8, UPB1*
IRF1	Transcription regulator	2.208	0.0203	*CXCL10, GSDMD, IFI44, IRF1, PIGR*
ERBB2	Kinase	2.2	0.0074	*BCAT2, BEX2, CES1, CXCL10, CXCL6, DUSP6, EIF4EBP1, EPHX2, IGFBP5, IRX3, LMO4, NT5E, PHGDH, PLAC8, PTGES, S100A4*
IFNAR1	Transmembrane receptor	2.184	0.0038	*BATF2, CXCL10, CXCL6, DUSP6, IFI44, IRF1*
MYD88	Other	2.178	0.0391	*CSF3, CXCL10, CXCL6, IGFBP5, IRF1, PTGES*
Etoposide	Chemical drug	2.177	0.0217	*ABCG1, BATF2, CXCL10, IRF1, SVIL, TP73*
RIPK2	Kinase	2.175	0.0033	*CXCL10, CXCL6, IFI44, LMO4, PTGES*

Table B-4. Continued

Upstream Regulator	Biotype	z-score	*P*-value	Target molecules differentially expressed in dataset
VEGFA	Growth factor	2.156	0.0081	*ANPEP, BCAT2, COX8A, CSF3, CXCL10, CXCL6, IGFBP5*
EGF	Growth factor	2.155	0.0424	*ALCAM, ANPEP, CXCL6, DUSP6, FOXA2, Gsta4, IGFBP5, NT5E, PTGES, S100A4*
STING1	Ion channel	2.153	0.0126	*BATF2, C15orf48, CXCL10, IFI44, PLEKHA4*
NFKBIA	Transcription regulator	2.137	0.0006	*AZGP1, CITED4, CSF3, CXCL10, CXCL6, DUSP6, IRF1, IRX3, JDP2, PTGES, SERPINE2*
CTNNB1	Transcription regulator	2.117	0.0021	*ALCAM, CALM1, CSF3, CXCL10, CXCL6, EYA2, FOXA2, GPX2, IGFBP5, PMP22, PTCH1, S100A4, SERPINE2, SESN1, SIX1, TP73, UPB1*
CREBBP	Transcription regulator	2.116	0.0315	*CD81, CXCL10, EYA2, IRF1, KRT14, LORICRIN, SERPINE2*
RNY3	Other	2	4.08×10^{-5}	*BATF2, CXCL10, IFI44, SPATS2L*
IL17RA	Transmembrane receptor	2	0.0002	*ABCG1, CCL28, CSF3, CXCL6*
HNF1A	Transcription regulator	2	0.0020	*ANPEP, ASGR1, ASGR2, CCL28, CDO1, DUSP6, FMO1, FOXA2, GPX2, NRARP, PIGR*
Taurochenodeoxycholate	Chemical - endogenous mammalian	2	0.0023	*ANPEP, CXCL6, NT5E, SERPINE2*
Glycodeoxycholic acid	Chemical - endogenous mammalian	2	0.0024	*ANPEP, CXCL6, NT5E, SERPINE2*
Glycocholic acid	Chemical - endogenous mammalian	2	0.0025	*ANPEP, CXCL6, NT5E, SERPINE2*
5-O-mycolyl-beta-araf-(1->2)-5-O-mycolyl-alpha-araf-(1->1')-glycerol	Chemical - endogenous non-mammalian	2	0.0034	*CXCL10, NT5E, RND3, SERPINE2*

Table B-4. Continued.

Upstream Regulator	Biotype	z-score	*P*-value	Target molecules differentially expressed in dataset
Glycochenodeoxycholate	Chemical - endogenous mammalian	2	0.0040	*ANPEP, CXCL6, NT5E, SERPINE2*
DSCAM	Other	2	0.0051	*DAB1, KCNJ2, NEURL1B, ROR2*
Taurocholic acid	Chemical - endogenous mammalian	2	0.0072	*ANPEP, CXCL6, NT5E ,SERPINE2*
Mir-802	MicroRNA	2	0.0227	*CCDC68, FMO1, KRT23, PPP1R1B*
N6AMT1	Enzyme	2	0.0280	*ADRA2A, CDO1, FAM171A1, NFIA*
EBF1	Transcription regulator	2	0.0359	*CRABP1, CXCL10, EIF4EBP1, IRF1*
Concanavalin a	Chemical drug	1.999	0.0177	*CSF3, CXCL10, IRF1, TP73*
MAP3K7	Kinase	1.988	0.0029	*CXCL10, CXCL6, IFI44, IRF1*
E. coli B4 lipopolysaccharide	Chemical toxicant	1.98	0.0050	*ADCY7, CSF3, CXCL10, CXCL6, PPP1R1B, PTGES, PYCARD*
CASP4	Peptidase	1.969	0.0003	*CXCL6, GSDMD, PGLYRP1, PLAC8*
FOSL1	Transcription regulator	1.969	0.0047	*CSF3, CXCL6, NT5E, SERPINE2*
MEF2A	Transcription regulator	1.966	0.0034	*CXCL10, Gsta4, IFI44, IRF1*
Pyridostatin	Chemical reagent	1.961	0.0016	*BATF2, CXCL10, IFI44, IRF1*
IL2	Cytokine	1.949	0.0118	*CSF3, CTSL, CXCL10, DUSP6, IRF1, NEURL1B, NT5E, PHGDH, PLAC8, PTCH1, S100A4, SESN1*
IRF7	Transcription regulator	1.916	0.0386	*CXCL10, IFI44, IRF1, PLAC8*
PRL	Cytokine	1.82	0.0116	*CXCL10, GSTM1, IFI44, IGFBP5, IRF1, KRT14, PC*
Hydrogen peroxide	Chemical - endogenous mammalian	1.813	0.0383	*CD81, CSF3, CXCL6, Gsta4, GSTM3, ROR2, RUNX3, SESN1, TP73*

Table B-4. Continued

Upstream Regulator	Biotype	z-score	*P*-value	Target molecules differentially expressed in dataset
Interferon alpha	Group	1.784	0.0001	*BATF2, CD81, CES1, COX7A1, CXCL10, DUSP6, EIF4EBP1, FMO3, GSTM3, IFI44, IRF1, NT5E, PTGES, SEC14L3*
Doxorubicin	Chemical drug	1.758	0.0238	*CXCL10, CXCL6, GPX2, GSTM3, IRF1, LPIN1, NT5E, SESN1, SVIL, TP73*
IKBKE	Kinase	1.746	4.83×10^{-6}	*CSF3, CXCL10, CXCL6, FOXA2, PHGDH, PTCH1, PYGL*
Growth hormone	Group	1.741	0.0101	*FOXA2, GSTM1, IGFBP5, IRF1, S100A4, TFF3*
TLR3	Transmembrane receptor	1.725	0.0494	*CSF3, CXCL10, IFI44, IRF1, PTGES*
Peptidoglycan	Chemical - endogenous non-mammalian	1.715	0.0087	*CSF3, CXCL10, CXCL6, IRF1*
ZBTB16	Transcription regulator	1.71	0.0226	*CD81, CXCL10, EYA2, LMO4, RUNX3*
IGF1	Growth factor	1.682	0.0361	*ANPEP, ASGR2, CGNL1, CXCL6, DUSP6, IGFBP5, JDP2, PDLIM2, PPP1R1B*
Norepinephrine	Chemical - endogenous mammalian	1.673	0.0020	*CITED4, GMNN, PIGR, PTCH1, PTGES, WHRN*
CD40	Transmembrane receptor	1.651	0.0317	*ANPEP, COX8A, CSF3, CXCL10, DUSP6, IRF1*
MYC	Transcription regulator	1.617	0.0006	*ABCG1, ALCAM, CSRP2, CXCL10, DUSP6, EFEMP1, EIF4EBP1, FOXA2, FXYD1, IFI44, IRX3, JDP2, KRT14, LORICRIN, MTBP, PLAC8, PMP22, SCEL, SERPINE2, SLC16A7, SLC22A4, TP73*
AHR	Ligand-dependent nuclear receptor	1.592	3.77×10^{-5}	*CDO1, COX8A, CXCL10, DUSP6, EFEMP1, EPHX2, FMO3, FOXA2, GPX2, IRF1, NT5E, PMP22, PTGES, TFF3, TP73*

Table B-4. Continued

Upstream Regulator	Biotype	z-score	*P*-value	Target molecules differentially expressed in dataset
ATF4	Transcription regulator	1.588	0.0193	*EIF4EBP1, IGFBP5, PHGDH, PMP22, TFF3*
STAT4	Transcription regulator	1.561	0.0015	*CXCL10, IRF1, LPIN1, PLAC8, PYGL, S100A4, SELENBP1*
IL17A	Cytokine	1.502	0.0469	*C15orf48, CSF3, CXCL10, CXCL6, FMO1, IRF1*
Paclitaxel	Chemical drug	1.478	0.0038	*CXCL10, CXCL6, DUSP6, FMO3, NT5E, PHGDH, SVIL, TP73*
NFE2L2	Transcription regulator	1.468	0.0096	*COX7A1, CXCL10, CXCL6, FMO1, FXYD1, GPX2, Gsta4, GSTM1, PHGDH, PTCH1*
HRAS	Enzyme	1.463	0.0002	*ADRA2A, CD81, CHST12, CSF3, CSRP2, CXCL10, DUSP6, EFEMP1, EIF4EBP1, IGFBP5, IRX3, S100A4, SERPINE2, SESN1, TP73*
FOXA2	Transcription regulator	1.446	0.0459	*ABCG1, FOXA2, GPX2, GSTM3, IGFBP5, PYGL, TUBB4B*
RAF1	Kinase	1.408	0.0011	*CTSL, DUSP6, FAM171A1, PC, RND3, SELENBP1, SLC16A7*
CD38	Enzyme	1.408	0.0014	*CHST12, EIF4EBP1, NT5E, S100A4, SCEL, UPB1*
MYOD1	Transcription regulator	1.408	0.0378	*ADCY7, CDO1, IGFBP5, MYMK, SIX1*
SERPINE1	Other	1.406	0.0009	*CES1, CSF3, CXCL10, CXCL6, DUSP6*
IRF2	Transcription regulator	1.387	0.0034	*CES1, CXCL10, FCGBP, GSDMD, IRF1*
TYK2	Kinase	1.387	0.0117	*CSF3, CXCL10, IFI44, IRF1*
AR	Ligand-dependent nuclear receptor	1.362	1.79×10^{-5}	*ABCG1, ARMCX2, AZGP1, CDO1, CITED4, COX8A, GDAP1, GSTM1, IGFBP5, KCNJ2, KRT14, LRATD1, PIGR, PTCH1, PVALB, SCEL, SLC22A4, TFF3*
ESRRA	Transcription regulator	1.342	0.0022	*CCL28, CSF3, CSRP2, CXCL10, KRT23, PDLIM2, PPP1R1B, PTPRM*

Table B-4. Continued

Upstream Regulator	Biotype	z-score	*P*-value	Target molecules differentially expressed in dataset
RBPJ	Transcription regulator	1.342	0.0105	*ABCG1, CSF3, CXCL10, CXCL6, PLAC8, RUNX3*
Budesonide	Chemical drug	1.342	0.0286	*CGNL1, CSF3, CXCL10, ETNK2, LPIN1, SERPINE2*
BCOR	Transcription regulator	-1.342	4.07×10^{-5}	*FOXA2, IGFBP5, LMO4, PTCH1, ZNF503*
INSIG1	Other	-1.342	0.0014	*ABCG1, CXCL10, CXCL6, LPIN1, PTGES*
Trans-hydroxytamoxifen	Chemical drug	-1.342	0.0103	*CTSL, PTPRM, PVALB, RND3, SELENBP1*
CEBPA	Transcription regulator	-1.342	0.0225	*ADCY7, ANPEP, CSF3, FOXA2, KRT14, LORICRIN, RARRES2, RUNX3*
ALOX5	Enzyme	-1.414	0.0089	*ETNK2, FOXA2, IFI44, NPL, PLAC8, PVALB, S100A4, SELENBP1*
PD98059	Chemical - kinase inhibitor	-1.516	0.0015	*ANPEP, BATF2, CTSL, CXCL10, DUSP6, FAM171A1, PC, PTGES, S100A4, SELENBP1, SLC16A7, TP73*
SIRT1	Transcription regulator	-1.633	0.0222	*ABCG1, CD81, GSTM1, GSTM3, IFI44, NT5E, PC, TP73*
SB203580	Chemical drug	-1.651	0.0314	*CXCL10, EFEMP1, Gsta4, IRF1, KRT23, LORICRIN, PTGES, TCHH*
MAP3K8	Kinase	-1.664	0.0011	*ADCY7, CSF3, DUSP6, SESN1, SIX1, SPATS2L*
GLI1	Transcription regulator	-1.915	0.0026	*ABCG1, DUSP6, ELAVL2, FOXA2, JDP2, MALL, NEURL1B, PTCH1, S100A4, SELENBP1, SESN1*
SOCS1	Other	-1.941	0.0204	*CSF3, CXCL10, IFI44, IRF1*
MCC950	Chemical reagent	-1.964	0.0004	*CXCL10, CXCL6, GSDMD, PYCARD*
TRIM24	Transcription regulator	-1.964	0.0095	*CXCL10, IFI44, IRF1, PLAC8*

Table B-4. Continued

Upstream Regulator	Biotype	z-score	*P*-value	Target molecules differentially expressed in dataset
Irgm1	Enzyme	-1.982	0.0061	*CXCL10, GSDMD, IFI44, IRF1*
GSR	Enzyme	-2	0.0002	*GPX2, Gsta4, GSTM1, LPIN1*
TXNRD1	Enzyme	-2	0.0003	*GPX2, Gsta4, GSTM1, LPIN1*
Ttc39aos1	Other	-2	0.0012	*CXCL10, IFI44, IRF1, PYCARD*
RXRB	Ligand-dependent nuclear receptor	-2	0.0022	*CXCL10, GSTM1, LDHD, MATN4, PMP22, S100A4*
Colistin	Biologic drug	-2	0.0082	*ALCAM, IGFBP5, NAV2, PTPRM*
MiR-3648 (miRNAs w/seed GCCGCGG)	Mature microRNA	-2	0.0084	*CITED4, LYPD3, NRARP, SSBP4*
Kanamycin A	Chemical drug	-2	0.0087	*ALCAM, IGFBP5, NAV2, PTPRM*
Metronidazole	Chemical drug	-2	0.0120	*ALCAM, IGFBP5, NAV2, PTPRM*
CBX5	Transcription regulator	-2	0.0149	*C15orf48, SELENBP1, TCEAL1, TFF3*
RNASEH2B	Other	-2.219	0.0002	*CTSL, CXCL10, GSDMD, IFI44, IRF1, PYCARD*
TSC2	Other	-2.219	0.0080	*CXCL10, IFI44, IGFBP5, PDLIM2, PVALB*
EGLN	Group	-2.236	0.0066	*CCL28, CSRP2, EIF4EBP1, PYGL, SELENBP1*
SP600125	Chemical drug	-2.357	0.0475	*CHST12, CSF3, CXCL10, CXCL6, PTGES, SGPL1*
CITED2	Transcription regulator	-2.401	0.0063	*ARMCX6, C15orf48, CXCL10, IFI44, IRF1, PLAC8*
LY294002	Chemical drug	-2.884	0.0011	*ANPEP, CSF3, CXCL10, CXCL6, DUSP6, GMNN, Gsta4, GSTM3, IGFBP5, IRF1, LMO4, RND3*

LIST OF REFERENCES

Abdulrahman, N. and T. Fair. 2019. Contribution of the immune system to follicle differentiation, ovulation and early corpus luteum formation. Anim. Reprod. 16:440-448.

Abedel-Majed, M. A., S. M. Romereim, J. S. Davis, and A. S. Cupp. 2019. Perturbations in lineage specification of granulosa and theca cells may alter corpus luteum formation and function. Front. Endocrinol. 10:832.

Aerts, J. and P. Bols. 2010. Ovarian follicular dynamics: a review with emphasis on the bovine species. Part I: Folliculogenesis and pre-antral follicle development. Reprod. Dom. Anim. 45(1):171-179.

Ali, A., K. Coenen, D. Bousquet, and M.-A. Sirard. 2004. Origin of bovine follicular fluid and its effect during in vitro maturation on the developmental competence of bovine oocytes. Theriogenology 62(9):1596-1606.

Alila, H., R. Corradino, and W. Hansel. 1989. Differential effects of luteinizing hormone on intracellular free Ca2+ in small and large bovine luteal cells. Endocrinology. 124(5):2314-2320.

Amaral, T. F., J. G. V. de Grazia, L. A. G. Martinhao, F. De Col, L. G. B. Siqueira, J. H. M. Viana, and P. J. Hansen. 2022. Actions of CSF2 and DKK1 on bovine embryo development and pregnancy outcomes are affected by composition of embryo culture medium. Sci. Rep. 12(1):7503.

Amos, M. R., G. D. Healey, R. J. Goldstone, S. M. Mahan, A. Düvel, H. J. Schuberth, O. Sandra, P. Zieger, I. Dieuzy-Labaye, D. G. Smith, and I. M. Sheldon. 2014. Differential endometrial cell sensitivity to a cholesterol-dependent cytolysin links Trueperella pyogenes to uterine disease in cattle. Biol. Reprod. 90(3):54.

Amstalden, M., R. Cardoso, B. Alves, and G. Williams. 2014. Reproduction Symposium: Hypothalamic neuropeptides and the nutritional programming of puberty in heifers. J Anim. Sci. 92(8):3211-3222.

Anderson, D., R. E. Billingham, G. H. Lampkin, and P. B. Medawar. 1951. The use of skin grafting to distinguish between monozygotic and dizygotic twins in cattle. Heredity 5(3):379-397.

Arosh, J. A., J. Parent, P. Chapdelaine, J. Sirois, and M. A. Fortier. 2002. Expression of cyclooxygenases 1 and 2 and prostaglandin E synthase in bovine endometrial tissue during the estrous cycle. Biol. Reprod. 67(1):161-169.

Asaf, S., G. Leitner, O. Furman, Y. Lavon, D. Kalo, D. Wolfenson, and Z. Roth. 2014. Effects of Escherichia coli-and Staphylococcus aureus-induced mastitis in lactating cows on oocyte developmental competence. Reproduction. 147(1):33-43.

Ashworth, C. J. and F. W. Bazer. 1989. Changes in ovine conceptus and endometrial function following asynchronus embryo transfer or administration of progesterone. Biol. Reprod. 40(2):425-433.

Atli, M. O., M. Kose, M. Hitit, M. S. Kaya, and F. Bozkaya. 2018. Expression patterns of Toll-like receptors in the ovine corpus luteum during the early pregnancy and prostaglandin F2α-induced luteolysis. Theriogenology. 111:25-33.

Badinga, L., R. J. Collier, W. W. Thatcher, and C. J. Wilcox. 1985. Effects of climatic and management factors on conception rate of dairy cattle in subtropical environment. J Dairy Sci. 68(1):78-85.

Badinga, L., W. Thatcher, T. Diaz, M. Drost, and D. Wolfenson. 1993. Effect of environmental heat stress on follicular development and steroidogenesis in lactating Holstein cows. Theriogenology 39(4):797-810.

Badinga, L., W. Thatcher, C. Wilcox, G. Morris, K. Entwistle, and D. Wolfenson. 1994. Effect of season on follicular dynamics and plasma concentrations of estradiol-17β, progesterone and luteinizing hormone in lactating Holstein cows. Theriogenology 42(8):1263-1274.

Bakos, H. W., M. Mitchell, B. P. Setchell, and M. Lane. 2011. The effect of paternal diet-induced obesity on sperm function and fertilization in a mouse model. Int. J Androl. 34(5 Pt 1):402-410.

Bao, B. and H. A. Garverick. 1998. Expression of steroidogenic enzyme and gonadotropin receptor genes in bovine follicles during ovarian follicular waves: a review. J Anim. Sci. 76(7):1903-1921.

Bartol, F., R. Roberts, F. Bazer, G. Lewis, J. Godkin, and W. Thatcher. 1985. Characterization of proteins produced in vitro by periattachment bovine conceptuses. Biol. Reprod. 32(3):681-693.

Battaglia, D. F., J. M. Bowen, H. B. Krasa, L. A. Thrun, C. Viguié, and F. J. Karsch. 1997. Endotoxin inhibits the reproductive neuroendocrine axis while stimulating adrenal steroids: a simultaneous view from hypophyseal portal and peripheral blood. Endocrinol. 138(10):4273-4281.

Battaglia, D. F., H. B. Krasa, V. Padmanabhan, C. Viguié, and F. J. Karsch. 2000. Endocrine alterations that underlie endotoxin-induced disruption of the follicular phase in ewes. Biol. Reprod. 62(1):45-53.

Bauersachs, S., S. E. Ulbrich, V. Zakhartchenko, M. Minten, M. Reichenbach, H.-D. Reichenbach, H. Blum, T. E. Spencer, and E. Wolf. 2009. The endometrium responds differently to cloned versus fertilized embryos. Proc. Nat. Acad. Sci. 106(14):5681-5686.

Biggers, B. G., R. Geisert, R. Wetteman, and D. Buchanan. 1987. Effect of heat stress on early embryonic development in the beef cow. J Anim. Sci. 64(5):1512-1518.

Bishop, C. V., V. Selvaraj, D. H. Townson, J. L. Pate, and M. C. Wiltbank. 2022. History, insights, and future perspectives on studies into luteal function in cattle. J Anim. Sci. 100(7):skac143.

Bisinotto, R., L. Greco, E. Ribeiro, N. Martinez, F. Lima, C. Staples, W. Thatcher, and J. Santos. 2018. Influences of nutrition and metabolism on fertility of dairy cows. Anim. Reprod. 9(3):260-272.

Bisinotto, R., E. Ribeiro, L. Martins, R. Marsola, L. Greco, M. Favoreto, C. Risco, W. Thatcher, and J. Santos. 2010. Effect of interval between induction of ovulation and artificial insemination (AI) and supplemental progesterone for resynchronization on fertility of dairy cows subjected to a 5-d timed AI program. J Dairy Sci. 93(12):5798-5808.

Boivin, J., L. Bunting, J. A. Collins, and K. G. Nygren. 2007. International estimates of infertility prevalence and treatment-seeking: potential need and demand for infertility medical care. Hum. Reprod. 22(6):1506-1512.

Bondurant, R. 1999. Inflammation in the bovine female reproductive tract. J Anim. Sci. 77(suppl_2):101-110.

Bonnett, B. N., S. W. Martin, and A. H. Meek. 1993. Associations of clinical findings, bacteriological and histological results of endometrial biopsy with reproductive performance of postpartum dairy cows. Prev. Vet. Med. 15(2-3):205-220.

Borsberry, S. and H. Dobson. 1989. Periparturient diseases and their effect on reproductive performance in five dairy herds. Vet. Rec. 124(9):217-219.

Box, G. E. and D. R. Cox. 1964. An analysis of transformations. J Roy. Stat. Soc. Ser. B: Stat. Method. 26(2):211-243.

Brannstrom, M., V. Pascoe, R. J. Norman, and N. McClure. 1994. Localization of leukocyte subsets in the follicle wall and in the corpus luteum throughout the human menstrual cycle. Fert. Steril. 61(3):488-495.

Britt, J. H. 1985. Enhanced reproduction and its economic implications. J Dairy Sci. 68(6):1585-1592.

Britt, J. H. 2008. Oocyte development in cattle: physiological and genetic aspects. Rev. Brasil. Zoot. 37:110-115.

Bromfield, J. J., J. E. Santos, J. Block, R. S. Williams, and I. M. Sheldon. 2015. Physiology and Endocrinology Symposium: Uterine infection: linking infection and innate immunity with infertility in the high-producing dairy cow. J Anim. Sci. 93(5):2021-2033.

Bromfield, J. J. and I. M. Sheldon. 2011. Lipopolysaccharide initiates inflammation in bovine granulosa cells via the TLR4 pathway and perturbs oocyte meiotic progression in vitro. Endocrinology 152(12):5029-5040.

Bromfield, J. J. and I. M. Sheldon. 2013. Lipopolysaccharide reduces the primordial follicle pool in the bovine ovarian cortex ex vivo and in the murine ovary in vivo. Biol. Reprod. 88(4):98, 91-99.

Bruinjé, T., E. Morrison, E. Ribeiro, D. Renaud, and S. LeBlanc. 2023. Associations of postpartum health with progesterone after insemination and endocrine signaling during early pregnancy in dairy cows. J Dairy Sci.

Budipitojo, T., M. Sasaki, S. Matsuzaki, M. B. C. Cruzana, T. Iwanaga, N. Kitamura, and J. Yamada. 2003. Expression of gastrin-releasing peptide (GRP) in the bovine uterus during the estrous cycle. Arch. Histol. Cytol. 66(4):337-346.

Bustin, S. A., V. Benes, J. A. Garson, J. Hellemans, J. Huggett, M. Kubista, R. Mueller, T. Nolan, M. W. Pfaffl, G. L. Shipley, J. Vandesompele, and C. T. Wittwer. 2009. The MIQE guidelines: minimum information for publication of quantitative real-time PCR experiments. Clin. Chem. 55(4):611-622.

Cannon, M. J., M. G. Petroff, and J. L. Pate. 2003. Effects of prostaglandin F2α and progesterone on the ability of bovine luteal cells to stimulate T lymphocyte proliferation. Biol. Reprod. 69(2):695-700.

Cardoso, D. and E. Perucha. 2021. Cholesterol metabolism: a new molecular switch to control inflammation. Clin.Sci. 135(11):1389-1408.

Care, A. S., W. V. Ingman, L. M. Moldenhauer, M. J. Jasper, and S. A. Robertson. 2014. Ovarian steroid hormone-regulated uterine remodeling occurs independently of macrophages in mice. Biol. Reprod. 91(3):60, 61-12.

Carroll, D. J., R. R. Grummer, and M. K. Clayton. 1992a. Stimulation of luteal cell progesterone production by lipoproteins from cows fed control or fat-supplemented diets. J Dairy Sci. 75(8):2205-2214.

Carroll, D. J., R. R. Grummer, and F. C. Mao. 1992b. Progesterone production by cultured luteal cells in the presence of bovine low-and high-density lipoproteins purified by heparin affinity chromatography. J Anim. Sci. 70(8):2516-2526.

Carvalho, M., F. Peñagaricano, J. Santos, T. DeVries, B. McBride, and E. Ribeiro. 2019. Long-term effects of postpartum clinical disease on milk production, reproduction, and culling of dairy cows. J Dairy Sci. 102(12):11701-11717.

Cerri, R., I. Thompson, I. Kim, A. Ealy, P. Hansen, C. Staples, J. Li, J. Santos, and W. Thatcher. 2012. Effects of lactation and pregnancy on gene expression of endometrium of Holstein cows at day 17 of the estrous cycle or pregnancy. J Dairy Sci. 95(10):5657-5675.

Chandrappa, S. M., O. B. Pascottini, G. Opsomer, G. Meineri, N. A. Martino, P. Banchi, L. Vincenti, and A. Ricci. 2023. Circulating and endometrial cell oxidative stress in dairy cows diagnosed with metritis. Theriogenology 198:217-223.

Channing, C. P. and T. M. Crisp. 1972. Comparative aspects of luteinization of granulosa cell cultures at the biochemical and ultrastructural levels. Gen. Comp. Endocrinol. 3:617-625.

Chapwanya, A., K. G. Meade, C. Foley, F. Narciandi, A. C. Evans, M. L. Doherty, J. J. Callanan, and C. O'Farrelly. 2012. The postpartum endometrial inflammatory response: a normal physiological event with potential implications for bovine fertility. Reprod. Fert. Dev. 24(8):1028-1039.

Chenault, J., W. Thatcher, P. Kalra, R. Abrams, and C. Wilcox. 1975. Transitory changes in plasma progestins, estradiol, and luteinizing hormone approaching ovulation in the bovine. J Dairy Sci. 58(5):709-717.

Chenault, J. R., J. F. McAllister, S. T. Chester, K. J. Dame, F. M. Kausche, and E. J. Robb. 2004. Efficacy of ceftiofur hydrochloride sterile suspension administered parenterally for the treatment of acute postpartum metritis in dairy cows. J Am. Vet. Med. Ass. 224(10):1634-1639.

Cherradi, N., G. Defaye, and E. Chambaz. 1994. Characterization of the 3 beta-hydroxysteroid dehydrogenase activity associated with bovine adrenocortical mitochondria. Endocrinology 134(3):1358-1364.

Chirivi, M., C. J. Rendon, M. N. Myers, C. M. Prom, S. Roy, A. Sen, A. L. Lock, and G. A. Contreras. 2022. Lipopolysaccharide induces lipolysis and insulin resistance in adipose tissue from dairy cows. J Dairy Sci. 105(1):842-855.

Cordle, S. R., R. J. Colbran, and S. J. Yeaman. 1986. Purification of hormone-sensitive lipase from bovine adipose tissue. Port. Press

Coulter, G. H., R. B. Cook, and J. P. Kastelic. 1997. Effects of dietary energy on scrotal surface temperature, seminal quality, and sperm production in young beef bulls. J Anim. Sci. 75(4):1048-1052.

Coulter, G. H. and G. C. Kozub. 1984. Testicular development, epididymal sperm reserves and seminal quality in two-year-old Hereford and Angus bulls: effects of two levels of dietary energy. J Anim. Sci. 59(2):432-440.

Cronin, J. G., M. L. Turner, L. Goetze, C. E. Bryant, and I. M. Sheldon. 2012. Toll-like receptor 4 and MYD88-dependent signaling mechanisms of the innate immune system are essential for the response to lipopolysaccharide by epithelial and stromal cells of the bovine endometrium. Biol. Reprod. 86(2):51.

Cui, L., J. Guo, Z. Wang, J. Zhang, W. Li, J. Dong, K. Liu, L. Guo, J. Li, and H. Wang. 2023. Meloxicam inhibited oxidative stress and inflammatory response of LPS-stimulated bovine endometrial epithelial cells through Nrf2 and NF-κB pathways. Int. Immunopharm. 116:109822.

Daetz, R., F. Cunha, J. Bittar, C. Risco, F. Magalhaes, Y. Maeda, J. Santos, K. Jeong, R. Cooke, and K. Galvão. 2016. Clinical response after chitosan microparticle administration and preliminary assessment of efficacy in preventing metritis in lactating dairy cows. J Dairy Sci. 99(11):8946-8955.

Dance, A., J. Thundathil, R. Wilde, P. Blondin, and J. Kastelic. 2015. Enhanced early-life nutrition promotes hormone production and reproductive development in Holstein bulls. J Dairy Sci. 98(2):987-998.

Davies, D., K. G. Meade, S. Herath, P. D. Eckersall, D. Gonzalez, J. O. White, R. S. Conlan, C. O'Farrelly, and I. M. Sheldon. 2008. Toll-like receptor and antimicrobial peptide expression in the bovine endometrium. Reprod. Biol. Endocrinol. 6(1):1-12.

Davis, J. S. and H. A. LaVoie. 2019. Molecular regulation of progesterone production in the corpus luteum. Pages 237-253 in The ovary. Elsevier.

Day, M., K. Imakawa, M. Garcia-Winder, D. Zalesky, B. Schanbacher, R. J. Kittok, and J. Kinder. 1984. Endocrine mechanisms of puberty in heifers: estradiol negative feedback regulation of luteinizing hormone secretion. Biol. Reprod. 31(2):332-341.

De Kruif, A. 1978. Factors influencing the fertility of a cattle population. Reproduction 54(2):507-518.

de Oliveira, E., F. Cunha, R. Daetz, C. Figueiredo, R. Chebel, J. Santos, C. Risco, K. Jeong, V. Machado, and K. Galvão. 2020. Using chitosan microparticles to treat metritis in lactating dairy cows. J Dairy Sci. 103(8):7377-7391.

De Vries, A. 2006. Economic value of pregnancy in dairy cattle. J Dairy Sci. 89(10):3876-3885.

Dhaliwal, G., R. Murray, and Z. Woldehiwet. 2001. Some aspects of immunology of the bovine uterus related to treatments for endometritis. Anim. Reprod. Sci. 67(3-4):135-152.

Dickson, M. J., J. V. Bishop, T. R. Hansen, I. M. Sheldon, and J. J. Bromfield. 2022a. The endometrial transcriptomic response to pregnancy is altered in cows after uterine infection. PLoS One 17(3):e0265062.

Dickson, M. J., R. L. Piersanti, R. Ramirez-Hernandez, E. B. de Oliveira, J. V. Bishop, T. R. Hansen, Z. Ma, K. C. C. Jeong, J. E. P. Santos, M. I. Sheldon, J. Block, and J. J. Bromfield. 2020. Experimentally Induced Endometritis Impairs the Developmental Capacity of Bovine Oocytes. Biol. Reprod. 103(3):508-520.

Dickson, M. J., I. M. Sheldon, and J. J. Bromfield. 2022b. Lipopolysaccharide alters CEBPβ signaling and reduces estradiol production in bovine granulosa cells. CABI Ag. Biosci. 3(1):66.

Dieleman, S., T. A. Kruip, P. Fontijne, W. De Jong, and G. Van der Weyden. 1983. Changes in oestradiol, progesterone and testosterone concentrations in follicular fluid and in the micromorphology of preovulatory bovine follicles relative to the peak of luteinizing hormone. J Endocrinol. 97(1):31-NP.

Ding, S., M. M. Chi, B. P. Scull, R. Rigby, N. M. Schwerbrock, S. Magness, C. Jobin, and P. K. Lund. 2010. High-fat diet: bacteria interactions promote intestinal inflammation which precedes and correlates with obesity and insulin resistance in mouse. PloS One 5(8):e12191.

Duan, Y., L. Zeng, C. Zheng, B. Song, F. Li, X. Kong, and K. Xu. 2018. Inflammatory links between high fat diets and diseases. Front. Immunol. 9:2649.

Duffy, J. M. N., G. D. Adamson, E. Benson, S. Bhattacharya, M. Bofill, K. Brian, B. Collura, C. Curtis, J. L. H. Evers, R. G. Farquharson, A. Fincham, S. Franik, L. C. Giudice, E. Glanville, M. Hickey, A. W. Horne, M. L. Hull, N. P. Johnson, V. Jordan, Y. Khalaf, J. M. L. Knijnenburg, R. S. Legro, S. Lensen, J. MacKenzie, D. Mavrelos, B. W. Mol, D. E. Morbeck, H. Nagels, E. H. Y. Ng, C. Niederberger, A. S. Otter, L. Puscasiu, S. Rautakallio-Hokkanen, L. Sadler, I. Sarris, M. Showell, J. Stewart, A. Strandell, C. Strawbridge, A. Vail, M. van Wely, M. Vercoe, N. L. Vuong, A. Y. Wang, R. Wang, J. Wilkinson, K. Wong, T. Y. Wong, C. M. Farquhar, and P. S. P. f. Infertility. 2021. Top 10 priorities for future infertility research: an international consensus development study. Fertil. Steril. 115(1):180-190.

Ealy, A. D., M. Drost, and P. J. Hansen. 1993. Developmental changes in embryonic resistance to adverse effects of maternal heat stress in cows. J Dairy Sci. 76(10):2899-2905.

Ealy, A. D. and L. K. Wooldridge. 2017. The evolution of interferon-tau. Reproduction 154(5):F1-F10.

Ebner, K. E. 1971. Biosynthesis of lactose. J Dairy Sci. 54(8):1229-1233.

Elliott, L., K. McMahon, H. Gier, and G. Marion. 1968. Uterus of the cow after parturition: bacterial content. Am. J Vet. Res. 29(1):77-81.

Ellsworth, L. R. and D. T. Armstrong. 1973. Luteinization of transplanted ovarian follicles in the rat induced by dibutyryl cyclic AMP. Endocrinology 92(3):840-846.

Erickson, B.H. 1966 Development and senescence of the postnatal bovine ovary. J. Anim. Sci. 25:800-805.

Escandón, B. M., J. S. Espinoza, F. P. Perea, F. Quito, R. Ochoa, G. E. López, D. A. Galarza, and J. P. Garzón. 2020. Intrauterine therapy with ozone reduces subclinical endometritis and improves reproductive performance in postpartum dairy cows managed in pasture-based systems. Trop. Anim. Heal. Prod. 52:2523-2528.

Espey, L. L. 1980. Ovulation as an inflammatory reaction—a hypothesis. Biol.Reprod. 22(1):73-106.

Fair, T. 2015. The contribution of the maternal immune system to the establishment of pregnancy in cattle. Front. Immunol. 6:7.

Fairchild, D. and J. Pate. 1989. Interferon-γ induction of major histocompatibility complex antigens on cultured bovine luteal cells. Biol. Reprod. 40(3):453-457.

Farin, C., T. Nett, and G. Niswender. 1990. Effects of luteinizing hormone on luteal cell populations in hypophysectomized ewes. Reproduction 88(1):61-70.

Farkash, Y., R. Timberg, and J. Orly. 1986. Preparation of antiserum to rat cytochrome P-450 cholesterol side chain cleavage, and its use for ultrastructural localization of the immunoreactive enzyme by protein A-gold technique. Endocrinology 118(4):1353-1365.

Faust, J., M. Brown, and J. Goldstein. 1980. Synthesis of delta 2-isopentenyl tRNA from mevalonate in cultured human fibroblasts. J Biol. Chem. 255(14):6546-6548.

Fields, M. and P. Fields. 1996. Morphological characteristics of the bovine corpus luteum during the estrous cycle and pregnancy. Theriogenology 45(7):1295-1325.

Fields, M. J., C. M. Barros, W. B. Watkins, and P. A. Fields. 1992. Characterization of large luteal cells and their secretory granules during the estrous cycle of the cow. Biol. Reprod. 46(4):535-545.

Forde, N., T. E. Spencer, F. W. Bazer, G. Song, J. F. Roche, and P. Lonergan. 2010. Effect of pregnancy and progesterone concentration on expression of genes encoding for transporters or secreted proteins in the bovine endometrium. Phys. Genom. 41(1):53-62.

Fortune, J. 1986. Bovine theca and granulosa cells interact to promote androgen production. Biol. Reprod. 35(2):292-299.

Fortune, J. and S. Quirk. 1988. Regulation of steroidogenesis in bovine preovulatory follicles. J Anim. Sci. 66(suppl_2):1-8.

Freick, M., A. Kunze, O. Passarge, J. Weber, and S. Geidel. 2017. Metritis vaccination in Holstein dairy heifers using a herd-specific multivalent vaccine–Effects on uterine health and fertility in first lactation. Anim. Reprod. Sci. 184:160-171.

Fujimoto, T. and R. G. Parton. 2011. Not just fat: the structure and function of the lipid droplet. Persp. Biol. 3(3):a004838.

Fullston, T., E. M. C. O. Teague, N. O. Palmer, M. J. DeBlasio, M. Mitchell, M. Corbett, C. G. Print, J. A. Owens, and M. Lane. 2013. Paternal obesity initiates metabolic disturbances in two generations of mice with incomplete penetrance to the F2 generation and alters the transcriptional profile of testis and sperm microRNA content. FASEB J 27(10):4226-4243.

Földi, J., M. Kulcsar, A. Pecsi, B. Huyghe, C. De Sa, J. Lohuis, P. Cox, and G. Huszenicza. 2006. Bacterial complications of postpartum uterine involution in cattle. Anim. Reprod. Sci. 96(3-4):265-281.

Gadsby, J., A. Tyson Nipper, H. Faircloth, M. D'Annibale-Tolhurst, J. Chang, P. Farin, I. Sheldon, and D. Poole. 2017. Toll-like receptor and related cytokine mRNA expression in bovine corpora lutea during the oestrous cycle and pregnancy. Reprod. Dom. Anim. 52(3):495-504.

Gallagher, J. and L. Ball. 1980. Effect of infusion of uterine purulent exudate into the bovine uterus. Theriogenology 13(5):311-320.

Galvão, K. N., R. C. Bicalho, and S. J. Jeon. 2019. Symposium review: The uterine microbiome associated with the development of uterine disease in dairy cows. J Dairy Sci. 102(12):11786-11797.

Garrett, J., R. Geisert, M. Zavy, and G. Morgan. 1988. Evidence for maternal regulation of early conceptus growth and development in beef cattle. Reproduction 84(2):437-446.

Geisert, R., M. Zavy, and B. Biggers. 1988. Effect of heat stress on conceptus and uterine secretion in the bovine. Theriogenology 29(5):1075-1082.

Geisert, R. D., G. A. Johnson, and R. C. Burghardt. 2015. Implantation and establishment of pregnancy in the pig. Regulation of Implantation and Establishment of Pregnancy in Mammals: Tribute to 45 Year Anniversary of Roger V. Short's" Maternal Recognition of Pregnancy" pages 137-163.

Ghanayem, B. I., R. Bai, G. E. Kissling, G. Travlos, and U. Hoffler. 2010. Diet-induced obesity in male mice is associated with reduced fertility and potentiation of acrylamide-induced reproductive toxicity. Biol. Reprod. 82(1):96-104.

Gilbert, I., C. Robert, S. Dieleman, P. Blondin, and M.-A. Sirard. 2011. Transcriptional effect of the LH surge in bovine granulosa cells during the peri-ovulation period. Reproduction 141(2):193-205.

Gilbert, R. O. and N. R. Santos. 2016. Dynamics of postpartum endometrial cytology and bacteriology and their relationship to fertility in dairy cows. Theriogenology 85(8):1367-1374.

Godkin, J., F. Bazer, J. Moffatt, F. Sessions, and R. Roberts. 1982. Purification and properties of a major, low molecular weight protein released by the trophoblast of sheep blastocysts at day 13–21. Reproduction 65(1):141-150.

Goldstone, R. J., M. Amos, R. Talbot, H.-J. Schuberth, O. Sandra, I. M. Sheldon, and D. G. Smith. 2014a. Draft genome sequence of Trueperella pyogenes, isolated from the infected uterus of a postpartum cow with metritis. Gen. An. 2(2):10.1128/genomea. 00194-00114.

Goldstone, R. J., R. Talbot, H.-J. Schuberth, O. Sandra, I. M. Sheldon, and D. G. Smith. 2014b. Draft genome sequence of Escherichia coli MS499, isolated from the infected uterus of a postpartum cow with metritis. Gen. An. 2(4):10.1128/genomea. 00217-00214.

Grant, E., S. Lilly, S. Herath, and I. Sheldon. 2007. Escherichia coli lipopolysaccharide modulates bovine luteal cell function. Vet. Rec. 161(20):695.

Gray, C. A., C. A. Abbey, P. D. Beremand, Y. Choi, J. L. Farmer, D. L. Adelson, T. L. Thomas, F. W. Bazer, and T. E. Spencer. 2006. Identification of endometrial genes regulated by early pregnancy, progesterone, and interferon tau in the ovine uterus. Biol. Reprod. 74(2):383-394.

Griffin, J., P. Hartigan, and W. Nunn. 1974. Non-specific uterine infection and bovine fertility: I. Infection patterns and endometritis during the first seven weeks post-partum. Theriogenology 1(3):91-106.

Guillemot-Legris, O., J. Masquelier, A. Everard, P. D. Cani, M. Alhouayek, and G. G. Muccioli. 2016. High-fat diet feeding differentially affects the development of inflammation in the central nervous system. J Neuroinflam. 13:1-11.

Gwazdauskas, F., W. Thatcher, C. Kiddy, M. Paape, and C. Wilcox. 1981. Hormonal patterns during heat stress following PGF2α-tham salt induced luteal regression in heifers. Theriogenology 16(3):271-285.

Gwynne, A. and W. Condon. 1982. Effects of cytochalasin B, colchicine, and vinblastine on progesterone synthesis and secretion by bovine luteal tissue in vitro. Reproduction 65(1):151-156.

Haimerl, P., W. Heuwieser, and S. Arlt. 2018. Meta-analysis on therapy of bovine endometritis with prostaglandin F2α—An update. J Dairy Sci. 101(11):10557-10564.

Hansen, J., M. Sato, R. Ruedy, K. Lo, D. W. Lea, and M. Medina-Elizade. 2006. Global temperature change. Proc. Nat. Acad. Sci. 103(39):14288-14293.

Hansen, L., A. Freeman, and P. Berger. 1983. Yield and fertility relationships in dairy cattle. J Dairy Sci. 66(2):293-305.

Hansen, P., M. Drost, R. Rivera, F. Paula-Lopes, Y. Al-Katanani, C. Krininger III, and C. Chase Jr. 2001. Adverse impact of heat stress on embryo production: causes and strategies for mitigation. Theriogenology 55(1):91-103.

Hansen, P. J., P. Soto, and R. P. Natzke. 2004. Mastitis and fertility in cattle - possible involvement of inflammation or immune activation in embryonic mortality. Am. J Reprod. Immunol. 51(4):294-301.

Harrison, T. D., E. M. Chaney, K. J. Brandt, T. B. Ault-Seay, L. G. Schneider, L. G. Strickland, F. N. Schrick, and K. J. McLean. 2022. The effects of differing nutritional levels and body condition score on scrotal circumference, motility, and morphology of bovine sperm. Transl. Anim. Sci. 6(1):txac001.

Harstine, B., M. Maquivar, L. Helser, M. Utt, C. Premanandan, J. DeJarnette, and M. Day. 2015. Effects of dietary energy on sexual maturation and sperm production in Holstein bulls. J Anim. Sci. 93(6):2759-2766.

Hayashi, K.-G., M. Hosoe, K. Kizaki, S. Fujii, H. Kanahara, T. Takahashi, and R. Sakumoto. 2017. Differential gene expression profiling of endometrium during the mid-luteal phase of the estrous cycle between a repeat breeder (RB) and non-RB cows. Reprod. Biol. Endocrinol. 15:1-18.

Hayes, J. D. and L. I. McLellan. 1999. Glutathione and glutathione-dependent enzymes represent a co-ordinately regulated defence against oxidative stress. Fr. Rad. Res. 31(4):273-300.

Heath, E., P. Weinstein, B. Merritt, R. Shanks, and J. Hixon. 1983. Effects of prostaglandins on the bovine corpus luteum: granules, lipid inclusions and progesterone secretion. Biol. Reprod. 29(4):977-985.

Herath, S., D. P. Fischer, D. Werling, E. J. Williams, S. T. Lilly, H. Dobson, C. E. Bryant, and I. M. Sheldon. 2006. Expression and function of Toll-like receptor 4 in the endometrial cells of the uterus. Endocrinology 147(1):562-570.

Herath, S., S. T. Lilly, N. R. Santos, R. O. Gilbert, L. Goetze, C. E. Bryant, J. O. White, J. Cronin, and I. M. Sheldon. 2009. Expression of genes associated with immunity in the endometrium of cattle with disparate postpartum uterine disease and fertility. Reprod. Biol. Endocrinol. 7:55.

Herath, S., E. J. Williams, S. T. Lilly, R. O. Gilbert, H. Dobson, C. E. Bryant, and I. M. Sheldon. 2007. Ovarian follicular cells have innate immune capabilities that modulate their endocrine function. Reproduction 134(5):683-693.

Hertl, J., Y. Gröhn, J. Leach, D. Bar, G. Bennett, R. Gonzalez, B. Rauch, F. Welcome, L. Tauer, and Y. Schukken. 2010. Effects of clinical mastitis caused by gram-positive and gram-negative bacteria and other organisms on the probability of conception in New York State Holstein dairy cows. J Dairy Sci. 93(4):1551-1560.

Herzog, K., K. Strve, J. Kastelic, M. Piechotta, S. E. Ulbrich, C. Pfarrer, K. Shirasuna, T. Shimizu, A. Miyamoto, and H. Bollwein. 2012. Escherichia coli lipopolysaccharide administration transiently suppresses luteal structure and function in diestrous cows. Reproduction 144(4):467.

Hirshfield, A. N. 1991. Theca cells may be present at the outset of follicular growth. Biol. Reprod. 44(6):1157-1162.

Hirshfield, A. N. 1992. Heterogeneity of cell populations that contribute to the formation of primordial follicles in rats. Biol. Reprod. 47(3):466-472.

Hirshfield, A. N. 1997. Overview of ovarian follicular development: considerations for the toxicologist. Environ. Mol. Mut. 29(1):10-15.

Holásková, I., G. S. Lewis, M. Elliott, K. P. Blemings, and R. A. Dailey. 2004. Effect of peptidoglycan-polysaccharide complex on reproductive efficiency in sheep. Am. J Reprod. Immunol. 52(3):197-203.

Horlock, A. D., T. J. Ormsby, M. J. Clift, J. E. Santos, J. J. Bromfield, and I. M. Sheldon. 2022. Cholesterol supports bovine granulosa cell inflammatory responses to lipopolysaccharide. Reproduction 164(3):109-123.

Horlock, A. D., R. L. Piersanti, R. Ramirez-Hernandez, F. Yu, Z. Ma, K. C. Jeong, M. J. D. Clift, J. Block, J. E. P. Santos, J. J. Bromfield, and I. M. Sheldon. 2020. Uterine infection alters the transcriptome of the bovine reproductive tract three months later. Reproduction 160(1):93-107.

Houfflyn, S., C. Matthys, and A. Soubry. 2017. Male Obesity: Epigenetic Origin and Effects in Sperm and Offspring. Curr. Mol. Biol. Rep. 3(4):288-296.

Husnain, A., U. Arshad, R. Zimpel, E. Schmitt, M. J. Dickson, M. C. Perdomo, M. N. Marinho, N. Ashrafi, S. F. Graham, and J. V. Bishop. 2023. Induced endometrial inflammation compromises conceptus development in dairy cattle. Biol. Reprod. 109(4):415-431.

Hussen, J., A. Düvel, O. Sandra, D. Smith, I. M. Sheldon, P. Zieger, and H.-J. Schuberth. 2013. Phenotypic and functional heterogeneity of bovine blood monocytes. PLoS One 8(8):e71502.

Hussen, J. and H.-J. Schuberth. 2017. Heterogeneity of bovine peripheral blood monocytes. Front. Immunol. 8:1875.

Ilic, Z., D. Crawford, P. A. Egner, and S. Sell. 2010. Glutathione-S-transferase A3 knockout mice are sensitive to acute cytotoxic and genotoxic effects of aflatoxin B1. Tox. App. Pharmacol. 242(3):241-246.

Imakawa, K., R. V. Anthony, M. Kazemi, K. R. Marotti, H. G. Polites, and R. M. Roberts. 1987. Interferon-like sequence of ovine trophoblast protein secreted by embryonic trophectoderm. Nature 330(6146):377-379.

Inchaisri, C., R. Jorritsma, P. Vos, G. Van der Weijden, and H. Hogeveen. 2011. Analysis of the economically optimal voluntary waiting period for first insemination. J Dairy Sci. 94(8):3811-3823.

Ireland, J. and J. Roche. 1983. Growth and differentiation of large antral follicles after spontaneous luteolysis in heifers: changes in concentration of hormones in follicular fluid and specific binding of gonadotropins to follicles. J Anim. Sci. 57(1):157-167.

Jeon, S. J., M. Oh, W. S. Yeo, K. N. Galvão, and K. C. Jeong. 2014. Underlying mechanism of antimicrobial activity of chitosan microparticles and implications for the treatment of infectious diseases. PLoS One 9(3):e92723.

Jinks, E., M. Smith, J. Atkins, K. Pohler, G. Perry, M. MacNeil, A. Roberts, R. Waterman, L. Alexander, and T. Geary. 2013. Preovulatory estradiol and the establishment and maintenance of pregnancy in suckled beef cows. J Anim. Sci. 91(3):1176-1185.

Johansson, A.-S. and B. Mannervik. 2001. Human glutathione transferase A3-3, a highly efficient catalyst of double-bond isomerization in the biosynthetic pathway of steroid hormones. J Biol. Chem. 276(35):33061-33065.

Kaltenbach, C., J. Graber, G. Niswender, and A. Nalbandov. 1968. Effect of hypophysectomy on the formation and maintenance of corpora lutea in the ewe. Endocrinology 82(4):753-759.

Kamat, M. M., S. Vasudevan, S. A. Maalouf, D. H. Townson, J. L. Pate, and T. L. Ott. 2016. Changes in myeloid lineage cells in the uterus and peripheral blood of dairy heifers during early pregnancy. Biol. Reprod. 95(3):68, 61-12.

Kasimanickam, R., T. Duffield, R. Foster, C. Gartley, K. Leslie, J. Walton, and W. Johnson. 2004. Endometrial cytology and ultrasonography for the detection of subclinical endometritis in postpartum dairy cows. Theriogenology 62(1-2):9-23.

Kelly, P., K. G. Meade, and C. O'Farrelly. 2019. Non-canonical inflammasome-mediated IL-1β production by primary endometrial epithelial and stromal fibroblast cells is NLRP3 and caspase-4 dependent. Front. Immunol. 10:102.

Kenny, D. A. and C. J. Byrne. 2018. Review: The effect of nutrition on timing of pubertal onset and subsequent fertility in the bull. Animal 12(s1):s36-s44.

Kesler, D. and H. Garverick. 1982. Ovarian cysts in dairy cattle: a review. J Anim. Sci. 55(5):1147-1159.

Kesner, J., E. Convey, and C. Anderson. 1981. Evidence that estradiol induces the preovulatory LH surge in cattle by increasing pituitary sensitivity to LHRH and then increasing LHRH release. Endocrinology 108(4):1386-1391.

Kim, I.-H. and H.-G. Kang. 2003. Risk factors for postpartum endometritis and the effect of endometritis on reproductive performance in dairy cows in Korea. J Reprod. Dev. 49(6):485-491.

Kim, K.-A., I.-H. Jung, S.-H. Park, Y.-T. Ahn, C.-S. Huh, and D.-H. Kim. 2013. Comparative analysis of the gut microbiota in people with different levels of ginsenoside Rb1 degradation to compound K. PloS one 8(4):e62409.

Kirby, C. J., M. F. Smith, D. H. Keisler, and M. C. Lucy. 1997. Follicular function in lactating dairy cows treated with sustained-release bovine somatotropin. J Dairy Sci. 80(2):273-285.

Knutti, B., J. Pycock, G. Van Der Weijden, and U. Küpfer. 2000. The influence of early postbreeding uterine lavage on pregnancy rate in mares with intrauterine fluid accumulations after breeding. Eq. Vet. Educ. 12(5):267-270.

Konishi, M., Y. Aoyagi, T. Takedomi, H. Itakura, T. Itoh, and S. Yazawa. 1996. Presence of granulosa cells during oocyte maturation improved in vitro development of IVM-IVF bovine oocytes that were collected by ultrasound-guided transvaginal aspiration. Theriogenology 45(3):573-581.

Lamming, G., D. Wathes, A. Flint, J. Payne, K. Stevenson, and J. Vallet. 1995. Local action of trophoblast interferons in suppression of the development of oxytocin and oestradiol receptors in ovine endometrium. Reproduction 105(1):165-175.

LeBlanc, S. 2012. Interactions of metabolism, inflammation, and reproductive tract health in the postpartum period in dairy cattle. Reprod. Dom. Anim. 47:18-30.

LeBlanc, S., T. Duffield, K. Leslie, K. Bateman, G. P. Keefe, J. Walton, and W. Johnson. 2002. Defining and diagnosing postpartum clinical endometritis and its impact on reproductive performance in dairy cows. J Dairy Sci. 85(9):2223-2236.

LeBlanc, S. J. 2008. Postpartum uterine disease and dairy herd reproductive performance: a review. Vet. J. 176(1):102-114.

LeBlanc, S. J. 2023. Postpartum reproductive disease and fertility in dairy cows. Animal 17:100781.

Leroy, J., T. Vanholder, J. Delanghe, G. Opsomer, A. Van Soom, P. Bols, and A. de Kruif. 2004. Metabolite and ionic composition of follicular fluid from different-sized follicles and their relationship to serum concentrations in dairy cows. Anim. Reprod. Sci. 80(3-4):201-211.

Leroy, J., T. Vanholder, B. Mateusen, A. Christophe, G. Opsomer, A. de Kruif, G. Genicot, and A. Van Soom. 2005. Non-esterified fatty acids in follicular fluid of dairy cows and their effect on developmental capacity of bovine oocytes in vitro. Reproduction 130(4):485-495.

Leroy, J., T. Vanholder, G. Opsomer, A. Van Soom, and A. de Kruif. 2006. The in vitro development of bovine oocytes after maturation in glucose and β-hydroxybutyrate concentrations associated with negative energy balance in dairy cows. Reprod. Dom. Anim. 41(2):119-123.

Liew, P. X. and P. Kubes. 2019. The neutrophil's role during health and disease. Physiol. Rev. 99(2):1223-1248.

Lima, F., R. Bisinotto, E. Ribeiro, L. Greco, H. Ayres, M. Favoreto, M. Carvalho, K. Galvão, and J. Santos. 2013. Effects of 1 or 2 treatments with prostaglandin F2α on subclinical endometritis and fertility in lactating dairy cows inseminated by timed artificial insemination. J Dairy Sci. 96(10):6480-6488.

Lima, F. S. d. 2020. Recent advances and future directions for uterine diseases diagnosis, pathogenesis, and management in dairy cows. Anim. Reprod. 17.

Lippolis, J. 2008. Immunological signaling networks: integrating the body's immune response. J Anim. Sci. 86(suppl_14):E53-E63.

Lopes, A., S. Butler, R. Gilbert, and W. Butler. 2007. Relationship of pre-ovulatory follicle size, estradiol concentrations and season to pregnancy outcome in dairy cows. Anim. Reprod. Sci. 99(1-2):34-43.

Lopez, D. and M. P. McLean. 1999. Sterol regulatory element-binding protein-1a binds to cis elements in the promoter of the rat high density lipoprotein receptor SR-BI gene. Endocrinology 140(12):5669-5681.

Loureiro, B., L. Bonilla, J. Block, J. M. Fear, A. Q. Bonilla, and P. J. Hansen. 2009. Colony-stimulating factor 2 (CSF-2) improves development and posttransfer survival of bovine embryos produced in vitro. Endocrinology 150(11):5046-5054.

Lüttgenau, J., B. Lingemann, O. Wellnitz, A.-K. Hankele, M. Schmicke, S. E. Ulbrich, R. M. Bruckmaier, and H. Bollwein. 2016a. Repeated intrauterine infusions of lipopolysaccharide alter gene expression and lifespan of the bovine corpus luteum. J Dairy Sci. 99(8):6639-6653.

Lüttgenau, J., B. Möller, D. Kradolfer, O. Wellnitz, R. M. Bruckmaier, A. Miyamoto, S. E. Ulbrich, and H. Bollwein. 2016b. Lipopolysaccharide enhances apoptosis of corpus luteum in isolated perfused bovine ovariesin vitro. Reproduction 151(1):17-28.

Ma, L., J. Cole, Y. Da, and P. VanRaden. 2019. Symposium review: Genetics, genome-wide association study, and genetic improvement of dairy fertility traits. J Dairy Sci. 102(4):3735-3743.

Machado, V. S., M. L. d. S. Bicalho, E. B. d. S. Meira Junior, R. Rossi, B. L. Ribeiro, S. Lima, T. Santos, A. Kussler, C. Foditsch, and E. K. Ganda. 2014. Subcutaneous immunization with inactivated bacterial components and purified protein of Escherichia coli, Fusobacterium necrophorum and Trueperella pyogenes prevents puerperal metritis in Holstein dairy cows. PloS one 9(3):e91734.

Mandl, A. M. and S. Zuckerman. 1951. The relation of age to numbers of oocytes. J Endocrinol. 7(2):190-193.

Mann, G., M. Fray, and G. Lamming. 2006. Effects of time of progesterone supplementation on embryo development and interferon-τ production in the cow. Vet. J. 171(3):500-503.

Martal, J., M.-C. Lacroix, C. Loudes, M. Saunier, and S. Wintenberger-Torres. 1979. Trophoblastin, an antiluteolytic protein present in early pregnancy in sheep. Reproduction 56(1):63-73.

Martins, T., M. Sponchiado, F. A. C. C. Silva, E. Estrada-Cortés, P. J. Hansen, F. Peñagaricano, and M. Binelli. 2022. Progesterone-dependent and progesterone-independent modulation of luminal epithelial transcription to support pregnancy in cattle. Physiol. Genom. 54(2):71-85.

Mascarenhas, M. N., S. R. Flaxman, T. Boerma, S. Vanderpoel, and G. A. Stevens. 2012. National, regional, and global trends in infertility prevalence since 1990: a systematic analysis of 277 health surveys. PLoS Med. 9(12):e1001356.

Mathew, D. J., K. D. Peterson, L. K. Senn, M. A. Oliver, and A. D. Ealy. 2022. Ruminant conceptus-maternal interactions: Interferon-tau and beyond. J Anim. Sci. 100(7):skac123.

Mathew, D. J., J. M. Sánchez, C. Passaro, G. Charpigny, S. K. Behura, T. E. Spencer, and P. Lonergan. 2019. Interferon tau-dependent and independent effects of the bovine conceptus on the endometrial transcriptome. Biol. Reprod. 100(2):365-380.

McDonald, T., G. Brester, A. Bekkerman, and J. Paterson. 2010. Case Study: Searching for the ultimate cow: The economic value of residual feed intake at bull sales. Prof. Anim. Sci. 26(6):655-660.

Medawar, P. B. 1953. Some immunological and endocrinological problems raised by the evolution of viviparity in vertebarates. Pages 320-338 in Proc. Symp. Soc. Exp. Biol.

Medawar, P. B. 1961. Immunological Tolerance: The phenomenon of tolerance provides a testing ground for theories of the immune response. Science. 133(3449):303-306.

Mehta, A., S. K. Onteru, and D. Singh. 2015. HDAC inhibitor prevents LPS mediated inhibition of CYP19A1 expression and 17β-estradiol production in granulosa cells. Mol. Cel. Endocrinol. 414:73-81.

Meidan, R., E. Girsh, O. Blum, and E. Aberdam. 1990. In vitro differentiation of bovine theca and granulosa cells into small and large luteal-like cells: morphological and functional characteristics. Biol. Reprod. 43(6):913-921.

Meira Jr, E., R. Ellington-Lawrence, J. Silva, C. Higgins, R. Linwood, M. Rodrigues, L. Bringhenti, H. Korzec, Y. Yang, and M. Zinicola. 2020. Recombinant protein subunit vaccine reduces puerperal metritis incidence and modulates the genital tract microbiome. J Dairy Sci. 103(8):7364-7376.

Merenda, V., D. Lezier, A. Odetti, C. Figueiredo, C. Risco, R. Bisinotto, and R. Chebel. 2021. Effects of metritis treatment strategies on health, behavior, reproductive, and productive responses of Holstein cows. J Dairy Sci. 104(2):2056-2073.

Meyerhoeffer, D., R. Wettemann, S. Coleman, and M. Wells. 1985. Reproductive criteria of beef bulls during and after exposure to increased ambient temperature. J Anim. Sci. 60(2):352-357.

Mitchell, M., H. W. Bakos, and M. Lane. 2011. Paternal diet-induced obesity impairs embryo development and implantation in the mouse. Fertil. Steril. 95(4):1349-1353.

Mitchell, M., R. Strick, P. L. Strissel, R. Dittrich, N. O. McPherson, M. Lane, G. Pliushch, R. Potabattula, T. Haaf, and N. El Hajj. 2017. Gene expression and epigenetic aberrations in F1-placentas fathered by obese males. Mol. Reprod. Dev. 84(4):316-328.

Miyamoto, T., N. Ogino, S. Yamamoto, and O. Hayaishi. 1976. Purification of prostaglandin endoperoxide synthetase from bovine vesicular gland microsomes. J Biol. Chem. 251(9):2629-2636.

Mohammed, Z. A., R. S. Robinson, R. Harris, Y. McLaughlin, K. E. Turnbull, G. E. Mann, and K. J. Woad. 2020. Detrimental effects of uterine disease and lipopolysaccharide on luteal angiogenesis. J Endocrinol. 245(1):79-92.

Molina-Coto, R., S. G. Moore, L. M. Mayo, W. R. Lamberson, S. E. Poock, and M. C. Lucy. 2020. Ovarian function and the establishment and maintenance of pregnancy in dairy cows with and without evidence of postpartum uterine disease. J Dairy Sci. 103(11):10715-10727.

Moraes, J. G., P. R. Silva, L. G. Mendonça, A. A. Scanavez, J. C. Silva, and R. C. Chebel. 2017. Effects of intrauterine infusion of Escherichia coli lipopolysaccharide on uterine health, resolution of purulent vaginal discharge, and reproductive performance of lactating dairy cows. J Dairy Sci. 100(6):4772-4783.

Murdoch, W. and R. McCormick. 1993. Mechanisms and physiological implications of leucocyte chemoattraction into periovulatory ovine follicles. Reproduction 97(2):375-380.

Murdoch, W. and L. Steadman. 1991. Investigations concerning the relationship of ovarian eosinophilia to ovulation and luteal function in the sheep. Am. J Reprod. Immunol. 25(2):81-87.

Nagy, L. and D. A. Freeman. 1990. Effect of cholesterol transport inhibitors on steroidogenesis and plasma membrane cholesterol transport in cultured MA-10 ley dig tumor cells. Endocrinology 126(5):2267-2276.

Nakamura, Y., M. Smith, A. Krishna, and P. Terranova. 1987. Increased number of mast cells in the dominant follicle of the cow: relationships among luteal, stromal, and hilar regions. Biol. Reprod. 37(3):546-549.

Ng, S. F., R. C. Lin, D. R. Laybutt, R. Barres, J. A. Owens, and M. J. Morris. 2010. Chronic high-fat diet in fathers programs β-cell dysfunction in female rat offspring. Nature 467(7318):963-966.

Nhu, Q. M., N. Cuesta, and S. N. Vogel. 2006. Transcriptional regulation of lipopolysaccharide (LPS)-induced Toll-like receptor (TLR) expression in murine macrophages: role of interferon regulatory factors 1 (IRF-1) and 2 (IRF-2). J Endotox. Res. 12(5):285-295.

Niswender, G. D. 2002. Molecular control of luteal secretion of progesterone. Reproduction 123(3):333-339.

Nomura, K., M. Maeda, K. Sugase, and S. Kusumoto. 2011. Lipopolysaccharide induces raft domain expansion in membrane composed of a phospholipid-cholesterol-sphingomyelin ternary system. Inn. Imm. 17(3):256-268.

O'Shea, J. 1987. Heterogeneous cell types in the corpus luteum of sheep, goats and cattle. J Reprod. Fertil. Suppl. 34:71-85.

Okuda, K., R. Sakumoto, Y. Uenoyama, B. Berisha, A. Miyamoto, and D. Schams. 1999. Tumor necrosis factor α receptors in microvascular endothelial cells from bovine corpus luteum. Biol. Reprod. 61(4):1017-1022.

Oliveira, L. J. and P. J. Hansen. 2009. Phenotypic characterization of macrophages in the endometrium of the pregnant cow. Am. J Reprod. Immunol. 62(6):418-426.

Oliveira, L. J., N. Mansourri-Attia, A. G. Fahey, J. Browne, N. Forde, J. F. Roche, P. Lonergan, and T. Fair. 2013. Characterization of the Th profile of the bovine endometrium during the oestrous cycle and early pregnancy. PLoS One 8(10):e75571.

Olsson, S. and R. Sundler. 2006. The role of lipid rafts in LPS-induced signaling in a macrophage cell line. Mol. Immunol. 43(6):607-612.

Opsomer, G., Y. Gröhn, J. Hertl, M. Coryn, H. Deluyker, and A. de Kruif. 2000. Risk factors for post partum ovarian dysfunction in high producing dairy cows in Belgium: a field study. Theriogenology 53(4):841-857.

Ott, T. L. 2019. Symposium review: Immunological detection of the bovine conceptus during early pregnancy. J Dairy Sci. 102(4):3766-3777.

Ott, T. L. 2020. Immunological detection of pregnancy: Evidence for systemic immune modulation during early pregnancy in ruminants. Theriogenology 150:498-503.

Owen, R. D. 1945. Immunogenetic consequences of vascular anastomoses between bovine twins. Science 102(2651):400-401.

Padmanabhan, V., J. Kesner, and E. Convey. 1978. Effects of estradiol on basal and luteinizing hormone releasing hormone (LHRH)-induced release of luteinizing hormone (LH) from bovine pituitary cells in culture. Biol. Reprod. 18(4):608-613.

Paisley, L., W. Mickelsen, and P. Anderson. 1986. Mechanisms and therapy for retained fetal membranes and uterine infections of cows: a review. Theriogenology 25(3):353-381.

Parry, D. M., D. Willcox, and G. Thorburn. 1980. Ultrastructural and cytochemical study of the bovine corpus luteum. Reproduction 60(2):349-357.

Pate, J. 1996. Intercellular communication in the bovine corpus luteum. Theriogenology 45(7):1381-1397.

Pate, J. L., K. Toyokawa, S. Walusimbi, and E. Brzezicka. 2010. The interface of the immune and reproductive systems in the ovary: lessons learned from the corpus luteum of domestic animal models. Am. J Reprod. Immunol. 64(4):275-286.

Payton, R. R., R. Romar, P. Coy, A. M. Saxton, J. L. Lawrence, and J. L. Edwards. 2004. Susceptibility of bovine germinal vesicle-stage oocytes from antral follicles to direct effects of heat stress in vitro. Biol. Reprod. 71(4):1303-1308.

Pennington, J., J. Albright, M. Diekman, and C. Callahan. 1985. Sexual activity of Holstein cows: seasonal effects. J Dairy Sci. 68(11):3023-3030.

Penny, L., D. Armstrong, T. Bramley, R. Webb, R. Collins, and E. Watson. 1999. Immune cells and cytokine production in the bovine corpus luteum throughout the oestrous cycle and after induced luteolysis. Reproduction 115(1):87-96.

Pereira, G., Y. Guo, E. Silva, M. F. Silva, C. Bevilacqua, G. Charpigny, L. Lopes-da-Costa, and P. Humblot. 2022. Subclinical endometritis differentially affects the transcriptomic profiles of endometrial glandular, luminal, and stromal cells of postpartum dairy cows. J Dairy Sci. 105(7):6125-6143.

Perrier, J.-P., D. A. Kenny, A. Chaulot-Talmon, C. J. Byrne, E. Sellem, L. Jouneau, A. Aubert-Frambourg, L. Schibler, H. Jammes, and P. Lonergan. 2020. Accelerating onset of puberty through modification of early life nutrition induces modest but persistent changes in bull sperm DNA methylation profiles post-puberty. Front. Genet. 11:945.

Perry, G., M. Smith, and T. Geary. 2004. Ability of intravaginal progesterone inserts and melengestrol acetate to induce estrous cycles in postpartum beef cows. J Anim. Sci. 82(3):695-704.

Perry, G. A., R. A. Cushman, B. L. Perry, A. K. Schiefelbein, E. J. Northrop, J. J. Rich, and S. D. Perkins. 2020. Role of preovulatory concentrations of estradiol on timing of conception and regulation of the uterine environment in beef cattle. Sys. Biol. Reprod. Med. 66(1):12-25.

Peter, A. T., W. Bosu, and R. DeDecker. 1989. Suppression of preovulatory luteinizing hormone surges in heifers after intrauterine infusions of Escherichia coli endotoxin. Am. J Vet. Res. 50(3):368-373.

Peñagaricano, F. and H. Khatib. 2012. Association of milk protein genes with fertilization rate and early embryonic development in Holstein dairy cattle. J Dairy Res. 79(1):47-52.

Peñagaricano, F., K. Weigel, and H. Khatib. 2012. Genome-wide association study identifies candidate markers for bull fertility in Holstein dairy cattle. Anim. Genet. 43:65-71.

Piersanti, R. L., J. Block, Z. Ma, K. C. Jeong, J. E. Santos, F. Yu, I. M. Sheldon, and J. J. Bromfield. 2020. Uterine infusion of bacteria alters the transcriptome of bovine oocytes. FASEB BioAdvances 2(8):506.

Piersanti, R. L., A. D. Horlock, J. Block, J. E. P. Santos, I. M. Sheldon, and J. J. Bromfield. 2019a. Persistent effects on bovine granulosa cell transcriptome after resolution of uterine disease. Reproduction 158(1):35-46.

Piersanti, R. L., R. Zimpel, P. C. C. Molinari, M. J. Dickson, Z. Ma, K. C. Jeong, J. E. P. Santos, I. M. Sheldon, and J. J. Bromfield. 2019b. A model of clinical endometritis in Holstein heifers using pathogenic Escherichia coli and Trueperella pyogenes. J Dairy Sci. 102(3):2686-2697.

Pierson, R., J. Kastelic, and O. Ginther. 1988. Basic principles and techniques for transrectal ultrasonography in cattle and horses. Theriogenology 29(1):3-20.

Pinedo, P., J. E. P. Santos, R. C. Chebel, K. N. Galvão, G. M. Schuenemann, R. C. Bicalho, R. O. Gilbert, S. L. Rodriguez-Zas, C. M. Seabury, G. Rosa, and W. Thatcher. 2020. Associations of reproductive indices with fertility outcomes, milk yield, and survival in Holstein cows. J Dairy Sci. 103(7):6647-6660.

Pinedo, P., J. Velez, H. Bothe, D. Merchan, J. Piñeiro, and C. Risco. 2015. Effect of intrauterine infusion of an organic-certified product on uterine health, survival, and fertility of dairy cows with toxic puerperal metritis. J Dairy Sci. 98(5):3120-3132.

Pinedo, P., J. Velez, G. Solano, N. Rodriguez, J. Naves, G. M. Schuenemann, and C. Risco. 2017. Effect of oral calcium administration on the cure and reproductive performance of Holstein cows diagnosed with puerperal metritis. J Dairy Sci. 100(4):2917-2927.

Plewes, M. R., C. Krause, H. A. Talbott, E. Przygrodzka, J. R. Wood, A. S. Cupp, and J. S. Davis. 2020. Trafficking of cholesterol from lipid droplets to mitochondria in bovine luteal cells: Acute control of progesterone synthesis. FASEB. 34(8):10731.

Poole, D. H. and J. L. Pate. 2012. Luteal microenvironment directs resident T lymphocyte function in cows. Biol. Reprod. 86(2):29, 21-10.

Potter, T. J., J. Guitian, J. Fishwick, P. J. Gordon, and I. M. Sheldon. 2010. Risk factors for clinical endometritis in postpartum dairy cattle. Theriogenology 74(1):127-134.

Price, J. C., J. J. Bromfield, and I. M. Sheldon. 2013. Pathogen-associated molecular patterns initiate inflammation and perturb the endocrine function of bovine granulosa cells from ovarian dominant follicles via TLR2 and TLR4 pathways. Endocrinology 154(9):3377-3386.

Przygrodzka, E., M. R. Plewes, and J. S. Davis. 2021. Luteinizing hormone regulation of inter-organelle communication and fate of the corpus luteum. Int. J Mol. Sci. 22(18):9972.

Pérez-Báez, J., T. V. Silva, C. A. Risco, R. C. Chebel, F. Cunha, A. De Vries, J. E. P. Santos, F. S. Lima, P. Pinedo, G. M. Schuenemann, R. C. Bicalho, R. O. Gilbert, S. Rodrigez-Zas, C. M. Seabury, G. Rosa, W. W. Thatcher, and K. N. Galvão. 2021. The economic cost of metritis in dairy herds. J Dairy Sci. 104(3):3158-3168.

Rajakoski, E. 1960. The ovarian follicular system in sexually mature heifers with special reference to seasonal, cyclical, and left-right variations. Eur. J. Endocrinol. 34(3_Suppl):S7-S68.

Reverchon, M., M. J. Bertoldo, C. Ramé, P. Froment, and J. Dupont. 2014. CHEMERIN (RARRES2) decreases in vitro granulosa cell steroidogenesis and blocks oocyte meiotic progression in bovine species. Biol. Reprod. 90(5):102, 101-115.

Ribeiro, E. S., G. Gomes, L. F. Greco, R. L. A. Cerri, A. Vieira-Neto, P. L. J. Monteiro, F. S. Lima, R. S. Bisinotto, W. W. Thatcher, and J. E. P. Santos. 2016. Carryover effect of postpartum inflammatory diseases on developmental biology and fertility in lactating dairy cows. J Dairy Sci. 99(3):2201-2220.

Richards, J. S., T. Jahnsen, L. Hedin, J. Lifka, S. Ratoosh, J. M. Durica, and N. B. Goldring. 1987. Ovarian follicular development: from physiology to molecular biology. Pages 231-276 in Proc. Proceedings of the 1986 Laurentian Hormone Conference. Elsevier.

Richards, J. S., Z. Liu, and M. Shimada. 2008. Immune-like mechanisms in ovulation. Tre. Endocrinol. Met. 19(6):191-196.

Roberts, R. M., D. W. Leaman, J. J. Hernandez-Ledezma, and N. C. Cosby. 1993. Trophoblast interferons: expression during development and gene organization. Pages 206-221 in Trophoblast Cells: Pathways for Maternal-Embryonic Communication. Springer.

Robinson, J., C. Ashworth, J. Rooke, L. Mitchell, and T. McEvoy. 2006. Nutrition and fertility in ruminant livestock. Anim. Fe. Sci. Tech. 126(3-4):259-276.

Rochlin, K., S. Yu, S. Roy, and M. K. Baylies. 2010. Myoblast fusion: when it takes more to make one. Dev. Biol. 341(1):66-83.

Romero-Arredondo, A. and G. Seidel Jr. 1994. Effects of bovine follicular fluid on maturation of bovine oocytes. Theriogenology 41(2):383-394.

Roth, Z. 2008. Heat stress, the follicle, and its enclosed oocyte: mechanisms and potential strategies to improve fertility in dairy cows. Reprod. Dom. Anim. 43:238-244.

Roth, Z., A. Dvir, D. Kalo, Y. Lavon, O. Krifucks, D. Wolfenson, and G. Leitner. 2013. Naturally occurring mastitis disrupts developmental competence of bovine oocytes. J Dairy Sci. 96(10):6499-6505.

Rowson, L. and R. Moor. 1967. The influence of embryonic tissue homogenate infused into the uterus, on the life-span of the corpus luteum in the sheep. Reproduction 13(3):511-516.

Rowson, L. E., G. E. Lamming, and R. M. Fry. 1953. Influence of Ovarian Hormones on Uterine Infection. Nature 171(4356):749-750.

Russe, I. 1983. Oogenesis in cattle and sheep. Bibl. Anat. 24:77-92.

Salilew-Wondim, D., S. Ibrahim, S. Gebremedhn, D. Tesfaye, M. Heppelmann, H. Bollwein, C. Pfarrer, E. Tholen, C. Neuhoff, K. Schellander, and M. Hoelker. 2016. Clinical and subclinical endometritis induced alterations in bovine endometrial transcriptome and miRNome profile. BMC Gen. 17:218.

Santos, J., R. Bisinotto, E. Ribeiro, F. Lima, L. Greco, C. Staples, W. Thatcher, M. Smith, M. Lucy, and J. Pate. 2011. Applying nutrition and physiology to improve reproduction in dairy cattle. Reprod. Dom. Rum. VII:387-403.

Sartori, R., P. M. Fricke, J. C. Ferreira, O. Ginther, and M. C. Wiltbank. 2001. Follicular deviation and acquisition of ovulatory capacity in bovine follicles. Biol. Reprod. 65(5):1403-1409.

Saunders, P. 2003. Germ cell-somatic cell interactions during spermatogenesis. Reproduction:91-101.

Sayers, N. and A. C. Hanyaloglu. 2018. Intracellular Follicle-Stimulating Hormone Receptor Trafficking and Signaling. Front. Endocrinol. 9:653.

Schrick, F. N., M. E. Hockett, A. M. Saxton, M. J. Lewis, H. H. Dowlen, and S. P. Oliver. 2001. Influence of subclinical mastitis during early lactation on reproductive parameters. J Dairy Sci. 84(6):1407-1412.

Seekford, Z. K., L. K. Wooldridge, N. W. Dias, C. L. Timlin, Á. Sales, S. L. Speckhart, K. G. Pohler, R. R. Cockrum, V. R. G. Mercadante, and A. D. Ealy. 2021. Interleukin-6 supplementation improves post-transfer embryonic and fetal development of in vitro-produced bovine embryos. Theriogenology 170:15-22.

Sekar, N. and J. D. Veldhuis. 2004. Involvement of Sp1 and SREBP-1a in transcriptional activation of the LDL receptor gene by insulin and LH in cultured porcine granulosa-luteal cells. Am. J Phys. Endocrinol. Met. 287(1):E128-E135.

Seo, H., G. D. Melo, R. V. Oliveira, G. A. Franco-Johannsen, F. W. Bazer, K. G. Pohler, and G. A. Johnson. 2024. Immunohistochemical examination of the uteroplacental interface of cows on days 21, 31, 40, and 67 of gestation. Reproduction 167(2).

Shan, X., T. Yu, X. Yan, J. Wu, Y. Fan, X. Guan, F. Fang, Y. Lin, Y. Zhang, and Y. Li. 2021. Proteomic analysis of healthy and atretic porcine follicular granulosa cells. J Proteo. 232:104027.

Sheldon, I., D. Noakes, A. Rycroft, D. Pfeiffer, and H. Dobson. 2002a. Influence of uterine bacterial contamination after parturition on ovarian dominant follicle selection and follicle growth and function in cattle. Reproduction. 123(6):837-845.

Sheldon, I. M., J. Cronin, L. Goetze, G. Donofrio, and H. J. Schuberth. 2009. Defining postpartum uterine disease and the mechanisms of infection and immunity in the female reproductive tract in cattle. Biol. Reprod. 81(6):1025-1032.

Sheldon, I. M., J. G. Cronin, and J. J. Bromfield. 2019. Tolerance and innate immunity shape the development of postpartum uterine disease and the impact of endometritis in dairy cattle. An. Rev. Anim. Biosci. 7:361-384.

Sheldon, I. M., J. G. Cronin, G. D. Healey, C. Gabler, W. Heuwieser, D. Streyl, J. J. Bromfield, A. Miyamoto, C. Fergani, and H. Dobson. 2014. Innate immunity and inflammation of the bovine female reproductive tract in health and disease. Reproduction 148(3):R41-R51.

Sheldon, I. M. and H. Dobson. 2004. Postpartum uterine health in cattle. Anim. Reprod. Sci. 82-83:295-306.

Sheldon, I. M., G. S. Lewis, S. LeBlanc, and R. O. Gilbert. 2006. Defining postpartum uterine disease in cattle. Theriogenology 65(8):1516-1530.

Sheldon, I. M., D. E. Noakes, A. N. Rycroft, D. U. Pfeiffer, and H. Dobson. 2002b. Influence of uterine bacterial contamination after parturition on ovarian dominant follicle selection and follicle growth and function in cattle. Reproduction 123(6):837-845.

Shen, W.-J., S. Asthana, F. B. Kraemer, and S. Azhar. 2018. Scavenger receptor B type 1: expression, molecular regulation, and cholesterol transport function. J Lip. Res. 59(7):1114-1131.

Shimizu, T., R. Echizenya, and A. Miyamoto. 2016. Effect of lipopolysaccharide on progesterone production during luteinization of granulosa and theca cells in vitro. J Biochem. Mol. Toxic. 30(4):206-211.

Short, R. V. 1969. Implantation and the maternal recognition of pregnancy. Foetal autonomy 2:31.

Sih, C. J., C. Takeguchi, and E. Kohno. 1971. Mechanism of prostaglandin biosynthesis. I. Characterization and assay of bovine prostaglandin synthetase. Biochemistry 10(12):2372-2376.

Silva, J., L. Siqueira, M. Rodrigues, M. Zinicola, P. Wolkmer, B. Pomeroy, and R. Bicalho. 2023. Intrauterine infusion of a pathogenic bacterial cocktail is associated with the development of clinical metritis in postpartum multiparous Holstein cows. J Dairy Sci. 106(1):607-623.

Simons, K. and R. Ehehalt. 2002. Cholesterol, lipid rafts, and disease. J Clin. Inves. 110(5):597-603.

Singh, A., S. Rajak, P. Kumar, S. Kerketta, and R. Yogi. 2018. Nutrition and bull fertility: a review. J. Entomol. Zool. Stud 6(6):635-643.

Skinner, J. and G. Louw. 1966. Heat stress and spermatogenesis in Bos indicus and Bos taurus cattle. J App. Phys. 21(6):1784-1790.

Skinner, J. D. 1981. Nutrition and fertility in pedigree bulls. Environmental Factors in Mammalian Reproduction. pp 160-168.

Soto, P., R. Natzke, and P. Hansen. 2003. Identification of possible mediators of embryonic mortality caused by mastitis: actions of lipopolysaccharide, prostaglandin F2α, and the nitric oxide generator, sodium nitroprusside dihydrate, on oocyte maturation and embryonic development in cattle. Am. J Reprod. Immunol. 50(3):263-272.

Staub, C. and L. Johnson. 2018. Spermatogenesis in the bull. Animal 12:s27-s35.

Steffan, J., S. Adriamanga, and M. Thibier. 1984. Treatment of metritis with antibiotics or prostaglandin F2 alpha and influence of ovarian cyclicity in dairy cows. Am. J Vet. Res. 45(6):1090-1094.

Steibel, J. P., R. Poletto, P. M. Coussens, and G. J. Rosa. 2009. A powerful and flexible linear mixed model framework for the analysis of relative quantification RT-PCR data. Genomics 94(2):146-152.

Stewart, H., S. McCann, P. Barker, K. Lee, G. Lamming, and A. Flint. 1987. Interferon sequence homology and receptor binding activity of ovine trophoblast antiluteolytic protein. J Endocrinol. 115(2):R13-R15.

Strüve, K., K. Herzog, F. Magata, M. Piechotta, K. Shirasuna, A. Miyamoto, and H. Bollwein. 2013. The effect of metritis on luteal function in dairy cows. BMC Vet. Res. 9(1):1-9.

Stumpf, T., M. Wolfe, M. Day, J. Stotts, P. Wolfe, R. Kittok, and J. Kinder. 1991. Effect of 17β-estradiol on the preovulatory surge of LH in the bovine female. Theriogenology 36(2):201-207.

Suleiman, J. B., V. U. Nna, Z. Zakaria, Z. A. Othman, A. B. A. Bakar, and M. Mohamed. 2020. Obesity-induced testicular oxidative stress, inflammation and apoptosis: Protective and therapeutic effects of orlistat. Reprod. Toxicol. 95:113-122.

Takahashi, M. 2012. Heat stress on reproductive function and fertility in mammals. Reprod. Med. Biol. 11(1):37-47.

Takahashi, T., A. Mori, H. Oda, I. Murayama, M. Kouno, and T. Sako. 2021. Comparison of cholesterol levels among lipoprotein fractions separated by anion-exchange high-performance liquid chromatography in periparturient Holstein–Friesian dairy cows. J Vet. Med. Sci. 83(2):260-266.

Takeda, K. and S. Akira. 2005. Toll-like receptors in innate immunity. Int. Immunol. 17(1):1-14.

Talbott, H. A., M. R. Plewes, C. Krause, X. Hou, P. Zhang, W. B. Rizzo, J. R. Wood, A. S. Cupp, and J. S. Davis. 2020. Formation and characterization of lipid droplets of the bovine corpus luteum. Sci. Rep. 10(1):11287.

Tall, A. R. and L. Yvan-Charvet. 2015. Cholesterol, inflammation and innate immunity. Nat. Rev. Immunol. 15(2):104-116.

Thatcher, W., M. Meyer, and G. Danet-Desnoyers. 1995. Maternal recognition of pregnancy. J Reprod. Fert. 49:15-28.

Townson, D. H. and J. L. Pate. 1996. Mechanism of action of TNF-α-stimulated prostaglandin production in cultured bovine luteal cells. Prostaglandins 52(5):361-373.

Triantafilou, M., K. Miyake, D. T. Golenbock, and K. Triantafilou. 2002. Mediators of innate immune recognition of bacteria concentrate in lipid rafts and facilitate lipopolysaccharide-induced cell activation. Journal of cell science 115(12):2603-2611.

Tsai, S.-J. and M. C. Wiltbank. 1998. Prostaglandin F2α regulates distinct physiological changes in early and mid-cycle bovine corpora lutea. Biol. Reprod. 58(2):346-352.

Turnbaugh, P. J., M. Hamady, T. Yatsunenko, B. L. Cantarel, A. Duncan, R. E. Ley, M. L. Sogin, W. J. Jones, B. A. Roe, and J. P. Affourtit. 2009. A core gut microbiome in obese and lean twins. Nature 457(7228):480-484.

Turner, M. L., J. G. Cronin, G. D. Healey, and I. M. Sheldon. 2014. Epithelial and stromal cells of bovine endometrium have roles in innate immunity and initiate inflammatory responses to bacterial lipopeptides in vitro via Toll-like receptors TLR2, TLR1, and TLR6. Endocrinology 155(4):1453-1465.

Vasudevan, S., M. M. Kamat, S. S. Walusimbi, J. L. Pate, and T. L. Ott. 2017. Effects of early pregnancy on uterine lymphocytes and endometrial expression of immune-regulatory molecules in dairy heifers. Biol. Reprod. 97(1):104-118.

Walsh, S., T. Fair, J. Browne, A. Evans, and P. McGettigan. 2012. Physiological status alters immunological regulation of bovine follicle differentiation in dairy cattle. J Reprod. Immunol. 96(1-2):34-44.

Walsh, S. W., E. J. Williams, and A. C. Evans. 2011. A review of the causes of poor fertility in high milk producing dairy cows. Anim. Reprod. Sci. 123(3-4):127-138.

Wang, Y., X. Mao, H. Chen, J. Feng, M. Yan, Y. Wang, and Y. Yu. 2019. Dexmedetomidine alleviates LPS-induced apoptosis and inflammation in macrophages by eliminating damaged mitochondria via PINK1 mediated mitophagy. Int. Immunophar. 73:471-481.

Watanabe, H., K. Tatsumi, H. Yokoi, T. Higuchi, M. Iwai, M. Fukuoka, H. Fujiwara, K. Fujita, H. Nakayama, and T. Mori. 1997. Ovulation defect and its restoration by bone marrow transplantation in osteopetrotic mutant mice of Mitf mi/Mitf mi genotype. Biol. Reprod. 57(6):1394-1400.

Waterman, R. 1988. Changes in Lipid Contents and Fatty Acid Compositions in Ovine Corpora Lutea during the Estrous Cycle and Early Pregnanancy. Biol. Reprod. 38(3):605-615.

Wathes, D. and G. Lamming. 1995. The oxytocin receptor, luteolysis and the maintenance of pregnancy. J Reprod. Fert. Supplement 49:53-67.

Wathes, D., G. Pollott, K. Johnson, H. Richardson, and J. Cooke. 2014. Heifer fertility and carry over consequences for life time production in dairy and beef cattle. Animal 8(s1):91-104.

Weber, D. M., P. A. Fields, L. J. Romrell, S. Tumwasorn, B. A. Ball, M. Drost, and M. J. Fields. 1987. Functional differences between small and large luteal cells of the late-pregnant vs. nonpregnant cow. Biol. Reprod. 37(3):685-697.

Wegmann, T. G., H. Lin, L. Guilbert, and T. R. Mosmann. 1993. Bidirectional cytokine interactions in the maternal-fetal relationship: is successful pregnancy a Th2 phenomenon? Immunol. Tod. 14(7):353-356.

Williams, E. J., D. P. Fischer, D. E. Noakes, G. C. England, A. Rycroft, H. Dobson, and I. M. Sheldon. 2007. The relationship between uterine pathogen growth density and ovarian function in the postpartum dairy cow. Theriogenology 68(4):549-559.

Williams, E. J., K. Sibley, A. N. Miller, E. A. Lane, J. Fishwick, D. M. Nash, S. Herath, G. C. England, H. Dobson, and I. M. Sheldon. 2008. The effect of Escherichia coli lipopolysaccharide and tumour necrosis factor alpha on ovarian function. Am. J Reprod. Immunol. 60(5):462-473.

Wilson, M., G. Lewis, and F. Bazer. 1979. Proteins of ovine blastocyst origin. Proc. Soc. Stud. Reprod. 11-21.

Wiltbank, M. C., M. G. Diskin, J. A. Flores, and G. D. Niswender. 1989. Regulation of the corpus luteum by protein kinase C. II. Inhibition of lipoprotein-stimulated steroidogenesis by prostaglandin F2α. Biol. Reprod. 42(2):239-245.

Wooding, F. 1992. The synepitheliochorial placenta of ruminants: binucleate cell fusions and hormone production. Placenta 13(2):101-113.

Wooding, F. 2022. The ruminant placental trophoblast binucleate cell: an evolutionary breakthrough. Biol. Reprod. 107(3):705-716.

Wooldridge, L. K. and A. D. Ealy. 2019. Interleukin-6 increases inner cell mass numbers in bovine embryos. BMC Dev. Biol. 19(1):2.

Wooldridge, L. K. and A. D. Ealy. 2021. Interleukin-6 promotes primitive endoderm development in bovine blastocysts. BMC Dev. Biol. 21(1):3.

Zhu, M. J., Y. Ma, N. M. Long, M. Du, and S. P. Ford. 2010. Maternal obesity markedly increases placental fatty acid transporter expression and fetal blood triglycerides at midgestation in the ewe. Am. J Phys. Reg. Integ. Comp. Phys. 299(5):R1224-R1231.

Zimbelman, R., R. Rhoads, M. Rhoads, G. Duff, L. Baumgard, and R. Collier. 2009. A re-evaluation of the impact of temperature humidity index (THI) and black globe humidity index (BGHI) on milk production in high producing dairy cows. Pages 158-169 in Proc. Southw. Nut. Con.

Zinicola, M., M. L. S. Bicalho, T. Santin, E. C. Marques, R. S. Bisinotto, and R. C. Bicalho. 2019. Effects of recombinant bovine interleukin-8 (rbIL-8) treatment on health, metabolism, and lactation performance in Holstein cattle II: Postpartum uterine health, ketosis, and milk production. J Dairy Sci. 102(11):10316-10328.

Zuckerman, S. 1951. The number of oocytes in the mature ovary. Rec. Prog. Horm. Res. 6:63-109.

BIOGRAPHICAL SKETCH

Zachary Seekford grew up on his family's dairy farm in McGaheysville, Virginia and received a Bachelor of Science degree in dairy science from Virginia Polytechnic Institute and State University. During his bachelor's degree, Zack was heavily involved in the dairy industry; learning more about improving management strategies and genetics in dairy cattle. This desire to learn led Zack to become an active participant in dairy related events such as dairy judging and Dairy Challenge where he focused on the roles of reproduction on dairy enterprises, and how fertility is important for profitability of dairy operations. Zack's interest in reproductive physiology allowed him to be exposed to research efforts at Virginia Tech targeted at improving fertility outcomes in cattle. Following graduation, Zack started a Master of Science degree in animal science at Virginia Polytechnic Institute and State University. Zack was co-advised by Dr. Alan Ealy and Dr. Vitor Mercadante and his thesis was titled "Interleukin-6 Supplementation Improves Post-Transfer Embryonic and Early Fetal Development of In Vitro Produced Bovine Embryos". After completion of his master's degree, Zack moved to Gainesville in August of 2020 to begin his doctoral studies. Zack's research under Dr. John Bromfield focused on uterine infections in dairy cows and the mechanisms regulating persistent subfertility in cows with uterine disease. After completion of his PhD, Zack plans to complete a postdoctoral position in reproductive physiology.